Neural Network Modelling of Present and Future Urban PM_{10} Concentrations based on Measurement Results

Von der Fakultät Energie-, Verfahrens- und Biotechnik der Universität Stuttgart zur Erlangung der Würde eines Doktors-Ingenieurs (Dr.-Ing.) genehmigte Abhandlung

Vorgelegt von
Keng Been Ang, M.Sc.

aus Singapur

Hauptberichter:	Prof. Dr.-Ing. habil. Günter Baumbach
Mitberichter:	Prof. Dr.-Ing. habil. Rainer Friedrich
Tag der Einreichung:	25.11.2009
Tag der mündlichen Prüfung:	25.02.2010

Institut für Feuerungs- und Kraftwerkstechnik der Universität Stuttgart
Abteilung Reinhaltung der Luft

2010

Acknowledgements

The writing of this dissertation has been one of the most significant challenges I have ever had to face. Without the support, patience and guidance of the following people, this study would not have been completed. It is to them that I owe my deepest gratitude.

First and foremost, I wish to express my deepest gratitude to Prof. Dr.-Ing. Günter Baumbach, who undertook to act as my supervisor despite his many other academic and professional commitments. His wisdom, knowledge and commitment to the highest standards inspired and motivated me. Not only has he taught me how to post questions and express my ideas, he showed me different ways to approach a research problem and the need to be persistent to accomplish my goal. He has been a mentor and a friend. For everything he has done, I thank him.

I am deeply indebted to Mr. Peter Pesch, Mr. Helmut Scheu-Hachtel, Dr. sc. nat. Ilona Heidmann and Dipl.-Ing. Alexandra Baltes from the Landesanstalt für Umwelt, Messungen und Naturschutz Baden-Württemberg for the continuous provision of measurement data from the air quality network since day one. My sincere appreciations go to Dipl.-Ing. Rainer Kapp and Mr Michael Brumbach from the Landeshauptstadt Stuttgart for the technical and logistic support during the street sweeping campaign at Stuttgart Neckartor. Special thanks also go to Dr. sc. agr. Karl Georg Gutbrod from meteoblue AG for his insightful comments and feedbacks. Working with these professionals has indeed been a fruitful learning experience.

I am very grateful to the institute director, Prof. Dr. techn. Günter Scheffknecht, for fostering a supportive and relaxed environment to work in. Special thanks go to Dipl.-Ing. Ulrich Vogt for his help in the German edition of the executive summary of this dissertation, and to Ing. Dieter Straub and Ing. Manfried Seitz for their excellent advice concerning both work and life. Very special thanks go to Antje Radszuweit, Marja Steinlechner, Renate Klein and Ursula Doctor for all the administrative assistance.

Being part of the WASTE family has been a special and invaluable experience for me. I thank all members, especially Dr.-Ing. Michael Waldbauer, Dipl.-Ing. Christine Dos Santos Costa and Dipl.-Ing. Adolf Neuwirth for the constant encouragements. Aaron DeWayne Fuller, Gloria Elizabeth Chávez Garcia, Sabrina Sanchez, Fabio Chui-Pressinotti, Carolina Andrea Acuña Caro, Marcelina Arkouli, Carlos Pacheco Bustos and so many others who have been my family in a foreign land since day one. Life as a foreigner away from the comfort of home would have been difficult without them.

Wong Chia Lee, my wife, without whom this effort would have been worth nothing. Her love, support and unwavering patience have not only taught me so much about sacrifice, discipline and compromise, they were also undeniably the bedrock upon which the past few years of my life have been built.

Ang Teng Hai and Yeo Seok Wah, my parents, who have always unconditionally supported, encouraged and believed in me, in all my endeavours and who so lovingly and unselfishly care for Chai Lee. It was under their faith in me and watchful eyes that I gained the drive and ability to accept challenges head on. Without them this dissertation would not have been possible.

Yang Lina, who has been taking care of the family despite her condition. Her perseverance in life has taught me an important lesson. Not everything is faced can be changed, but nothing can be changed until it is faced.

Last but not least, I must acknowledge the help of one very special person. Ang Bang Yao, my younger brother, who undertook the role as the elder brother for the past six years as the pillar of support in the family during my absence. This work would not have been possible without him at all possible and impossible times, for being self-sacrificing and for being there for the family at all times.

Keng Been Ang

Contents

Notations

Abbreviations

AfU	Landeshauptstadt Stuttgart, Amt für Umweltschutz
AMORE	A MORE
ANN	Artificial Neural Network
ARIMA	AutoRegressive Moving Average
AWS	Abfallwirtschaft Stuttgart
BMU	Bundesministerium für Umwelt, Naturschutz und Reaktorsicherheit
CALGRID	CALifornia photochemical GRID model
CALINE	CAlifornia LINe source model
CFD	Computation Fluid Dynamics
CMAQ	Community Multiscale Air Quality
DET	DETerministic modelling system
DWD	Deutscher Wetterdienst
EDX	Energy Dispersive X-Ray
EU	European Union
IFK-RdL	Institut für Feuerungs- und Kraftwerkstechnik, Abteilung Reinhaltung der Luft
ISC3	Industrial Source Complex
LEZ	Low Emission Zones
LUBW	Landesanstalt für Umwelt, Messungen und Naturschutz Baden-Württemberg
LUWG	Landesamt für Umwelt, Wasserwirtschaft und Gewerbeaufsicht
MIMO	Multiple-Input Multiple-Output
MISKAM	Mikroskaliges Klima- und Ausbreitungsmodell
MISO	Multiple-Input Single-Output
NMM	Numerical Mesoscale Model
NOAA	National Oceanic and Atmospheric Administration
OSPM	Operational Street Pollution Model
PCA	Principal Component Analysis
PM	Particulate Matter
ROM	Regional Oxidant Model
SEM	Scanning Electron Microscopy
STEM	Sulphur Transport and Emission Model
TVAREX	Time-Varying AutoRegressive model with EXogenous input
UAM	Urban Airshed Model
USEPA	United States Environmental Protection Agency
UTC	Universal Time, Coordinated

Mathematical functions and abbreviations

A	overall accuracy
C	cross-correlation coefficient
FAR	false alarm ratio
FN	number of missed predictions on PM_{10} exceedances
FP	number of false alarms
FB	fractional bias
IA	index of agreement
IS	index of success
MAE	mean absolute error
MBE	mean bias error
Q-Q	quantile-quantile
R^2	squared correlation coefficient
RMSE	root mean square error
TP	number of correction predictions on PM_{10} exceedances

Latin symbols and abbreviations

a	modelled value of output neuron
b	bias
d	measured value of output neuron
E	error function
f	transfer function for hidden layer
g	transfer function for output layer
Ib	input bias
Iw	input weight
Lb	layer bias
Lw	layer weight
n	activation
N	size of data set
O	measured PM_{10} concentration
p	input
P	modelled PM_{10} concentration
R	number of inputs
s_D	standard deviation
S	number of hidden neurons
T	number of output units
t	time
w	weight
y	model input parameter

Greek symbols and abbreviations

α	momentum
Δ	update value for weight
ε	learning rate
η_1	effect of street sweeping on ambient PM_{10} concentrations
η_2	effect of fireworks on ambient PM_{10} concentrations
η_{10}	reduction efficiency of PM_{10} on street surfaces
η_{75}	reduction efficiency of silt (PM_{75}) on street surfaces
η_{Total}	reduction efficiency of total dust load on street surfaces
η^-	negative multiplication factor
η^+	positive multiplication factor
θ	summation of biases

Zusammenfassung

Luftreinhaltung ist einerseits erforderlich, um die Situation weiterer Verschlechterung auf lange Sicht hin zu verhindern, andererseits sind auch Vorhersagen notwendig, um während Feinstaub-Episoden präventive Maßnahmen zur Verbesserung der Luftqualität ergreifen zu können.

In den letzten zehn Jahren sind neuronale Netzmodelle in der Luftreinhaltung ein effizientes Instrument zur Feststellung der räumlichen und zeitlichen Variabilität der Luftverunreinigung geworden. Eine der wichtigsten Eigenschaften von neuronalen Netzmodellen ist ihre Fähigkeit gelernte Sachverhalte zu verallgemeinern und darauf basierend, neue Situationen zu simulieren oder zu prognostizieren. Ein Anwendungsfall des neuronalen Netzwerks in der Luftreinhaltung kann darin bestehen, dass Messdaten als Eingangsparameter verwendet werden und sich Schadstoffkonzentrationen als Ausgangsparameter ergeben.

Ziel dieser Arbeit ist die simulative Bestimmung der PM_{10}-Konzentrationen in Stuttgart auf Basis von Tageswerten, mit Hilfe von zwei unterschiedlichen Modellen, die für diesen Zweck entwickelt wurden. Die beiden entwickelten Modelle sind ein PM_{10}-Nowcasting-Modell und ein PM_{10}-Forecasting-Modell.

Um eine gründliche und aufschlussreiche Bewertung der modellierten PM_{10}-Konzentrationen durchführen zu können, mussten mehrere Leistungsindikatoren für das PM_{10}-Nowcasting-Modell und das PM_{10}-Forecasting-Modell festgelegt und ausgewertet werden. Die Leistungsindikatoren sind der Fractional-Bias, der Grad der Übereinstimmung, das Quadrat des Korrelationskoeffizienten, der mittlere absolute Fehler, der mittlere quadratische Fehler und die mittlere quadratische Abweichung. Um die Anzahl der täglichen PM_{10}-Überschreitungen bestimmen zu können, mussten zusätzliche Leistungsgrade berücksichtigt werden. Für die beiden Modelle wurden auch eingehende Analysen der Restfehler und Quantil-Quantil-Plots zur Identifizierung von möglichen Ausreißern durchgeführt, um eine Verbesserung der modellierten Ergebnisse zu erlangen.

Als Anwendungsfall für das PM_{10}-Nowcasting-Modell wurden Untersuchungen herangezogen, die am Stuttgarter Neckartor durchgeführt wurden. Von November 2006 bis März 2007 wurden in der Umgebung der Luftmessstation am Neckartor die Straßen gereinigt. Dies galt als mögliche Maßnahme gegen hohe Feinstaubkonzentrationen im Bereich dieser Messstation. Basierend auf den Ergebnissen von Einzelpartikelanalysen, der Messungen von PM- und NO_X-Konzentrationen sollte eine Reduktion der PM_{10}-Konzentrationen in der Außenluft nachweisen werden. Allerdings war eine quantitative Auswertung über die Wirkung der Straßenreinigung anhand der Messergebnisse nicht möglich, da durch die meteorologischen Einflüsse und u.U. durch weitere Parameter überlagert wurden. Das neuronale Netzwerk bietet jedoch den Vorteil, dass die PM_{10}-Konzentrationen als Funktion der meteorologischen Einflüsse simuliert werden können. Das PM_{10}-Nowcasting-Modell wurde somit als ein Instrument zur Ergänzung von Immissionsmessungen entwickelt. Das Ziel des entwickelten Modells ist, die PM_{10}-Konzentrationen am Stuttgarter Neckartor zu simulieren, für den Fall dass keine Straßenreinigungsaktivitäten stattgefunden haben. Der Nachweis der Wirkung der Straßenreinigung wird dadurch geführt, dass die Differenzen zwischen den modellierten PM_{10}-Konzentrationen (ohne Straßenreinigung) und den entsprechenden gemessenen PM_{10}-Konzentrationen (mit Straßenreinigung) bestimmt werden. Basierend auf den ausführlichen statistischen Analysen konnte die Leistungsfähigkeit des entwickelten PM_{10}-Nowcasting-Modells festgestellt werden. Somit konnten mit dem Modell

die PM_{10}-Konzentrationen auf Basis von Tageswerten für den Zeitraum von mehreren Jahren (Januar 2004 bis Oktober 2006) am Stuttgarter Neckartor simulativ bestimmt werden. Anschließend wurde das PM_{10}-Forecasting-Modell eingesetzt, um die PM_{10}-Konzentrationen während der Straßenreinigung zu simulieren. Die Ergebnisse aus der linearen Regressionsanalyse, die einen Vergleich zwischen den modellierten PM_{10}-Konzentrationen und den gemessenen Werten erlauben, zeigen, dass die gemessenen PM_{10}-Werte im Allgemeinen etwa 4 % niedriger als die modellierten Werte waren, was auf einen Effekt der Straßenreinigung hindeutet. Dieser Trend war allerdings nicht an allen Straßenreinigungstagen zu beobachten.

Im Gegensatz dazu wurde das PM_{10}-Forecasting-Modell entwickelt, um die täglichen PM_{10}-Konzentrationen für die folgenden drei Tage in zwei städtischen Gebieten in Stuttgart mit unterschiedlichen Eigenschaften vorherzusagen. Der erste Messort repräsentierte ein verkehrsreiches Gebiet, wohingegen der zweite Messort städtischen Hintergrundkonzentrationen widerspiegelt. Die Eingangsparameter für die Simulation bestanden zum einen aus Messdaten von zwei Luftmessstationen, die Messstation am Neckartor (verkehrsreich) und die Messstation Bad Cannstatt (städtischer Hintergrund). Zum anderen wurden meteorologische Daten aus Wettervorhersagen für die folgenden drei Tage verwendet. Diese stammen aus einem Numerischen Mesoskaligen Modell. Das PM_{10}-Forecasting-Modell liefert statistisch gesicherte Ergebnisse für Vorhersagen von PM_{10}-Konzentrationen für die folgenden drei Tage, sowohl für das verkehrsreiche Gebiet als auch für das städtische Gebiet mit Hintergrundkonzentration. Allerdings sind Abstriche bei der Genauigkeit der simulierten Werte im Echtzeitbetrieb hinzunehmen, da die Wettervorhersagen nicht immer den auftretenden Wetterbedingungen entsprechen. Daher ist eine wichtige Voraussetzung für die erfolgreiche Vorhersage von PM_{10}-Konzentrationen die Verfügbarkeit von präzisen Wettervorhersagedaten, da die Qualität der PM_{10}-Vorhersagen stark von diesen Parametern abhängt.

Bei der Simulation von PM_{10}-Episoden mit hohen PM_{10}-Konzentrationen traten sowohl mit dem Modell zum PM_{10}-Nowcasting als auch mit dem PM_{10}-Forecasting-Modell Probleme auf. Vom mathematischen Aspekt her könnte die Tatsache eine Rolle spielen, dass die neuronalen Netzmodelle nur auf Konzentrationsbereiche angewendet werden dürfen, die während des Trainierens der Modelle vorlagen, aber nicht auf Konzentrationsbereiche extrapoliert werden dürfen, die nicht trainiert werden. Vom wissenschaftlichen Aspekt her könnte eine Unterschätzung der PM_{10}-Konzentrationen da durch erklärt werden, dass durch die Zusatzbelastung bei PM_{10}-Episoden deren Quellen nicht genau von den Eingangsparametern beschrieben werden können und daher nicht ausreichend genau simuliert werden können. Die drei Arten von PM_{10}-Episoden sind: Inversionswetterlagen während der kalten Jahreszeit, Feuerwerke und Feinstaub aus Ferntransport.

Eine allgemeine Schlussfolgerung ist, dass neuronale Netzmodelle für Anwendungen im Rahmen der Modellierung von PM_{10}-Konzentrationen in städtischen Gebieten eingesetzt werden können. Allerdings haben diese Modelle auch Einschränkungen, z.B. sind die entwickelten Modelle gebietspezifisch. Trotzdem kann festgehalten werden, dass bestimmte Sachverhalte und Zusammenhänge vom Modell korrekt abgebildet werden, wenn diese in einem vorher erzeugten und statistisch geprüfen Datensatz, mit dem das neuronale Netzmodell traniert wird, enthalten waren.

Executive summary

The problem of air pollution is a frequently recurring situation and its management has considerable social and economic effects. On one hand, air pollution control is necessary to prevent the situation from worsening in the long run. On the other hand, forecasting of air quality in days in advance is also necessary in order to adopt preventive actions during episodes of airborne pollutions.

In the past decade, neural network models have become an efficient tool for establishing both temporal and spatial characteristics of ambient air quality in the field of air pollution. Neural network models are capable of learning to model a relationship during a supervised training procedure, when they are repeatedly presented with series of input and associated output data. In the case of modelling ambient air pollutant concentrations, the input data could consist of meteorological or air quality data from measurements, and the outputs would be the air pollutant concentrations.

In this dissertation, the objectives are to realise and to evaluate two air quality neural network models that, correlating the air quality data with the meteorological information, are able to simulate daily urban PM_{10} concentrations in Stuttgart. For that, two models are developed for PM_{10} Nowcasting and PM_{10} Forecasting.

To conduct a thorough and insightful evaluation on the modelled PM_{10} concentrations, several performance indices which were used for both the PM_{10} Nowcasting and PM_{10} Forecasting models included the fractional bias, the index of agreement, the squared correlation coefficient, the mean absolute error, the mean bias error and the root mean square error. For the PM_{10} Forecasting model, additional performance indices to evaluate the correct number of PM_{10} exceedances were considered. For both models, thorough analyses of the error residuals and quantile-quantile plots were performed for the identification of possible outliers and for the better understanding in the patterns across the two sets of univariate modelled and measured data.

From 15.11.2006 to 18.03.2007, intensive street sweeping was conducted along the paved roadway of Stuttgart Neckartor as an urban PM abatement strategy. Based on results from single particle analyses and measurements of PM and NO_X concentrations, reductions in ambient PM_{10} concentrations could be suggested. However, an exact quantitative evaluation on the effectiveness of street sweeping on ambient PM_{10} was complicated by the possible influence of different meteorological conditions and other unknown factors during sweeping and non-sweeping days. With the neural network approach, these influencing meteorological conditions could be parameterised as functions to PM_{10} concentrations. The PM_{10} Nowcasting model was thus developed as a tool to complement the results of the past measurements. The aim of the developed model is to Nowcast the original state of PM_{10} concentrations at Neckartor, assuming that no street sweeping activities took place during the sweeping periods. Any effect of street sweeping could then be suggested by any differences between the modelled PM_{10} concentrations and the corresponding measured PM_{10} values. Through extensive statistical evaluation on the performance of the developed model, it was capable of accurately simulating past PM_{10} concentrations from January 2004 to October 2006. For the next step, the suitability of the developed model for operational use was then evaluated for the modelling of PM_{10} concentrations at the Neckartor site on the 41 days with street sweeping. Although results from linear regression analysis between the modelled PM_{10} concentrations against the measured values showed that the measured PM_{10} values were approximately 4 %

lower than the modelled values, trends of lower PM_{10} concentrations were not observable during all sweeping periods. Interesting, this reduction trend from the modelling results was in accordance to the measurement results.

The PM_{10} Forecasting model was developed to forecast the daily PM_{10} concentrations in one, two and three days in advance for two urban sites of different characteristics in Stuttgart. The first site represented the heavily trafficked site Neckartor, and the second site represented the urban background site Bad Cannstatt. The input parameters were on the one hand measurement data from the two ambient air monitoring stations at Neckartor and Bad Cannstatt. On the other hand common forecasted weather parameters up to three days in advance, which were obtained from a Numerical Mesoscale Model, were included. The overall model's results illustrate a possibility of effective use on the operational level for performing future PM_{10} forecasts up to three days at both the traffic and urban background sites. However, in real-time forecasting conditions, a compromise in performance should be expected, due to the possibility of less accurate meteorological forecasts. Therefore, a prerequisite for the successful implementation for PM_{10} forecasting is the availability of high quality meteorological forecasts, as the model performs according to the accuracy of these parameters.

Both the PM_{10} Nowcasting and PM_{10} Forecasting models encountered difficulties in accurately simulating PM_{10} concentrations during several distinct PM_{10} episodes. From the mathematical aspect, the underpredicting behaviours of both models during episodic events verifies the general assumption that neural network models will fail to extrapolate on data which have not been presented during the training procedure. From the scientific aspect, the underpredicting behaviours of the models could be attributed to the additional loads of PM from episodic events, whose presence could not be accurately modelled by the input parameters. The three most probable types of PM_{10} episodes are the extreme wintertime inversion-induced PM_{10} episodes, recreational PM_{10} episodes and regional and long-range PM_{10} transport.

A general conclusion is that neural network models can be useful and fairly accurate tools of assessment in PM_{10} concentrations in urban areas. However neural network models have inherent limitations. In this dissertation, the main limitation is that both PM_{10} Nowcasting and PM_{10} Forecasting models are strictly site-specific. Nevertheless, the general approach can be followed, especially in the case of neural networks, where a number of key decisions on their formulation, topology and operating parameters are necessary for the accurate simulation of PM_{10} concentrations.

1 Introduction

In urban environments where population and traffic density are relatively high, human exposure to hazardous substances is expected to be significantly increased. This is often the case near trafficked sites in city centres, where urban topography and microclimate may contribute to the creation of poor air dispersion conditions, thus giving rise to pollution hotspots. Under such conditions, pedestrians, cyclists, drivers and residents are likely to be exposed to pollutant concentrations exceeding the regulated air quality standards. The impact of air pollutants on human exposures depends on the location of pollution: large stationary sources, often located at a distance from densely populated city centres, emit air pollutants into the higher layers of the atmosphere, while the emissions from households and traffic are usually near ground levels in highly populated areas. As a result, mobile and small stationary sources may contribute more to ambient pollution concentrations and the resulting health effects, than their share in total emissions loads indicate.

1.1 Particulate matter

Among the various air pollutants, particulate matter (PM) pollution in particular is an issue of increasing public concern due to its recognised adverse effects on human health. The issue of PM or fine dust has been heavily discussed, and is still a very present and explosive topic in science and politics [1-4]. Although there is evidence that certain particle properties, such as the chemical composition and aerodynamic size, have different effects on human health [5], current EU legislation only regulates the mass concentration of particles with aerodynamic diameters below 10 µm and 2.5 µm in ambient air [6]. According to the EU framework Directive 1999/30/EC [7], the limit value for the daily PM_{10} average is 50 µg/m³ and must not be exceeded on more than 35 days of the calendar year (valid for the years 2005 to 2009). In addition, the annual PM_{10} average must not exceed the limit value of 40 µg/m³. In June 2008, a new edition of the Air Quality Directive [6] came in force which merges the former framework Directive and the Daughter Directives into a single Directive, with no change to existing air quality objectives. This new Directive includes the possibility to discount natural sources of pollution when assessing compliance against limit values, and the possibility of time extension of three years for PM_{10} concentrations with EU approval. However, the recommendations from the 1999 Daughter Directive, which foresaw that the annual limit value would be reduced to 20 µg/m³, and that the number of allowed exceedances of the daily PM_{10} average limit value would be reduced to seven per year by 2010, are no longer valid. In addition to the changes in the PM_{10} guidelines, new $PM_{2.5}$ regulations which introduce a concentration cap of 25 µg/m³ and an exposure reduction target are also now in force.

In Germany, the 2005 EU PM_{10} limit values were transposed by the 7th amendment of the Federal Immission Control Act (BImSchG) and by the 22nd Ordinance for the Implementation of the Federal Immission Control Act (22. BImSchV) [8]. With regard to PM_{10} concentration, it is important that the threshold concentration is not exceeded, below which the association of PM_{10} concentrations and human health can no longer be detected [9, 10]. For this reason, particularly strict criteria must be applied for the compliance with PM_{10} standards for the protection of human health.

1.2 PM situation in Europe

The main causes of PM pollution episodes in European cities can be summarised as follows:

- strong traffic-related emission sources and poor local atmospheric dispersion conditions (e.g. calm winds, temperature inversions, etc.) [11]
- synoptic weather conditions that favour long-range transport of particles [12, 13]
- natural sources of coarse particles that are not easily controllable (e.g. windblown dust, sea salt, etc.) [14]

The increased number of diesel-powered vehicles in the European vehicle fleets may have offset some of the gains in primary emission reductions due to the tightening of PM emission limits (e.g. EU-5 Regulation of the European Parliament) for such vehicles through technological improvements. Although the highest PM_{10} concentrations are generally expected to occur at roadsides, urban background monitoring stations can also record high PM_{10} values [11]. That raises concern about the exposure of a large proportion of the European urban population to PM pollution.

1.3 Ambient PM abatement strategy

The adoption of an effective air pollution abatement strategy has the ultimate aim to improve the ambient air quality in the areas of implementation. Forming long-term and successful air pollution control strategies require, however, the knowledge of the implementation costs, the economic benefits that might result from the reduction of emitted pollutants into the atmosphere, as all as other possible benefits (or damages) arising from the adoption of the proposed strategies. Some measures to mitigate the negative effects of ambient PM_{10} may focus on separating pollution sources and receptors, reducing the polluting activity, reducing its pollution characteristics, and controlling emissions with filtering devices [15]. Two examples of such measures are the designation of Low Emission Zones (LEZ) and the implementation of street sweeping activities.

1.3.1 Low emissions zones

17 air schemes/action plans have been worked out to date for the particularly polluted regions of the state of Baden-Württemberg in Germany [16]. Low Emission Zones are a central feature of these plans which involve a ban on vehicles with high emission levels. The Low Emission Zones are clearly delimited, generally urban areas where a ban on vehicles with high emission levels applies. Concentrations of PM and NO_2 in excess of the critical values occur in Baden-Württemberg only in areas with adjoining roads [17]. Consequently, road traffic is a factor of significant importance in the endeavour in improving ambient air quality. The quality of air can hence be improved by restricting traffic in Low Emission Zones as these regulations are designed to lower the high level of PM emission and NO_2 pollution in the ambient air. The traffic restrictions in these zones apply all the time; i.e. irrespective of whether the levels of air pollution are higher or lower at any one time.

Since 01.03.2008, the Low Emission Zones have been established in the following cities of Baden-Württemberg: Stuttgart, Mannheim, Reutlingen, Ludwigsburg, Tübingen, Schwäbisch Gmünd, Leonberg, Ilsfeld and Pleidelsheim (since 01.07.2008). This means that only vehicles in certain emission categories may drive in the urban area of these cities. From 01.01.2009, more Low Emission Zones came into force in Karlsruhe, Heilbronne, Ulm, Pforzheim, Herrenberg and Mühlacker.

1.3.2 Street sweeping

Reduction in traffic-induced PM will not be optimal by focusing exclusively on vehicle emissions control technology. Düring et al. [18] reported that a portion of the traffic-related PM_{10} can be attributed to non-exhaust emissions such as the resuspension of road dust, which comprises of PM from abrasion of the street surface, abrasion of clutch, brakes or tyres, and the emission of the road dust deposited on the road, which originated from outside the street and which may be crushed by the tyres.

To date, several studies have been conducted on the different reduction measures of PM emission from streets. These measures ranged from the application of road dust binding chemicals to the operation of street sweepers [19-24]. The reason behind the use of these measures to control PM is not unfounded. Assuming that street sweeping can remove particles which may eventually evolve into resuspended PM, then it is possible that the removal of large grains of geological particles could reduce the PM loads, which would otherwise be available for emission. A modified mechanical broom and water wash street sweeper was operated along the paved roadway at Stuttgart Neckartor, Germany, from 15.11.2006 to 18.03.2007. Based on results from single particle analyses and measurements of PM and NO_X concentrations, reductions in ambient PM_{10} concentrations could be suggested. However, an exact quantitative evaluation on the effectiveness of street sweeping was complicated by the possible influence of local meteorological conditions and other unknown effects [25]. Although conclusions cannot be drawn at this point, that street sweeping is entirely effective as an emission reduction strategy for ambient PM_{10} even for such modified street sweepers, it should be emphasised that the reduction of dust loads on street surfaces was clearly demonstrated.

1.4 The need of air quality modelling

Ambient air quality assessment and management are becoming increasingly dependent on air quality modelling [26]. In terms of assessment, air quality modelling can support optimisation of measurement networks, provides more comprehensive temporal and spatial information of air pollutants, and also delivers additional information in understanding of the contributing sources of pollution [27]. In terms of management, prediction of the next day's air pollution levels can call for proper actions and better controlling strategies from the concerned authorities [28].

Considering highly urbanised areas where the population spends most of their time at home, workplaces, schools and recreational areas, warnings can be helpful to alert health care as well as traffic and environmental management in scenarios whereby air quality limit values are exceeded. Such warning systems must be sufficiently reliable and understandable by the majority of the people. These warnings are aimed at specific population groups that are particularly sensitive to air pollution (e.g. asthmatics). Interests in finding ways to protect these individuals are also vital in recognising the lack of a discernable health threshold for exposure to ambient air pollutants, which implies that no level of emission reduction will protect all individuals [29]. Air quality forecasting system should therefore provide accurate advance notice that the ambient air concentration levels might exceed the air quality guidelines or the limit values.

However, a system for modelling urban air quality cannot by itself, solve ambient air pollution problems. The modelled results, if they are reliable and sufficiently accurate, can play an important role in complimenting actual measurement results. An example is the implementation of the air pollutant dispersion models, which have been widely used for assessing roadside air quality by providing predictions of present and future air pollutant levels, as well as the temporal and spatial variations [30]. When applied in a knowledgeable way, they can be useful in providing insights into the physical and chemical processes that govern the transport and transformation of atmospheric pollutants [31].

1.5 Objective

The objective of this dissertation is to develop a core model of neural network, which on one hand, is able to compute the Nowcast of PM_{10} concentrations when provided with certain sets of measured parameters. On the other hand the model is able to perform the forecast of probable concentrations of urban PM_{10}.

For the first task, a PM_{10} Nowcasting model shall be developed to complement the measurement results at Neckartor in winter 2006/2007, during which street sweeping was conducted as an urban PM abatement strategy [25]. The evaluation on the effect of street sweeping at Neckartor during the investigation period was, however, complicated by influence from varying weather conditions. Using the neural network approach, the varying weather conditions shall be parameterised as model inputs. The aim of the model is to Nowcast the original state of daily PM_{10} concentrations at Neckartor, assuming that no street sweeping activities took place during the sweeping periods. Any effect of street sweeping could then be suggested by any differences between the modelled PM_{10} concentrations and the corresponding measured PM_{10} values on street sweeping days.

For the second task, a PM_{10} Forecasting model shall be developed to forecast 24 h average PM_{10} concentrations three days in advance for two urban sites of different characteristics in Stuttgart. The first site represents a heavily trafficked site, and the second site represents an urban background site. The model shall rely on forecasted weather parameters from a Numerical Mesoscale Model (NMM) and measured PM_{10} concentrations from two existing ambient air monitoring stations at Neckartor and Bad Cannstatt. The benefits of developing such a model are two-folds. Firstly, the modelled results could act as both an alarm for bad weather (from the weather forecaster) and the quality of ambient air (from the PM_{10} Forecasting). Secondly, the information derived from the model could also aid in public education.

2 State-of-the-art of air quality models

Air quality models use mathematical and numerical techniques to simulate the physical and chemical processes that affect air pollutants as they disperse and react in the atmosphere. Based on inputs of meteorological data and source information, the developed models can be designed to characterise primary pollutants that are emitted directly into the atmosphere [32, 33]. These models are important to air quality management system as they can be used by agencies or parties tasked with controlling air pollution to identify source contributions to air quality problems, or to assist in the design of effective strategies to reduce harmful air pollutants via appropriate abatement strategies. In addition, air quality models can also be used to predict future pollutant concentrations after the implementation of a new regulatory program, in order to estimate the effectiveness of the program in reducing harmful exposures to humans and the environment.

The development of air quality models progressed in two main phases. In a first phase from about 1950 to 1970, empirical and theoretical investigations suggested that the concentration of atmospheric pollutants in a smoke trail could be approximated by a Gaussian distribution. Local scale transport models based on this assumption came to be known as “Gaussian models” or “Diffusion models” [34]. For the permission on the constructions of huge emission sources, such models were used to simulate pollutant transport and diffusion from single stacks, and to predict the concentration of pollutants at the receptors. The second phase began in the late 1970s; the Urban Airshed Model (UAM) [35], followed by the Regional Oxidant Model (ROM) [36, 37] which provided Eulerian-based models for O_3, the former for urban and the latter for regional scale modelling. The Sulphur Transport and Emission Model (STEM) focused on regional and continental acid deposition modelling [38-40]. The Community Multiscale Air Quality (CMAQ) modelling system is capable of processing large and diverse information from complicated emission mixtures and distribution of sources, to modelling the complexities of atmospheric process that transport and transform these mixtures to a dynamic environment [41]. This system operates in large time scales covering minutes to days and weeks.

An air quality modelling system typically consists of a meteorological model, an emissions model and an air quality model [42]. The meteorological model calculates as a function of time, the three-dimensional fields of wind, temperature, relative humidity, pressure and in some cases, turbulent eddy diffusivity, clouds and precipitation. The emissions model estimates the amount and chemical speciation of primary pollutants deriving from point to area sources based on process information (e.g., traffic loads, land use etc) and day-specific meteorological parameters. The outputs of the meteorological and emissions models are then introduced into the air quality model, which calculates the concentrations and deposition rates of gases and aerosols as a function of space and time.

For modelling purpose, two main classifications to the models can be made: Nowcasting and Forecasting models. As the names suggest, a Nowcasting model allows air quality for any given model domain to be shown in an up-to-date fashion. A Forecasting model, on the other hand, predicts the probable air quality in time-steps in advance, for instance a day to a week. Depending on the requirements, the respective models may require information on emissions, either archive or real time, as well as real time meteorological information.

2.1 Nowcasting models

In recent years, Nowcasting models for predicting air pollutant concentrations have been frequently used in the “what-if” scenarios. These types of hypothetical scenarios can be essential for policy makers to determine whether the costs of implementing measures justify the benefits brought about by reducing the concentrations of the targeted ambient air pollutants. For instance, the effect of Low Emission Zones in central London as a means of reducing ambient NO_2 concentrations was investigated with a stochastic model [43, 44]. In the work, two principal types of Low Emission Zones were considered; the reduction of vehicle flows and the restriction of certain higher emitting vehicle types. Although the results showed that significant reductions in traffic emissions did not appreciably affect the NO_2 concentrations, the importance of considering other options to reduce emissions from non-road traffic sources was raised. In another study, a quantitative evaluation of PM_{10} mitigation measure via the construction of a bypass road in Berlin was performed with a combination of numerical dispersion models [45]. Using this “what-if” approach, significant reductions in PM_{10} and NO_2 loads in the study area were reported.

The next common application of Nowcasting models in the field of air quality control is the modelling of air pollution concentrations for areas, on which no measurement results are available. With a stochastic model, the spatial distributions of O_3, NO_X and PM in Sydney were successfully mapped [46]. In another study, a multivariate neural network method which incorporated results from a Gaussian model and regression approach to calculate the average spatial distribution of NO_2 concentrations covering Cyprus was developed [27]. From the results, it was possible to account for the actual air quality situations at many sites for the research area.

Nowcasting systems are also used in the understanding and predicting of air pollutant concentrations and pathways within build up areas [47, 48]. With advances in computing power, computational fluid dynamics (CFD) models can now resolve individual buildings and predict wind pathways through different terrain types. Such models are increasingly being used to simulate the transport and diffusion, and subsequently concentrations of air pollutants within urban areas, where the population is at risk [49, 50].

2.2 Forecasting models

During the last decades several Forecasting models have been designed on the basis of different computational methods to provide air quality forecasts. The first systems generally implemented statistical approaches based on empirical observations, such as neural network models taking advantage of their limited computational resources demand. For instance, evaluations and intercomparisons of these forecasting models for NO_2, PM_{10} and O_3 concentrations were previously performed [51, 52]. A variety of approaches based on empirical methods were applied to forecast air pollutant concentrations for different urban locations: multilayer perceptron based neural network models were used to forecast O_3 peaks in the Orleans region [53], NO_2 and O_3 hourly average concentrations in Bilbao [54], and PM_{10} concentrations in Thessaloniki [55] and in Bordeaux [56]. Later the increase in computer processing speed and memory capacity of new generation computers allowed the development and implementation of forecasting systems based on deterministic or semi-deterministic models [57, 58]. Presently, some examples of national and regional scale forecasts can be obtained from the USEPA, NOAA [59] and different European institutions such as the University of Cologne [60] and the French Institute National de l’Environnement

Industriel et des Risques. Urban scale forecasting systems have also been successfully developed and are now in use in some European cities for both urban air quality forecast and also for emergency preparedness [61-63].

2.3 Classification of Nowcasting and Forecasting models

As a general classification, both Nowcasting and Forecasting models can be categorised as follows:

- Deterministic model
- Numerical model
- Stochastic model
- Hybrid model
- Neural network model

In Table 2.1 a summary of some available PM models which have been widely used is given. The classification here follows the type of the model and the mathematical principle of the method respectively.

Table 2.1: Classification of air quality models

Type	Theoretical background	Models
Deterministic	Gaussian principle	DET [51] AIRPOL [64] ISC3 [65] HIWAY [66, 67] CALINE [68-70]
Numerical	K-models	AUSTAL2000 [71] CALPUFF [72, 73] DRAIS [74, 75] Micro-CALGRID [76] MISKAM [49, 77, 78]
Stochastic	Regression, time series technique	ARIMA [79, 80] Linear model [51, 81-84] Multiple linear regression model [85, 86] TVAREX [87]
Hybrid	Combination of deterministic, stochastic and neural network	Hybrid ARIMA-ANN model [79, 88] OSPM [88]
Neural network	Multilayer perceptron	Neural network model [51, 81-84, 85, 89-93]

2.3.1 Deterministic model

The deterministic models estimate air pollutant concentrations from emission inventories and meteorological variables, according to solution of various equations that represent the relevant physical processes. In other words, differential equation is developed by relating the rate of change of air pollutant concentrations in terms of average wind characteristics and turbulent diffusion, which in turn, is derived from the mass conservation principle. The common Gaussian line source model is based on the superposition principle, namely pollutant concentration at a receptor, which is the sum of concentrations from all the point sources making up a line source.

Although the deterministic modelling approach may be a logical way to predict air pollutant concentrations, it is, however, not free from limitations. These models are developed by deducing the transportation of air pollutants with mathematical formulae, which may reflect more or less accurately the physics of the process. To be useful, these formulae require first an adequate amount of meteorological input about the state of the atmosphere (wind characteristics, stability, turbulence, etc.) and then the detailed information on relevant emissions.

2.3.2 Numerical model

Numerical air quality models are based on numerical solution of partial differential equations representing the atmospheric dispersion phenomena. Example of such numerical models is the K-models, which are derived by using the K-theory approximation for the closure of the turbulent diffusion equation. These models are time dependent and applied through computer codes: Eulerian models and Lagrangian models.

For the Eulerian models, the transport of inert air pollutants may be simulated by means of models which numerically solve the equation for conservation of mass of the pollutants. Such models are usually embedded in prognostic meteorological models. Advanced Eulerian models include refined sub-models for the description of turbulence (e.g. second-order closure models and large-eddy simulation models).

As an alternative to the Eulerian models, the Lagrangian approach consists in describing fluid elements that follow the instantaneous flow. They include all models in which plumes are broken up into elements such as segments, puffs or particles. Lagrangian models use a certain number of fictitious particles to simulate the dynamics of a selected physical parameter. Particle motion can be produced by both deterministic velocities and semi-random pseudo-velocities generated using the Monte Carlo techniques. Hence, transport caused by both the wind and turbulent terms due to wind fluctuations is taken into account.

All numerical models have common limitations arising from employing the K-theory for the closure of diffusion equation [94]. For instance, the K-theory diffusion equation is valid only when considering neural and stable atmospheric conditions, and when the size of the plume of pollutants is greater than the size of the dominant turbulent eddies.

2.3.3 Stochastic model

In contrast to deterministic modelling, the stochastic models calculate air pollutant concentrations from meteorological and traffic parameters after an appropriate statistical relationship has been empirically computed from the measured concentrations. In short, these models are summarisation of the data already on record completed by the assumption that the record is either stable or contain trends or cycles, which may somehow be extrapolated. Regression, multiple regression and time series technique are some of the used methods [86]. Example of the time series techniques are the Box-Jenkins models, which are widely used to describe the dispersion of exhaust emissions at trafficked intersection and at busy arterial roads.

Stochastic models can be very useful in situations such as real-time short-term forecasting, where the information available from measured trends in concentration is generally more relevant than that obtained from the deterministic models [94].

Limitations of stochastic models include the requirements of long historical data sets and the lack of physical interpretation. For instance, regression modelling often underperforms when applied to describe non-linear systems [95]. The quality of the Box-Jenkins models relies frequently on individual user's experiences and knowledge of pollutant time series statistics. Thus, different analyst may render contradictory interpretations when given the same data [96].

2.3.4 Hybrid model

The hybrid models may combine the useful components of both deterministic and stochastic models [97]. Other variations of hybrid models may also combine components from both stochastic and neural network models [79, 98].

For hybrid models, the deterministic component can facilitate the strengthening of the models' accuracies, i.e., to use it for predicting air pollutant concentrations that occur frequently. The stochastic component can be used to analyse the parametric distributional form of air pollutant data in order to estimate percentiles including the extreme values. This approach is largely based on the ability of deterministic models to establish links between emissions, meteorological and pollutant concentrations, and the ability of stochastic models to predict the distribution of all events, once the appropriate distributional form is identified for the historical air pollutant data [97].

The combination with the neural network component allows the hybrid models to approximate complex functions between the training variables and the target [79].

2.3.5 Neural network model

Due to difficulties in understanding the physical parameters in neural network models, they are often referred as "black box models". Nevertheless, researches have been conducted to implement possible nonlinear differential equations inside the network in order to use the available knowledge [99]. An example of such application is the development of neural network model as a non-linear tool for air quality modelling, principally using the multilayer perceptron architecture [100]. To date, numerous papers have shown that a feed-forward network is potentially capable of approximating any non-linear function. Gardner and Dorling [95, 100] concluded that neural network models generally provide better results compared to statistical linear methods, especially where the problem being analysed includes nonlinear behaviour.

As neural networks are not based on any physical theory and may contain nonlinearities, the predictions may be ambiguous when extrapolating predictions beyond the range of the original training data. In another words, the drawback of the neural approach is that no information on the physical phenomena can be gained, since the network resembles the behaviour of a black-box method [101]. Even when not extrapolating, the predictions may already possess inherent errors which are caused by the network's local minima resulting from the non-uniform distribution of training parameters and noise over the domain [102].

2.4 Evaluation on air quality models

The potential scenarios to be considered by the air quality models in this dissertation cover two main areas:

- Nowcasting of daily PM_{10} concentrations at Neckartor during street sweeping periods
- Forecasting of daily PM_{10} concentrations three days in advance for two sites of different characteristics in Stuttgart

Judging from the scenarios and the background information of the air quality models which have been reviewed, the following criteria and methodology have been used in order to conduct a credible and objective review of all models. Four model evaluation categories have been suggested as follows:

Science and credibility: Describes how well the model simulates processes in air pollution meteorology (dispersion, chemistry, transport, numerical methods, etc.)

Ease of use (from user's perspective): Describes how easily the user can manage and use the model with or without prior knowledge, and configuration of input data files

Computational requirements: Describes whether the model and any supporting programs have system requirements that are difficult to meet

Availability, restrictions and terms: Describes the legal restrictions on procuring the model, permission for code changes by end-user, and acquisition methods (from the vendor or download from the internet)

The evaluation of the respective models are summarised in Table 2.2.

Table 2.2: Evaluation of air quality models

Evaluation categories	**Ratings**				
	Deterministic model	**Numerical model**	**Stochastic model**	**Hybrid model**	**Neural network model**
Science and credibility	fairly good	average	average	fairly good	average
Ease of use	poor	poor	average	poor	poor
Computational requirements	poor	poor	average	poor	average
Availability, restrictions, terms	fairly good	fairly good	average	average	good

Based on results from Table 2.2, both the stochastic and neural network air quality models seem to be the better choices among the five evaluated models in terms of overall ratings. It should be emphasised that stochastic model is a general classification of the simple regression model to the complicated Box-Jenkins model. Thus, although the model scores average ratings for all four evaluation categories, the actual ratings depend largely on the specific type of model considered.

In general, the neural network model outperforms the other four models in terms of availability, restrictions and terms. Some better-known commercially available neural network programmes include the Wolfram Research Neural Network package [103], the AMORE [104], MathWorks Neural Network Toolbox [105] and the GBLearn2 library [106], which are based on programming codes and can be modified or improved without restrictions based on the end-user’s requirements. However, the requirement of use in terms of programming can greatly hinder the ease of use when considering users who have no prior knowledge to computer programming.

To summarise, the use of neural network model can be flexible, which enables one to solve highly complex non-linear problems. When properly trained, the model is able to self-extract functional relationships between the model inputs and outputs from the data set without requiring explicit consideration on the actual data generation process, which makes the model easy to handle in principle. Neural network model can be trained with real measurement and forecasted data, and subsequently updated with new data, enhancing its quality and making it an ideal method for the purpose of this dissertation.

3 Air pollution situation at Stuttgart Neckartor and Bad Cannstatt

3.1 Description of study areas

Stuttgart is the capital of the state of Baden-Württemberg in southern Germany. Being the sixth largest city in Germany, Stuttgart has a population of over 590 thousand while the metropolitan area has a population of over 5 million inhabitants. The centre of Stuttgart city is located off the Neckar valley, which inherits a basin topography. A 2 km long narrow valley runs from Kaltental through Nesenbach and ends in Heslach, which is in the basin structure. From northeast to southwest in the direction along the Neckar valley, the slopes incline from 5 to 10° and heights from 100 to 240 m over 6 km in distance. To the northeast of Karlshöhe lies the 2.5 km wide Stuttgart city centre. Between Kreigsberg and Uhlandshöhe, a constriction of approximately 1 km wide is located at Bad Cannstatt in the Neckartal.

The locations of the traffic and urban background sites in Stuttgart are depicted in Fig. 3.1. The traffic site (latitude 48°47’16’’N and longitude 9°11’25’’E) is located approximately 30 m before a traffic junction of the Neckartor roadway. The roadway belongs to the federal highway B14 and is oriented from southwest to northeast. It is surrounded by a non-permeable barrier of buildings on one side, where air pollution build-up is favoured. The urban background site (latitude 48°48’31’’N and longitude 9°13’47’’E) is distanced from the

Fig. 3.1: Locations of Neckartor (traffic) and Bad Cannstatt (urban background) in Stuttgart, Germany data source: Google Maps

main artery roadways to the city centre and is, in general, a good representation of city-wide background PM_{10} concentrations.

3.2 PM situation at Stuttgart

Transport can be considered as one of the most important sources of PM, and is largely involved in major urban air pollution issue [107, 108]. At the heavily trafficked site of Stuttgart Neckartor the 24 h average limit value of 50 µg/m³ for PM_{10} prescribed by the European legislation was exceeded 110 and 89 times in 2007 and 2008 respectively. The PM_{10} annual average values for 2007 and 2008 were 44 µg/m³ and 41 µg/m³ respectively, which exceeded the limit value of 40 µg/m³.

During the winter season, the basin area of Stuttgart is exposed to weather conditions such as high atmospheric pressure and little wind which often result in the formation of temperature inversion. In the past, these special weather conditions resulted in extensive PM episodes in the ambient air [109, 110]. During the particular PM_{10} pollution episode in January to February 2006, approximately 54 % of the PM_{10} in Neckartor originated from traffic [110], as illustrated in Fig. 3.2. The portion was calculated by the Landesanstalt für Umwelt, Messungen und Naturschutz Baden-Württemberg (LUBW) from the sum of PM_{10} from the traffic and exhaust from traffic sectors. The next largest portion originated from the urban background, which constituted approximately 33 % of the total PM_{10}.

This traffic-related PM_{10} proportion was among the highest compared to other ambient air monitoring stations in the state of Baden-Württemberg. One reason for the exceeding PM_{10} limit values at the traffic site of Neckartor is the local road dust generation. Three main groups of potential PM sources were previously identified at this site with a method of size-fractionated PM samplings coupled with Scanning Electron Microscopy (SEM) and Energy Dispersive X-Ray (EDX) analyses [111]. The PM coarse fractions of 2.1 to 10.0 µm, which accounted for 44 % of the PM_{10}, were identified as resuspended road dust. The PM fractions of 0.7 to 2.1 µm, which accounted for 38 % of the PM_{10}, were identified as background and agglomerated particles with N and S containing crystals. The finer PM fractions smaller than 0.7 µm, which accounted for 18 % of the PM_{10}, were identified as agglomerated diesel soot particles with traces of S. The results from cascade impactor samplings and single particle analyses with SEM/EDX at Neckartor during high PM concentrations ($PM_{10,\ 24h}$ > 80 µg/m^3) were averaged and depicted in one summarising diagram in Fig. 3.3.

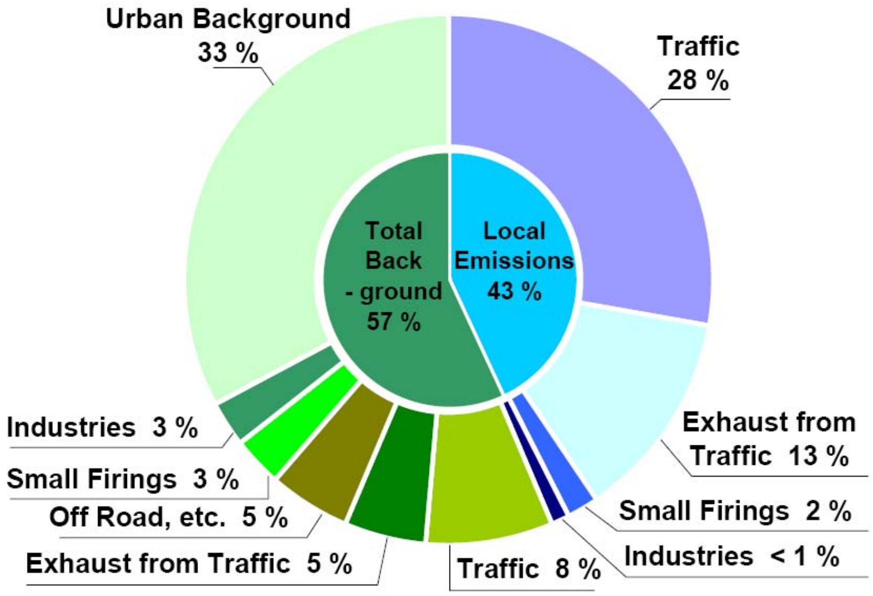

Fig. 3.2: Sources of PM_{10} at Stuttgart Neckartor [110]

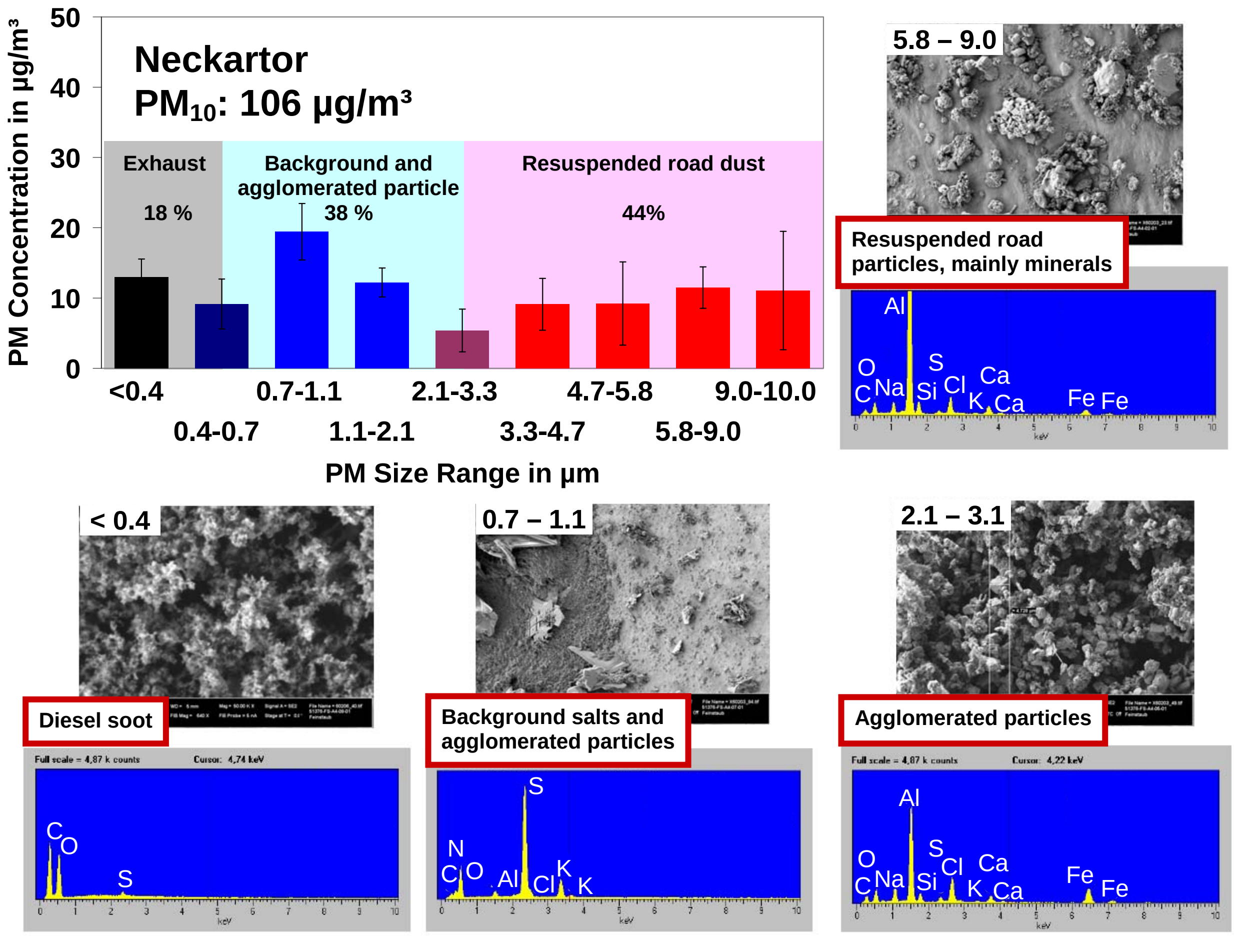

Fig. 3.3: Single particle analyses of size fractionated PM at Stuttgart Neckartor during high PM concentrations ($PM_{10,\ 24h} > 80\ \mu g/m^3$) [111]

3.3 Air quality measurements from 2004 to 2007

3.3.1. 24 h average and annual mean PM_{10} concentrations

The 24 h average PM_{10} concentrations are exemplarily shown for the traffic site of Neckartor and urban background site of Bad Cannstatt in Fig. 3.4a to 3.4d, and 3.5a to 3.5d respectively. Despite differences in local emissions and dispersion conditions between the two studied areas, the profile of 24 h average PM_{10} concentrations over the course of the four years are similar, being determined by PM episodes.

For comparison purposes, the annual mean PM_{10} concentrations and number of days exceeding the EU PM_{10} 24 h average limit values at Neckartor and Bad Cannstatt from 2004 to 2007 are summarised in Table 3.1 and 3.2.

From 2004 to 2007, the lowest annual mean PM_{10} concentration at Neckartor was 44.3 µg/m³ in 2007, which exceeded 40 µg/m³. This is the same as the annual limit established by the 2008/50/EC Directive for PM_{10} concentrations. At Bad Cannstatt, the lowest annual mean PM_{10} concentration was recorded in 2007, which was 22.5 µg/m³. On the account of EU-wide legislation (e.g. emission standards for vehicles, Large Combustion Plant Directive), national legislation and the implementation of both in Member States, Görgen and Lambrecht [112] estimated that the urban background concentrations for PM_{10} in Germany will decline between 2005 and 2015 by an annual average of about 5 µg/m³. Should this reduction be realised, Bad Cannstatt could then comply with the binding annual limit. Adopting the PM_{10} model as proposed by Lenschow et al. [113], a 5.0 µg/m³ reduction in PM_{10} concentration from the urban origin would also suggest similar reduction in PM_{10} concentration at the traffic site. However, this hypothetical reduction is somewhat insufficient when considering Neckartor from 2004 to 2006, as the annual mean PM_{10} concentrations for the three years before reduction has already exceeded 51.1 µg/m³.

As depicted in Fig. 3.4c, the Neckartor site recorded the highest 24 h average PM_{10} concentration of 191.0 µg/m³ on 01.02.2006. In general, higher PM_{10} concentrations are recorded from December to early March in the following year. During the colder months, high PM_{10} concentrations were resulted due to the formation of winter time surface inversions and low wind speed [114]. Inversions occur during night-times in winter, under clear weather conditions, with slow wind speed and high atmospheric pressure. Surface inversions are usually dissolved after sunrise when the ground is heated by radiation and temperature of the lower boundary level increases. Occasionally in winter the inversions can also be found evaluated during the daytimes. At the urban background site of Bad Cannstatt, significantly lower PM_{10} concentrations were recorded in comparison to Neckartor. Nevertheless, the maximum PM_{10} concentration of 117.0 µg/m³ on 01.02.2006 was also measured, coinciding with the behaviour of the Neckartor site under temperature inversions.

In regard to the number of 24 h average PM_{10} exceedances in a calendar year, the Neckartor site is unable to comply with the regulated 35 exceedance days. Bad Cannstatt, on the other hand, has no difficulties in fulfilling the criteria.

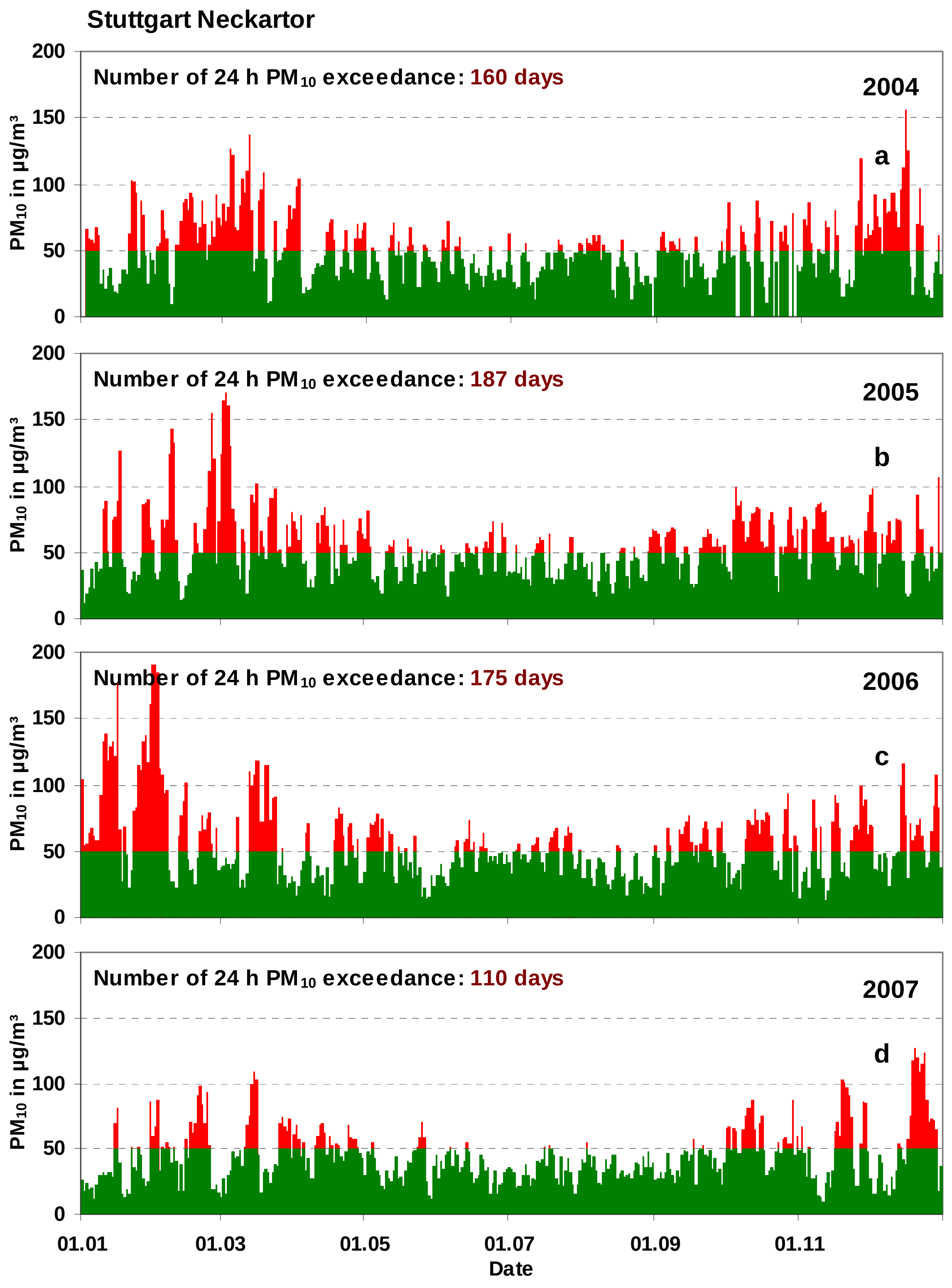

Fig. 3.4a-d: 24 h average PM_{10} concentrations at Stuttgart Neckartor for the period 2004 to 2007 data source: LUBW

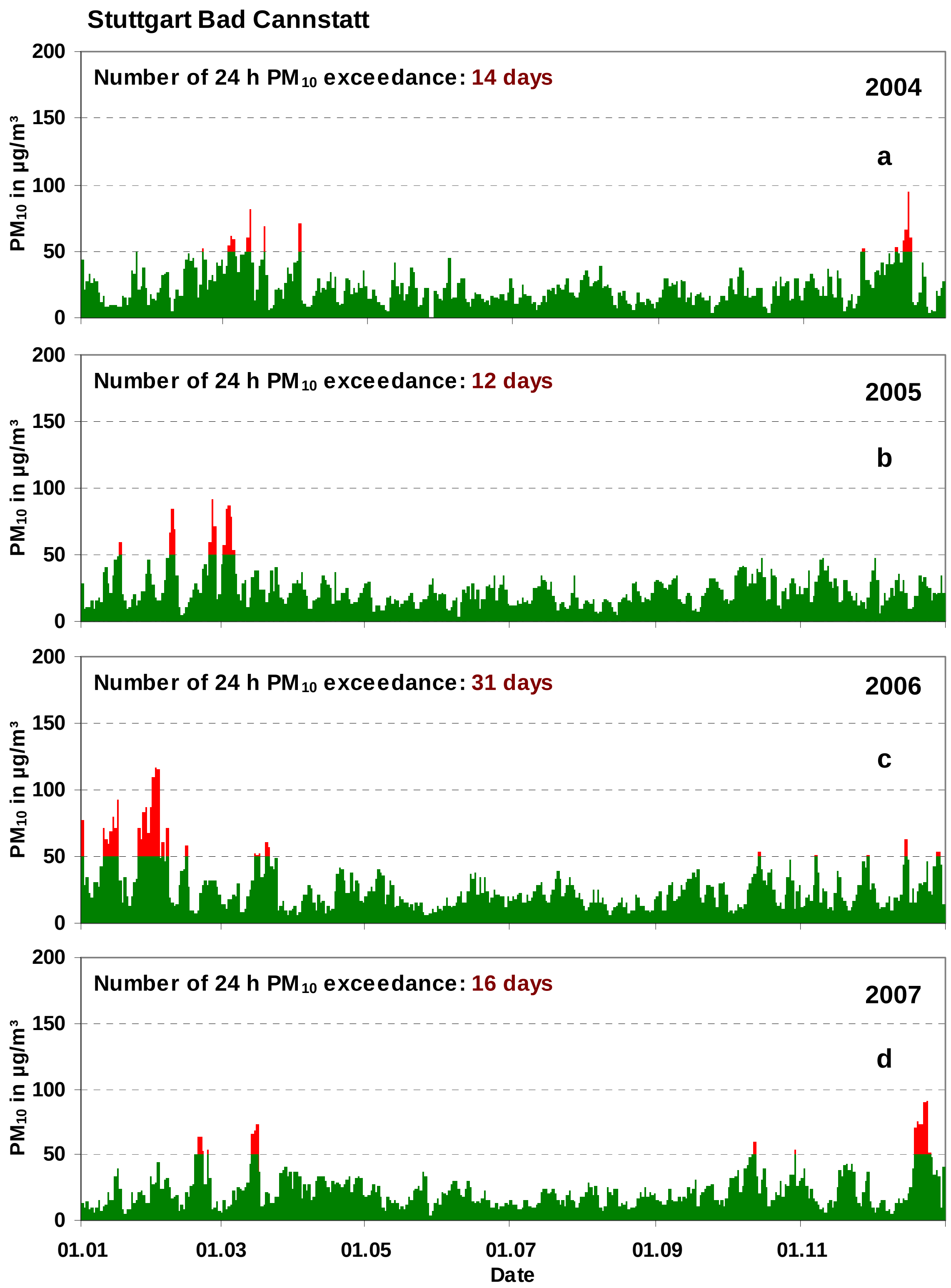

Fig. 3.5a-d: 24 h average PM_{10} concentrations at Stuttgart Bad Cannstatt for the period 2004 to 2007 data source: LUBW

Table 3.1: Annual mean PM_{10} concentrations and number of days exceeding the EU PM_{10} 24 h limit values at Stuttgart Neckartor for the period 2004 to 2007 [6, 8]

Year	Mean in µg/m³	98th percentile in µg/m³	Minimum in µg/m³	Maximum in µg/m³	Number of 24 h exceedances
2004	51.1	109.9	9.0	156.0	160
2005	54.5	126.8	12.0	171.0	187
2006	55.3	132.7	13.0	191.0	175
2007	44.3	103.0	10.0	127.0	110
2008					

Table 3.2: Annual mean PM_{10} concentrations and number of days exceeding the EU PM_{10} 24 h limit values at Stuttgart Bad Cannstatt for the period 2004 to 2007 [6, 8]

Year	Mean in µg/m³	98th percentile in µg/m³	Minimum in µg/m³	Maximum in µg/m³	Number of 24 h exceedances
2004	23.2	59.7	3.0	95.0	14
2005	23.5	65.0	4.0	92.0	12
2006	25.9	79.2	6.0	117.0	31
2007	22.5	67.4	4.0	91.0	16

3.3.2 Regularities in PM_{10}, NO and NO_2 concentrations depicted by average diurnal courses

The significance of the principal cyclic influences on the variability of pollution concentration at a receptor is the average diurnal cycle. First, the diurnal pattern to pollutants' source strength can be depicted. Second, the diurnal pattern of meteorological conditions on the influence on pollutants' dispersion can also be illustrated.

For the analyses of diurnal courses of PM_{10}, NO and NO_2 concentrations, the weekday-weekend cycle at Neckartor and Bad Cannstatt were investigated. The diurnal courses were prepared for days with PM_{10} exceedances, i.e., $PM_{10,\,24h}$ > 50 µg/m³.

3.3.2.1 Average diurnal courses of PM_{10}, NO and NO_2 concentrations for weekdays

The average diurnal courses of PM_{10}, NO and NO_2 concentrations with their respective standard deviations at Neckartor and Bad Cannstatt from August 2005 to November 2006 for weekdays are depicted in Fig. 3.6 and 3.7.

For the diurnal courses during weekdays at Neckartor, assuming a constant emission cycle with two peaks in the morning and evening rush hours, the time evolution of the air pollutant concentrations can be conceptualised in the following ways:

1. The morning peaks occur in the morning hours at around 08:00 in stable conditions, during which the PM_{10}, NO and NO_2 concentrations increase, but are counteracted by the destabilisation of the boundary layer due to ground heating via sun radiation [115, 116].

2. The minimum PM_{10}, NO and NO_2 concentrations are reached mid afternoon at around 12:00 to 15:00 when the traffic emissions are lower and atmospheric stability is at its minimum.

3. The build-ups of PM_{10}, NO and NO_2 concentrations become significant about when the evening peak emissions due to traffic and other sources are coincident with the stabilisation of the boundary layer. Compared to mid-afternoon, the vertical mixing is significantly reduced. Especially during low temperatures in winter, the formation of secondary aerosols under these conditions can be favoured [111, 117, 118].

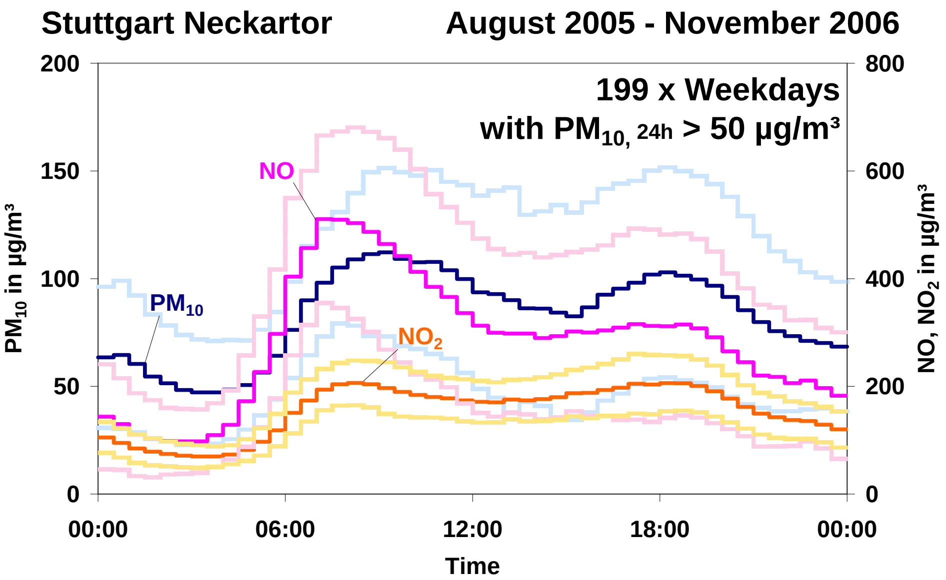

Fig. 3.6: Average diurnal courses of PM_{10}, NO and NO_2 concentrations with standard deviations at Stuttgart Neckartor from August 2005 to November 2006 for weekdays with $PM_{10,\ 24h}$ exceedances of 50 µg/m³ only data source: LUBW

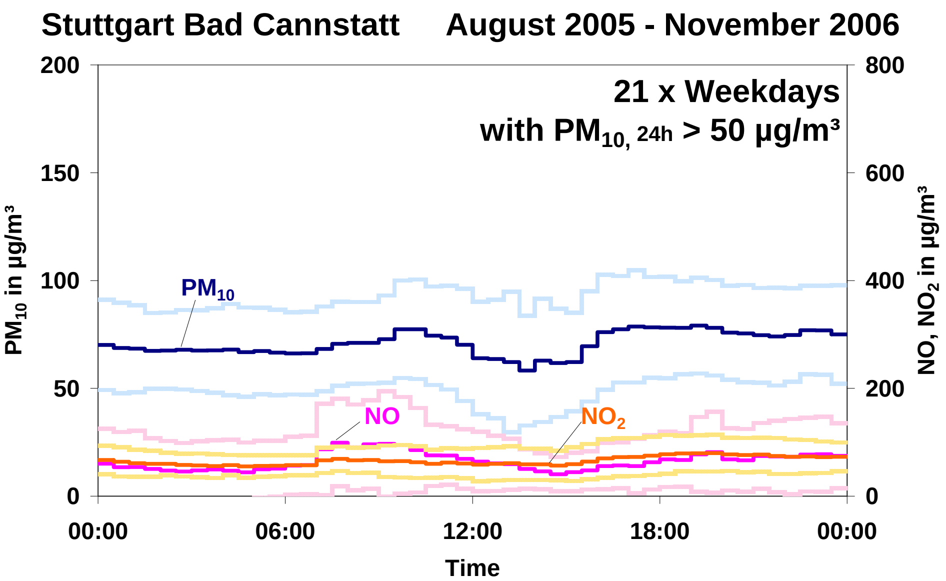

Fig. 3.7: Average diurnal courses of PM_{10}, NO and NO_2 concentrations with standard deviations at Stuttgart Bad Cannstatt from August 2005 to November 2006 for weekdays with $PM_{10,\ 24h}$ exceedances of 50 µg/m³ only data source: LUBW

In Fig. 3.6, the build-ups of air pollutant concentrations at Neckartor are much more significant in the morning hours than in the evening hours. For instance, PM_{10} concentrations increase from 47.2 µg/m³ to 112.2 µg/m³ from 03:00 to 09:00, and from 82.5 µg/m³ to 102.9 µg/m³ from 15:00 to 18:00. NO concentrations increase from 97.9 µg/m³ to 510.3 µg/m³ from 02:30 to 07:30, and from 289.5 µg/m³ to 314.9 µg/m³ from 14:00 to 18:30. NO_2 concentrations increase from 69.7 µg/m³ to 206.4 µg/m³ from 03:00 to 08:00, and from 170.5 µg/m³ to 206.1 µg/m³ from 12:30 to 18:00. Considering Bad Cannstatt, the two traffic-induced emission peaks which are observable at the Neckartor site are absent in the urban background site, as depicted in Fig. 3.7. This observation can be explained by the location of Bad Cannstatt, which is sited away from the artery roadways.

3.3.2.2 Average diurnal courses of PM_{10}, NO and NO_2 concentrations for weekends

The average diurnal courses of PM_{10}, NO and NO_2 concentrations with their respective standard deviations at Neckartor and Bad Cannstatt from August 2005 to November 2006 for weekends are depicted in Fig. 3.8 and 3.9 respectively. Given the paucity of day of the week-specific activity data for sources other than road traffic at Neckartor and Bad Cannstatt, it has been assumed that non-traffic sources of PM_{10}, NO and NO_2 are uniform throughout the week, thus allowing the analyses of the diurnal courses for weekends. While this approach may neglect a weekday-weekend difference in emission sources from factories, households, etc., the effects from these sources are assumed to be negligible.

Variations in the air pollutant concentrations at Neckartor are higher at weekdays than on weekends. This can be explained by the traffic flow originating from the B14 federal highway, from which traffic-induced PM_{10} are produced. At Bad Cannstatt, no significant changes in the pollutants' concentrations profiles can be observed when comparing Fig. 3.7 and 3.9.

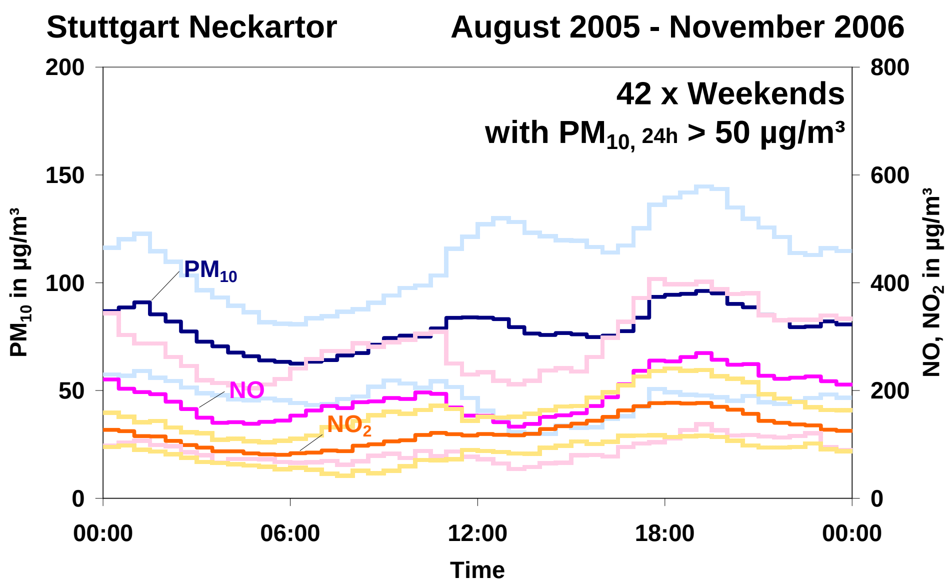

Fig. 3.8: Average diurnal courses of PM_{10}, NO, and NO_2 concentrations with standard deviations at Stuttgart Neckartor from August 2005 to November 2006 for weekends with $PM_{10,\,24h}$ exceedances of 50 µg/m³ only data source: LUBW

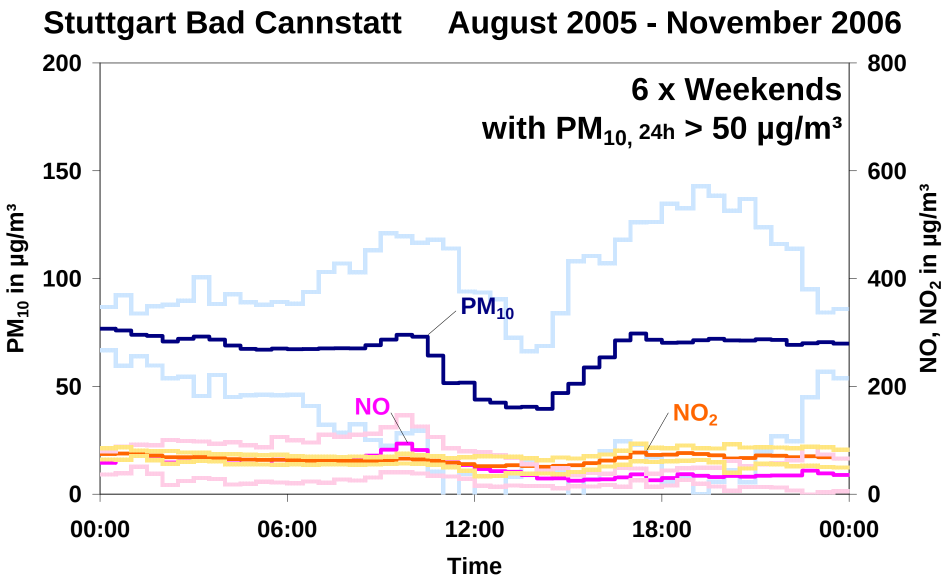

Fig. 3.9: Average diurnal courses of PM_{10}, NO, and NO_2 concentrations with standard deviations at Stuttgart Bad Cannstatt from August 2005 to November 2006 for weekends with $PM_{10,\ 24h}$ exceedances of 50 µg/m³ only data source: LUBW

During weekends at Neckartor, three concentration peaks of PM_{10}, NO and NO_2 are observed, which can be summarised in the following ways:

1. The first concentration peaks occur at around midnight and subsequently decrease when emissions are reduced gradually. The nocturnal air pollutant concentrations may appear surprising high in relation to the night-time typical reduction of major emissions, like those to traffic from the B14 federal highway, to domestic heating originating from the residential areas in the urban background, to industries, and to other human activities. Considering the night-time activities in the Stuttgart city centre, the cause of the concentration peaks points at the emission contribution from vehicles as the main source of these pollutants.

2. The second and third concentration peaks which occur around 10:00 to 12:00 and 17:00 suggest the weekend activities of the general population. The minimum PM_{10}, NO and NO_2 concentrations are reached mid afternoon at around 15:00 when the atmospheric stability is at its minimum. Such similar diurnal behavioural observations have also been reported in previous studies [119, 120].

To summarise, three important points can be highlighted through the analyses of the average diurnal courses of PM_{10}, NO and NO_2 concentrations from Fig. 3.6 to 3.9.

1. The influence of traffic on the average diurnal courses of the pollutants can be clearly illustrated by the differences in pollutant concentrations between the traffic site Neckartor and the urban background site Bad Cannstatt. The build-ups of air pollutant concentrations in the morning and evening rush hours at Neckartor can be solely attributed to traffic. As expected, these observations are not seen at Bad Cannstatt due to the apparent absence of traffic influence.

2. The peak concentrations depend on the stability of the boundary layer at the time of the morning and evening emission peaks. The more stable the conditions near

ground, the higher the air pollutant concentrations, which can be sustained by the roadside emissions considering Neckartor [121]. The night-time reduction in air pollutant concentrations testifies to the fact that such high levels of concentrations cannot be sustained in the absence of sources. Conversely, a destabilisation of the boundary layer from the solar heating of the land leads to faster dispersion of air pollutants and subsequent reduction in air pollutant concentrations.

3. The variations between the average diurnal profiles of the pollutants during weekdays and weekends at Neckartor suggest that the overall decrease in concentrations have been attributed to the decrease in traffic density and change in human activities in the city centre. The variations are not as significant at Bad Cannstatt.

3.4 Determination of street sweeping efficiency – results of experiments

3.4.1 Measurement approach

3.4.1.1 Site description

The traffic site selected for this research was the existing LUBW ambient air quality monitoring station of Neckartor as depicted in Fig. 3.1.

Parallel measurements were performed at a second measurement site in Schlosspark (latitude 48°47’14’’N and longitude 9°11’17’’E). This monitoring station was jointly operated by the LUBW and the Institut für Feuerungs- und Kraftwerkstechnik, Abteilung Reinhaltung der Luft (IFK-RdL). The measuring equipments were deployed in the middle of the park, 180 m to the traffic monitoring station at Neckartor, and 90 m away from the federal highway B14. Being located in the urban green belt, the measurement data from this measurement station was ideal for the evaluation for the urban background concentrations of PM without the direct local influence of traffic activities from B14.

A third monitoring station (latitude 48°47’38’’N and longitude 9°12’00’’E) was installed at approximately 900 m in the downstream traffic along the federal highway B14 from the Neckartor monitoring station in November 2006. This monitoring station, which was jointly operated by IFK-RdL and the Amt für Umweltschutz, Abteilung Stadtklimatologie (AfU), was sited about 160 m before a traffic junction of the Cannstatter Strasse. Oriented from southwest to northeast, Cannstatter Strasse is surrounded by a wall of tall vegetations on one side of the roadway and Schlosspark on the other side of the road. This monitoring site functioned as a reference station. In a situation whereby unusual PM episodes occurred at the Neckartor site, the measurement data from this reference station could be important in the validation of such events.

3.4.1.2 Street sweeping

The approach was based on operating a modified mechanical broom and water wash street sweeper equipped with fine dust filter in its hopper along the six lanes roadway at the Neckartor traffic site.

The specifications and operation conditions for the street sweeper used in this research are listed in Table 3.3. In Fig. 3.10 shows the street sweeper in operation.

Table 3.3: Specifications and operation conditions for the street sweeper

Street sweeper	
Item	**Specification**
Length in mm	6,200
Width in mm	2,500
Height in mm	3,300
Empty weight in kg	9,000
Turning circle in mm	10,000
Capacity in c.c.	6,000
Maximum power in hp	240
Capacity of water tank in l	1,900
	Operation conditions
Water spray in l/h	50
Sweeping speed in km/h	3 – 8
Spray pressure in bar	120
Brush speed in rpm	110
Maximum cleaning capacity in m²/h	15,000

Fig. 3.10: Street sweeper in operation during street cleaning periods from 15 November 2006 to 18 March 2007

The street sweeper is operated at 3 km/h to 8 km/h for its sweeping velocity. During its operation, a mechanical broom sweeps the street dust towards the centre of the sweeper with a brush speed of 110 rpm. The side brush is installed on a central column together with the return and suction air duct. The recirculating air system continuously conveys air from the hopper to the blowing nozzle, thus resulting in a small proportion of the air reaching the atmosphere in the process. The blower nozzle forces the recirculated air against the street surface and any road dust is then vacuumed up through the suction air duct. In its hopper, debris such as leaves is removed from the air stream by a screen. The larger particles are removed by a centrifugal separator. The vented air then goes through a fine dust filter. To suppress any resuspension of road dust, water is sprayed at 50 l/h with a pressure of 120 bar.

The street sweeping activities were conducted by the Abfallwirtschaft Stuttgart (AWS) and all sweeping events with corresponding meteorological conditions were protocolled accordingly. In total, there were 52 days with street sweeping during the investigation period.

3.4.1.3 Measurements

To monitor the temporal variability of ambient air pollutants during sweeping and non-sweeping periods, the measurements from ß-attenuation PM monitors and chemiluminescence analysers were evaluated. To monitor the 24 h average PM_{10} concentrations, the measurements from PM_{10} samplers were evaluated. To have a better comparison between the morphological and elemental compositions of the ambient PM from the three monitoring sites, single particle analyses were performed on the samples collected by cascade impactors. The procedure of investigation on the morphology, elemental characterisation, and mineralogy of ambient PM was documented in Baumbach et al. [25]. To summarise, the effect of street sweeping on ambient PM concentrations were evaluated based on results from both continuous and non-continuous (PM samplings with samplers and cascade impactors) measurements of ambient air pollutants.

In parallel to the continuous measurements during the investigation period, a series of direct road dust samplings from the street surfaces at Neckartor were performed. The areas, from which road dust samplings were conducted, were individually measured and marked. Silt loadings on the street surfaces were determined by vacuuming the active traffic lanes and then separating the material according to their sizes. The collection procedure was performed using a handheld vacuum cleaner equipped with dust-restrainting features [122, 123]. Paper dust bags were installed in the vacuum cleaner. In Fig. 3.11 shows the procedure of road dust sampling at Neckartor.

Fig. 3.11: Direct road dust sampling at Neckartor

A total of ten road dust samples were collected from 17.01.2007 to 15.03.2007, only on days when the road was visibly dry. Five samples were collected when no street sweeping took place prior to the sampling. The other five were collected immediately after street sweeping. To ensure comparability of the data sets, the respective samplings were performed at the same time of the working day. Weather characteristics, road conditions, time, and the studied surface areas were documented. The weight of the dust bag before and after vacuuming was determined on site. With reference to the method of dry sieve analysis as prescribed by DIN 18123 [124], two fractions PM (> 75µm) and PM (< 75 µm) were classified. However, the process of the classical dry sieving method is unable to further separate PM into fractions smaller than 30 µm. Thus, a BACHO separator was brought into operation in order to obtain the finer PM_{10} fractions. The separation of PM is realised by rotating the drum of the BACHO separator in high velocity. Through centrifugal separation, the PM_{10} and 10<PM<75 fractions could be obtained. To summarise, the effects of street sweeping on dust loads on street surfaces were evaluated based on results from direct street dust samplings followed by PM size distributions.

3.4.2 Results

In this chapter, only measurement results pertaining to PM_{10} concentrations at Neckartor from 15.11.2006 to 18.03.2007 are included. The measurement results from the other two comparison stations, and the results from the morphological, elemental and chemical analyses of the size-fractionated ambient PM and road dust are detailed in Baumbach et al. [25].

3.4.2.1 Average diurnal courses of PM_{10} and NO_X concentrations

The entire measured data from Neckartor was separated into two subsets: 31 working days with street sweeping and 26 working days without street sweeping. Average diurnal courses of PM_{10} and NO_X concentrations were evaluated to determine if there were any regular effects of street sweeping. The diurnal courses of PM_{10} and NO_X concentrations are depicted in Fig. 3.12 and 3.13. The three street sweeping periods from 00:00 h to 01:30 h, 10:30 h to 12:00 h, and 15:00 h to 16:30 h are depicted as the vertical grey bars in the figures.

In Fig. 3.12, the diurnal PM_{10} concentrations decreased temporally right after the street sweeping from 02:00 to 06:00 h, and similar observations were made after the second street sweeping from 12:00 to 14:00 h. However, the trend was not observed after the third sweeping period. Any positive effects of street sweeping could not be concluded at this juncture as the diurnal courses of NO_X concentrations showed a similar reduction behaviour, see Fig. 3.13. One possible explanation for the discrepancies between the NO_X concentrations from 06:00 to 16:00 h could be the frequent natural cleaning processes from precipitation and winds during the investigation period. If this argument was valid, then the reductions in PM_{10} concentrations could not be induced by the street sweeping after all.

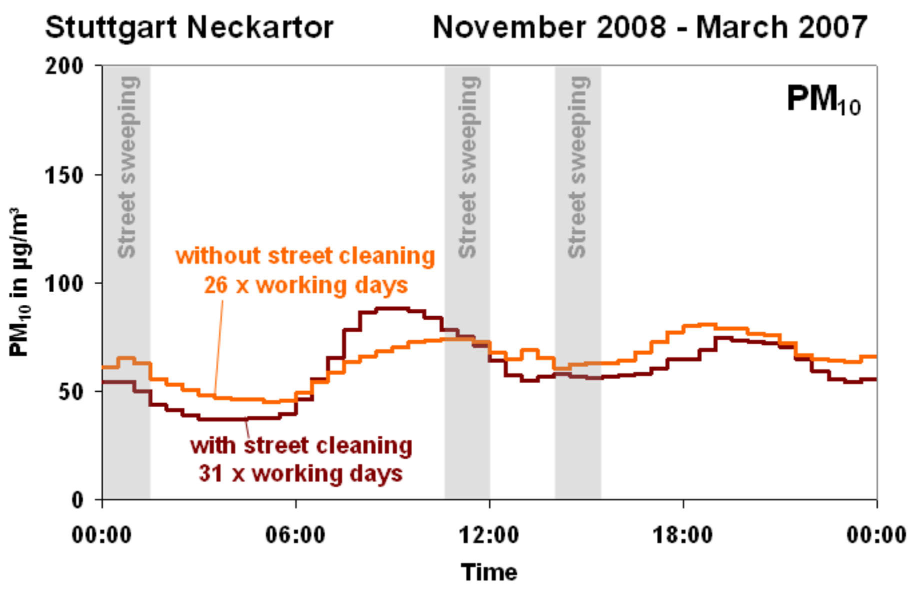

Fig. 3.12: Average diurnal courses of PM_{10} at Stuttgart Neckartor from 15 November 2006 to 18 March 2007 data source: LUBW

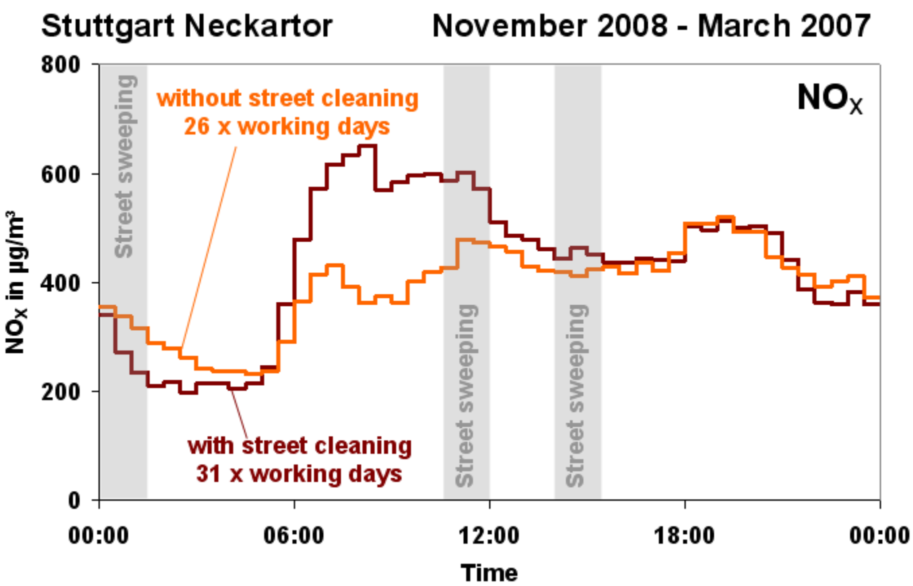

Fig. 3.13: Average diurnal courses of NO_X at Stuttgart Neckartor from 15 November 2006 to 18 March 2007 data source: LUBW

3.4.2.2 PM_{10}/NO_X ratio for compensation of meteorological influences

In a hypothetical situation whereby the traffic-induced NO_X emissions at Neckartor remain always the same during all working days, any variations in the average diurnal course of NO_X concentrations would then be primarily influenced by the different meteorological conditions. In this case, the changes in NO_X concentrations could actually be used as a meteorological indicator. According to Ketzel et al. [125], this method of analysis has the advantage that the influence of dispersion conditions of the air pollutants is neutralised.

A comparative analysis of the diurnal PM_{10} measurements was therefore proposed by plotting the PM_{10} concentrations normalised by NO_X concentrations, as shown in Fig. 3.14 and Fig. 3.15. If any effect of street sweeping on ambient PM_{10} concentrations were expected to take place, the following interpretation could then be made: in the absence of precipitation, strong wind, or unusual local events, a positive street sweeping effect could be indicated by a decrease in the PM_{10}/NO_X ratio following street sweeping activities, compared to the average diurnal course of PM_{10}/NO_X ratio without street cleaning.

In Fig. 3.14, the average diurnal normalised PM_{10}/NO_X ratio decreased noticeably after the first sweeping period from 02:00 to 05:00 h. However, the decrease from 05:00 to 09:00 h could not be explained here. During the daytime after 09:00 h, differences between the two diurnal courses were not noticeable before and after the second and third street sweeping periods. By computing these average values of the normalised PM_{10}/NO_X ratio for days without street sweeping and days with street sweeping, the values of 0.165 and 0.155 were obtained respectively, which could also infer a reduction potential of approximately 6 % in ambient PM_{10} concentrations after street sweeping.

In Fig. 3.15, the 24 h average normalised PM_{10}/NO_X ratio is depicted over the entire investigation period. The average values of the normalised ratio for days without street

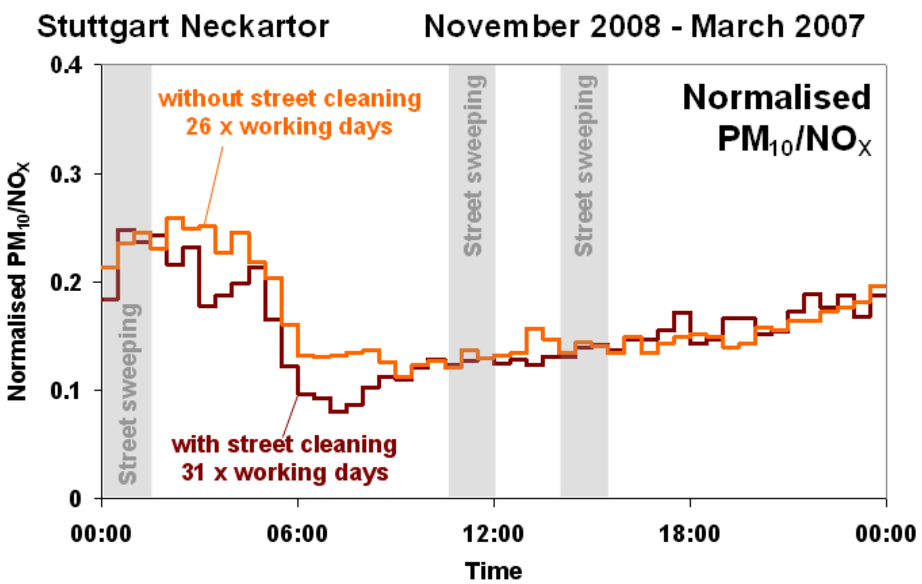

Fig. 3.14: Average diurnal courses of normalised PM_{10}/NO_X at Stuttgart Neckartor from 15 November 2006 to 18 March 2007 data source: LUBW

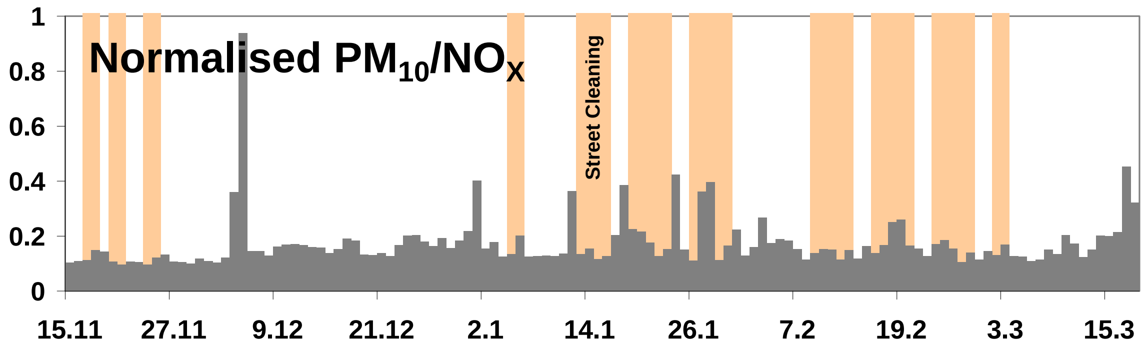

Fig. 3.15: 24 h average normalised PM_{10}/NO_X ratio at Stuttgart Neckartor from 15 November 2006 to 18 March 2007 data source: LUBW

sweeping and days with street sweeping were found to be 0.162 and 0.151 respectively, which worked out to be approximately 7 % reduction. Although both the analyses in Fig. 3.12 and 3.13 could suggest a reduction effect, it was difficult to conclude if this small reduction trend could be attributed to street sweeping or to other unknown factors.

In Table 3.4, all averages of the normalised PM_{10}/NO_X ratio are summarised according to the evaluated days. Based on the results, a reduction potential of approximately 13 % in ambient PM_{10} concentrations was computed on days with street sweeping. In comparison to other related studies, Chang et al. [19] reported a reduction efficiency of ambient TSP of up to 30 % when using a regenerative-air vacuum sweeper and a washer. However, the effect was short-lived lasting no more than 3 h to 4 h. With intense washing of street surfaces with high-pressure water systems, a 6 % reduction in ambient PM_{10} could be observed [23]. Considering other PM control measure, Norman and Johansson [23] estimated an average reduction of around 35 % in the 24 h average PM_{10} concentrations with the application of calcium magnesium acetate (CMA) on street surfaces.

Table 3.4: Averages of normalised PM_{10}/NO_X ratio at Stuttgart Neckartor from 15 November 2006 to 18 March 2007

Description	**Evaluated days**	
	All days	**Working days only**
Without street sweeping (based on average diurnal courses)	0.179	0.165
With street sweeping (based on average diurnal courses)	0.155	0.155
Without street sweeping (based on 24 h average values)	0.163	0.162
With street sweeping (based on 24 h average values)	0.151	0.151

3.4.2.3 Gravimetric analyses of road dust

Besides the evaluation of ambient PM_{10} behaviour, the direct effect of road dust on street surfaces before and after street sweeping was also evaluated based on results from gravimetric analyses of the collected road dust. For this purpose, a definition of street sweeping efficiency was defined and used here. Respectively, η_{Total} represents the reduction efficiency of total road dust, η_{75} represents the reduction efficiency of silt (PM_{75}), and η_{10} represents the reduction efficiency of PM_{10} on the street surfaces. The dust load removal efficiencies of PM_{Total}, PM_{75} and PM_{10}, from street surfaces before and after street sweeping are presented in Table 3.5.

Table 3.5: Dust load removal efficiency of PM_{Total}, PM_{75}, and PM_{10} on street surfaces before and after street sweeping

	Dust load before street sweeping in mg/m²	**Dust load after street sweeping in mg/m²**	**Removal efficiency in %**
PM_{Total}	1358 ± 459.7	538 ± 235.1	60.4
PM_{75}	94 ± 5.6	40 ± 21.8	57.4
PM_{10}	1.3 ± 0.3	0.6 ± 0.1	54.8

The results indicated that following the street sweeping at Neckartor, η_{Total} was approximately 60 %, η_{75} was approximately 57 %, and η_{10} was approximately 55 %. While these results were specific to the Neckartor site, similar quantitative findings would be anticipated in other trafficked areas, where the roadways are of similar conditions to those at Neckartor.

The duration of effects from street sweeping on dust loads on street surfaces which were conducted at Neckartor from 17.09.2007 to 28.09.2007 are shown in Fig. 3.16. The effect lasted over one rush hour (approximately 6 h to 8.5 h) and the dust load was generated again within the next rush hour.

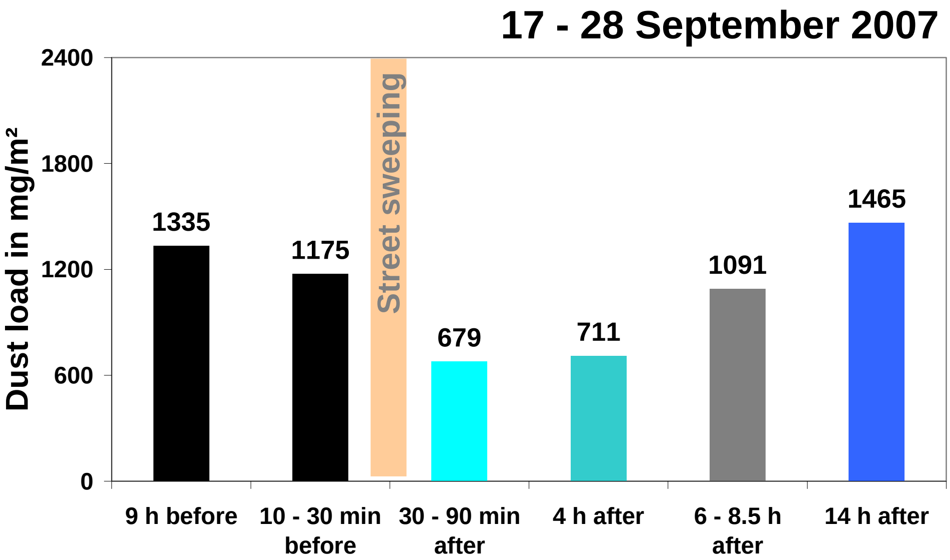

Fig. 3.16: Duration of effects from street sweeping on dust loads on street surfaces at Neckartor from 17 to 28 September 2007

3.4.3 Conclusions

Street sweeping is often proposed as a PM abatement strategy in cities to reduce resuspended road dust contributions to ambient PM concentrations. For this investigation, the effectiveness of street sweeping on the reduction of ambient PM_{10} concentrations and dust loads on street surfaces at Neckartor was investigated.

The effects of street sweeping on the ambient PM_{10} concentrations were evaluated based on results from continuous beta-attenuation PM_{10} measurements, gravimetric PM_{10} samplings and NO_X measurements. While reductions in ambient PM_{10} concentrations could be suggested during street sweeping periods, an exact quantitative evaluation on the effectiveness was overlaid by possible meteorological influences and other unknown effects. It is unclear which of these factors most influenced the reduction of ambient PM_{10} concentrations. Coupled with certain degree of uncertainty, it could still be a subject of controversy for the validity of these results. Although the method of normalised PM_{10}/NO_X ratio was used to compensate for the varying meteorological influences, it was still unclear if the reduction of ambient PM_{10} concentrations was directly caused by street sweepings or by the frequent natural cleaning processes from precipitation and wind during the investigation period in winter 2006/2007. By using an appropriate air quality model, a “what-if” scenario could in fact be simulated to Nowcast the original state of 24 h average PM_{10} concentrations at Neckartor, assuming that no street sweeping activities took place during the sweeping periods. This approach would be possible considering the use of neural network modelling in parameterising all the varying weather conditions as model inputs. Any effect of street sweeping could then be suggested by any differences between the modelled PM_{10} concentrations and the corresponding measured PM_{10} values on street sweeping days.

A series of direct dust samplings from street surfaces in Neckartor were performed from mid January 2007 to mid March 2007 in parallel to ambient PM measurements. The results demonstrated favourable sweeping efficiency from 60 to 80 % for reducing the dust loads on street surfaces depending on the particle size group. The direct impact of street sweeping on the dust loads of street surfaces lasted over one rush hour (approximately 6 h to 8.5 h), and the dust load was generated again within the next rush hour.

4 Methodology

4.1 Artificial neural network

An artificial neural network (ANN) is an information processing paradigm that is inspired by the way biological nervous systems, such as the brain, processes information. The key element of this paradigm is the structure of the information processing system. It is composed of a large number of highly interconnected processing elements (neurons) working in unison to solve specific problems. Artificial neural networks, like human, learn by example. A network is configured for a specific application, such as pattern recognition or data classification, through a learning process. Learning in biological systems involves adjustments to the synaptic connections that exist between the neurons. This is true of artificial networks as well [126, 127].

4.2 Biological neuron model

Neurons (also called nodes) can be referred to the building bricks of a neural network. To understand the physics behind the operation of the network, it is important to know the function of the neurons. In Fig. 4.1, the schematic drawing of the major components of a typical neuron, including the cell body with nucleus, the dendrites that receive signals from the other neurons, and the axon, which relays nerve signals to other neurons at a specialised structure called a synapse, is depicted.

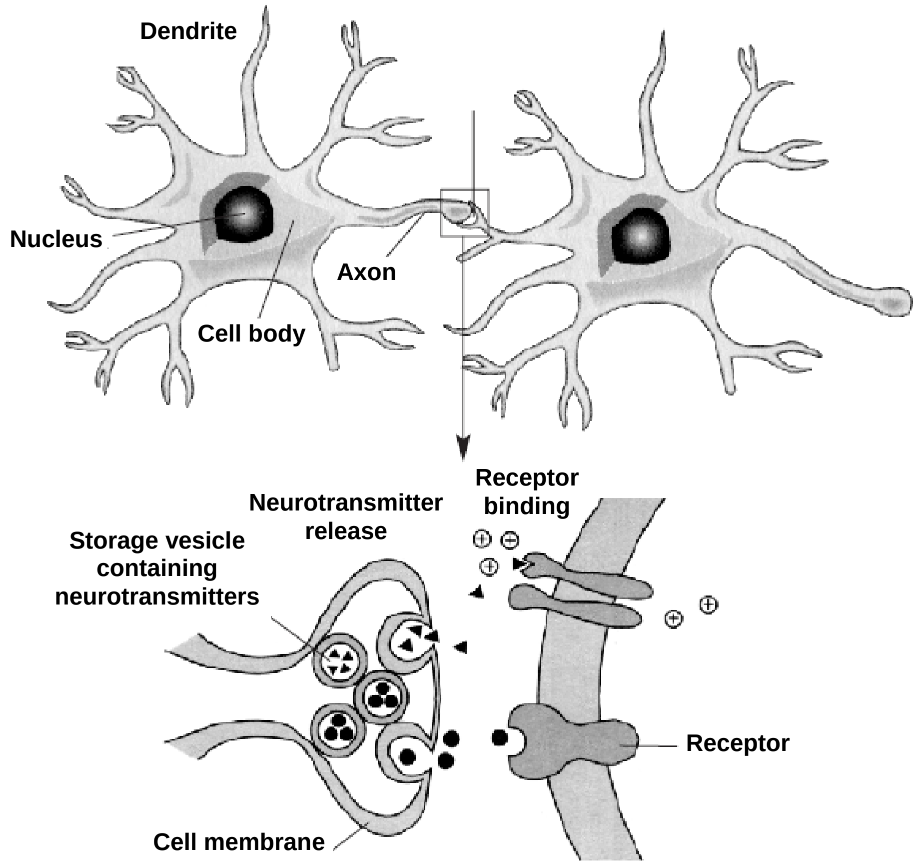

Fig. 4.1: Structural features of a typical nerve cell (neuron) and synapse [127]

The neuron sends out spikes of electrical activity through a stand known as an axon, which splits into numerous branches. At the end of each branch, the synapse converts the activity from the axon into electrical charges that may inhibit or excite activity in the connected neuron(s). When a neuron receives an excitatory input that is sufficiently large compared with its inhibitory input, it sends a spike of electrical activity down its axon. This type of synapse which encourages depolarisation activity in the membrane of the post-synaptic cell is called excitatory, and the other which discourages it is called inhibitory synapse. Learning occurs by changing the effectiveness of the synapses so that the influence of one neuron on another changes. As a result, if the decrease in the polarisation is sufficient to exceed a threshold, then the post synaptic neuron "fires" to produce an output signal.

4.3 Artificial neuron model

The transmission of a signal from one neuron to another through synapses is a complex process, in which specific transmitter substances are released from the sending side of the junction. The effect is to increase or lower the electrical potential inside the body of the receiving cell. As mentioned earlier, if this potential reaches a threshold, the neuron fires. It is this characteristic that the artificial neuron model attempts to reproduce [126]. The artificial neuron model depicted in Fig. 4.2 is one that is widely used in artificial neural networks with modifications on it.

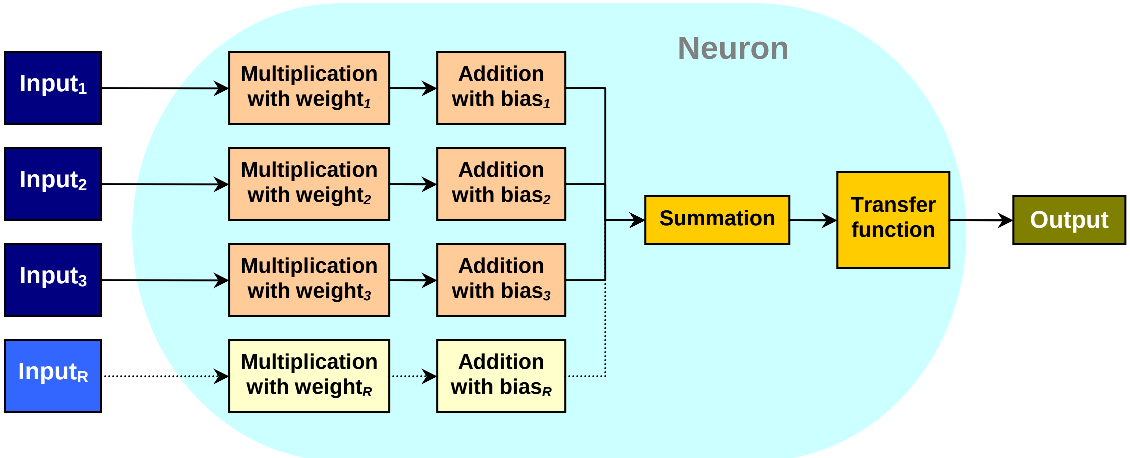

Fig. 4.2: Structural features of an artificial neuron model without feedback, modified from [126]

The artificial neuron as depicted in Fig. 4.2 has R number of inputs. Each line connecting to these inputs to the neuron is assigned a weight, which corresponds to the synaptic connections in biological neurons. The threshold in an artificial neuron is represented by the biases. Networks with biases can represent relationships between inputs and output(s) easier than networks without biases. For example, a neuron without a bias will always have a net input to the transfer function of zero when all of its inputs are zero. However, a neuron with a bias can learn to have any net transfer input function under the same conditions by learning an appropriate value for the bias. The activation corresponding to the "electrical potential" to fire the neuron can be described by Eq. (4.1)

$$n = \sum_{i=1}^{R} (w_i p_i + b_i) , \tag{4.1}$$

where n is the activation, R is the number of inputs, w is the weight, p is the input, and b is the bias. The summation of the biases is also denoted by Eq. (4.2) in some literatures,

$$\theta = \sum_{l=1}^{N} b_l , \tag{4.2}$$

where N represents the size of the data set.

The inputs, weights, biases and output are real values. A negative value for the weight indicates an inhibitory connection while a positive value indicated an excitatory one. The output value of the neuron is defined as a function of its activation in an analogy to the firing frequency of the biological neuron, which can be described by Eq. (4.3)

$$a = f(n), \tag{4.3}$$

where $f(n)$ represents a transfer function. The most commonly used functions are depicted in Fig. 4.3a to 4.3d respectively. Originally, the neuron output function $f(n)$ in the McCulloch and Pits' model [126] was proposed as a hard-limit function as shown in Fig. 4.3a, with which the output of the neuron is either zero, when the net input argument n value is less than zero, or one, when the n value is greater than or equal to zero. This type of function is usually used for making classification decisions. An example for such implementation is the description of basic Boolean functions such as the AND, OR and NOT logic gates. In Fig. 4.3b the linear transfer function is depicted. Transfer function of this type is used for linear approximation, which can take on any output value. However, non-linear relationships between the input and output values cannot be accurately represented by a linear function. Thus, if the relationship between the input and output values is linear or a linear approximation is desired, then linear function is made for the job. Otherwise, the use of sigmoid transfer functions may be the solution. The sigmoid transfer functions in Fig. 4.3c and 4.3d takes the input value, which may have any value between plus and minus infinity, and limit the output into the range of minus and positive one, or zero to one.

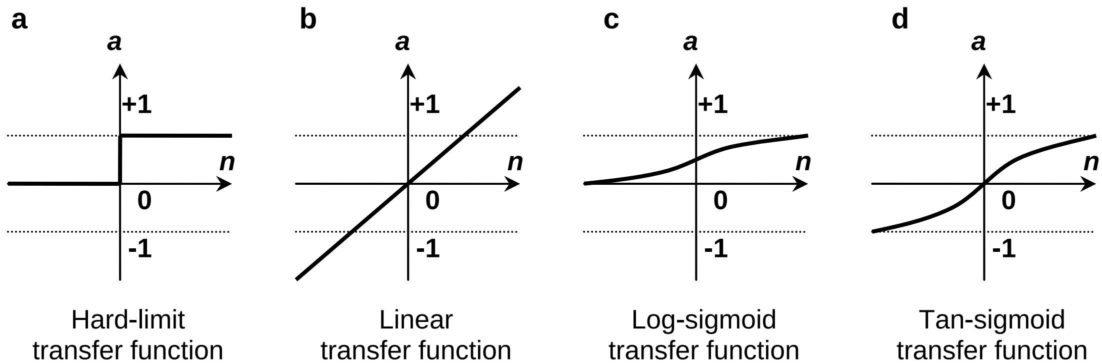

Fig. 4.3a-d: Various transfer functions for neural network model

4.4 PM_{10} Nowcasting and PM_{10} Forecasting with neural network

Based on the knowledge of the various components which constitute an artificial neuron model, the process with which data are being assimilated and processed, to being modelled and checked for accuracies by a neural network model is summarised and depicted in Fig. 4.4. The respective components that constitute the model are as follows:

1. Data set preparation
2. Input layer
3. Hidden layer
4. Output layer
5. Training algorithm
6. Validation
7. Quality assurance
8. Data set post processing

These individual components detailed in the following chapters.

Developing a neural network model is an iterative process which requires a systematic approach. It is, however, not possible to document all results and development steps. Thus, only the most important findings and results are documented here. It should be emphasised that there is no difference in the flowchart of data assimilation to modelling when comparing PM_{10} Nowcasting to PM_{10} Forecasting; the only difference lies on the way the modelled values are being handled.

4.4.1 Data set preparation

Neural network training can be made more efficient if pre-processing steps are performed on the network inputs and targets. The two techniques which are commonly used are the principal component analysis (PCA) and data normalisation.

4.4.1.1 Principal component analysis

The principal component analysis is a pre-processing technique which can significantly reduce the complexity of the neural networks employed. Since many of the meteorological parameters are somewhat related to the same synoptic process, they can be strongly interrelated [93]. In addition, the complexities of urban areas may also result in high cross-correlations among the topographical, traffic and air quality variables [55]. By applying principal component analysis to the entire data set, an independent linear combination of all the variables can be provided, and therefore effectively anticipate substantial autocorrelations between the data set. As a result, the dimensionality of the input space of the data can be greatly reduced while the relevant information can be preserved as much as possible.

4.4.1.2 Data normalisation

The second pre-processing stage is the data normalisation which follows the principal component analysis for the purpose of enhancing the features in a data set. Data normalisation is an independent linear scaling of the respective input features to avoid large dynamic ranges in one or more dimensions. There are many applications in which two or more input features may differ by several orders of magnitude. The large variations in feature sizes can dominate the more important but smaller trends in the data. Therefore, the harmful effects can be removed through normalisation.

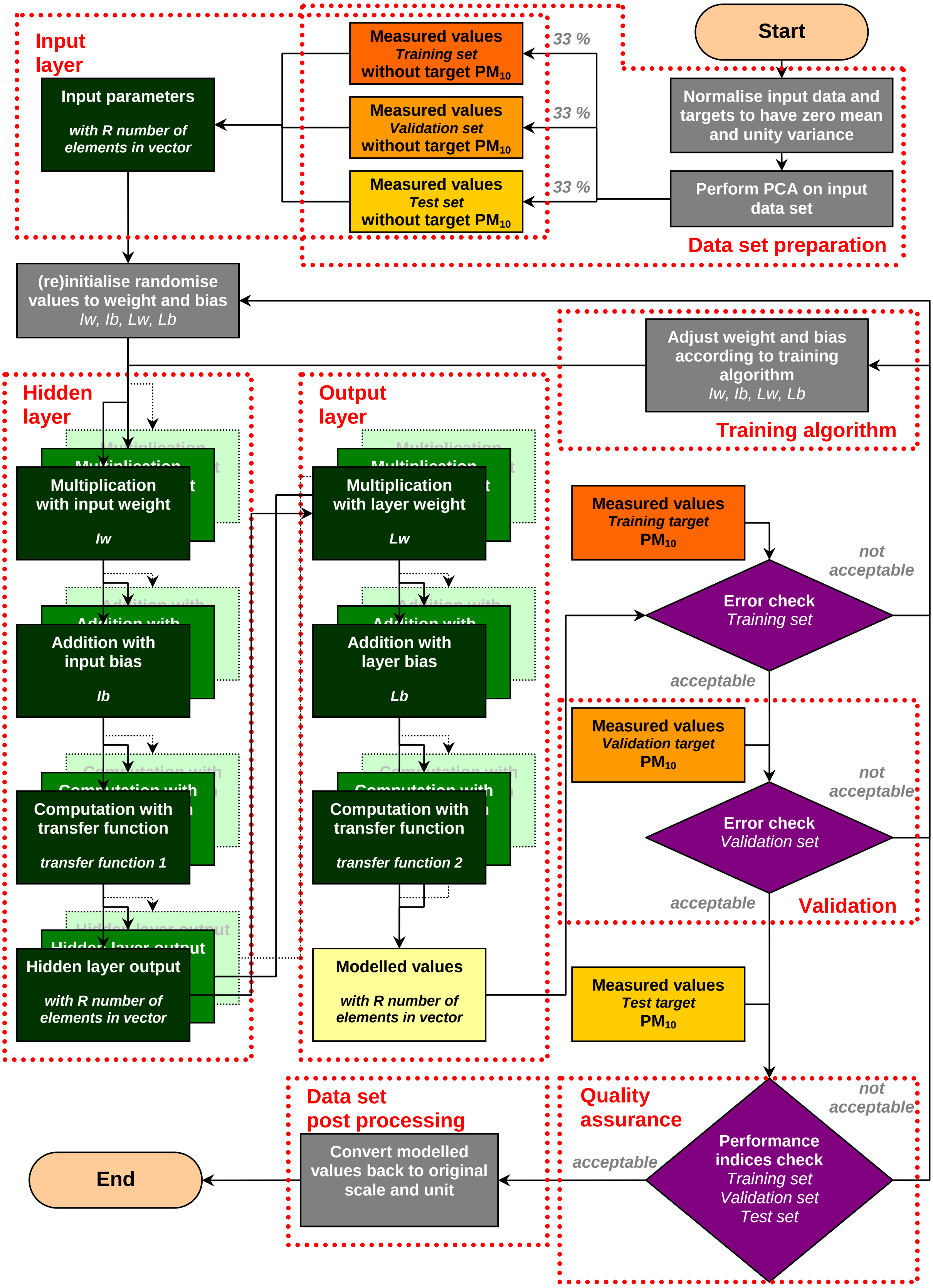

PCA: Principal component analysis, Iw: input weight, Ib: input bias, Lw: layer weight, Lb: layer bias

Fig. 4.4: Flowchart of data assimilation to modelling for PM_{10} Nowcasting and PM_{10} Forecasting with feedback

4.4.2 Neural network model's structure

As the term neuron can also be interpreted as a biological nerve cell, the more general term, node, shall be used instead to describe its functions in the artificial neural network models in the subsequent chapters.

4.4.2.1 Input layer

In the input layer, the post-processed data set are divided into three subsets: training, validation and test sets respectively.

The training set is a set of data used to adjust the initial weights of the neural network to produce the desired outcome. The validation set is a set of data used to find the best network configuration and training parameters. For example, it can be employed to monitor the network error during training to determine the optimal number of training iterations or epochs. It can also be used to determine the optimal number of hidden nodes. When the validation set is used to stop training, the neural network is optimistically biased, having exposed to the data.

The test set is a set of data used only to evaluate the fully trained neural network, without changing the configuration of the network. Often, it is collected separately from the training and validation sets to help ensure independence. The neural network is biased towards both the training and validation sets, so the independent test must be used to determine the generalisation error. The test set should never be used to choose between neural networks, so that it remains an unbiased estimate of the network's performance. This practice for generalisation error estimation is characterised as split-sample or hold-out validation.

4.4.2.2 Hidden and output layers

While a single node is able to perform single function such as classification, linear and non-linear approximations, it may not be sufficient to approximate more complex functions with a finite number of discontinuities. A solution to this limitation is by connecting the outputs of node(s) as input to the others, so constituting an output layer and thus completing the structure of a neural network.

The determination of the optimal number of nodes in the hidden layer is an important issue; a network with a small number of hidden nodes will probably fail to learn the data, whilst a network with too many nodes will fatefully overfit the training patterns and results in a poor generalisation performance, an observation which is usual in common prediction tasks [95].

Considering a large network, increasing the number of hidden nodes in a network does not guarantee better results than those obtained with a smaller number of hidden nodes [128]. If the function being learnt happens to be a Tan-sigmoid function as presented in Fig. 4.3d, a network with one Tan-sigmoid hidden node will perform substantially better than any more complex networks. Even if the true function can only be exactly represented by an infinite network, it is possible that it is very close to a function that can be represented by a smaller network.

According to the structure of the connections between nodes in a network, two main classes of network architectures can be identified as the feedforward network and the recurrent network. To simplify the notations, equations will be restricted to consider a two-layered network, i.e. network with two layers of nodes excluding the input layer (leaving with one hidden and one output layer). Each layer will have its own index variable: i for input nodes j

for hidden, and k for output nodes. In a feedforward network, the input vector, p, is propagated through a weight layer as described by Eq. (4.4) and (4.5),

$$a_{ij}(t) = f(n_{ij}(t)), \tag{4.4}$$

$$n_{ij}(t) = \sum_{i=1}^{R} w_{ij} \cdot p_i(t) + \theta_j, \tag{4.5}$$

where $a(t)$ represents the time series of output, $n(t)$ denotes the activation, w is the weight, $p(t)$ is the time series of input, and θ_j is the bias of unit j.

Recurrent networks are fundamentally different from the feedforward architectures in the sense that they do not operate on an input space, but also on an internal state space, in which a trace of what already has been processed by the network [129]. In a simple recurrent network, the input values are similarly propagated through a weight layer, and also combined with the previous state activation through an additional recurrent weight layer

$$n_{ij}(t) = \sum_{i=1}^{R} w_{ij} \cdot p_i(t) + \sum_{j=1}^{S} w_{jk} \cdot p_j(t-1) + \theta_j, \tag{4.6}$$

where S denotes the number of hidden nodes. The output of the network is, in both cases, determined by Eq. (4.7) and (4.8)

$$a_{jk}(t) = g(n_{jk}(t)), \tag{4.7}$$

$$n_{jk}(t) = \sum_{k=1}^{T} w_{jk} \cdot p_k(t) + \theta_k \tag{4.8}$$

where g is the transfer function for the output layer, T represents the number of output units, and θ_k is the bias of unit k.

4.4.3 Validation

For validation, the deviations of the modelled values from the measured values are evaluated as an error function. This error function is defined as the mean square sum of differences between the values of the output values and the desired target values. This function is calculated for the whole input data set as described by Eq. (4.9)

$$E_{ik} = \sum_{k=1}^{T} (d_{ik} - a_{ik})^2 \text{ ,} \tag{4.9}$$

where E_{ik} is the difference between the input nodes i and output nodes k, and d_{ik} and a_{ik} are the measured and the modelled value of output neuron k corresponding to the input i. The total error E can be computed by Eq. (4.10)

$$E = \frac{1}{2} \cdot \sum_{i=1}^{R} E_{ik} = \frac{1}{2} \cdot \sum_{i=1}^{R} \sum_{k=1}^{T} (d_{ik} - a_{ik})^2 \text{ .} \tag{4.10}$$

Should the total error exceed the acceptable tolerance, the neural network model will be reinitialised by adjusting the initial weight and bias values. The method of adjustment is dependant on the training algorithm of the model.

In this dissertation, one-third of the entire data set was used for training, one-third for validation, and one-third as an independent test data set. There is no "rule of thumb" on the correct division of the entire data sets into their subsets. For instance, Hooybergs et al. [90] and McKendry [81] used four-fifth of their entire data set as training and validation sets, and one-fifth as test set. Grivas and Chaloulakou [89] used three-fourth as training set, one-eighth as validation set, and one-eighth as test set. Gardner and Dorling [130] used one-half as training set, one-fourth as validation set, and one-fourth as test set. Lu et al. [131] used seven-eighth as training set, one-eighth as validation set, and no data as test set. In a more recent study, Diaz-Robles et al. [79] portioned the data set into two: 92 % as training set and only 8 % as validation set. The reason behind the use of larger training set is not unfounded. When training neural network model, it is important for the model to extract all underlying patterns in the entire data set. This means that the training data set should be both adequately extensive and fully representative of all cases that the model is required to generalise. However the developed model performance statistics will be artificially biased if no truly independent test data set existed [100]. Thus, it is desirable that any data set should be divided into the three independent training, validation and test sets.

4.4.4 Training algorithm

An important aspect of a neural network is the learning step, based on a set of measured numerical values. Representative examples are presented to the network so that this knowledge can be integrated within its structure. The accuracy of network representation depends directly on the interconnections between the neurons.

The leaning process consists of identifying the weights and biases that produce the best fit of the output data over the entire training data set. At the beginning of the learning step, random values are chosen to initialise weight data. During the learning step, the weights of the network are continuously adjusted, based on the error signal generated by the deviation between the output data computed through the network and the data from the target values used in the training set.

This can be accomplished by the backpropagation training algorithm which involves performing computations backwards through the network. Should the training algorithm become trapped in local minima, the final model may be sub optimal. Generally when the global minimum is not reached, a good local minimum can also be treated as an acceptable solution [95].

4.4.4.1 Backpropagation

Backpropagation algorithms for feedforward networks use the gradient of the performance function to determine how to adjust the weights and biases in order to minimise errors of the modelled values. The total error function E as described by Eq. (4.10) is minimised using a gradient-descent technique. The necessary adjustments to the weights of the network are obtained by calculating the partial derivative of the error function in relation to each weight w_{ij}. A gradient vector representing the steepest increasing direction in the weight space is thus obtained. The following step is to compute the resulting weight update. In its simplified form, the weight update is a scaled step in the opposite direction of the gradient. Hence, the weight update Δw can be defined by Eq. (4.11)

$$\Delta w_{ij}(t) = -\varepsilon \cdot \frac{\partial E}{\partial w_{ij}}(t), \tag{4.11}$$

where ε represents the learning rate. In some cases, a momentum may be used with the idea of incorporating in the present weight update some influence of the past iteration. Thus, the weight update becomes

$$\Delta w_{ij}(t) = -\varepsilon \cdot \frac{\partial E}{\partial w_{ij}}(t) + \alpha \cdot \Delta_i w_{ij}(t-1), \tag{4.12}$$

where α is the momentum term and determines the amount of influence from the previous iteration to the current one.

In this dissertation, the resilient backpropagation training algorithm was used for the development of the neural network models due to its simplicity. This algorithm is developed based on the backpropagation method and the procedures, with which the weights are adjusted, are presented in detail in Annex A1. Some other more sophisticated techniques which are also frequently used include the conjugate gradient decent method [100, 131], quasi-Newton method [52] and Levenberg-Marquardt method [91], which are sometimes referred as second order training algorithms in some literatures [132]. Unfortunately, the error surface is often complex and may contain several local minima. An inter-comparison between the different training algorithms was, however, not performed in the scope of this work.

4.4.5 Quality assurance

4.4.5.1 Definition of performance indices

Several performance indices were computed in this dissertation in order to compare and evaluate the modelling performance of the developed neural network models: the **Fractional bias (*FB*)**, the **index of agreement (*IA*)**, the **squared correlation coefficient (*R²*)**, the **mean absolute error (*MAE*)**, the **mean bias error (*MBE*)** and the **root mean square error (*RMSE*)**. For the PM_{10} Forecasting model, additional performance indices to evaluate the correct number of PM_{10} exceedances, false alarms and PM_{10} missed exceedances were also considered: the **index of success (*IS*)**, the **false alarm value (*FAR*)** and the overall accuracy (*A*). These performance indices have been discussed extensively in several literatures [51, 93, 130, 131, 133, 134].

The **Fractional bias (*FB*)** value is defined as the difference between the means of two series divided by the average of the means of the two series, i.e.,

$$FB = \frac{\sum_{i=1}^{N}(P_i - O_i)}{0.5 \cdot \sum_{i=1}^{N}(P_i + O_i)}, \tag{4.13}$$

where P_i and O_i are the modelled and measured PM_{10} concentrations respectively. N is the data size.

The **index of agreement (*IA*)** value can be defined as the measure of agreement between the mean values of the modelled and measured PM_{10} concentrations. It is calculated as

$$IA = 1 - \frac{\sum_{i=1}^{N}(P_i - O_i)^2}{\sum_{i=1}^{N}(\left|P'_i\right| + \left|O'_i\right|)^2}, \tag{4.14}$$

where $P'_i = P_i - \overline{O}, O'_i = O_i - \overline{O}$. The overbar refers to the average over the series.

Indifferent to the deviation between the modelled and measured PM_{10} concentrations, the **squared correlation coefficient (*R²*)** value shows the ability of the developed neural network model to capture the variability in the PM_{10} concentrations. It is defined as

$$R^2 = \frac{(N \cdot \sum_{i=1}^{N} O_i \cdot P_i - \sum_{i=1}^{N} O_i \cdot \sum_{i=1}^{N} P_i)^2}{(N \cdot \sum_{i=1}^{N} O^2{}_i - (\sum_{i=1}^{N} O_i)^2 \cdot (N \cdot \sum_{i=1}^{N} P^2{}_i - (\sum_{i=1}^{N} P_i)^2}. \tag{4.15}$$

The **mean absolute error (*MAE*)** value is the measure of residual error between the modelled and measured PM_{10} concentrations, which is computed as

$$MAE = \frac{1}{N} \cdot \sum_{i=1}^{N} \left|P_i - O_i\right|. \tag{4.16}$$

The **mean bias error (*MBE*)** value indicates, on average, if the modelled PM_{10} concentrations are underpredicted or overpredicted. It is defined as

$$MBE = \frac{1}{N} \cdot \sum_{i=1}^{N} (P_i - O_i) \,. \tag{4.17}$$

Similar to the mean absolute error (*MAE*) value, the **root mean square error (*RMSE*)** value is a measure of residual error. In addition, the power term makes it more sensitive to extreme values compared to mean absolute error (*MAE*) value. It is defined as

$$RMSE = \left[\frac{1}{N} \cdot \sum_{i=1}^{N} (P_i - O_i)^2 \right]^{\frac{1}{2}} . \tag{4.18}$$

The **index of success (*IS*)** value indicates how well the PM_{10} exceedances are predicted. It is defined as

$$IS = \frac{TP}{TP + FP + FN} \,, \tag{4.19}$$

where *TP* is the number of correct predictions on PM_{10} exceedances, *FP* is the number of false alarms, and *FN* is the number of missed predictions on PM_{10} exceedances. *IS* is not affected by a large number of correctly predicted non-exceedances and therefore it can be useful for evaluating rare events.

The **false alarm value (*FAR*)** value indicates the fraction of predictions of PM_{10} exceedances which did not occur in the study period. It is defined as

$$FAR = \frac{FP}{FP + TP} \,. \tag{4.20}$$

In reality, false alarms are highly undesirable for practical reasons since the prediction of PM_{10} exceedances could result in expensive emission management strategy [135].

The **overall accuracy (*A*)** value indicates the fraction of PM_{10} predictions that correctly predicts an event (exceedance) or a non-event (non-exceedance). It is defined as

$$A = \frac{N - FP - FN}{N} \,. \tag{4.21}$$

4.4.6 PM_{10} Nowcasting

Street sweeping was conducted from 15.11.2006 to 18.03.2007 at Neckartor as an urban PM abatement strategy [25]. Based on measurement results, the evaluation on the effect of street sweeping during the investigation period was complicated by influence from varying weather conditions. Using the neural network approach, the varying weather conditions could be parameterised as model inputs. The aim of the Nowcasting model was to simulate a "what-if" scenario which could describe the original state of 24 h average PM_{10} concentrations at Neckartor, assuming that no street sweeping activities took place during the sweeping periods. Any effect of street sweeping could then be suggested by any differences between the modelled PM_{10} concentrations and the corresponding measured PM_{10} values.

The development of this type of model was an iterative process as depicted in Fig. 4.5. The model was initially trained with 24 h average measured parameters from the Schnarrenberg meteorological station, Neckartor traffic site, Bad Cannstatt urban background site and Erpfingen rural background site on days without street sweeping for the period from 03.01.2004 to 14.11.2006. The training parameters are described in Table 4.1 accordingly. The architecture of this model can also be termed as a Multiple-Input Single-Output (MISO) structure. It should be noted here that the wind direction data were dichotomised using sine and cosine functions, enabling the neural network algorithm to take into account of the discontinuities in the original cyclic signals [51, 100]. The corresponding output from the PM_{10} Nowcasting was the 24 h average PM_{10} concentrations on days when the training parameters were measured.

For the next step, the suitability of the developed model for operational use was then evaluated for the modelling of PM_{10} concentrations at the Neckartor site on the 52 days with street sweeping. The model input parameters, which functioned as a second test data set, were similar to the previously described training parameters except for the PM_{10} concentrations measured at Neckartor.

By definition, comparison between the modelled and measured values from a test set provides information on the generalisation behaviour of the model; the closer the modelled and measured values, the better the generalisation. Due to this application, the test set can also be termed as the generalisation set. The second test set for the PM_{10} Nowcasting did not, however, function as a generalisation set; the difference between the modelled and measured values as described by Eq. (4.22) would provide insights on the effect of street sweeping at Neckartor on ambient PM_{10} concentrations.

$$\eta_1 = \frac{PM_{10,\,Modelled} - PM_{10,\,Measured}}{PM_{10,\,Modelled}} \cdot 100\% \,, \tag{4.22}$$

where η_1 is the effect due to street sweeping. A positive value would indicate a positive effect, while a negative value would indicate a counteractive effect.

As street sweeping is a mechanical process which removes road dust from street surfaces, it can be expected that the sweeping activities at Neckartor will not affect the measured NO and NO_2 concentrations, meteorological conditions and air pollutant mixing heights on site. In another words, any effect of street sweeping can only be monitored by a change in PM_{10} concentrations. Although the model input parameters were based on days with street sweeping, the modelled PM_{10} concentrations would represent the original state of PM_{10} concentrations without sweeping hypothetically.

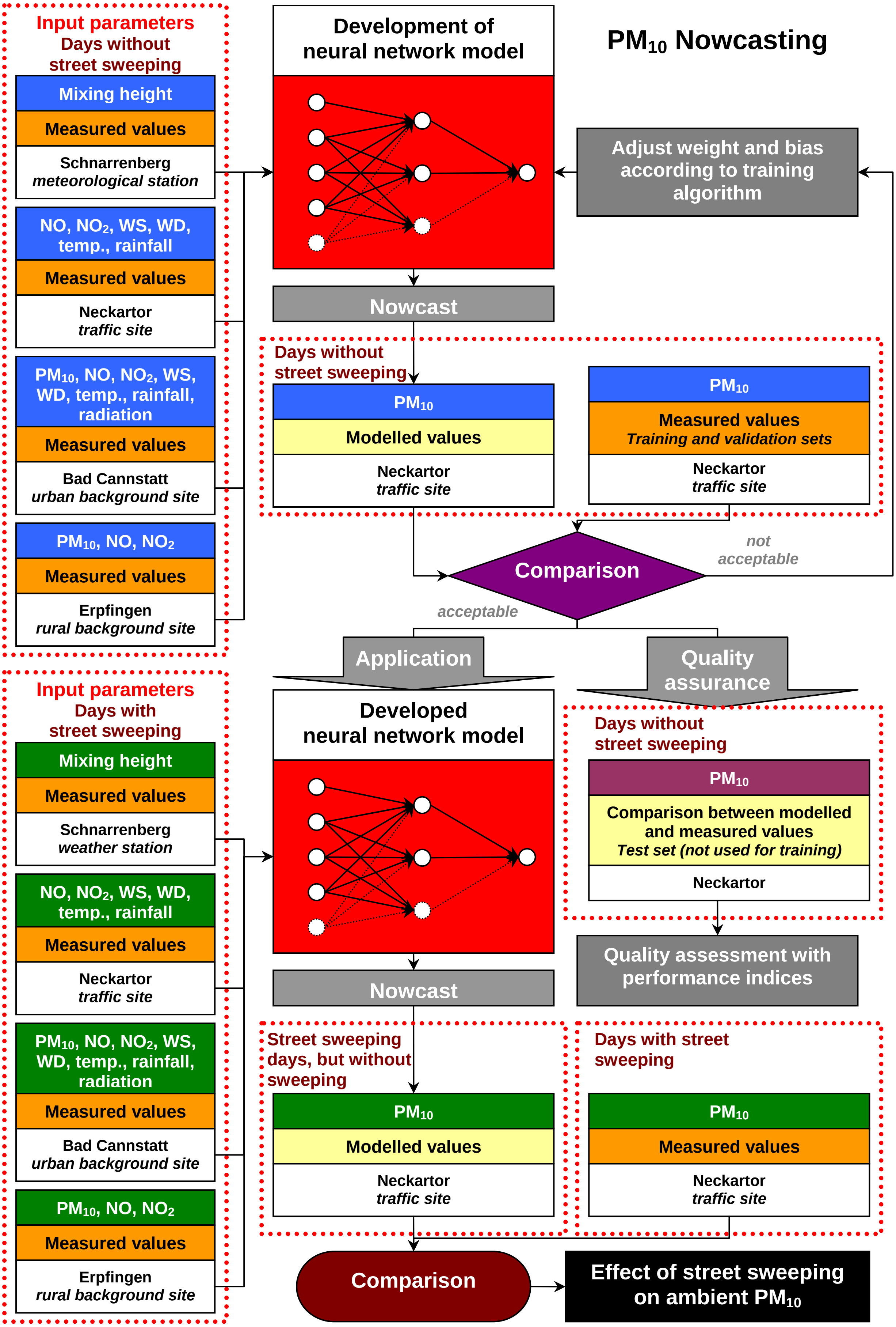

Fig. 4.5: PM_{10} Nowcasting for investigation on effect of street sweeping on ambient PM_{10} concentrations at Stuttgart Neckartor

Table 4.1: Training and input parameters for PM_{10} Nowcasting

Site	Parameters	Units	Mean	
			without street sweeping	with street sweeping
Neckartor (traffic)	PM_{10} [1]	µg/m³	52.9	-
	NO	µg/m³	176.6	258.0
	NO_2	µg/m³	113.9	127.0
	Wind speed	m/s	0.5	0.7
	Cosine wind direction	°	-0.4	-0.4
	Sine wind direction	°	-0.8	-0.8
	Temperature	°C	14.2	8.2
	Rainfall	mm	0.0	0.0
Bad Cannstatt (urban background)	PM_{10}	µg/m³	24.1	25.1
	NO	µg/m³	16.8	34.3
	NO_2	µg/m³	33.3	46.6
	Wind speed	m/s	1.2	1.5
	Cosine wind direction	°	-0.6	-0.8
	Sine wind direction	°	0.0	0.1
	Temperature	°C	10.5	7.4
	Rainfall	mm	0.0	0.0
	Global radiation	W/m²	93.1	46.9
Erpfingen (rural background)	PM_{10}	µg/m³	15.8	12.6
	NO	µg/m³	0.8	0.5
	NO_2	µg/m³	6.8	8.3
Schnarrenberg (meteorological station)	Mixing height [2]	m	1523.6	1310.7

[1]: only as training parameter; [2]: measured at 12:00 UTC daily

4.4.7 PM_{10} Forecasting

A model for PM_{10} Forecasting was developed to forecast 24 h average PM_{10} concentrations three days in advance for two urban sites of different characteristics in Stuttgart. The first site represented a heavily trafficked site, and the second site represented an urban background site. The developed model was looked upon as a system that under varying sets of forecasted meteorological inputs (weather conditions) and expected traffic flow, would respond by predicting the PM_{10} concentrations up to three days in advance for the two sites of different characteristics in Stuttgart. The development of this type of model for the traffic and urban background sites is depicted in Fig. 4.6. The training and input parameters to the model are described in Table 4.2.

In the model development phase, the model was trained using measured 24 h average PM_{10} concentrations from two ambient air monitoring stations at Neckartor and Bad Cannstatt, traffic counts at the Neckartor site, mixing height data from the Schnarrenberg meteorological station and four forecasted meteorological parameters (wind speed, temperature, rainfall and radiation) for day_{d+1}, day_{d+2} and day_{d+3} from a Numerical Mesoscale Model (NMM) [136]. Unlike the model which was developed for PM_{10} Nowcasting, wind direction was not considered as a training parameter due to the site characteristics of Neckartor. At Neckartor, the ambient air monitoring station is surrounded by a non permeable barrier of buildings on one side, where the build-up of air pollution is favoured. Hence, the forecasted wind direction may not be fully representative of the on-site wind characteristics. Comparisons between the

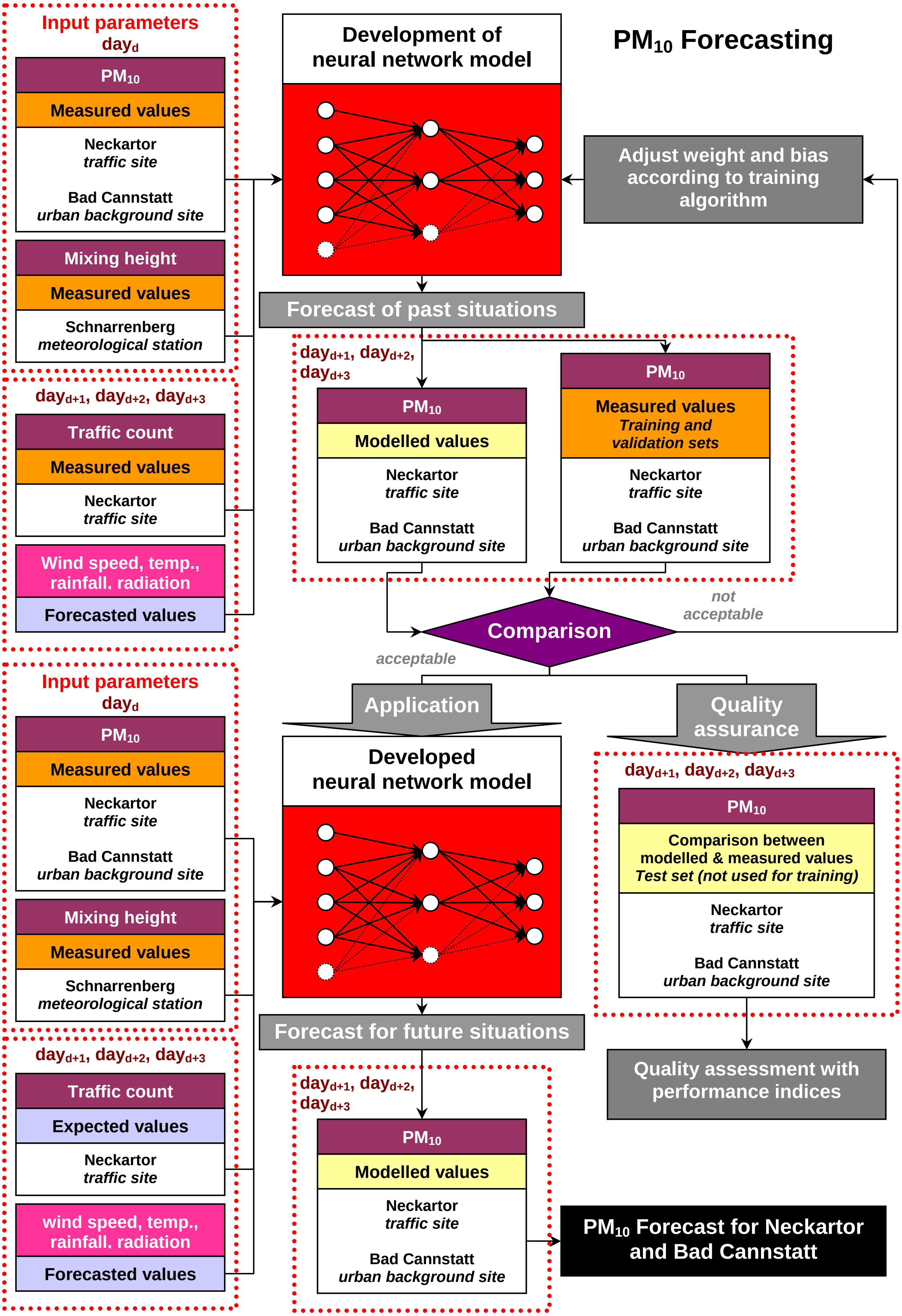

Fig. 4.6: PM_{10} Forecasting for the traffic and urban background sites

forecasted and measured meteorological parameters at the traffic and urban background sites on day_{d+1}, day_{d+2} and day_{d+3} are detailed in Annex B1. The model input parameters included past PM_{10} measurements, traffic counts and weather forecast from 01.05.2007 to 30.04.2008. The corresponding six outputs were the PM_{10} concentrations for day_{d+1}, day_{d+2} and day_{d+3} at the traffic and urban background sites. For the next step, the suitability of the developed model for operational use is envisioned for the modelling of future PM_{10} concentrations for the two sites using future weather forecasts and expected traffic counts.

By definition, the architecture of this type of model can also be termed as a Multiple-Input Multiple-Output (MIMO) structure. As the model's objective function is defined as a weighted sum squared error of multiple outputs, this type of model is expected to produce only a compromising optimisation of all outputs and cannot guarantee to have minimum error for each individual forecasted output [137]. As stated by Huang and Lian [138], the difficulty of MIMO systems is to overcome the coupling effects between the degrees of freedom of the nodes. Thus, the accuracy of the PM_{10} Forecasting can be expected to be lower than the PM_{10} Nowcasting because of the greater and more complex interactions of the weights and biases for different outputs. Owing to the Multiple-Output solutions, the searching process in the error domain is more complicated than that for a single target.

Table 4.2: Training and input parameters for PM_{10} Forecasting

Site/Source	Parameters	Unit	Input time	Mean
Neckartor (traffic)	PM_{10}	µg/m³	day_d	43.3
	PM_{10} [1]	µg/m³	day_{d+1}	42.3
	Traffic flow	number	day_{d+1}	73316
	PM_{10} [1]	µg/m³	day_{d+2}	41.8
	Traffic flow	number	day_{d+2}	73316
	PM_{10} [1]	µg/m³	day_{d+3}	42.5
	Traffic flow	number	day_{d+3}	73316
Bad Cannstatt (urban background)	PM_{10}	µg/m³	day_d	21.4
	PM_{10} [1]	µg/m³	day_{d+1}	20.7
	PM_{10} [1]	µg/m³	day_{d+2}	20.5
	PM_{10} [1]	µg/m³	day_{d+3}	21.0
Schnarrenberg (meteorological station)	Mixing height [2]	m	day_d	1529.2
Numerical Mesoscale Model (weather forecaster)	Temperature	°C	day_{d+1}	10.0
	Rainfall	mm	day_{d+1}	0.1
	Global radiation	W/m²	day_{d+1}	163.5
	Wind speed	m/s	day_{d+1}	0.9
	Temperature	°C	day_{d+2}	10.0
	Rainfall	mm	day_{d+2}	0.1
	Global radiation	W/m²	day_{d+2}	159.0
	Wind speed	m/s	day_{d+2}	0.9
	Temperature	°C	day_{d+3}	10.3
	Rainfall	mm	day_{d+3}	0.1
	Global radiation	W/m²	day_{d+3}	160.0
	Wind speed	m/s	day_{d+3}	1.0

[1]: only as training parameters; [2]: measured at 12:00 UTC daily

4.5 Sensitivity analyses between PM_{10} concentrations and influencing parameters

The analyses of the parametric correlation coefficients between PM_{10} concentrations and their influencing parameters were conducted here, aiming to evaluate the influence of each variable on the PM_{10} concentrations. These correlation coefficients provide a measure of the association between the two considered variables. The comparisons were performed using 24 h average data. Whenever correlations were performed and a data point was not available for a parameter, the correspondent data point of the other was withdrawn from the analyses.

In regard to the developed PM_{10} Nowcasting and PM_{10} Forecasting models, the influencing parameters represented the input parameters, whilst the PM_{10} concentrations represented the output. By performing the sensitivity analyses between these parameters, the calculated correlation coefficient could hint on the relative importance of each respective input parameter to the network response.

4.5.1 PM_{10} vs. PM_{10} at different sites

Based on the 24 h average PM_{10} measurements at Neckartor, Bad Cannstatt and Erpfingen, the field structure of PM_{10} concentrations for the Stuttgart region from 03.01.2004 to 14.11.2006, based on the Lenschow's model [113], is depicted schematically in Fig. 4.7.

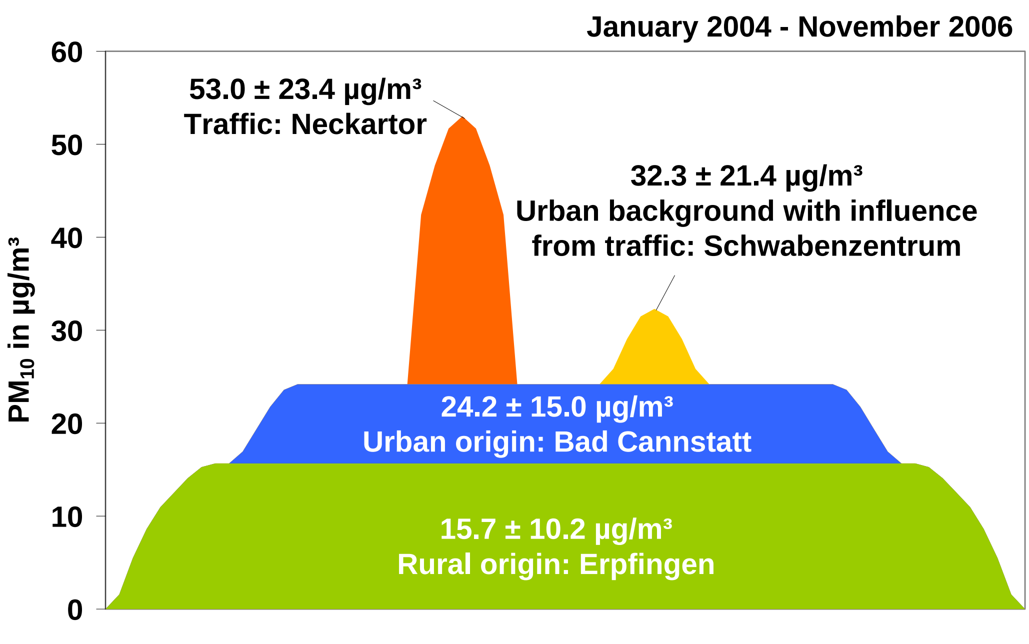

Fig. 4.7: Schematic horizontal profile of the 24 h average PM_{10} concentrations at Stuttgart for the period 03.01.2004 to 14.11.2006 data souce: AfU, LUBW

The field structure of PM_{10} concentrations at Stuttgart can provide an overview on the proportion of background PM_{10} on traffic PM_{10} loads. Based on the results, approximately 30 % of the PM loads at Neckartor could be attributed to the rural background, 15 % to the urban

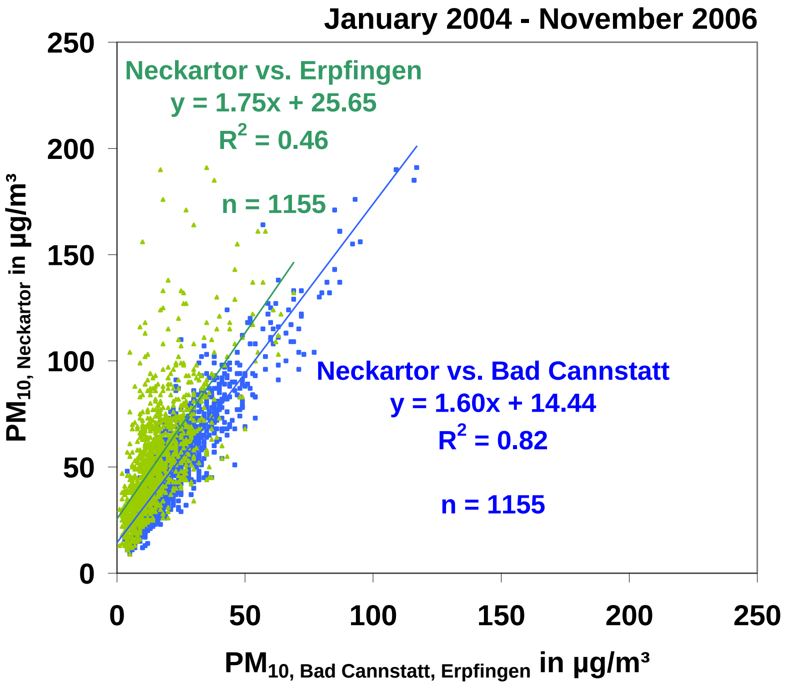

Fig. 4.8: 24 h average $PM_{10,\ Neckartor}$ vs. $PM_{10,\ Bad\ Cannstatt,\ Erpfingen}$ for the period 03.01.2004 to 14.11.2006 data source: LUBW

background, and the remaining 55 % to PM sources of local origin. In line with the results from Baumbach et al. [25], traffic-induced PM was found to account for approximately 62 % of the PM_{10} at Stuttgart Neckartor. In order to investigate on the dependence of varying background PM_{10} loads on the traffic PM_{10} loads, a statistical approach was adopted, whereby linear regression analyses on the correlations between 24 h average traffic PM_{10} concentrations and background PM_{10} concentrations were performed and the results are depicted in Fig. 4.8 accordingly. For these analyses, a high correlation coefficient R^2 value would imply that any increase in background PM_{10} concentrations would consequently lead to an increase in PM_{10} concentrations at the traffic site. The PM_{10} increment may be associated with one of the following:

1. Continuous periods of temperature inversion which may result in PM_{10} pollution episodes [11, 109, 111, 114, 115, 139]
2. PM_{10} pollution due to festive events [142]
3. PM_{10} pollution due to long-range or medium-range PM_{10} transport from background sites to traffic sites [140, 141]

Good correlation between the 24 h average PM_{10} concentrations at Neckartor and Bad Cannstatt was computed with a R^2 value of 0.82. Taking into account of the basin topological characteristics of the Neckar valley and the proximity between Neckartor and Bad Cannstatt, the influence on PM_{10} at these two sites under local meteorological conditions such as ground-level inversions can be expected to be similar [109, 110, 114, 117], and therefore explaining the high R^2 value. In another words, the PM_{10} trends at Neckartor and Bad Cannstatt are similar due to the comparable meteorological dispersion conditions. The absolute PM_{10} concentrations are different due to the difference in local emissions.

The traffic PM_{10} concentrations increased proportionally with a factor of 1.60 to the urban background PM_{10} concentrations, and with a positive offset of 14.44. From the mathematical aspect, this offset implies that whenever no background PM_{10} loads were expected, a minimum PM_{10} concentration of 14.44 µg/m³ at Neckartor would be observed.

The correlation between the 24 h average PM_{10} concentrations at Neckartor and Erpfingen was, however, not as strong, with a lower R^2 value of 0.46. This can be explained by the location of Erpfingen, which is sited in an entirely different environment, and is also probably above any ground-level inversions. Overall, an increasing trend in the PM_{10} concentrations at Neckartor could still be observed with increasing rural background PM_{10} concentrations at Erpfingen.

4.5.1.1 PM_{10} persistence models

A persistence model simulates the complete persistence of the initial state. In this work, the method of persistence modelling assigned the 24 h average PM_{10} concentrations on day_d equal to the values on the present day. The measured PM_{10} concentrations on day_{d+1}, day_{d+2} and day_{d+3} were subsequently plotted against the measured PM_{10} concentrations on day_d. Based on this method, the PM_{10} persistence models for up to three days in advance at Neckartor and Bad Cannstatt are depicted in Fig. 4.9a to 4.9c respectively.

In Fig. 4.9a, it is interesting to note that fairly good R^2 values exceeding 0.52 were computed for both Neckartor and Bad Cannstatt, inferring that the prevailing lag effects of PM_{10} concentrations from the previous day had rather strong influences on PM_{10} concentrations on the following day_{d+1}. Considering the three modes of particles, the smallest nucleation mode particles with diameter between 10 nm to 0.1 µm are known to be capable of residing in the atmosphere for a few hours [143-145]. Even though such particles may be present in large numbers, they usually form a small proportion of the total PM mass. The accumulation mode particles with diameter between 0.1 to 2.5 µm can have atmospheric residence time up to ten days, and usually have a more significant fraction of the total PM mass. The coarse mode particles with diameter between 2.5 to 10.0 µm have shorter residence time than the former modes, and can contribute substantially to the total PM mass. Using this knowledge, the persistent behaviours of PM_{10} on day_{d+2} and day_{d+3} are most likely caused by the accumulation mode particles. Although temperature inversions at Stuttgart have been shown to be a major cause for exceeding air-quality legislation thresholds for the allowable PM_{10} concentrations [109], the phenomenon, during which the lag effects of PM_{10} concentrations become prominent, can be expected to occur during the colder months of the year. Thus, considerations have to be made to the fact that the PM_{10} Forecasting should be capable of taking into account the possible prevailing lag effects of PM_{10} concentrations that could continue to persist for long periods of time when inversion conditions prevail.

The inherent problems on the accuracy of long-term persistence models can be observed by comparing the R^2 values in Fig. 4.9a and 4.9b. At Neckartor, the R^2 value weakened significantly from 0.52 to 0.21, and similar trend could be observed at Bad Cannstatt, where the value reduced from 0.56 to 0.27. By extending the persistence model to one day more as presented in Fig. 4.9c, the R^2 values were further halved from 0.21 to 0.10, and 0.27 to 0.14 at Neckartor and Bad Cannstatt respectively. When considering the diurnal evolution of the heights of mixing layer [146, 147], the decrease in R^2 values with days is a logical conclusion.

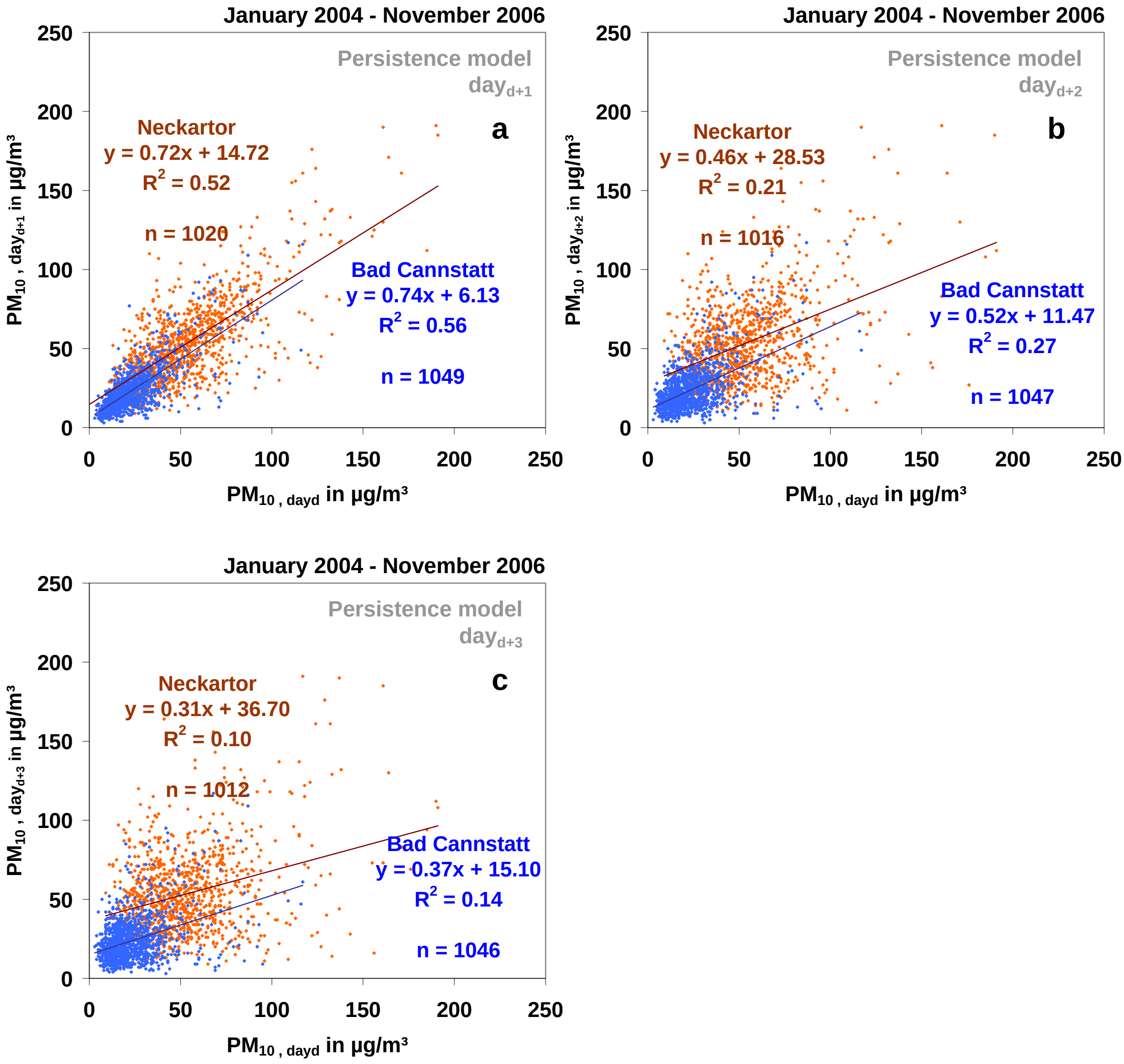

Fig. 4.9a-c: 24 h average PM_{10}, day$_{d+n}$ vs. PM_{10}, day$_d$ for the period 03.01.2004 to 14.11.2006 data source: LUBW

4.5.2 PM_{10} vs. NO_X

The high NO concentrations which are measured at both the Neckartor and Bad Cannstatt sites can be associated as primary NO emissions from local sources [148]. After NO is emitted to the atmosphere, NO can be oxidised by O_3 and peroxy radicals (HO_2, RO_2) to form NO_2. Compared to Bad Cannstatt, the higher NO_2 load at Neckartor originates from the direct exhaust emissions of vehicles from the B14 federal highway. As a result of modern exhaust after-treatment technologies mainly used in diesel vehicles, directly emitted NO_2 can be expected to be higher at the traffic sites. The share of the different NO_2 sources on the total NO_2 concentration may vary, depending on the traffic situation (e.g. traffic volume, share of diesel vehicles), local ventilation as well as meteorological parameters [149]. NO_2 concentration may also vary according to the time of day, season and meteorological parameters such as temperature, inversion, wind speed, O_3 availability etc [150]. During colder seasons, higher NO_2 concentration can also be expected due to frequent temperature inversions. Since the NO_2/NO ratio is not constant and depends on the various NO_2 formation conditions, the sum of NO + NO_2 is used to consider the NO_X emissions from traffic. It should be noted that not all NO_X originate from the traffic; an urban background portion of NO_X exists as well.

To investigate on the probable relationships between PM_{10} and NO_X concentrations, linear regression analyses were performed between PM_{10} and NO_X concentrations at Neckartor and Bad Cannstatt, as depicted in Fig. 4.10 accordingly. For this type of analyses, a high correlation coefficient R^2 value would indicate that high PM_{10} occur with high NO_X concentrations. In Fig. 4.10, a linear correlation between the two parameters could be established. The fairly good correlation coefficient R^2 value of 0.64 at Neckartor could infer that both the PM_{10} and NO_X were associated to a common origin; the higher the traffic-induced NO_X concentrations, the higher the PM_{10} concentrations.

At Bad Cannstatt, the background PM_{10} concentrations had weaker correlation to NO_X. This could imply that there were different sources of PM_{10} and NO_X over the urban background site. If both PM_{10} and NO_X originated from vehicle exhaust, one would expect less scatter in the data.

In regard to the two regression lines in Fig. 4.10, it is interesting to note that whenever no traffic-induced NO_X loads were expected at Neckartor, an urban background PM_{10} concentration of 12.38 µg/m³ would be expected. In the case for Bad Cannstatt, the expected PM_{10} concentration in the absence of NO_X would be 10.17 µg/m³.

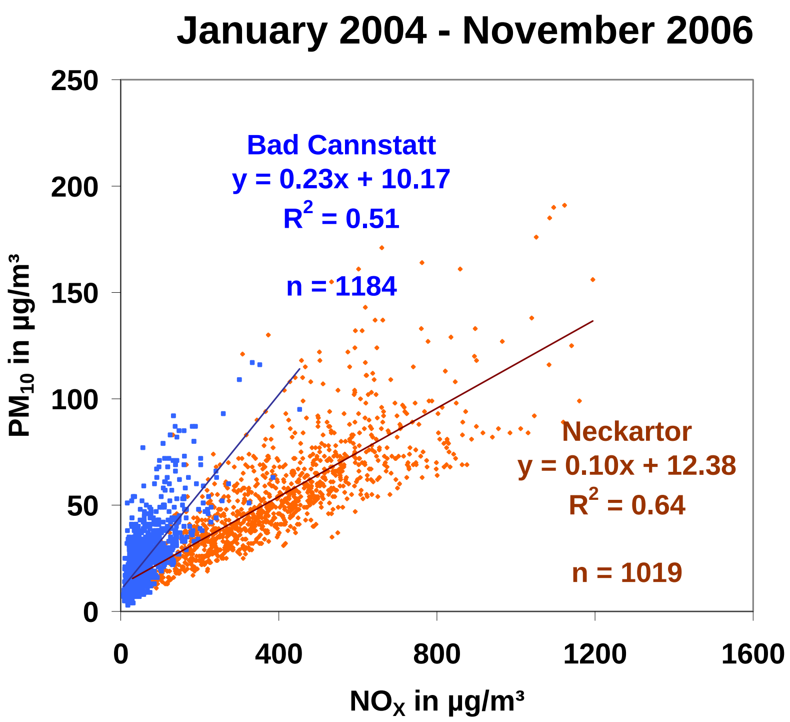

Fig. 4.10: 24 h average PM_{10} vs. NO_X concentrations at Stuttgart Neckartor and Bad Cannstatt for the period 03.01.2004 to 14.11.2006 data source: LUBW

4.5.3 PM_{10} vs. traffic

PM emissions from traffic may include contributions from exhaust emissions (fuel and lubricating oil combustion) to non-exhaust emissions from abrasion processes (tire-wear emissions, brake linings, catalyst deterioration, etc.) and resuspension of road dust induced by the vehicle-generated turbulence and most importantly road material abrasion. It is commonly assumed that most primary fine particles ($PM_{2.5}$) are emitted from the exhaust, whereas many of the coarse particles ($PM_{2.5\text{-}10.0}$) are considered to originate from non-exhaust sources. The traffic sector may also be responsible for a large part of the secondary PM formed via gas-to-particle conversion and the agglomeration mode ($PM_{1.0\text{-}2.5}$) [151]. At Stuttgart Neckartor, traffic-induced PM, which were previously identified as resuspended road dust in the size fraction of 2.1 to 10.0 µm and agglomerated diesel soot particles in the size fraction smaller than 0.7 µm, accounted for approximately 62 % of the PM_{10} [25]. Thus, it can be expected that good correlation may be computed between the measured PM_{10} concentrations and traffic count at Neckartor.

The relationship between the traffic PM_{10} concentrations and the traffic densities at Neckartor was investigated, as depicted in Fig. 4.11. The number of cars, lorries, buses and motorcycles passing through the Neckartor site was recorded and analysed for the period from 01.07.2007 to 29.02.2008 by LUBW. Data prior to July 2007 were not available. As expected, the PM_{10} concentrations agreed strongly to the traffic density, with a high R^2 value of 0.74. The PM_{10} concentrations increased with traffic density with a polynomial function. The lowest PM_{10} concentration was 21.3 µg/m³ when the traffic count was between 0 to 30,000; and the highest value was 88.0 µg/m³ when the traffic count was between 90,000 to 100,000. In an event when there was no traffic at Neckartor, an urban background PM_{10} concentration of 14.75 µg/m³ would be expected. This result is somewhat in consistent with the other hypothesis tests conducted in the earlier chapters.

In Fig. 4.12 the variation in PM_{10} concentrations with respect to the day of week is illustrated. It can be observed here that the PM_{10} levels tracked the traffic counts, with high levels occurring during weekdays when there was more traffic. With the exception on Friday when there was a slight reduction of PM_{10} concentrations from 48.5 µg/m³ to 47.1 µg/m³ and an increase in traffic count from 78786 to 80929, there was no evidence of a positive correlation between PM_{10} and traffic count on this day.

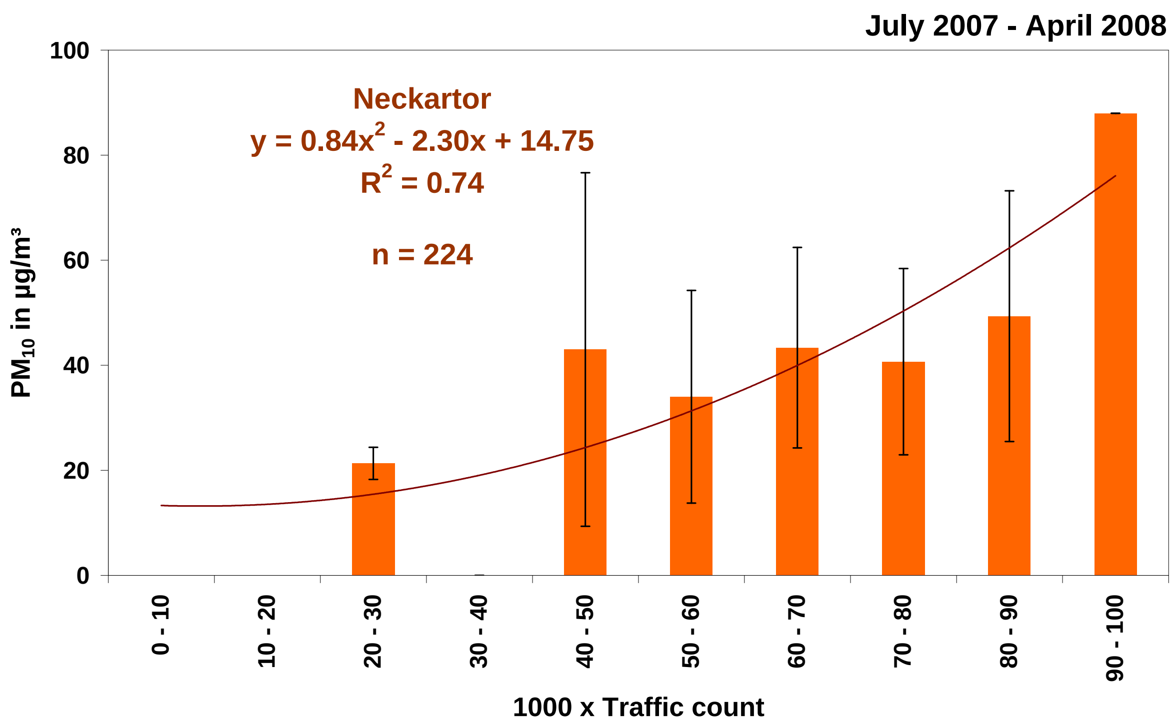

Fig. 4.11: 24 h average PM_{10} concentrations vs. traffic count at Stuttgart Neckartor for the period 01.07.2007 to 29.02.2008 data source: LUBW

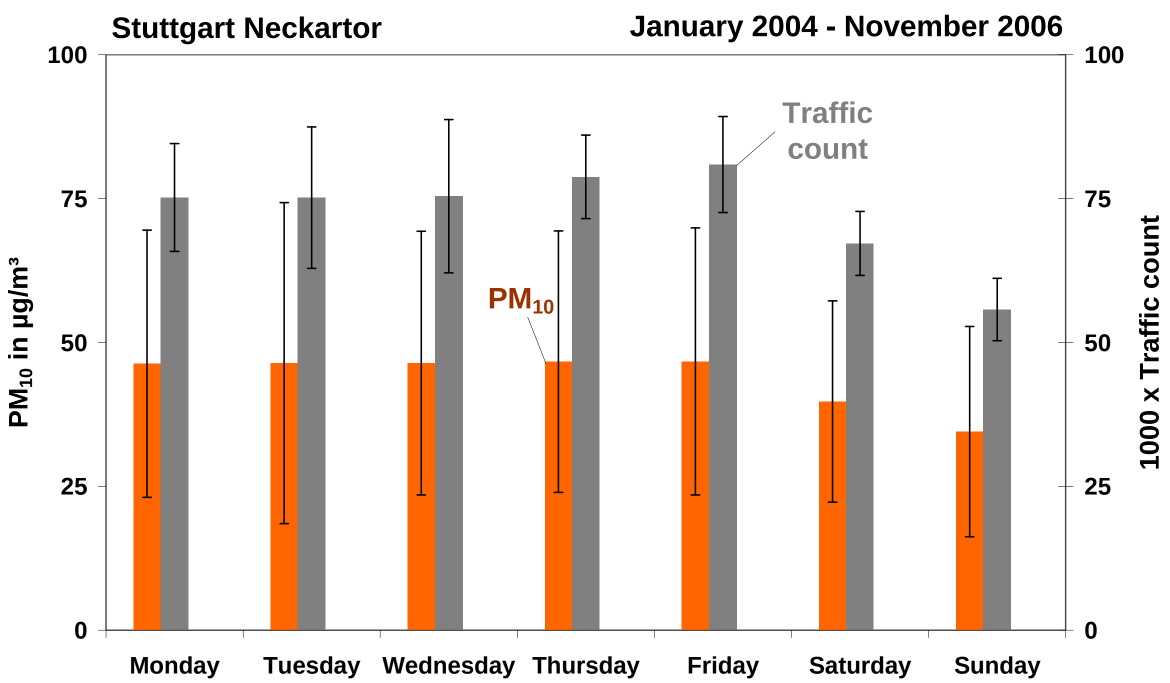

Fig. 4.12: 24 h average PM_{10} concentrations vs. traffic count on different days of week at Stuttgart Neckartor for the period 01.07.2007 to 29.02.2008 data source: LUBW

4.5.4 PM_{10} vs. rain duration

The influences of rain duration on the 24 h average PM_{10} concentrations at Neckartor and Bad Cannstatt were computed as logarithmic functions in Fig. 4.13 accordingly. These functions were only influenced by the length of the period of rain and other precipitation, ranging from lowering the average PM_{10} concentrations at Neckartor from 47.6 µg/m³ (1 rainy day) to 38.7 µg/m³ (> 3 rainy days), and at Bad Cannstatt from 21.0 µg/m³ (1 rainy day) to 16.0 µg/m³ (> 3 rainy days). The PM_{10} concentrations on dry days were higher compared with average, up to 66.9 µg/m³ at Neckartor, and 31.5 µg/m³ at Bad Cannstatt.

At both sites, the wet deposition of ambient PM_{10} with rain was demonstrated in Fig. 4.13. It means that due to scavenging of small particles by rain, the atmospheric PM_{10} loads decrease during rainy periods. However the impact of rain should not be solely regarded as the main cause of the washout effect, as rain influences the state of the roadways and its silt loading, while long drought periods may correspond to strong anticyclonic conditions, which also have a removal effect on ambient PM_{10} [152].

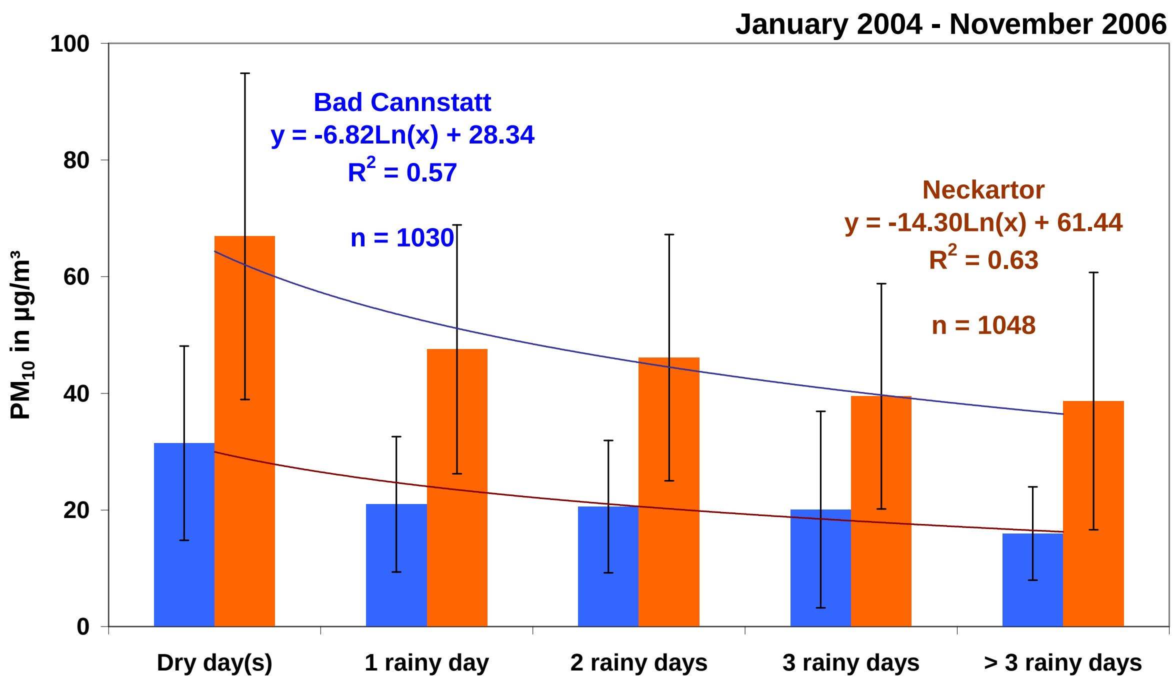

Fig. 4.13: 24 h average PM_{10} concentrations vs. rain duration at Stuttgart Neckartor and Bad Cannstatt for the period 03.01.2004 to 14.11.2006 data source: LUBW

4.5.5 PM_{10} vs. wind

Wind speed has long been recognised as an important control on ambient PM_{10} concentrations dependent on dry or wet conditions [153]. In the scope of this dissertation, no differentiation was made between the dry and wet months.

In Fig. 4.14, the logarithmic regressions of PM_{10} concentrations at Neckartor and Bad Cannstatt against wind speed were calculated to investigate the effect of wind speed on ambient PM_{10} concentrations. At Neckartor, a high 24 h average PM_{10} concentration of 61.8 µg/m³ was determined when the wind speed was less that 0.4 m/s. At Bad Cannstatt, similar finding was noticeable, with a high 24 h average PM_{10} concentrations of 33.3 µg/m³ when the wind speed was less than 0.4 m/s.

The difference in the R^2 values between Neckartor and Bad Cannstatt was significant. At Neckartor, the weaker R^2 value of 0.33 could be attributed to the limited wind data, as these wind data were only available starting from 10 March 2006. At Bad Cannstatt, wind speed was found to have a strong influence on PM_{10} concentrations, as indicated by the high R^2 value of 0.80. A general trend could be observed here: the stronger the wind, the lower the ambient PM_{10} concentrations.

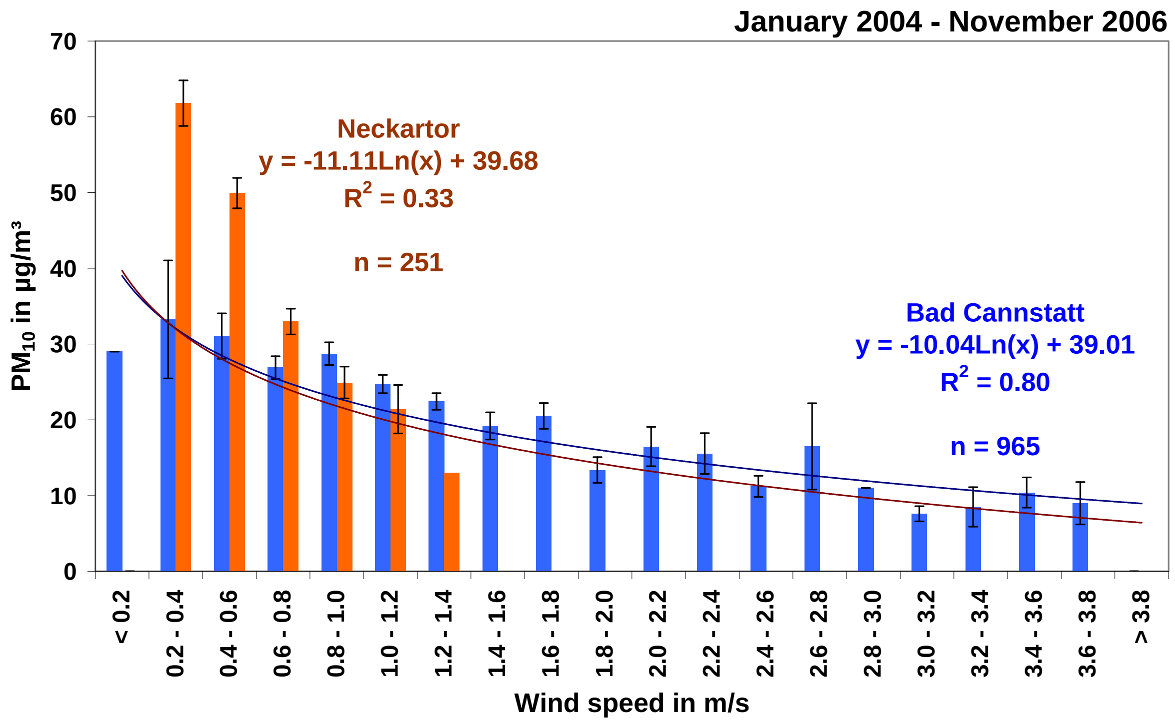

Fig. 4.14: 24 h average PM_{10} concentrations vs. wind speed at Stuttgart Neckartor and Bad Cannstatt for the period 03.01.2004 to 14.11.2006 data source: LUBW

4.5.6 PM_{10} vs. global radiation

Atmospheric aerosols may interact in different ways with the climatic system as follows [154]:

1. Scattering of solar radiation leads to a reduction of net solar radiation and therefore to a cooling of climate
2. Absorbing of solar and terrestrial radiation leads to the heating of the atmosphere

In Fig. 4.15, the influence of global radiation on ambient PM_{10} concentrations is depicted. At Neckartor, the maximum 24 h average PM_{10} concentration was 50.8 µg/m³ when the global radiation was between 0 to 25 W/m². At Bad Cannstatt, the corresponding maximum PM_{10} concentration was 23.6 µg/m³. On days when the global radiation was at its highest between 225 and 250 W/m², minimum 24 h average PM_{10} concentrations of 46.9 µg/m³ and 18.7 µg/m³ at Neckartor and Bad Cannstatt were observed respectively.

It is worth noting that the PM_{10} concentrations at both Neckartor and Bad Cannstatt were linearly proportional to the amount of global radiation with the same factor of -0.42 and a different offset. This could indicate that global radiation affects both traffic-induced and background PM_{10} with a similar magnitude. This observation is in agreement with many previous studies, which have shown that aerosols and global radiation are indeed closely correlated, especially those of anthropogenic origins [155-158]. The global radiation can also represents the different seasons. In winter with lower radiation, higher PM_{10} concentrations can be expected than in summer with high radiation.

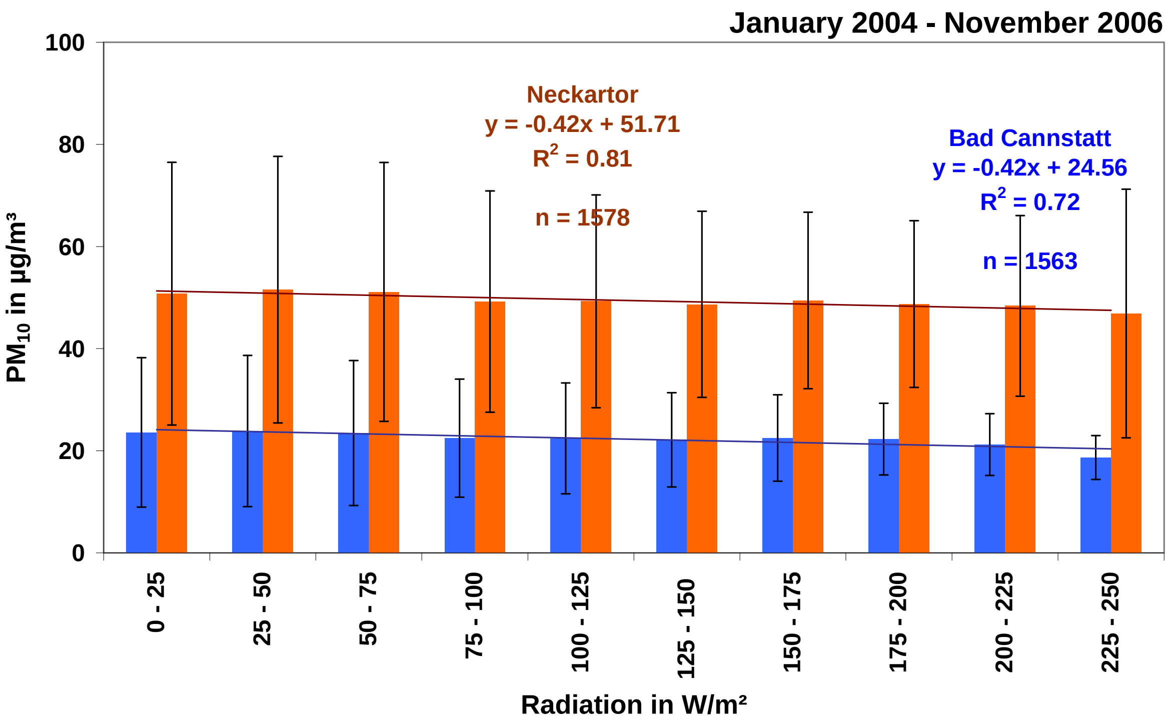

Fig. 4.15: 24 h average PM_{10} concentrations vs. global radiation at Stuttgart Neckartor and Bad Cannstatt for the period 03.01.2004 to 14.11.2006 data source: LUBW

4.5.7 PM_{10} vs. mixing height

Calculations of the daily average mixing height layers were based on the radio-soundings data from the Deutscher Wetterdienst (DWD) meteorological station at Stuttgart Schnarrenberg. The mixing heights can provide information on the air volume available for vertical dispersion of PM_{10} via convection or mechanical turbulence, and understanding it is of importance for various applications such as environmental monitoring. Thus, an accurate representation of the mixing height depth may play an essential role in the ability of air quality models to calculate the pollutant concentrations [90, 159]. Since mixing height is not measured by standard meteorological practices, much effort is often invested in improving its estimation. Although there are several definitions and methods for determining the mixing heights [147, 160-162], the process can somewhat be unspecific, whose definition and estimate are not precise. In this work, the method in determining the daily mixing heights was described in Zeng [114].

The 24 h average PM_{10} concentrations for different classes of mixing heights up to 1700 m at Neckartor and Bad Cannstatt for the period 03.01.2004 to 14.11.2006 are depicted in Fig. 4.16 accordingly. Particularly, lower mixing heights occurred in the colder months, during which higher PM_{10} concentrations were measured. This observation was evident for both the Neckartor and Bad Cannstatt sites. In extreme situations with low mixing heights of 0 to 400 m, the traffic PM_{10} concentrations increased significantly up to 120.0 µg/m³, compared to at Bad Cannstatt with 52.2 µg/m³. In situations with higher mixing heights, the PM_{10} concentrations decreased logarithmically. High R^2 values of 0.61 for Neckartor and 0.75 for Bad Cannstatt were calculated, underlining the overwhelming influence of the mixing heights on ambient PM_{10} concentrations.

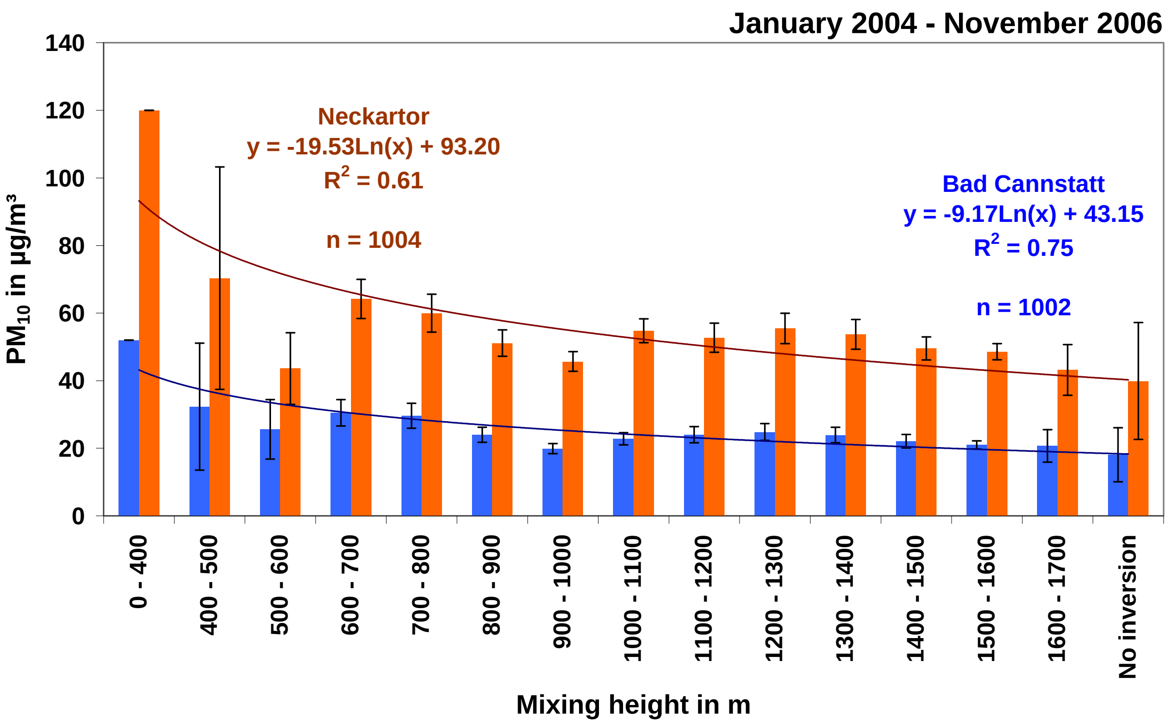

Fig. 4.16: 24 h average of PM_{10} concentrations for classes of mixing heights at Stuttgart Neckartor and Bad Cannstatt for the period 03.01.2004 to 14.11.2006

data source: DWD, LUBW

4.5.8 Conclusions

A major task of Chap. 4.5 was to find out the probable relative importance of each respective input parameter to the neural network response. In Table 4.3, the correlation coefficients of all investigated input parameters (PM_{10} at different sites, PM_{10} persistence behaviours, NO_X, traffic, rain duration, wind speed, global radiation, mixing height) to the reference parameter ($PM_{10,\ \mathrm{Neckartor,\ Bad\ Cannstatt}}$) is summarised. The R^2 value infers the degree of variability between the parameters.

From Table 4.3, the urban background PM_{10} is closely correlated to the traffic PM_{10} at Neckartor. At Bad Cannstatt, wind speed has the highest influence on the urban PM_{10}. In regard to neural network modelling, these respective R^2 values could already provide some hints on the respective weight distributions (w_{ij}) of nodes in the hidden layer based on Eq. (4.1) to (4.3); the higher the R^2 value, the greater the weight distribution, and vice versa. It should be emphasised that high R^2 values do not necessarily indicate the overall accuracy in neural network modelling. The quality of the model should be assessed considering the various performance indices as described in Chap. 4.4.5.

Table 4.3: Relative importance and association of all input to output parameters

Output parameter	Input parameter	R^2	Association
$PM_{10,\ \mathrm{Neckartor}}$	$PM_{10,\ \mathrm{Bad\ Cannstatt}}$	0.82	Linear
	$PM_{10,\ \mathrm{Erpfingen}}$	0.46	Linear
	$NO_{X,\ \mathrm{Neckartor}}$	0.64	Linear
	Traffic count$_{,\ \mathrm{Neckartor}}$	0.74	Polynomial
	Rain duration	0.63	Logarithmic
	Wind speed	0.33	Logarithmic
	Global radiation	0.81	Linear
	Mixing height	0.61	Logarithmic
$PM_{10,\ \mathrm{Neckartor,\ dayd+1}}$	$PM_{10,\ \mathrm{Neckartor,\ dayd}}$	0.52	Linear
$PM_{10,\ \mathrm{Neckartor,\ dayd+2}}$	$PM_{10,\ \mathrm{Neckartor,\ dayd}}$	0.21	Linear
$PM_{10,\ \mathrm{Neckartor,\ dayd+3}}$	$PM_{10,\ \mathrm{Neckartor,\ dayd}}$	0.10	Linear
$PM_{10,\ \mathrm{Bad\ Cannstatt}}$	$NO_{X,\ \mathrm{Bad\ Cannstatt}}$	0.51	Linear
	Rain duration	0.57	Logarithmic
	Wind speed	0.80	Logarithmic
	Global radiation	0.72	Linear
	Mixing height	0.75	Logarithmic
$PM_{10,\ \mathrm{Bad\ Cannstatt,\ dayd+1}}$	$PM_{10,\ \mathrm{Bad\ Cannstatt,\ dayd}}$	0.56	Linear
$PM_{10,\ \mathrm{Bad\ Cannstatt,\ dayd+2}}$	$PM_{10,\ \mathrm{Bad\ Cannstatt,\ dayd}}$	0.27	Linear
$PM_{10,\ \mathrm{Bad\ Cannstatt,\ dayd+3}}$	$PM_{10,\ \mathrm{Bad\ Cannstatt,\ dayd}}$	0.14	Linear

5 Results and discussion

5.1 Determination of the optimal number of hidden nodes for PM_{10} Nowcasting and PM_{10} Forecasting

Various rules of thumb have been proposed for the determination of the optimal number of hidden nodes, based on numerical relations between the number of training patterns and the number of weights, or the number of input variables [163]. As the number of hidden nodes is considered to be a matter of great significance, the use of empirical rules as suggested by Swingler [164] and Berry and Linoff [165] were avoided, and a trial-and-error procedure was adopted. The number of hidden nodes was varied from one to fifteen, and the corresponding performance indices, as described in Chap. 4.4.5, were computed and presented in Annex C1 for the PM_{10} Nowcasting, and in Annex C2 for the PM_{10} Forecasting. The number of hidden nodes for the network with the highest Index of Agreement (*IA*) and correlation coefficient (R^2) values was selected. Based on the selection criteria, the selected number of hidden nodes was three for the PM_{10} Nowcasting, and eight for the PM_{10} Forecasting.

5.2 PM_{10} Nowcasting

The performance of the PM_{10} Nowcasting model with a network topology of twenty input parameters, three hidden nodes and one output parameter was evaluated. This configuration can also be denoted by 20 - 3 - 1. Upon decreasing the number of hidden nodes, better overall performance and less error were derived. The results presented here were obtained with a hidden layer with three nodes, which was sufficient to perform the Nowcast function on the PM_{10} concentrations with all the considered input parameters. In order to study the regular pattern of convergence for the neural network model, the mean square error curves for the training, validation and test sets are depicted in Fig. 5.1.

At the first epoch, all mean square errors of the three data sets reduced significantly from over 811.0 $\mu g^2/m^6$ to 250.0 $\mu g^2/m^6$. These high error values were attributed by the initial assignment of randomise weights and biases to the network. Beyond the first epoch, moderate rates of decrease in the mean square errors were observed. Training was terminated at the seventeenth epoch, which resulted in minimum mean square error values of 22.3 $\mu g^2/m^6$ for

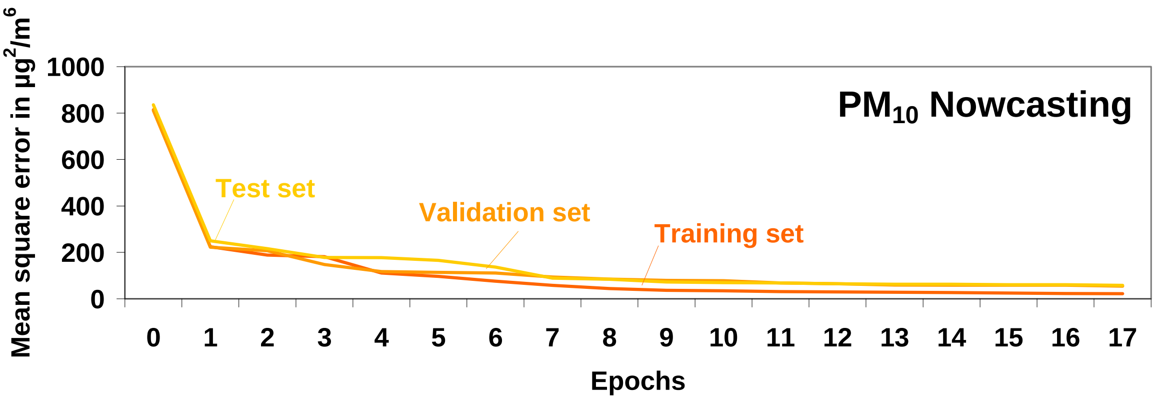

Fig. 5.1: Mean square error curves for training, validation and test sets vs. epochs for PM_{10} Nowcasting

the training set, 54.8 $\mu g^2/m^6$ for the validation set, and 58.0 $\mu g^2/m^6$ for the test set. Comparing the error curves from the three data sets, it can be seen that the evolution of errors over epochs are similar to one another, indicating comparable distributions of data for the training, validation and test sets.

5.2.1 Statistical evaluation

The overall statistical model evaluation on the modelled 24 h average PM_{10} concentrations at Neckartor are summarised in Table 5.1. The fractional bias (*FB*), index of agreement (*IA*), correlation coefficient (R^2), mean absolute error (*MAE*), mean bias error (*MBE*) and root mean square error (*RMSE*) values are presented as average values and their respective standard deviations in brackets for the period from 03.01.2004 to 14.11.2006.

The *FB* and *MBE* values were computed as -3.35 ± 2.93 % and -1.89 ± 1.73 µg/m³ respectively, which indicated a tendency of the model to underpredict. When the *IA* value approaches 1, then the model is more appropriate to simulate the measured PM_{10} concentrations. A high *IA* value of 0.97 ± 0.03 was computed, which implied that 97 % of the modelled values were error free. Based on the R^2 value, the PM_{10} Nowcasting model was able to capture 89 ± 8 % in the variability in the PM_{10} measured concentrations. The calculated values for *MAE* and *RMSE* were found to be 5.86 ± 3.41 µg/m³ and 7.44 ± 4.11 µg/m³ respectively.

Considering the high *IA* value which exceeded 0.9, and the R^2 value which exceeded 0.8, these results were comparable with those obtained in other studies for the modelling of 24 h average PM_{10} concentrations [81, 85, 97]. However, the differences should be mainly attributed to the different climatic characteristics of the different study sites and to the different approach for the estimation of generalisation error used.

Table 5.1: Overall statistical model evaluation parameters of modelled 24 h average PM_{10} concentrations at Stuttgart Neckartor, presented as average values and their standard deviations for the period 03.01.2004 to 14.11.2006

Site		**Overall results from training, validation and test sets**					
		***FB* in %**	***IA***	**R^2**	***MAE* in µg/m³**	***MBE* in µg/m³**	***RMSE* in µg/m³**
Neckartor		-3.35	0.97	0.89	5.86	-1.89	7.44
	s_D	(2.93)	(0.03)	(0.08)	(3.41)	(1.73)	(4.11)

FB: fractional bias, IA: index of agreement, R^2: correlation coefficient, MAE: mean absolute error, MBE: mean bias error, RMSE: root mean square error, s_D: standard deviation

5.2.2 Scatter plot of modelled and measured PM_{10} concentrations

The scatter plot of the modelled and measured 24 h average PM_{10} concentrations at the site of Neckartor for the period from 03.01.2004 to 14.11.2006 is depicted in Fig. 5.2. The 95 % confidence intervals of the linear regression between the modelled and measured PM_{10} concentrations are also included. In total 1029 pairs of data were available. Based on the profile of the scatter plot, the modelled PM_{10} concentrations agreed relatively well to the measured values, with the exception of ten outliers which were notably underpredicted from the PM_{10} Nowcasting. Interestingly, all the ten outliers were modelled on days with PM_{10} episodes. The respective PM_{10} episodes are further described in the following chapters.

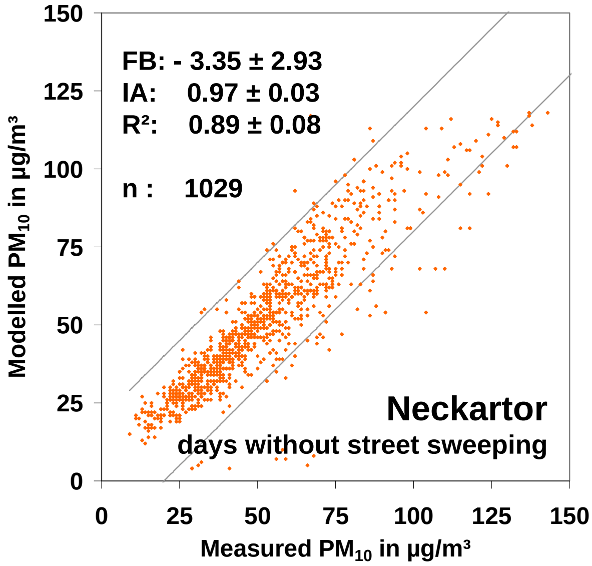

Fig. 5.2: Scatter plot of modelled and measured PM_{10} concentrations at Stuttgart Neckartor with 95 % confidence intervals for the period 03.01.2004 to 14.11.2006

5.2.3. Time series of modelled and measured PM_{10} concentrations

In order to visualise the performance of the PM_{10} Nowcasting model for the period from 03.01.2004 to 14.11.2006, the time series of the modelled and measured 24 h average PM_{10} concentrations at Neckartor are presented in Fig. 5.3a to 5.3c respectively.

Although the modelled PM_{10} concentrations followed the general trend of the measured PM_{10} concentrations reasonably well, the PM_{10} Nowcasting seemed to encounter difficulties in modelling the particularly high PM_{10} concentration peaks. For instance, the measured PM_{10} concentration on 16.12.2004 was 156 µg/m³ whilst the corresponding modelled value was 127 µg/m³. In 2005 and 2006, the quality of the predictions regarding episodic concentration levels was again undermined by the model's inability to correctly spot some distinct high-concentration events from mid January 2005 till late April 2005, and mid January 2006 till late April 2006. On 04.03.2005 the highest measured PM_{10} concentration was 171 µg/m³, whilst the corresponding modelled value was 123 µg/m³. During another inversion episode in early 2006, the highest PM_{10} concentration of 191 µg/m³ was measured on 02.02.2006, whilst the corresponding modelled value was 127 µg/m³.

From the mathematical aspect, the underpredicting behaviour of the PM_{10} Nowcasting model during episodic events verifies the general assumption that neural network models will fail to extrapolate on data which have not been presented during the training procedure [95]. There are two approaches to address this issue, aiming to increase the frequency of extreme values in the training process either by reserving most of the available episodes for the training set, or by including each episode case more times [51, 85].

From the scientific aspect, the underpredicting behaviour of the PM_{10} Nowcasting model could be attributed to the additional loads of PM from episodic events, whose presence could not be accurately modelled by the model input parameters. The three most probable types of PM_{10} episodes are listed in Table 5.2.

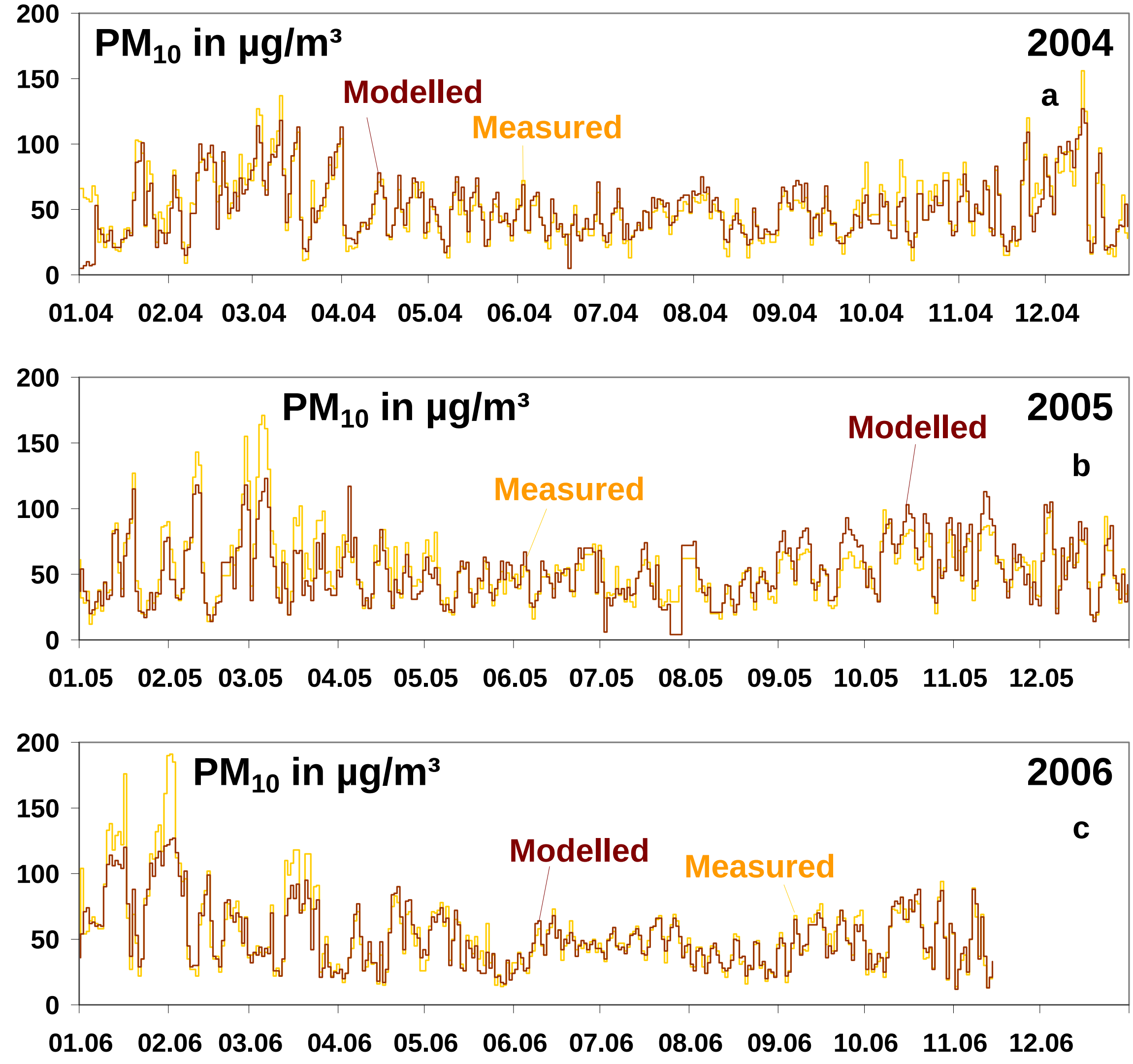

Fig. 5.3a-c: Modelled and measured 24 h average PM_{10} concentrations at Stuttgart Neckartor for the period 03.01.2004 to 14.11.2006

Table 5.2: General classification of PM_{10} episodes at Stuttgart Neckartor

Description	Characteristic season of the year	Characteristic meteorological factors	Main emission source category	References
Local-scale episodes				
Wintertime inversion-induced episodes	Winter	Inversion, stable stratification, low wind velocity	Local	[11, 111, 115, 166, 167]
Recreational pollution episodes	Whole season (but more critical during winter and spring)	Inversion, stable stratification, low wind velocity	Local	[139, 168, 169]
Regional and long-range transport episodes				
Long-range and regional transport episodes	Winter	Stable stratification, low wind velocity	Regional and long-term transport scales	[12, 13, 170, 171]

5.2.3.1 Wintertime inversion-induced PM_{10} episodes

During wintertime inversion-induced episodes, atmospheric inversions result in the accumulation of PM_{10} components emitted close to ground-level. In addition, the atmospheric stability enhances the formation of secondary PM components [109, 172]. An association between the increases in concentrations of ammonium salts during temperature inversion episodes could, in fact, be established in Stuttgart [117, 121]. In particular to ammonium nitrate, the concentrations are clearly dependent on the local production on nitric acid, which eventually reacts with ammonia to form ammonium nitrate.

For the production of ammonium chloride to take place, there must be a source of hydrochloric acid or precursor gas such as a chlorinated hydrocarbon to react with ammonia. However, no major sources of these species are known to Neckartor. Nevertheless, hydrochloric acid can also be produced as a product of the nitric acid reaction with salts, as described in Eq. (5.1)

$$NaCl(s) + HNO_3(g) \rightarrow NaNO_3(s) + HCl(g)\,. \tag{5.1}$$

Considering that the underprediction of PM_{10} concentrations at Neckartor occurred mainly during the winter months, the most probable source of sodium chloride could be from the application of road salts on street surfaces. Thus, the road salts could serve as a source of hydrochloric acid in the atmosphere and subsequently form ammonium chloride via reaction with ammonia [173].

To have better comparisons between the modelled and measured PM_{10} concentrations during wintertime inversion episodes at Neckartor, the corresponding values during several selected inversion periods, during which PM_{10} underpredictions were observed, are listed in Table 5.3. The PM_{10} underprediction ratio, which provides an estimation on the extent of modelling error, is defined as Eq. (5.2)

$$Ratio = \frac{PM_{10,\,Modelled}}{PM_{10,\,Measured}}\,. \tag{5.2}$$

From Table 5.3, the PM_{10} Nowcasting model underpredicted up to 30 % of the measured PM_{10} concentrations during the selected inversion episodes. A closer look at the model input parameters showed a comparatively uniform pattern, which seemed to be mainly formed by the prevailing meteorological conditions during these periods. Considering the two successive PM_{10} episodes at the beginning of 2006, both episodes were characterised by very weak exchange conditions (extreme inversion conditions) during an extensive high pressure system. The mixing height level was below 500 m in the first PM_{10} episode, and was reported to be even below 300 m in the second episode [139]. Therefore, it was clear that the maximum measured PM_{10} concentration in the second episode was higher than the first due to the smaller air volume available for vertical dispersion of PM_{10}. This observation is in accordance to the results from the sensitivity analysis test for PM_{10} vs. mixing height in Chap. 4.5.7; the lower the mixing height, the higher the PM_{10} concentration.

Table 5.3: Modelled and measured PM_{10} concentrations during several selected inversion periods at Stuttgart Neckartor from 2004 to 2006

Date	Modelled PM_{10} in µg/m³	Measured PM_{10} in µg/m³	PM_{10} underprediction ratio
22.01.2004 – 29.01.2004	63.8	71.3	0.9
30.01.2004 – 02.02.2004	30.5	44.0	0.7
02.02.2004 – 07.02.2004	47.8	56.3	0.8
10.02.2004 – 20.02.2004	74.0	74.1	0.9
24.02.2004 – 08.03.2004	74.3	80.6	0.9
08.03.2004 – 14.03.2004	85.9	92.0	0.9
16.01.2005 – 24.01.2005	42.9	48.1	0.9
28.01.2005 – 03.02.2005	49.6	57.9	0.9
05.02.2005 – 14.02.2005	61.9	68.4	0.9
22.02.2005 – 02.03.2005	83.4	104.6	0.8
02.03.2005 – 12.03.2005	67.2	90.5	0.7
12.03.2005 – 16.03.2005	50.0	67.6	0.7
16.03.2005 – 20.03.2005	43.6	62.8	0.7
20.03.2005 – 23.03.2005	51.3	76.0	0.7
23.03.2005 – 31.03.2005	49.3	64.2	0.8
10.01.2006 – 18.01.2006	98.0	115.7	0.8
24.01.2006 – 06.02.2006	108.9	130.9	0.8
11.02.2006 – 18.02.2006	60.8	58.5	1.0
19.02.2006 – 26.02.2006	62.3	63.4	1.0
14.03.2006 – 25.03.2006	73.7	91.3	0.8

5.2.3.2 Festive PM_{10} pollution episodes

One of the more unusual anthropogenic activities that can result in notable PM_{10} episodes at Stuttgart is the festive usage of fireworks to celebrate popular fiestas, a practice that, while common worldwide (e.g. New year), is more prevalent in some places than others. In Stuttgart, fireworks displays commonly accompany fiestas, the popular events being the spring festival (Frühlingsfest) event, Stuttgart beer festival (Cannstatter Volksfest) event, and New Year celebrations. The modelled and measured PM_{10} concentrations during several exemplary days with fireworks from 2004 to 2006 at Neckartor are listed in Table 5.4.

The effect of fireworks on the ambient PM_{10} concentrations at Neckartor is defined with Eq. (5.3)

$$\eta_2 = \frac{PM_{10,\,Measured} - PM_{10,\,Modelled}}{PM_{10,\,Modelled}} \cdot 100\%, \qquad (5.3)$$

where η_2 is the effect due to fireworks, and $PM_{10,\,Modelled}$ represents the original state of PM_{10} concentrations without any influence from fireworks. A positive value would suggest an additional load to ambient PM_{10} concentrations, while a negative value would suggest a reduction in ambient PM_{10} concentrations.

Table 5.4: Modelled and measured 24 h average PM_{10} concentrations during selected fiestas at Stuttgart Neckartor from 2004 to 2006

Event	Date	Modelled PM_{10} in µg/m³	Measured PM_{10} in µg/m³	η_2 in %
53. Stuttgarter Lichterfest in Höhenpark, Killesberg	10.07.2004	26	29	-10.3
159. Cannstatter Volksfest in Bad Cannstatt	30.09.2004	55	66	20.0
New year	01.01.2005	30	37	23.3
67. Stuttgarter Frühlingsfest in Bad Cannstatt	26.04.2005	35	46	31.4
54. Stuttgarter Lichterfest in Höhenpark, Killesberg	16.07.2005	43	41	4.9
160. Cannstatter Volksfest in Bad Cannstatt	30.09.2005	54	56	3.7
New year	01.01.2006	54	104	92.6
68. Stuttgarter Frühlingsfest in Bad Cannstatt	25.04.2006	70	71	1.4
55. Stuttgarter Lichterfest in Höhenpark, Killesberg	15.07.2006	39	41	5.1
161. Cannstatter Volksfest in Bad Cannstatt	08.10.2006	38	40	5.3

η_2: effect due to fireworks

On both days of New Year in 2005 and 2006, the additional loads on the ambient PM_{10} concentrations due to fireworks events in Germany were 20 % more than the modelled values. On 01.01.2006 the maximum measured concentration was 104 µg/m³, which was almost double of the modelled value. It should be emphasised that these values should not be evaluated quantitatively as the PM_{10} Nowcasting model was not trained for days with fireworks. During other events such as the Volksfest and Frühlingsfest, the increase in measured PM_{10} concentrations is partly attributed to the increase in traffic as well.

The negative value in Table 5.4 which indicated that fireworks reduce the PM_{10} concentration on 10.07.2004 should be considered as modelling errors. Nevertheless, in line with the results presented here, Vecchi et al. [142] reported that the PM_{10} concentrations attributed to fireworks can be as much as 53 % of the mass.

Ravindra et al. [169] observed an increase in NO_2 concentrations during pyrotechnic display. Vecchi et al. [142] reported, however, that no significant NO_2 emissions could be ascribed to fireworks. To investigate this discrepancy in observations, the diurnal courses of PM_{10} and NO_2 concentrations on 01.01.2004 and 01.01.2005 (New Year) at the ambient air monitoring station of Bad Cannstatt, where the station is located near the major pyrotechnic displays, are depicted in Fig. 5.4. Interestingly, the PM_{10} concentrations reached the maximum of 145 µg/m³ on 01.01.2004 at 00:30, and 329 µg/m³ on 01.01.2005 at 01:00, whilst the NO_2 concentration profiles on both days indicated no significant changes. The NO_2 diurnal patterns in the early hours could be explained by the traffic flows, likely due to people returning home. Hence, it can be expected that the PM_{10} Nowcasting will fail to simulate PM_{10} concentrations on days with fireworks, during which associations between the modelled PM_{10} concentrations and the corresponding model input parameters such as NO_2 concentrations and weather conditions cannot be established on such days.

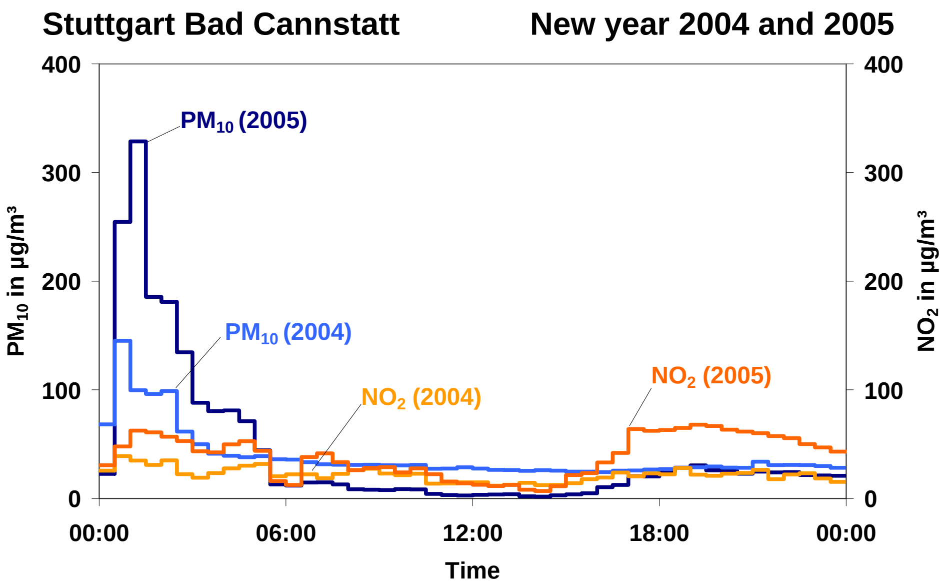

Fig. 5.4: Diurnal course of PM_{10} and NO_2 concentrations at Stuttgart Bad Cannstatt on 01.01.2004 and 01.01.2005 data source: LUBW

5.2.3.3 Regional and long-range PM_{10} transport

Besides winter-time inversion induced episodes and fireworks, ambient PM_{10} concentrations can also be substantially affected by long-range transport in areas characterised by low local emissions [142, 170, 174]. Long-range PM_{10} transport can result in episodic events when air masses arrive during suitable meteorological conditions (no precipitations and/or weak mixing of air masses) from regions with higher emissions of particles or from Sahara dust plumes [142]. In fact, dust transport can usually be observed over Central Europe several times a year via lofted aerosol layers [175]. While such detached layers may remain relatively stable, they need to mix with boundary layer air for the dust particles to reach the ground. Consequently, the dust plumes spread and dilute over larger areas and appear at the ground only at moderate concentrations.

A recent PM_{10} episode which affected Germany was reported by Bruckmann et al. [12], during which a belt of high PM_{10} concentrations extended from Ukraine to a large part of Europe was observed on 24.05.2007. On this particular day, extremely high half-hourly PM_{10} concentrations up to 360 µg/m³ were measured at many background ambient air monitoring stations in Germany, sparing only southern Bavaria, Baden-Württemberg and the Saar regions.

The hypothesis of long-range transport for air masses towards Stuttgart can be suggested by performing back trajectory analysis, a method which has often been used to identify sources and sinks areas of ambient PM_{10} or to construct their average spatial distribution [176]. However, PM_{10} back trajectories analysis was not performed in the scope of this dissertation, and information on PM_{10} episodes caused by long-range transport from 2004 to 2006 for the region of Baden-Württemberg was not documented in recent literatures. Although there was insufficient information to suggest that the underprediction of PM_{10} concentrations on certain days was due to long-range transport of PM_{10}, the possibility of such occurrence should not be ruled out entirely.

5.2.4 Error residuals

Comparison between the modelled and measured PM_{10} concentrations from the PM_{10} Nowcasting can provide information on the accuracy of the model; the closer the modelled and measured values, the higher the accuracy. Based on a method proposed by Kolehmainen et al. [134] and Ordieres et al. [177], the comparison between the modelled and measured PM_{10} concentrations can be described by Eq. (5.4)

$$Error\ residual = PM_{10,\ Modelled} - PM_{10,\ Measured}\ , \tag{5.4}$$

where $PM_{10,\ Modelled}$ and $PM_{10,\ Measured}$ are corresponding data sets.

With this definition, the error residuals of the PM_{10} Nowcasting for the period from 03.01.2004 to 14.11.2006 at Neckartor are presented in Fig. 5.5a to 5.5c respectively. Based on the results, the occurrences of PM_{10} underprediction were easily distinguishable during continuous temperature inversion periods in the early months of 2005 and 2006, and also on New Year's eves to the following day when pyrotechnic displays took place.

In Fig. 5.6, an error residual plot is depicted in order to compare the modelled and measured PM_{10} concentrations. The lower and upper ends of the vertical bars represent the 2^{nd} and 98^{th} percentile of the ratio of modelled PM_{10} to measured PM_{10} concentrations. The lower and upper limits of the boxes indicate the 16^{th} and 84^{th} percentiles of the ratio, and the horizontal line in between represents the median. As least 50 % of the modelled PM_{10} concentrations should be within a factor of 2 to the corresponding measured values (within the dotted lines) [178-180].

The PM_{10} Nowcasting model achieved a close agreement between the modelled PM_{10} concentrations to the measured PM_{10} concentrations, with a median of 0.96. More than 50 % of the data were found within the limits [180]. In addition, the small 2^{nd} and 98^{th} percentiles values illustrated that the main bulk of the modelled PM_{10} concentrations agreed relatively well to the measured values, thus indicating the high accuracy of the developed model.

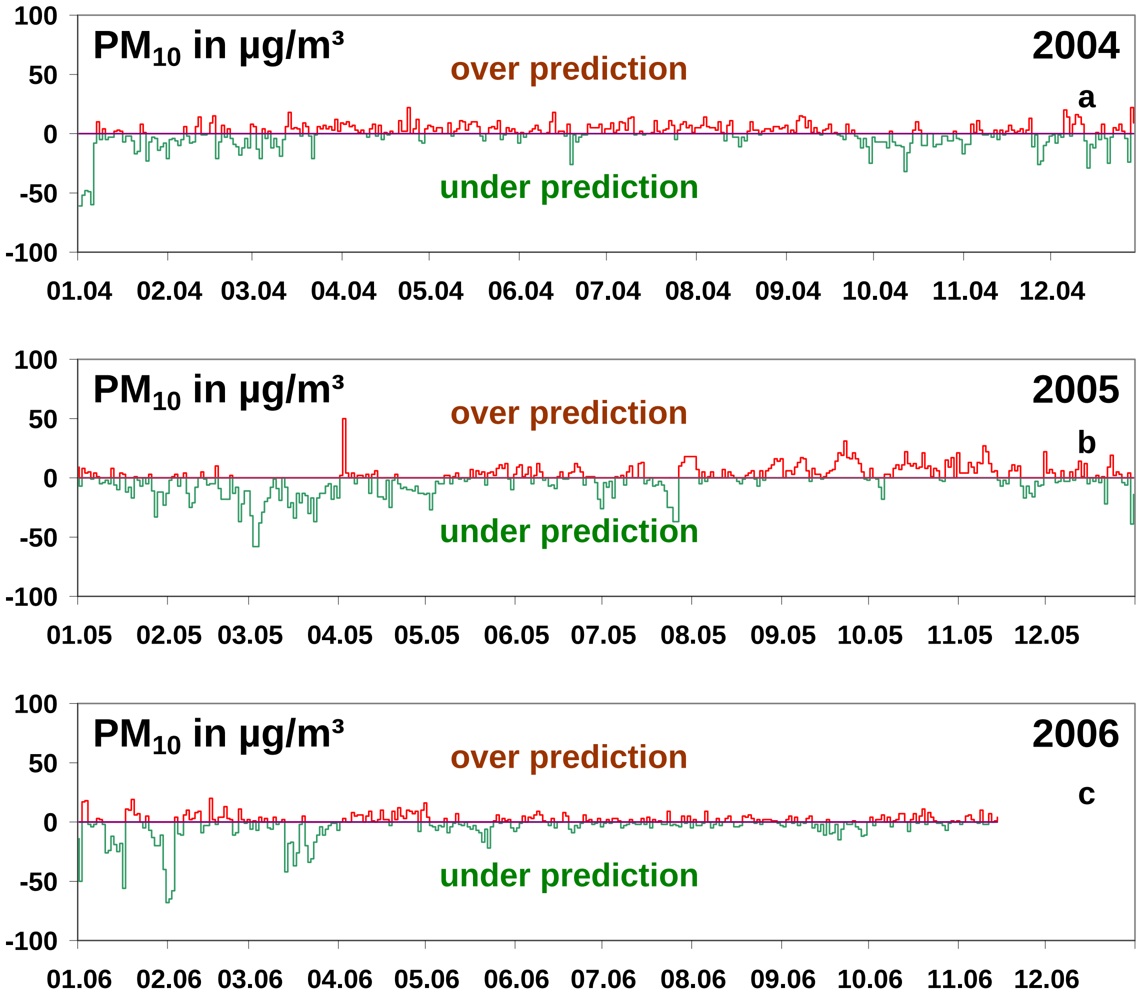

Fig. 5.5a-c: Error residuals of modelled 24 h average PM_{10} concentrations at Stuttgart Neckartor for the period 03.01.2004 to 14.11.2006

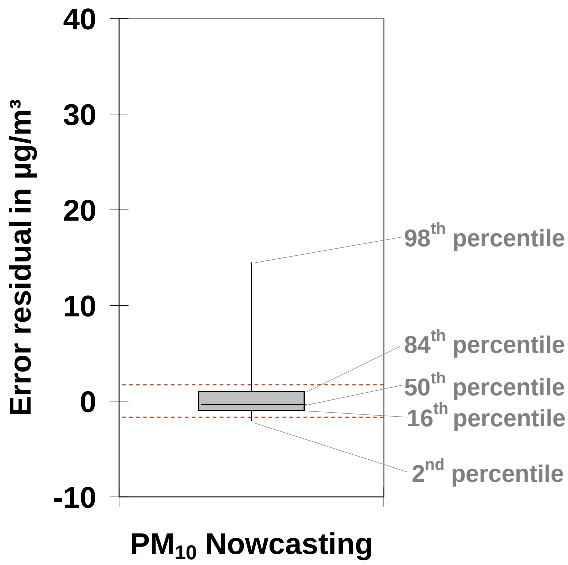

Fig. 5.6: 2nd, 16th, 50th, 84th and 98th percentiles of ratio between modelled PM_{10} and measured PM_{10} concentrations

5.2.4.1 Frequency distributions of error residuals

A more precise understanding in the goodness of fit between the modelled PM_{10} and measured PM_{10} concentrations can be demonstrated by plotting the histogram of error residuals. Based on Eq. (5.4), a good model shall consist of a shape where the frequency distributions of the PM_{10} error residuals near 0 µg/m³ is maximised and where the total range is as narrow as possible.

Fourteen class intervals of 10 µg/m³, from -60 µg/m³ to 70 µg/m³, were identified, which represented the respective range of data. The histogram of PM_{10} error residuals for the PM_{10} Nowcasting model is depicted in Fig. 5.7. The residuals were more or less normally distributed, which can be seen by the bell-shaped curve with an almost equal number of values to the left and right of centre of the data distribution. Symmetry of the distribution can be described by its skewness. In Fig. 5.7, the residuals appeared slightly skewed to the left.

Satisfactory results from the distribution frequency of PM_{10} error residuals were observed; approximately 77 % of the residuals fell between ± 10 µg/m³ with respect to 0 µg/m³. This information is important since the work was intended to simulate 24 h average PM_{10} concentrations of high accuracy. Thus, the frequency distribution of the residuals should suffice to establish the good agreement between the modelled and measured PM_{10} concentrations at the Neckartor site during the investigation period.

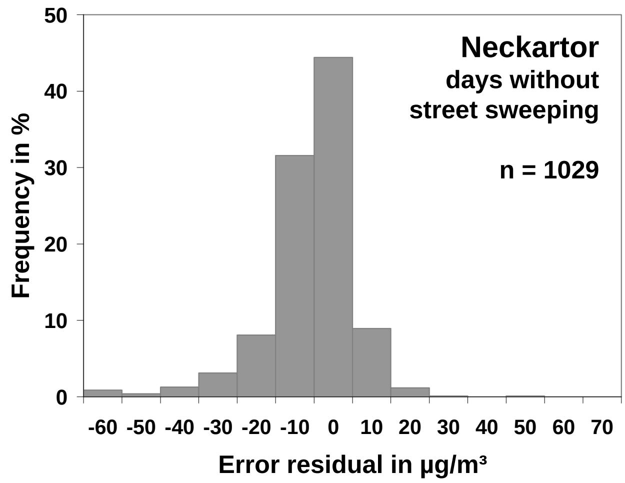

Fig. 5.7: Histogram of error residuals for the period 03.01.2004 to 14.11.2006

5.2.5 Quantile-quantile plot

A quantile-quantile plot (Q-Q plot) provides the graphical representation of the magnitude of one set of quantiles plotted against that of another. Thus, it can be a good visual means for understanding the underlying patterns across two sets of univariate numerical data. When comparing sets of data, it is common to consider measures of central tendency such as the median. If greater distributional detail is required, then finer graduations like quantiles may be examined. In Fig. 5.8, the quantile-quantile plot of the modelled PM_{10} concentrations against the measured values is depicted. The quantile-quantile plot, which was evaluated here, was created by plotting all 100 percentiles of both the modelled and measured PM_{10} concentrations. Working with the quantiles is, in effect, the same as working with the two sets of data that have been ordered from the smallest value to the largest value.

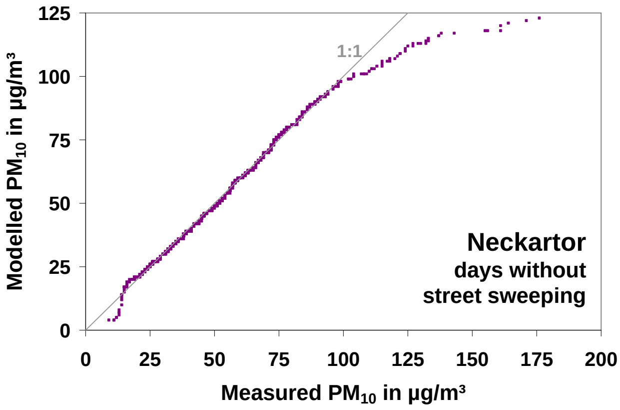

Fig. 5.8: Quantile-quantile plot of modelled 24 h average PM_{10} concentrations against measured PM_{10} concentrations at Stuttgart Neckartor for the period 03.01.2004 to 14.11.2006

55 out of 1029 data points in the top right indicated that the underprediction behaviour of the PM_{10} Nowcasting model began to show higher than 99 µg/m³. A closer look at the data points beyond 99 µg/m³ revealed that the most extreme underprediction case was caused by fireworks (or increase in traffic flow) on 01.01.2006, whilst the remaining 54 data sets were found in the colder months from January to March, during which temperature inversions were expected to form.

Six quantiles from Fig. 5.8 were identified and further analysed in Table 5.5. The various point estimates for the quantiles of the modelled PM_{10} concentrations agreed well to the measured PM_{10} concentrations up to q_{90}; underpredictions of PM_{10} concentrations were observed after the 92.5th quantile. In another words, the two sets of modelled and measured PM_{10} concentrations possessed similar distribution of data up to 99 µg/m³.

Table 5.5: Quantiles of modelled and measured PM_{10} concentrations

Quantiles	Modelled PM_{10} in µg/m³	Measured PM_{10} in µg/m³
q_{10}	26	25
q_{25}	34	35
q_{50}	48	49
q_{75}	66	67
q_{90}	86	84
$\boldsymbol{q_{92.5}}$	**91**	**91**

5.2.6 Cross-correlation coefficients of model input parameters to modelled PM_{10} concentrations

To investigate the influence of each model input parameter on the simulation of PM_{10} concentration at Neckartor during days without street sweepings, the cross-correlation coefficients between all parameters were computed. It is defined as Eq. (5.5)

$$C_{Pj} = \frac{N \cdot \sum_{i=1}^{N} P_i \cdot y_{ji} - \sum_{i=1}^{N} P_i \cdot \sum_{i=1}^{N} y_{ji}}{\sqrt{N \cdot \sum_{i=1}^{N} P^2{}_i - (\sum_{i=1}^{N} P_i)^2} \cdot \sqrt{N \cdot \sum_{i=1}^{N} y^2{}_{ji} - (\sum_{i=1}^{N} y_{ji})^2}}, \tag{5.5}$$

where y_j represents the model input parameters to the PM_{10} Nowcasting. C_{Pj} varies between 1 (total linear correlation) and -1 (total anti-linear correlation). A value zero implies no correlation at all. The cross-correlation coefficients of all model input parameters with respect to modelled PM_{10} concentrations at Neckartor are summarised in Table 5.6.

For NO and NO_2 concentrations at Neckartor, the positive cross-correlation coefficients exceeding 0.74 could indicate that both PM_{10} and NO_X concentrations mostly originated from the same source. The cross-correlation coefficient between the PM_{10} concentrations measured at Neckartor and Bad Cannstatt was clearly the highest, and approximately a third lower at Erpfingen. At Bad Cannstatt, the PM_{10} concentrations represented the urban background which included PM originating from other sources and mechanisms, except for those from the local vehicular traffic from the federal highway of B14. The good correlation was probably related to the pronounced influence of local PM sources, since the two sites of Neckartor and Bad Cannstatt are only approximately 3.8 km apart from each other. Considering the schematic horizontal profile of the 24 h average PM_{10} concentrations at Stuttgart in Fig. 4.7, the fact that an increase in background concentrations of PM_{10} would consequently result in an increase in PM_{10} concentrations at Neckartor could be established. Thus, the results from Table 5.6 revealed that the modelled PM_{10} concentrations possessed the same characteristics as the measured values.

Among the model input parameters, wind speed, temperature and rainfall parameters at Neckartor and Bad Cannstatt showed the strongest anticorrelation behaviours to the modelled PM_{10} concentrations. These findings were no surprise as typical temperature inversion can usually be described by low wind speed and temperature. Coupled with low mixing height, an accumulation of air pollutants above the ground surface can be expected to take place.

Table 5.6: Cross-correlation coefficients of model input parameters (measured values) to modelled PM_{10} concentrations for the period 03.01.2004 to 14.11.2006

Site	Input parameters from measurements	Cross-correlation coefficient
Neckartor (traffic)	NO	0.77
	NO_2	0.74
	Wind speed	-0.23
	Cosine wind direction	-0.05
	Sine wind direction	0.26
	Temperature	-0.27
	Rainfall	-0.20
Bad Cannstatt (urban background)	PM_{10}	0.91
	NO	0.66
	NO_2	0.77
	Wind speed	-0.39
	Cosine wind direction	-0.05
	Sine wind direction	0.51
	Temperature	-0.32
	Rainfall	-0.23
	Global radiation	-0.03
Erpfingen (rural background)	PM_{10}	0.67
	NO	0.22
	NO_2	0.40
Schnarrenberg (weather station)	Mixing height	-0.10

5.2.7 Application of PM_{10} Nowcasting for investigation on effect of street sweeping on ambient PM_{10} concentrations

The model input parameters for PM_{10} Nowcasting comprised of only information other than PM_{10} concentrations measured at Neckartor during the street sweeping periods. These parameters were necessary to simulate the original state of ambient PM_{10} concentrations at Neckartor during these periods, but assuming that no sweeping activities took place. Based on the modelling results, any positive effect of street sweeping as a PM_{10} abatement strategy at Neckartor would be suggested by higher modelled PM_{10} concentrations in comparison to the corresponding measured PM_{10} values. Conversely, no influence on the ambient PM_{10} concentrations after street sweeping would be implied by similar or lower modelled PM_{10} concentrations than the measured values.

To establish any relationship between the modelled PM_{10} concentrations (no street sweeping assumed) and the corresponding measured PM_{10} values (with street sweeping), the two sets of data are plotted against each other in Fig. 5.9. In addition, the temporal courses of the modelled and measured 24 h average PM_{10} concentrations are depicted in Fig. 5.10.

Using the neural network approach, the developed PM_{10} Nowcasting model was able to accurately perform the Nowcast of PM_{10} concentrations at Neckartor during street sweeping periods. Based on the results in Fig. 5.9, the gradient of 0.96 implied that the measured PM_{10} values were approximately 4 % lower than the modelled values, suggesting slight influence of street sweeping activities on ambient PM_{10} concentrations at Neckartor. However, the results based on Fig. 5.9 should not be conclusive as the trends of lower PM_{10} concentrations were not obvious during all sweeping periods, as depicted in Fig. 5.10. For instance, based on Eq. (4.22), more than 23 % reductions in the ambient PM_{10} concentrations were computed for three street sweeping days on 19.01.2007, 27.02.2007 and 03.03.2007. However, more than 10 % increments in the ambient PM_{10} values were also computed for street sweeping days on 17.02.2007, 23.02.2007 and 24.02.2007. The complete modelling results of PM_{10} concentrations during all street sweeping periods are included in Annex D1.

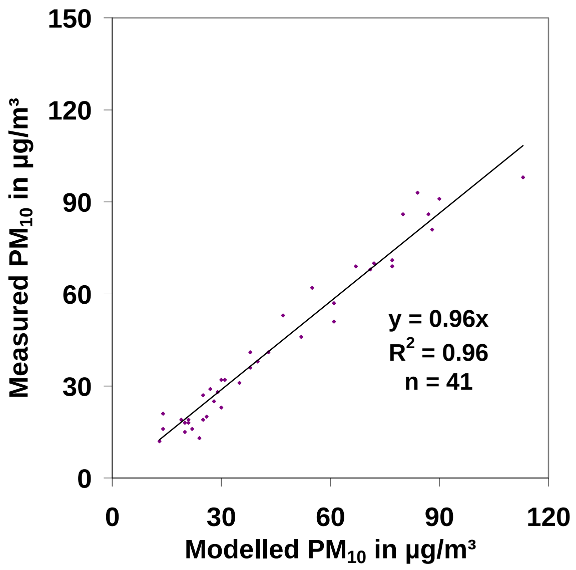

Fig. 5.9: Measured PM_{10} concentrations (with street sweeping) against modelled PM_{10} concentrations (no street sweeping assumed) at Stuttgart Neckartor for the period 15.11.2006 to 18.03.2007

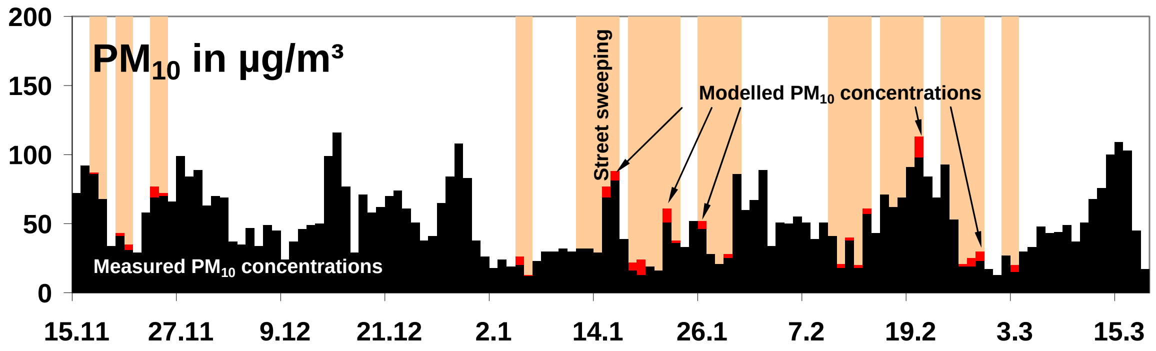

Fig. 5.10: Modelled and measured 24 h average PM_{10} concentrations at Stuttgart Neckartor for the period 15.11.2006 to 18.03.2007

5.2.8 Comparisons between modelling and measurement results from street sweeping

Based on the actual measurement results performed from 15.11.2007 to 18.03.2007, a small reduction potential of 6 % from street sweeping during working days at Neckartor was computed from the analyses of normalised PM_{10}/NO_X ratio. Although this method of analysis has the advantage of compensating the varying meteorological influences on ambient PM_{10}, it was difficult to conclude if the small reduction trend could be attributed to street sweeping or to other unknown factors.

To take into account of these uncertainties, such influences of meteorological conditions were parameterised as input parameters for the PM_{10} Nowcasting. Through extensive statistical evaluation on the performance of the developed neural network model, it was shown that the PM_{10} Nowcasting was capable of accurately simulating the PM_{10} concentrations from 03.01.2004 to 14.11.2006. On days with street sweeping, the measured PM_{10} concentrations were approximately 4 % lower than the corresponding modelled values, which could infer a slight reduction potential of ambient PM_{10} concentrations from the street sweeping activities. Interesting, this reduction trend was somewhat similar to the measurement results. However, it should be emphasised that the trends of lower PM_{10} concentrations were not obvious from the modelling results during all sweeping periods.

5.3 PM_{10} Forecasting

The performance of the PM_{10} Forecasting model with a network topology of eighteen input parameters, eight hidden nodes and six output parameters was evaluated. As described earlier for the PM_{10} Nowcasting model, the network configuration for the PM_{10} Forecasting model can also be denoted by 18 - 8 - 6. The mean square errors for the training, validation and test sets are depicted in Fig. 5.11.

After the first epoch, the mean square errors of the three data sets decreased notably, an observation which was also seen during the training of the PM_{10} Nowcasting model. For the training set, the mean square error decreased from 2100.0 $\mu g^2/m^6$ to 1075.0 $\mu g^2/m^6$ during the first epoch, then gradually to 536.5 $\mu g^2/m^6$ at the fourth epoch, and finally to 365.1 $\mu g^2/m^6$ at the tenth epoch. For both the validation and test sets, the mean square error decreased sharply from over 1349.4 $\mu g^2/m^6$ to 343.3 $\mu g^2/m^6$ during the first epoch, and gradually to 282.5 $\mu g^2/m^6$ for the validation set, and 289.3 $\mu g^2/m^6$ for the test set. Nevertheless, the errors of all three data sets converged to their minimum at the tenth epoch.

In comparison to the PM_{10} Nowcasting model (see Fig. 5.1), the magnitudes of the corresponding mean square errors for the training, validation and test sets in Fig. 5.11 were more than five folds. These results were anticipated due to the way the errors were calculated for the PM_{10} Forecasting, with which the total errors of the six outputs were summed after each epoch (see Eq. (4.09) and (4.10)).

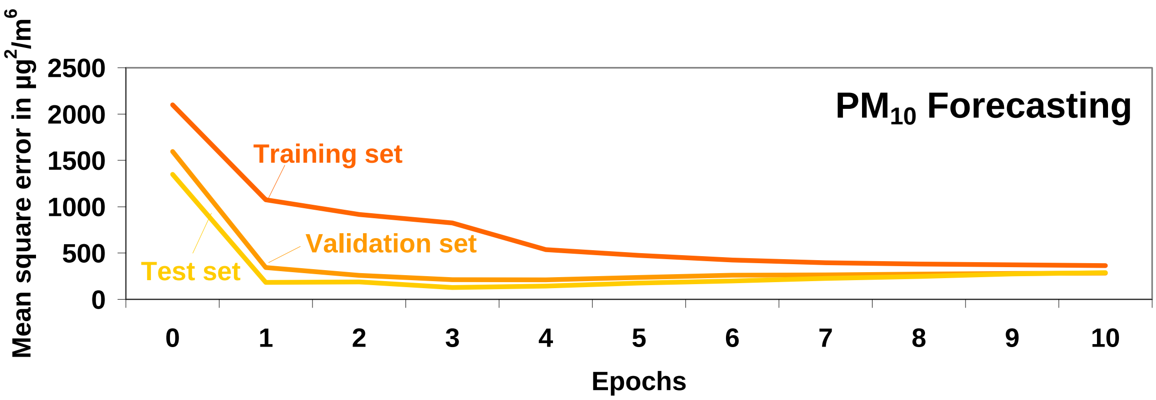

Fig. 5.11: Mean square error curves for training, validation, and test sets vs. epochs for PM_{10} Forecasting

5.3.1 Statistical evaluation

The overall statistical model evaluation on the modelled 24 h average PM_{10} concentrations at both traffic and urban background sites on day_{d+1}, day_{d+2} and day_{d+3} are summarised in Table 5.7 and Table 5.8. In Table 5.7 the fractional bias (*FB*), index of agreement (*IA*), correlation coefficient (R^2), mean absolute error (*MAE*), mean bias error (*MBE*) and root mean square error (*RMSE*) values are presented as average values and their respective standard deviations. In Table 5.8 the number of correct predictions on exceedances (*TP*), number of false alarms (*FP*), number of missed exceedances (*FN*), index of success (*IS*), false alarms values (*FAR*) and overall accuracy (*A*) values are presented.

Table 5.7: Overall statistical model evaluation parameters of modelled 24 h average PM_{10} concentrations at the traffic and urban background sites, presented as average values and their standard deviations for the period 01.05.2007 to 30.04.2008 on day_{d+1}, day_{d+2} and day_{d+3}

Site		Overall results from training, validation and test sets					
		***FB* in %**	***IA***	***R²***	***MAE* in µg/m³**	***MBE* in µg/m³**	***RMSE* in µg/m³**
day_{d+1}							
Traffic		-5.84	0.86	0.63	9.10	-2.40	13.01
	s_D	(2.89)	(0.04)	(0.08)	(2.79)	(1.48)	(4.93)
Urban background		-4.58	0.79	0.50	5.68	-0.93	9.24
	s_D	(5.90)	(0.07)	(0.07)	(1.89)	(1.35)	(4.15)
day_{d+2}							
Traffic		-3.28	0.86	0.61	9.73	-1.35	13.01
	s_D	(4.31)	(0.05)	(0.16)	(2.28)	(2.07)	(3.55)
Urban background		-3.59	0.82	0.51	6.18	-0.72	8.96
	s_D	(5.08)	(0.04)	(0.13)	(1.08)	(1.20)	(2.73)
day_{d+3}							
Traffic		1.20	0.84	0.54	10.96	0.51	14.78
	s_D	(7.52)	(0.03)	(0.15)	(2.26)	(3.38)	(3.82)
Urban background		-5.07	0.80	0.48	6.87	-1.04	10.12
	s_D	(4.67)	(0.03)	(0.13)	(1.40)	(1.17)	(3.65)

FB: fractional bias, IA: index of agreement, R^2: correlation coefficient, MAE: mean absolute error, MBE: mean bias error, RMSE: root mean square error, s_D: standard deviation

Table 5.8: Performance indices on the overall successful predictions of exceedances of 24 h average PM_{10} concentrations at the traffic and urban background sites for the period 01.05.2007 to 30.04.2008 on day_{d+1}, day_{d+2} and day_{d+3}

Site		Overall results from training, validation and test sets					
		TP	***FP***	***FN***	***IS***	***FAR***	***A***
day_{d+1}							
Traffic		66	16	13	0.69	0.20	0.91
	s_D	(18)	(3)	(3)	(0.22)	(0.12)	(0.01)
Urban background		0	0	10	0	N.A.	0.97
	s_D	(0)	(0)	(4)	(0)		(0.04)
day_{d+2}							
Traffic		62	22	15	0.63	0.26	0.89
	s_D	(18)	(2)	(4)	(0.28)	(0.23)	(0.02)
Urban background		0	0	10	0	N.A.	0.97
	s_D	(0)	(0)	(4)	(0)		(0.04)
day_{d+3}							
Traffic		64	33	14	0.58	0.34	0.86
	s_D	(19)	(3)	(2)	(0.26)	(0.26)	(0.01)
Urban background		0	0	12	0	N.A.	0.96
	s_D	(0)	(0)	(6)	(0)		(0.06)

TP: number of correct predictions of exceedances, FP: number of false alarms, FN: number of missed exceedances, IS: index of success, FAR: false alarms value, A: overall accuracy, s_D: standard deviation

On day_{d+1} and day_{d+2}, both *FB* and *MBE* values for the traffic site were negative-indicating a tendency of the model to underpredict; while these two performance indices were slightly positive on day_{d+3} and hence indicating a tendency of the model to overpredict. At the urban background site, the behaviour of underprediction was observed for all three days.

At the traffic site, the modelled PM_{10} concentrations showed good agreement with the measured PM_{10} concentrations. The *IA* values were 0.86 ± 0.04 on day_{d+1}, 0.86 ± 0.05 on day_{d+2}, and 0.84 ± 0.03 on day_{d+3}. It implied that 86 % of the predictions were error free on day_{d+1} and day_{d+2}, while 84 % of the predictions were error free on day_{d+3}. Through assessing the R^2 values, the PM_{10} Forecasting model captured 63 ± 8 % variability in the PM_{10} concentrations on day_{d+1}, 61 ± 16 % on day_{d+2}, and 54 ± 15 % on day_{d+3}. At the urban background site, the modelled PM_{10} concentrations showed also good agreement with the measured PM_{10} concentrations. The *IA* values were 0.79 ± 0.07 on day_{d+1}, 0.82 ± 0.04 on day_{d+2}, and 0.80 ± 0.03 on day_{d+3}. It implied that 79 % of the predictions on day_{d+1}, 82 % on day_{d+2}, and 80 % on day_{d+3}, were error free. In terms of R^2 values, the model captured 50 ± 7 % variability in the PM_{10} concentrations on day_{d+1}, 51 ± 13 % on day_{d+2}, and 48 ± 13 % on day_{d+3}.

In terms of *MAE* and *RMSE* values, the large errors could be caused by some unexpected events, which were not anticipated and therefore considered during the development of the PM_{10} Forecasting model. In fact, urban prediction of PM_{10} concentrations can be difficult due to several highly variable sources, which can be of either local or non-local origins [50]. In this case, the most probable explanation to the errors could be due to the local, regional and long-range transported contributions of additional PM_{10} loads, whose origins could not be fully described by the model input parameters. Fireworks events took place on several occasions in the study period from 01.05.2007 to 30.04.2008. For instance, the Frühlingsfest event in Bad Cannstatt on 13.05.2007, the 56th Lichterfest event in Höhenpark Killesberg on 07.07.2007, 162th Cannstatter Volksfest event in Bad Cannstatt on 14.10.2007, Christmas celebration in the last week of December 2007, and New Year celebration in the first week of January 2008. Thus, it can be expected that the model will fail to accurately simulate the PM_{10} concentrations including the additional anthropogenic loads on all these occasions. The possibility of occurrence of traffic congestions along the Neckartor federal highway B14 was also not taken into account. Consequently, all these uncertainties challenged the robustness of the model, which could be seen by the large *MAE* values of 9.10 ± 2.79 µg/m³ on day_{d+1}, 9.73 ± 2.28 µg/m³ on day_{d+2}, and 10.96 ± 2.26 µg/m³ on day_{d+3} for the traffic site. The corresponding *RMSE* values were 13.01 ± 4.93 µg/m³, 13.01 ± 3.55 µg/m³, and 14.78 ± 3.22 µg/m³ respectively. For the urban background site, smaller *MAE* values of 5.68 ± 1.89 µg/m³, 6.18 ± 1.08 µg/m³, and 6.87 ± 1.40 µg/m³, and *RMSE* values of 9.24 ± 4.15 µg/m³, 8.96 ± 2.73 µg/m³, and 10.12 ± 3.65 µg/m³ were computed respectively. In line with the observations made by Kousa et al. [181], the modelling of air quality at urban traffic site was indeed more demanding compared to that for an urban background site.

For the period from 01.05.2007 to 30.04.2008, the model showed acceptable performance on the basis of 66 out of 79 correct predictions of PM_{10} daily exceedances on day_{d+1}, 62 out of 77 on day_{d+2}, and 64 out of 78 on day_{d+3} at the traffic site. The number of false alarms increased with the forecasted days; there were only 16 false alarms on day_{d+1} compared to 33 on day_{d+3}. The decrease in prediction accuracy with forecasted days could also be observed by the weaker *IS* value on day_{d+3}, with a lower score of 0.58 ± 0.26 compared to 0.69 ± 0.22 on day_{d+1}. Nevertheless, the PM_{10} Forecasting model scored high *A* values exceeding 0.85 on all three days. At the urban background site, although high *A* values exceeding 0.95 were computed, the model failed to spot any PM_{10} exceedance. As a result, all *IS* values were computed as zero.

The evaluation of all these performance indices demonstrated the importance of considering more than one performance index when assessing the model's performance. For instance, a high *IA* value does not necessary infer high accuracy of the model in predicting PM_{10} exceedances (high *A* value). Conversely, having the highest accuracy in predicting PM_{10} exceedances does not imply a high R^2 value. Thus, the statistical evaluation of the PM_{10} Forecasting model could only be complete by thoroughly examining all concerned performance indices.

To summarise, in regard to the statistical assessment of PM_{10} Forecasting models, it is highly recommended to select a model with the highest *IA* value, followed by the R^2 and subsequently the *A* values. With a high *IA* value, a good degree of agreement between the mean values of the modelled and measured PM_{10} concentrations can be assured. Although the R^2 value is widely used in statistical analyses to describe the variability between two sets of values, this performance index has its inherent flaw. As an example, a neural network model which only simulates a constant output value regardless of its input parameters and values will always score a perfect R^2 value of one. This happens when correlations between all input and output parameters of the neural network model cannot be established, a phenomenon which was previously documented by Khare and Nagendra [163]. While a high *A* value infers high accuracy in predicting PM_{10} exceedances, the trend of the modelled PM_{10} concentrations may not necessary be similar to the comparison measured PM_{10} values, since this performance index does not calculate the deviations (errors) between the modelled and measured values.

5.3.2 Scatter plots of modelled and measured PM_{10} concentrations

Modelled 24 h average PM_{10} concentrations at both traffic and urban background sites on day_{d+1}, day_{d+2} and day_{d+3} were regressed over measured data. The results of the analyses with 95 % confidence intervals are depicted in Fig. 5.12a to 5.12f respectively.

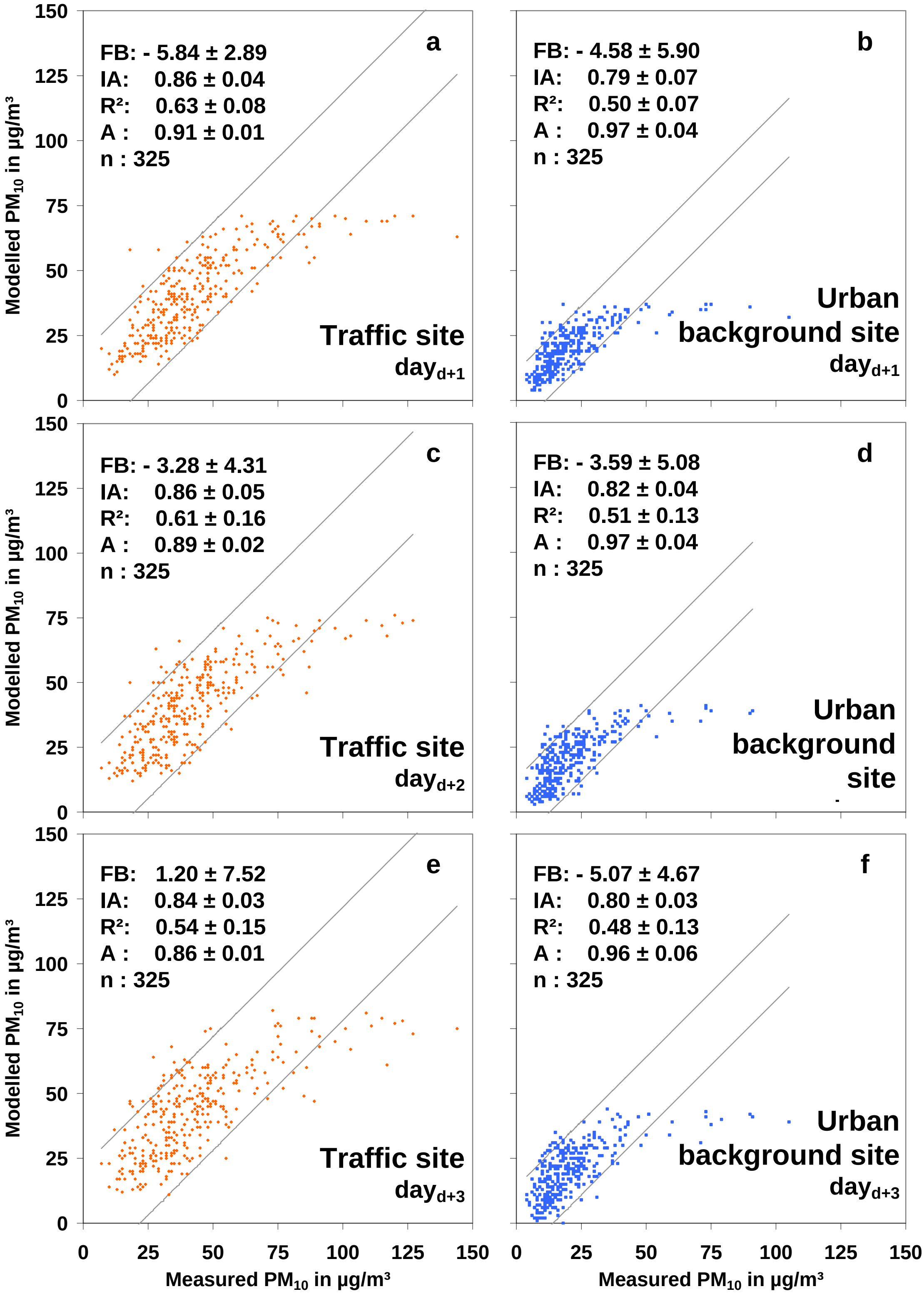

Fig. 5.12a-f: Scatter plots of modelled and measured 24 h average PM_{10} concentrations at the traffic and urban background sites with 95 % confidence intervals for the period 01.05.2005 to 30.04.2008 (from training, validation and test sets with deviations)

5.3.3 Time series of modelled and measured PM_{10} concentrations

The modelled and measured 24 h average PM_{10} concentrations at the traffic and urban background sites for the investigated period from 01.05.2007 to 30.04.2008 are presented in Fig. 5.13a to 5.13c and Fig. 5.14a to 5.14c respectively.

In general, the modelled PM_{10} concentrations were found to agree relatively well to the measured values. However, the underpredicting behaviour of the PM_{10} Forecasting model was revealed during periods with high PM_{10} concentrations originating from episodic events. The different types of episodic events which have been identified from 01.05.2007 to 30.04.2008 are described in the following chapters.

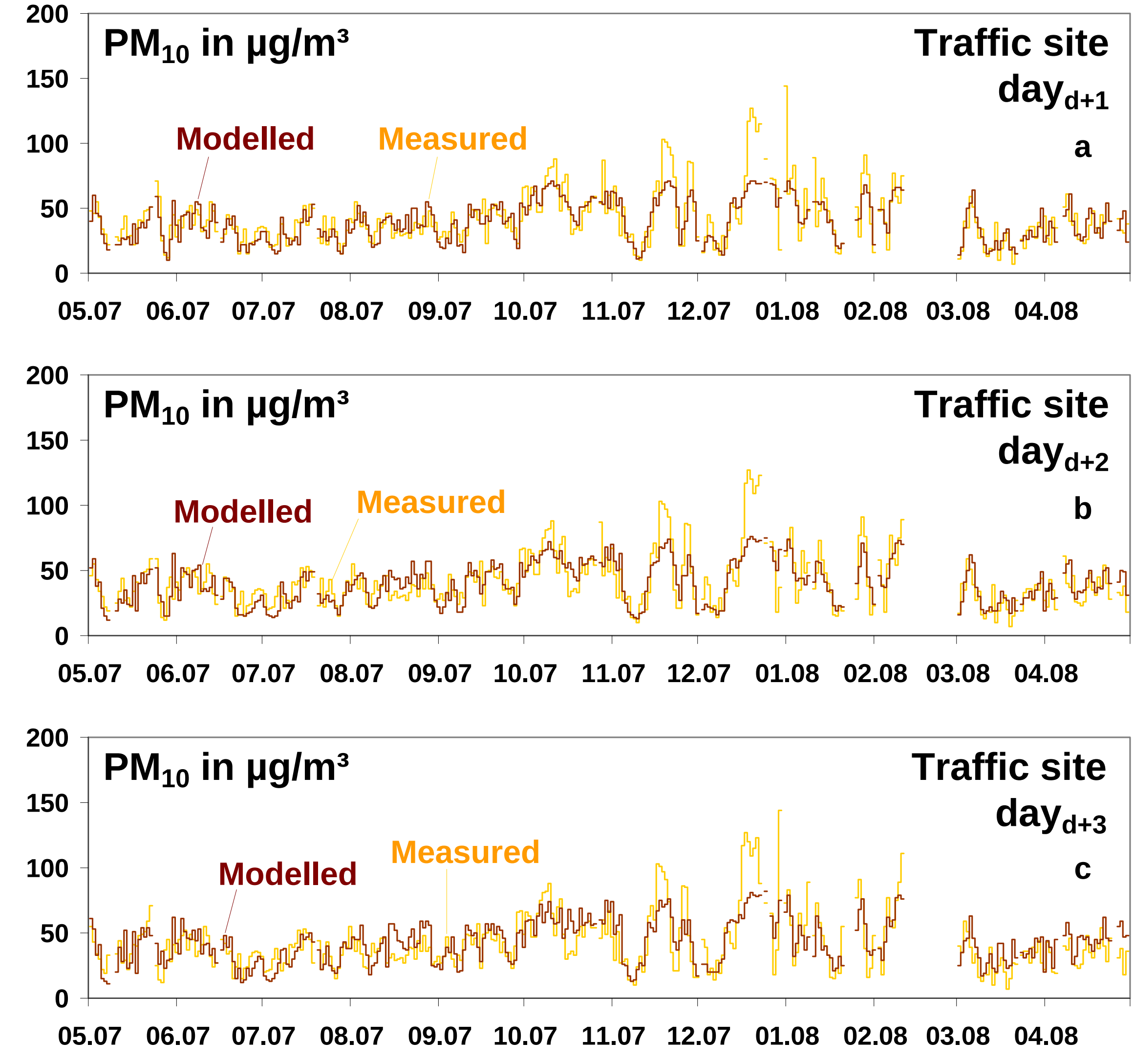

*: *Meteorological forecasts were not available from 11.02.2008 to 31.02.2008; modelling of PM_{10} concentrations was not performed for these days*

Fig. 5.13a-c: Modelled and measured 24 h average PM_{10} concentrations at the traffic site for day_{d+1}, day_{d+2} and day_{d+3}, 01.05.2007 to 30.04.2008

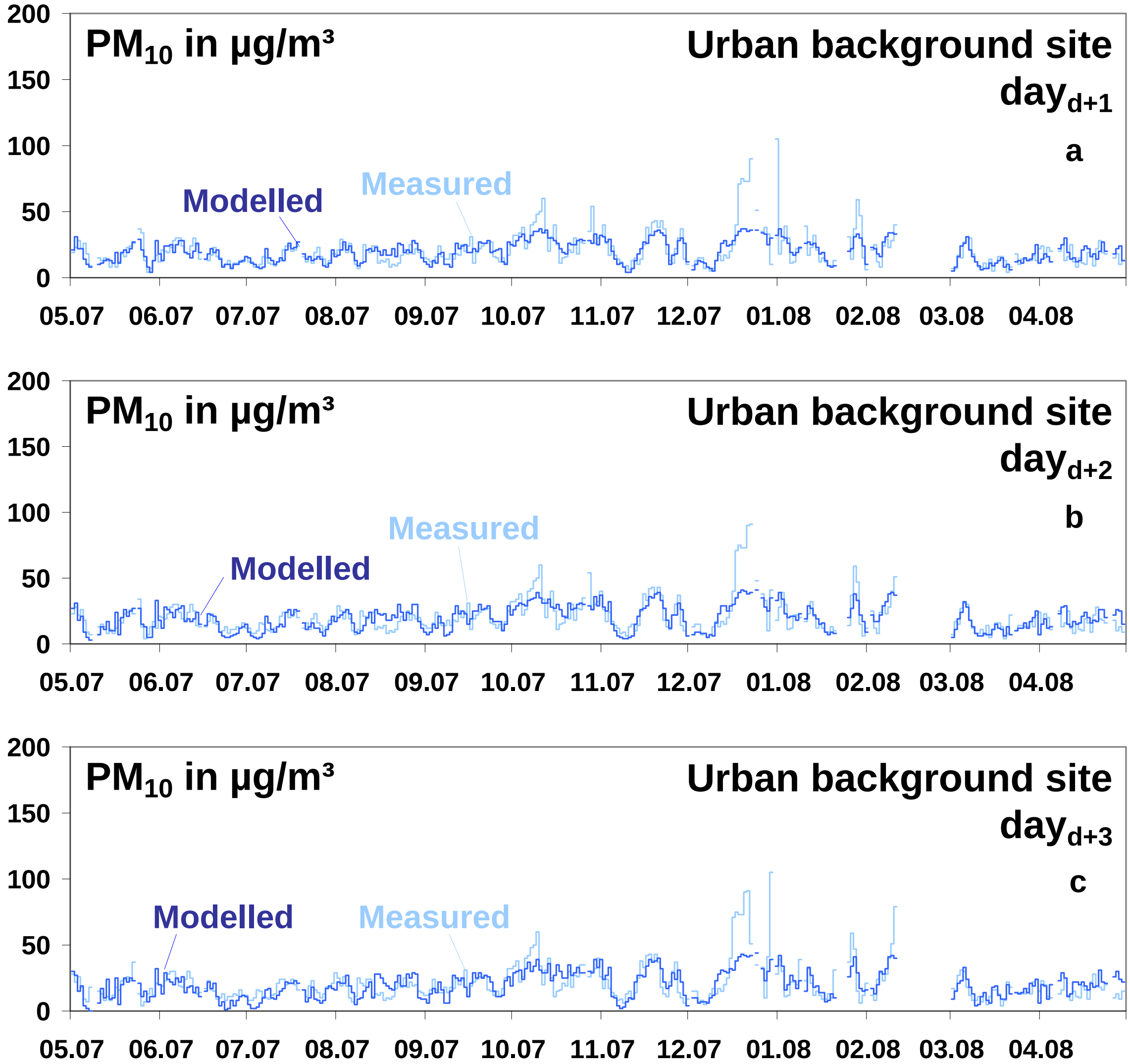

Fig. 5.14a-c: Modelled and measured 24 h average PM$_{10}$ concentrations at the urban background site for day$_{d+1}$, day$_{d+2}$ and day$_{d+3}$, 01.05.2007 to 30.04.2008

5.3.3.1 Wintertime inversion-induced PM$_{10}$ episodes

In Fig. 5.13a to 5.13c and Fig. 5.14a to 5.14c, two distinct inversion periods were identified in late December 2007 and late February 2008. The corresponding modelled and measured PM$_{10}$ concentrations for both inversion periods at the traffic and urban background sites are listed in Table 5.9 and Table 5.10.

During the first inversion period from 16.12.2007 to 30.12.2007, 24 h average PM$_{10}$ concentrations exceeding 100 µg/m³ were recorded in many parts of southern Germany [182]. Even in the Rheinland-Pfalz, such high PM$_{10}$ concentrations were very seldom encountered. From 23.12.2007 to 26.12.2007, the lowest mixing height level recorded at the Schnarrenberg weather station was below 400 m, with daily wind speed lower than 0.6 m/s at both traffic and urban background sites. During this period with relatively stable atmospheric conditions, the PM$_{10}$ Forecasting model underpredicted up to 50 % of the measured PM$_{10}$ concentrations at the traffic site, and up to 60 % of the measured PM$_{10}$ concentrations at the urban background site. In comparison to the PM$_{10}$ Nowcasting, the latter underpredicted only up to 30 % of the measured PM$_{10}$ concentrations during the selected inversion episodes (see Table 5.3).

Table 5.9: Modelled and measured 24 h average PM_{10} concentrations during an inversion period from 16.12.2007 to 30.12.2007 at the traffic and urban background sites

Site	Modelled PM_{10} in µg/m³			Measured PM_{10} in µg/m³	PM_{10} underprediction ratio		
	day$_{d+1}$	***day$_{d+2}$***	***day$_{d+3}$***		***day$_{d+1}$***	***day$_{d+2}$***	***day$_{d+3}$***
16.12.2007							
Traffic	41	42	39	38	1.1	1.1	1.0
Urban background	15	15	20	20	0.8	0.8	1.0
17.12.2007							
Traffic	58	57	58	58	1.0	1.0	1.0
Urban background	18	19	19	25	0.7	0.8	0.8
18.12.2007							
Traffic	63	61	64	75	0.8	0.8	0.7
Urban background	32	30	32	40	0.8	0.8	0.8
19.12.2007							
Traffic	69	68	61	117	0.6	0.6	0.5
Urban background	35	35	31	71	0.5	0.5	0.4
20.12.2007							
Traffic	71	74	73	127	0.6	0.6	0.6
Urban background	37	39	38	75	0.5	0.5	0.5
21.12.2007							
Traffic	71	76	77	120	0.6	0.6	0.6
Urban background	37	41	41	73	0.5	0.6	0.6
22.12.2007							
Traffic	69	74	81	109	0.6	0.7	0.7
Urban background	35	40	43	73	0.5	0.5	0.6
23.12.2007							
Traffic	69	72	79	115	0.6	0.6	0.7
Urban background	36	38	42	90	0.4	0.4	0.5
24.12.2007							
Traffic	-	73	78	123	-	0.6	0.6
Urban background	-	39	41	91	-	0.4	0.5
25.12.2007							
Traffic	70	-	79	88	0.8	-	0.9
Urban background	36	-	42	51	0.7	-	0.8
26.12.2007							
Traffic	-	75	-	71	-	1.1	-
Urban background	-	41	-	48	-	0.9	-
27.12.2007							
Traffic	69	-	82	73	0.9	-	1.1
Urban background	34	-	34	35	1.0	-	1.0
28.12.2007							
Traffic	68	68	-	72	0.9	0.9	-
Urban background	33	35	-	38	0.9	0.9	-
29.12.2007							
Traffic	51	57	63	65	0.8	0.9	1.0
Urban background	25	28	32	33	0.8	0.8	1.0
30.12.2007							
Traffic	18	16	16	18	1.0	0.9	0.9
Urban background	9	8	9	10	0.9	0.8	0.9

Table 5.10: Modelled and measured 24 h average PM_{10} concentrations during an inversion period from 26.01.2008 to 31.01.2008 at the traffic and urban background sites

Site	Modelled PM_{10} in µg/m³			Measured PM_{10} in µg/m³	PM_{10} underprediction ratio		
	day$_{d+1}$	*day$_{d+2}$*	*day$_{d+3}$*		*day$_{d+1}$*	*day$_{d+2}$*	*day$_{d+3}$*
26.01.2008							
Traffic	41	-	-	51	0.8	-	-
Urban background	20	-	-	31	0.6	-	-
27.01.2008							
Traffic	22	20	-	28	0.8	0.7	-
Urban background	12	10	-	14	0.9	0.7	-
28.01.2008							
Traffic	61	53	52	77	0.8	0.7	0.7
Urban background	31	27	26	37	0.8	0.7	0.7
29.01.2008							
Traffic	68	71	68	91	0.7	0.8	0.7
Urban background	33	38	34	59	0.6	0.6	0.6
30.01.2008							
Traffic	62	64	76	76	0.8	0.8	1.0
Urban background	30	33	41	47	0.6	0.7	0.9
31.01.2008							
Traffic	41	35	37	38	1.1	0.9	1.0
Urban background	14	12	15	15	0.9	0.8	1.0

During the second inversion period from 26.01.2008 to 31.01.2008, the PM_{10} underprediction ratios were, on average, slightly higher compared to the first inversion period; indicating that the magnitude of prediction errors was related to the strength of the inversion; the stronger the inversion, the larger the errors. The lowest mixing height recorded was below 700 m, and the highest PM_{10} concentrations were 91.0 µg/m³ and 59.0 µg/m³ at the traffic and background sites respectively. Low wind speeds of 0.4 m/s at the traffic site, and 0.6 m/s at the urban background site were measured on 29.01.2008, which coincided on the day with the maximum PM_{10} concentrations. From these results, the high PM_{10} concentrations could be associated with typical inversion weather conditions: low mixing heights with cold temperature on the ground and warmer air mass above, combined with very low wind speeds over a period of several days. With these weather conditions, the air mass above ground remains stagnant and the measured PM_{10} concentrations subsequently increase through the accumulation of air pollutants. For the PM_{10} Nowcasting model, the influence of temperature inversions on the modelled PM_{10} concentrations was better taken into account in comparison to the PM_{10} Forecasting model. During an inversion, it can be expected that the concentrations of other air pollutants increase with PM_{10}. In the case of the former model, such air pollutants included NO and NO_2 from Neckartor, and PM_{10}, NO and NO_2 from Bad Cannstatt. Therefore, the inclusion of these model input parameters can clearly improve the overall prediction accuracy for the PM_{10} Nowcasting. In the case of the PM_{10} Forecasting, the model emulated an improved PM_{10} persistence model (see Fig. 4.9a to 4.9c), with which only the persistence behaviour of PM_{10} concentrations on day_d and the accuracies of the forecasted meteorological parameters on day_{d+1}, day_{d+2} and day_{d+3} were used in simulating PM_{10} concentrations during inversion periods. As a result, the extend of underprediction with the PM_{10} Forecasting was greater than the PM_{10} Nowcasting.

5.3.3.2 Festive PM_{10} pollution episodes

One distinct PM_{10} pollution episode which was caused by the usage of fireworks was dated on 01.01.2008, on which the measured 24 h average PM_{10} concentrations were 144 µg/m³ at the traffic site, and 105 µg/m³ at the urban background site. The modelled and measured PM_{10} concentration on 01.01.2008 for day_{d+1}, day_{d+2} and day_{d+3} at the traffic and urban background sites are listed in Table 5.11 accordingly. The effect of fireworks on the ambient PM_{10} concentrations can be denoted by the η_2 value, which was described earlier by Eq. (5.3). Based on results in Table 5.11, fireworks has a greater influence on the measured PM_{10} concentrations at the urban background site compared to the values at the traffic site. This could be attributed to the closer proximity of the location of pyrotechnic displays to where the PM_{10} concentrations were measured at the urban background site. At the urban background site, η_2 values for day_{d+1} and day_{d+3} were 228.1 % and 169.2 %, whilst the corresponding values at the traffic site were 128.9 % and 95.0 % accordingly.

Table 5.11: Modelled and measured PM_{10} concentrations on 01.01.2008 for day_{d+1}, day_{d+2} and day_{d+3} at the traffic and urban background sites; η_2 effect due to fireworks

Site	Modelled PM_{10} in µg/m³	Measured PM_{10} in µg/m³	η_2 in %
day_{d+1}			
Traffic	63	144	128.9
Urban background	32	105	228.1
day_{d+2} *			
Traffic	-	144	-
Urban background	-	105	-
day_{d+3}			
Traffic	75	144	95.0
Urban background	39	105	169.2

η_2: effect due to fireworks

**: Measured PM_{10} concentrations at the traffic and urban background sites were not available on 30.12.008 (day_d) for batch modelling; modelling of PM_{10} concentrations on 31.12.2007 (day_{d+1}), 01.01.2008 (day_{d+2}), and 02.01.2008 (day_{d+3}) with reference to 30.12.2008 (day_d) was not performed*

5.3.3.3 Regional and long-range PM_{10} transport

As back trajectory analysis of PM_{10} was not performed for the period from 01.05.2007 to 30.04.2008 in this dissertation, it was not possible to discern from the results if the regional and long-range PM_{10} transport was responsible for any of the PM_{10} episodes during the investigation period. Nevertheless, the possibility of such occurrence should not be omitted.

5.3.4 Error residuals

The error residuals of the PM_{10} Forecasting model for the investigated period from 01.05.2007 to 30.04.2008 at the traffic and urban background sites for day_{d+1}, day_{d+2} and day_{d+3}, are presented in Fig. 5.15a to 5.15c, and Fig. 5.16a to 5.16c respectively. By comparing the error residuals between the two sites, the magnitude of errors at the traffic site was significantly greater than at the urban background site. A possible explanation to this discrepancy could be the exposure of the traffic site to varying traffic loads, which was clearly absent at the urban background site. Even though the expected traffic loads for day_{d+1}, day_{d+2} and day_{d+3} were considered as model input parameters, the deviations between the actual and expected values could still be substantial. In general, the prediction error of PM_{10} concentrations for a site with a higher variability of PM_{10} loads (e.g. traffic) can be expected to be higher compared to sites with less varying PM_{10} concentration courses (background).

At both sites, the underprediction behaviour of the PM_{10} Forecasting was clearly demonstrated from 16.12.2007 to 30.12.2007, and on 01.01.2008, as the model was unable to accurately simulate the additional PM loads from episodic events with the considered input parameters.

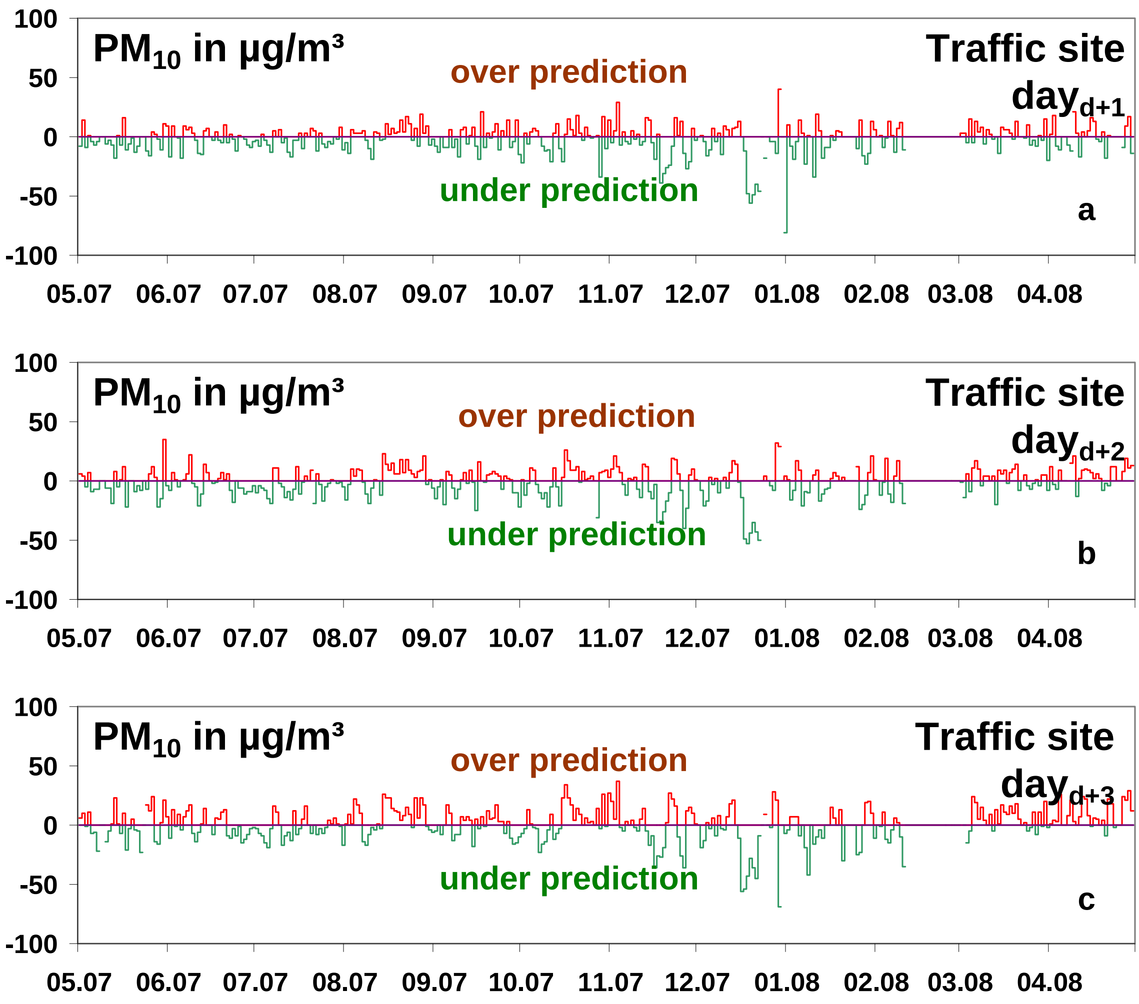

Fig. 5.15a-c: Error residuals of modelled 24 h average PM_{10} concentrations at the traffic site for day_{d+1}, day_{d+2} and day_{d+3} from 01.05.2007 to 30.04.2008

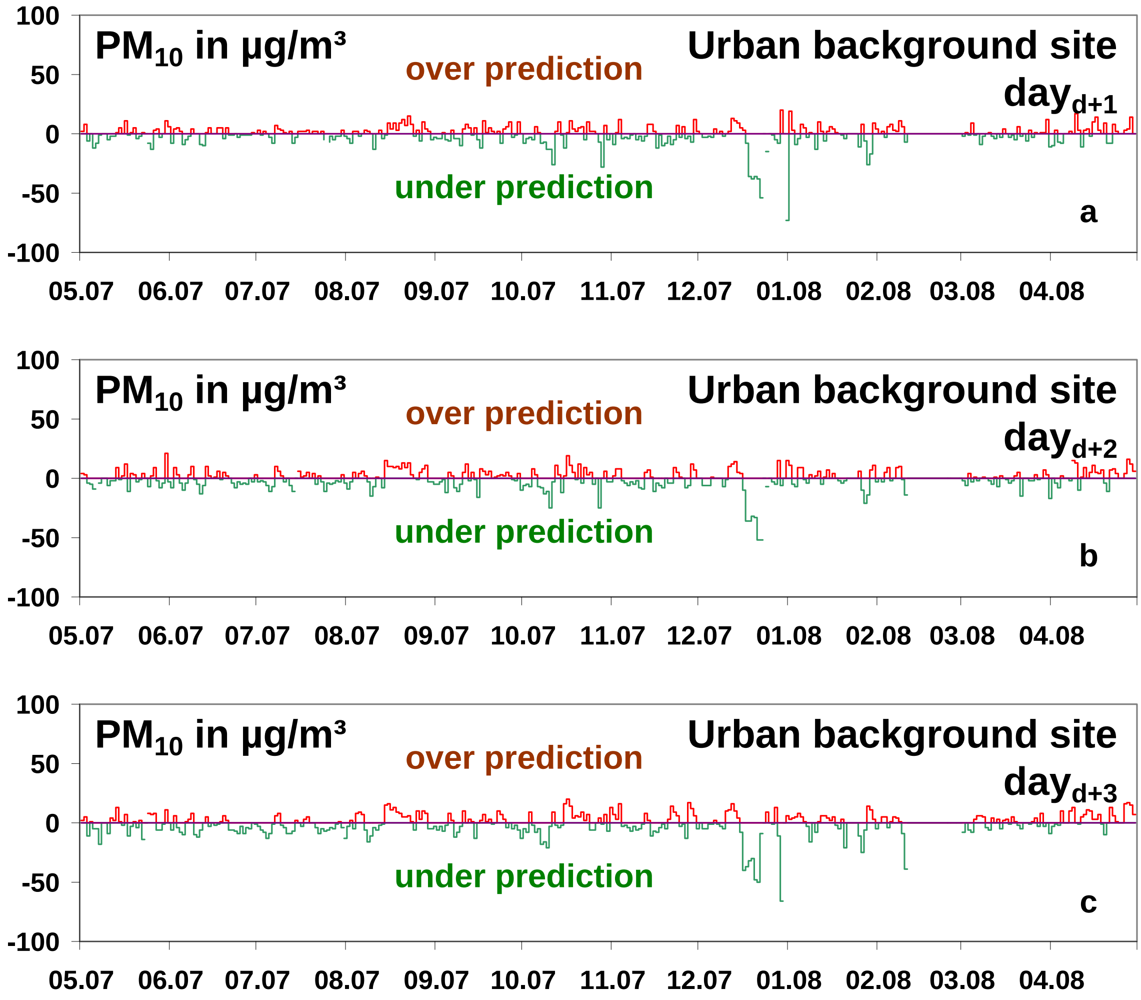

Fig. 5.16a-c: Error residuals of modelled 24 h average PM_{10} concentrations at the urban background site for day_{d+1}, day_{d+2} and day_{d+3} for the period 01.05.2007 to 30.04.2008

The ratio of the modelled PM_{10} to the measured PM_{10} concentrations for day_{d+1}, day_{d+2} and day_{d+3} at the traffic and urban background sites from 01.05.2007 to 30.04.2008 are depicted in Fig. 5.17. For a good model, the median should be close to 1 and 50 % of the ratio should be within a factor of 2 [180].

The smaller gaps between the 16^{th} and 84^{th} percentiles for the traffic site on day_{d+1}, day_{d+2} and day_{d+3} indicated that the PM_{10} Forecasting model achieved on average a closer agreement between the modelled PM_{10} concentrations and the measured values at the traffic site than at the urban background site. In general, the ratio of the modelled PM_{10} to the measured PM_{10} concentrations increased with the forecasted days at both sites. These observations were anticipated due to the inherent characteristics of forecasted meteorological parameters with days; the longer the forecast periods, the larger the error. Nevertheless, a comparable range of ratios of modelled PM_{10} to measured PM_{10} concentrations was computed for both sites, with medians ranging from 0.97 to 1.00.

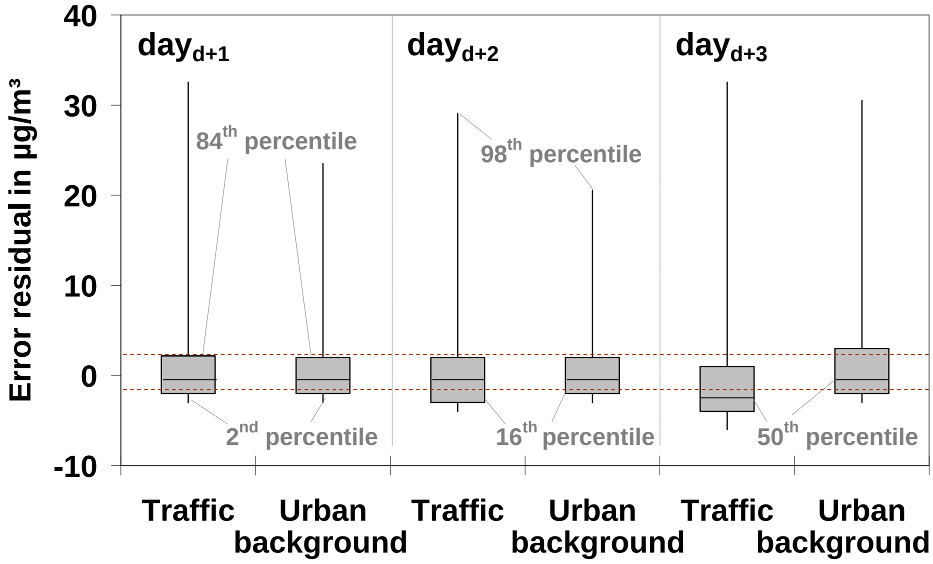

Fig. 5.17: 2nd, 16th, 50th, 84th and 98th percentiles of ratio between modelled PM_{10} and measured PM_{10} concentrations

5.3.4.1 Frequency distributions of error residuals

Histograms of the PM_{10} error residuals for the traffic and urban background sites for day$_{d+1}$, day$_{d+2}$ and day$_{d+3}$ are depicted in Fig. 5.18a to 5.18f respectively.

The similar fourteen class intervals, which were described earlier for the PM_{10} Nowcasting model, were also identified here. In an ideal situation, the difference between the modelled and measured PM_{10} concentrations would be close to zero. At the traffic site, the histograms showed that the PM_{10} forecasts on day$_{d+1}$, day$_{d+2}$ and day$_{d+3}$ exhibited single modal distributions of PM_{10} error residuals. Compared to day$_{d+1}$ and day$_{d+2}$, the data for day$_{d+3}$ exhibited considerable left-skewness with a higher frequency of PM_{10} residuals in the interval class of -30 µg/m³, indicating lower modelled PM_{10} concentrations on day$_{d+3}$.

At the urban background site on day$_{d+1}$, day$_{d+2}$ and day$_{d+3}$, the PM_{10} forecasts were more or less normally distributed, which can be seen by the almost-symmetrical bell-shaped curve along the centre of the data distribution at 0 µg/m³. On day$_{d+1}$, more than 86 % of the PM_{10} error residuals fell between ± 10 µg/m³ with respect to 0 µg/m³. On day$_{d+2}$ and day$_{d+3}$, the percentages were calculated as 83 % and 82 % respectively. The corresponding values calculated at the traffic site were significantly lower, with 67 % on day$_{d+1}$, 64 % on day$_{d+2}$, and 57 % on day$_{d+3}$.

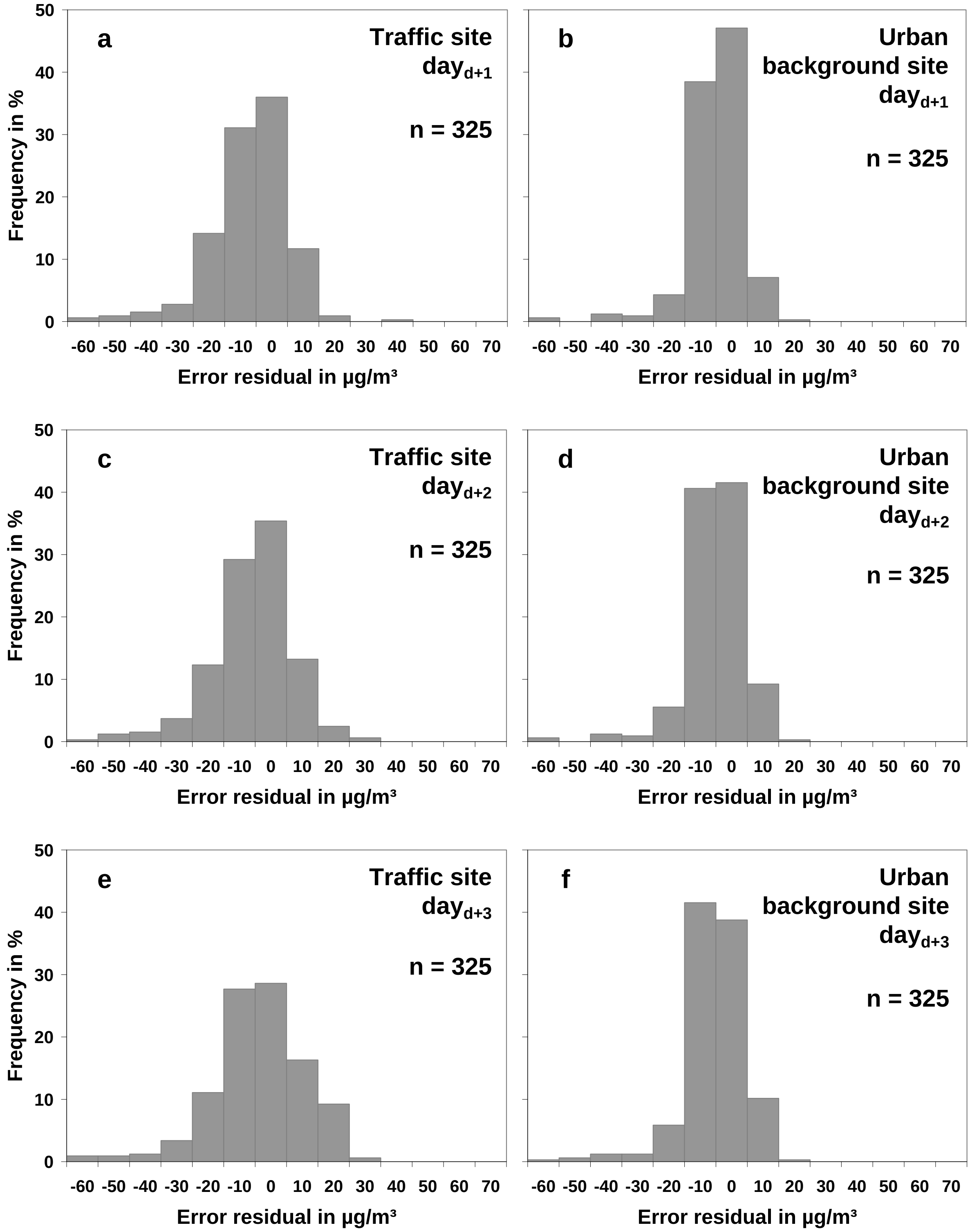

Fig. 5.18a-f: Histograms of error residuals for the traffic and urban background sites for day$_{d+1}$, day$_{d+2}$ and day$_{d+3}$ for the period 01.05.2007 to 30.04.2008

5.3.5 Quantile-quantile plots

The quantile-quantile plots of the modelled 24 h average PM_{10} concentrations against the measured PM_{10} concentrations for day_{d+1}, day_{d+2} and day_{d+3} at the traffic and urban background sites from 01.05.2007 to 30.04.2008 are depicted in Fig. 5.19a to 5.19f.

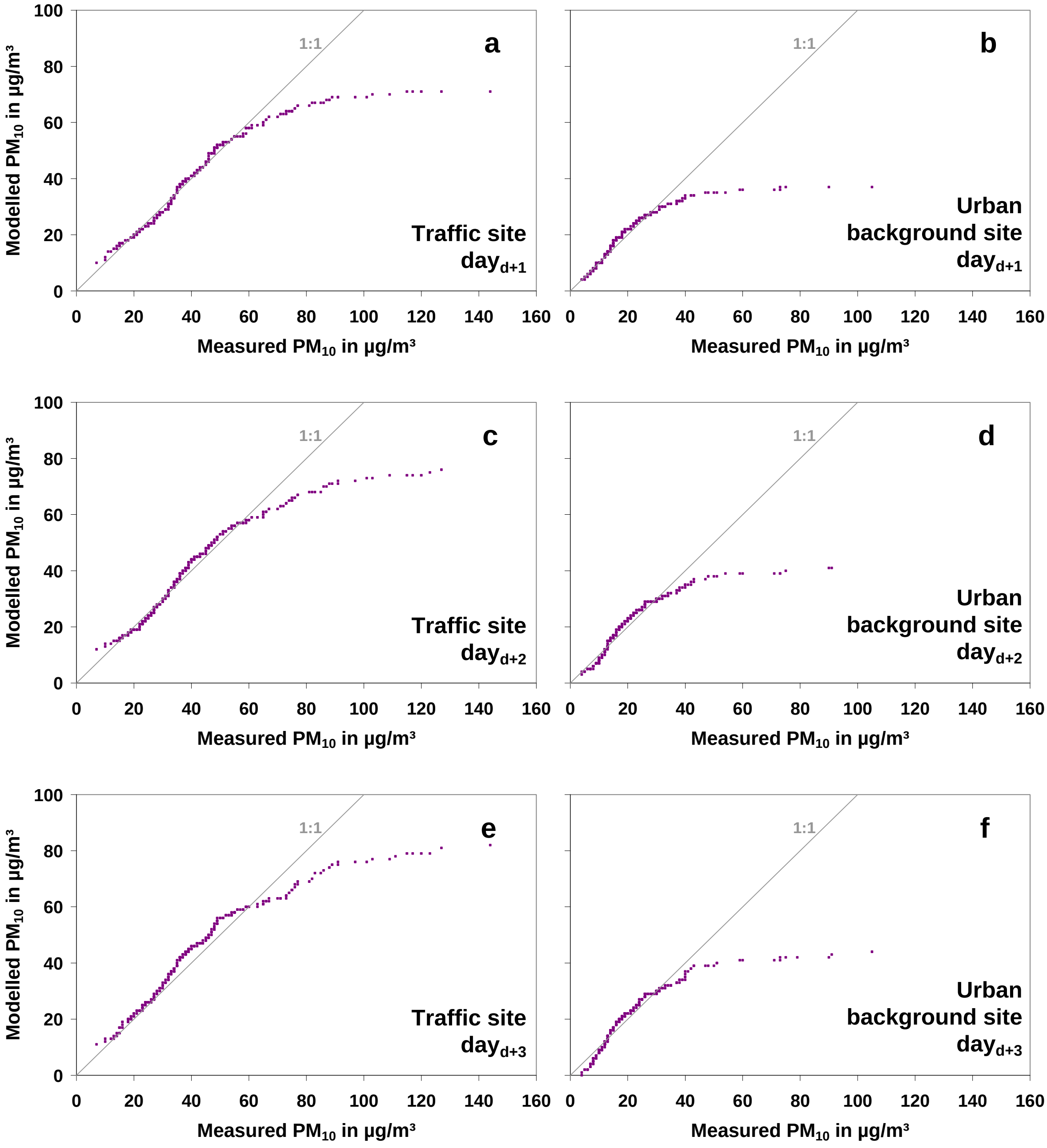

Fig. 5.19a-f: Quantile-quantile plots of modelled 24 h average PM_{10} concentrations against measured PM_{10} concentrations at the traffic and urban background sites for day_{d+1}, day_{d+2} and day_{d+3} for the period 01.05.2007 to 30.04.2008

The quantile-quantile plots indicated that the PM_{10} Forecasting model did a reasonable good job in simulating PM_{10} concentrations with rather similar frequency distributions to the measured PM_{10} concentrations, except for the higher values. Scattering of the data points around the ideal line 1:1 increased at the right ends of the plots. The effect of PM_{10} episodes on the underestimating behaviour of the model could be observed for both the traffic and urban background sites. The reasons were described earlier for the single events. At the traffic site, the underprediction behaviour of the PM_{10} Forecasting model began to show at concentrations higher than 61 µg/m³ for all three days of forecast. At the urban background site, this phenomenon became obvious for concentrations higher than 33 µg/m³. In comparison to the PM_{10} Nowcasting model, agreement between the modelled and measured values from the quantile-quantile plot was observed up to 100 µg/m³ (see Fig. 5.8). The better agreement in values for the PM_{10} Nowcasting model could probably be explained by the fact that the Nowcasting model input parameters were more effective in simulating the PM_{10} concentrations in comparison to the Forecasting model.

To have a better understanding on the distributions of data set, the six quantiles, namely q_{10}, q_{25}, q_{50}, q_{75}, q_{85} and q_{90}, were identified and evaluated. The results are listed in Table 5.12 accordingly. Based on Table 5.12, the best modelling results for the traffic and urban background sites were obtained before the 85th quantile; beyond that underpredictions of PM_{10} were observable at both sites.

Table 5.12: Quantiles of modelled and measured PM_{10} concentrations

Quantiles	Traffic site		Urban background site	
	Modelled PM_{10} in µg/m³	**Measured PM_{10} in µg/m³**	**Modelled PM_{10} in µg/m³**	**Measured PM_{10} in µg/m³**
day_{d+1}				
q_{10}	20	21	9	9
q_{25}	27	28	13	13
q_{50}	39	38	19	17
q_{75}	52	49	26	25
$\boldsymbol{q_{85}}$	**60**	**61**	**29**	**31**
q_{90}	63	71	31	35
day_{d+2}				
q_{10}	19	20	7	9
q_{25}	27	28	12	12
q_{50}	40	37	20	17
q_{75}	52	49	27	25
$\boldsymbol{q_{85}}$	**61**	**60**	**30**	**30**
q_{90}	62	69	32	35
day_{d+3}				
q_{10}	22	20	7	9
q_{25}	29	28	12	12
q_{50}	43	38	20	18
q_{75}	55	49	27	25
$\boldsymbol{q_{85}}$	**61**	**62**	**31**	**31**
q_{90}	63	72	33	37

5.3.6 Cross-correlation coefficients of model input parameters to modelled PM_{10} concentrations

As explained earlier, the cross-correlation coefficient was computed to investigate the linear relationship between the respective model input parameters to the corresponding modelled PM_{10} concentrations (see Eq. (5.5)). The cross-correlation coefficient is 1 in the case of an increasing perfect linear relationship, −1 in the case of a decreasing perfect linear relationship. The closer the coefficient is to either −1 or 1, the stronger the correlation between the variables. If the variables are independent, the cross-correlation coefficient is 0, but the converse is not true because the correlation coefficient detects only linear dependencies between two variables.

The cross correlation coefficients of all model input parameters with respect to the modelled PM_{10} concentrations at the traffic and urban background sites on day_{d+1}, day_{d+2} and day_{d+3} are summarised in Table 5.13 to 5.15 respectively.

At both sites, the model input parameter PM_{10} (measured value) on day_d showed high cross-correlation coefficients to the modelled PM_{10} concentrations for all three forecasted days. On day_{d+1}, the highest correlation could be explained by the persistent behaviour of ambient PM_{10} concentrations on the previous day (day_d). In the presence of continuous surface inversions, the accumulation of ambient PM_{10} loads from the previous day may be resulted [146, 147]. As a consequence, the modelled PM_{10} concentrations, especially on day_{d+1}, could be very much influenced by the input parameter PM_{10} concentrations on day_d. This phenomenon is expected to be more prominent during the colder months of the year, during which the persistent behaviour of PM_{10} concentrations may even last for several days. In line with the results from the PM_{10} persistence models described earlier (see Fig. Fig. 4.9a to 4.9c), slight positive correlations between the measured PM_{10} (day_d) and PM_{10} (day_{d+2} and day_{d+3}) were also observed.

Under stable atmospheric conditions, there is minimal vertical dispersion of traffic-induced PM_{10} loads above the ground surface. Thus, the traffic flows on day_{d+1}, day_{d+2} and day_{d+3} can be expected to be directly proportional to the modelled PM_{10} concentrations respectively. However, low cross-correlation coefficients between the traffic flows and modelled PM_{10} concentrations were computed for all three days of forecasts; suggesting that the influence of expected traffic flows as the model's input parameters were not as significant as originally anticipated. This is not surprising since the traffic flow is more or less constant at the traffic site, apart from weekend (see Fig. 4.12).

The negative cross-correlation coefficients between the forecasted rainfall and the modelled PM_{10} concentrations at both sites highlighted the "cleaning" effect of rainfall on ambient PM_{10}. In general, the more amount of rainfall, the lower the concentrations of PM_{10}.

The results from evaluating the cross-correlation coefficients between the forecasted temperature, global radiation and wind speed to the modelled PM_{10} concentrations were consistent with the observations that elevations of ambient PM_{10} concentrations occur predominantly in the colder months, during which periods of low ambient temperature, high atmospheric pressure and little wind support the formation of temperature inversions.

Contrary to expectation, the model input parameter mixing height (day_d) had little to no influence on the predicted PM_{10} (day_{d+1}). The mixing height data were established using the radio sounding data from the Schnarrenberg monitoring station, which is located 79 m higher

Table 5.13: Cross-correlation coefficients of all model input parameters to modelled PM_{10} concentrations on day_{d+1} for the period 01.05.2007 to 30.04.2008

Site	Input parameters from measurements and forecasts	Cross-correlation coefficient
Traffic site PM_{10}, day_{d+1}		
Neckartor (traffic)	PM_{10}, day_d	0.68
	Traffic flow, day_{d+1}	0.16
Bad Cannstatt (urban background)	PM_{10}, day_d	0.65
Schnarrenberg* (weather station)	Mixing height, day_d	-0.07
Numerical Mesoscale Model (weather forecaster)	Temperature, day_{d+1}	-0.26
	Rainfall, day_{d+1}	-0.28
	Global radiation, day_{d+1}	-0.15
	Wind speed, day_{d+1}	-0.60
Urban background site PM_{10}, day_{d+1}		
Bad Cannstatt (urban background)	PM_{10}, day_d	0.69
Schnarrenberg (weather station)	Mixing height, day_d	-0.06
Numerical Mesoscale Model (weather forecaster)	Temperature, day_{d+1}	-0.21
	Rainfall, day_{d+1}	-0.23
	Global radiation, day_{d+1}	-0.13
	Wind speed, day_{d+1}	-0.53

Table 5.14: Cross-correlation coefficients of all model input parameters to modelled PM_{10} concentrations on day_{d+2} for the period 02.05.2007 to 30.04.2008

Site	Input parameters from measurements and forecasts	Cross-correlation coefficient
Traffic site PM_{10}, day_{d+2}		
Neckartor (traffic)	PM_{10}, day_d	0.52
	Traffic flow, day_{d+2}	0.20
Bad Cannstatt (urban background)	PM_{10}, day_d	0.50
Schnarrenberg* (weather station)	Mixing height, day_d	-0.05
Numerical Mesoscale Model (weather forecaster)	Temperature, day_{d+2}	-0.23
	Rainfall, day_{d+2}	-0.31
	Global radiation, day_{d+2}	-0.13
	Wind speed, day_{d+2}	-0.60
Urban background site PM_{10}, day_{d+2}		
Bad Cannstatt (urban background)	PM_{10}, day_d	0.56
Schnarrenberg (weather station)	Mixing height, day_d	0.01
Numerical Mesoscale Model (weather forecaster)	Temperature, day_{d+2}	-0.20
	Rainfall, day_{d+2}	-0.28
	Global radiation, day_{d+2}	-0.11
	Wind speed, day_{d+2}	-0.53

Table 5.15: Cross-correlation coefficients of all model input parameters to modelled PM_{10} concentrations on day_{d+3} for the period 03.05.2007 to 30.04.2008

Site	Input parameters from measurements and forecasts	Cross-correlation coefficient
Traffic site PM_{10}, day_{d+3}		
Neckartor (traffic)	PM_{10}, day_d	0.42
	Traffic flow, day_{d+3}	0.15
Bad Cannstatt (urban background)	PM_{10}, day_d	0.41
Schnarrenberg* (weather station)	Mixing height, day_d	-0.03
Numerical Mesoscale Model (weather forecaster)	Temperature, day_{d+3}	-0.21
	Rainfall, day_{d+3}	-0.28
	Global radiation, day_{d+3}	-0.15
	Wind speed, day_{d+3}	-0.51
Urban background site PM_{10}, day_{d+3}		
Bad Cannstatt (urban background)	PM_{10}, day_d	0.46
Schnarrenberg (weather station)	Mixing height, day_d	0.02
Numerical Mesoscale Model (weather forecaster)	Temperature, day_{d+3}	-0.21
	Rainfall, day_{d+3}	-0.25
	Global radiation, day_{d+3}	-0.13
	Wind speed, day_{d+3}	-0.46

in elevation than the Neckartor monitoring station. Thus, accurate representation of the mixing heights (if any) of air pollutants lower than the Schnarrenberg station could be questionable and likely lead to the weak cross-correlation coefficients. In general, it is expected that lower mixing height will result in higher pollutant loads in the ambient air.

To summarise, the results in Table 5.13 to 5.15 show that the persistent behaviour of ambient PM_{10} concentrations on day_d had the highest linear correlation to the modelled PM_{10} concentrations for all three forecasted days at both the traffic and urban background site. Among the considered forecasted meteorological parameters, wind speed exhibited the highest anti-linear correlation behaviour to the modelled PM_{10} concentrations.

5.3.7 Test and improvement of PM_{10} Forecasting model

The main drawback of the developed PM_{10} Forecasting model is its inability to accurately simulate PM_{10} concentrations during episodic events during the investigated period from 02.05.2007 to 30.04.2008. At the traffic site, the maximum measured PM_{10} concentration was 144 µg/m³ on 14.08.2007, while the corresponding modelled value was 82 µg/m³. At the urban background site, the maximum measured and modelled values were 105 µg/m³ and 44 µg/m³ respectively (see Fig. 5.12a to 5.12f and Fig. 5.19a to 5.19f).

To address the underprediction problem of the PM_{10} Forecasting, two different approaches in improving the PM_{10} Forecasting accuracy during episodic events could be adopted. The first method is the so-called boosting, which refers to increasing the frequency of extreme values in the training process by reserving most or all of the available episodes for the training set in order to improve the ability of the neural network model to identify their characteristics [183, 184]. The second method is the so-called bagging, which refers to including each episode case more times in the training data set [184, 185].

5.3.7.1 Results from boosting method

In this dissertation, a simplified boosting method was in fact used in the development of the PM_{10} Forecasting model (see Annex C2 for data distributions in the training, validation and test sets). In regard to neural network modelling, it is important to assess the quality of the independent test data set, as this data set can be used to determine the generalisation error of the model. In the case of the developed PM_{10} Forecasting model, the shortcoming of the boosting training method was that high PM_{10} concentrations were not reflected in the test set as these values were all reserved for the training data set. Nevertheless, the highest PM_{10} concentrations were still intentionally reserved for the training data set for two reasons. As neural network models will fail to extrapolate on data which have not been presented during the training procedure, it is recommended that the training data set should consist of extreme training values [95]. As for the second reason, a diversity of training data set will ensure that the model is adequately trained to respond to a larger number of input data variations, in the expectation that the PM_{10} Forecasting can cover all the possible behaviours of the model input parameters under study.

As a comparison model, a test PM_{10} Forecasting model which was not trained with the boosting method was developed. The data for the training, validation and test sets were distributed in a way that all three data sets possessed similar data distributions, i.e. data containing low and high PM_{10} concentrations was equally divided among the three sets. The number of hidden nodes for this test model was varied from one to fifteen, and selected performance indices, such as the *FB* (fractional boas), *IA* (index of agreement), R^2 (correlation coefficient) and *A* (overall accuracy) values, were computed. A network topology of fourteen hidden nodes was eventually derived, based on the highest *IA* value, followed by the R^2 and subsequently the *A* values.

In Fig. 5.20a to 5.20f, the modelled PM_{10} concentrations from the test set for day_{d+1}, day_{d+2} and day_{d+3} at the traffic and urban background sites were regressed over the corresponding measured data. The results of the analyses with the combined training and validation sets are included in Annex C3. Based on results from the test sets, it can be deduced that the boosting method did little to improve the prediction accuracy of the PM_{10} Forecasting model, as the overall *IA*, R^2 and *A* values were comparable to the corresponding values which were computed for the original model trained with the boosting method (see Fig. 5.12a to 5.12f).

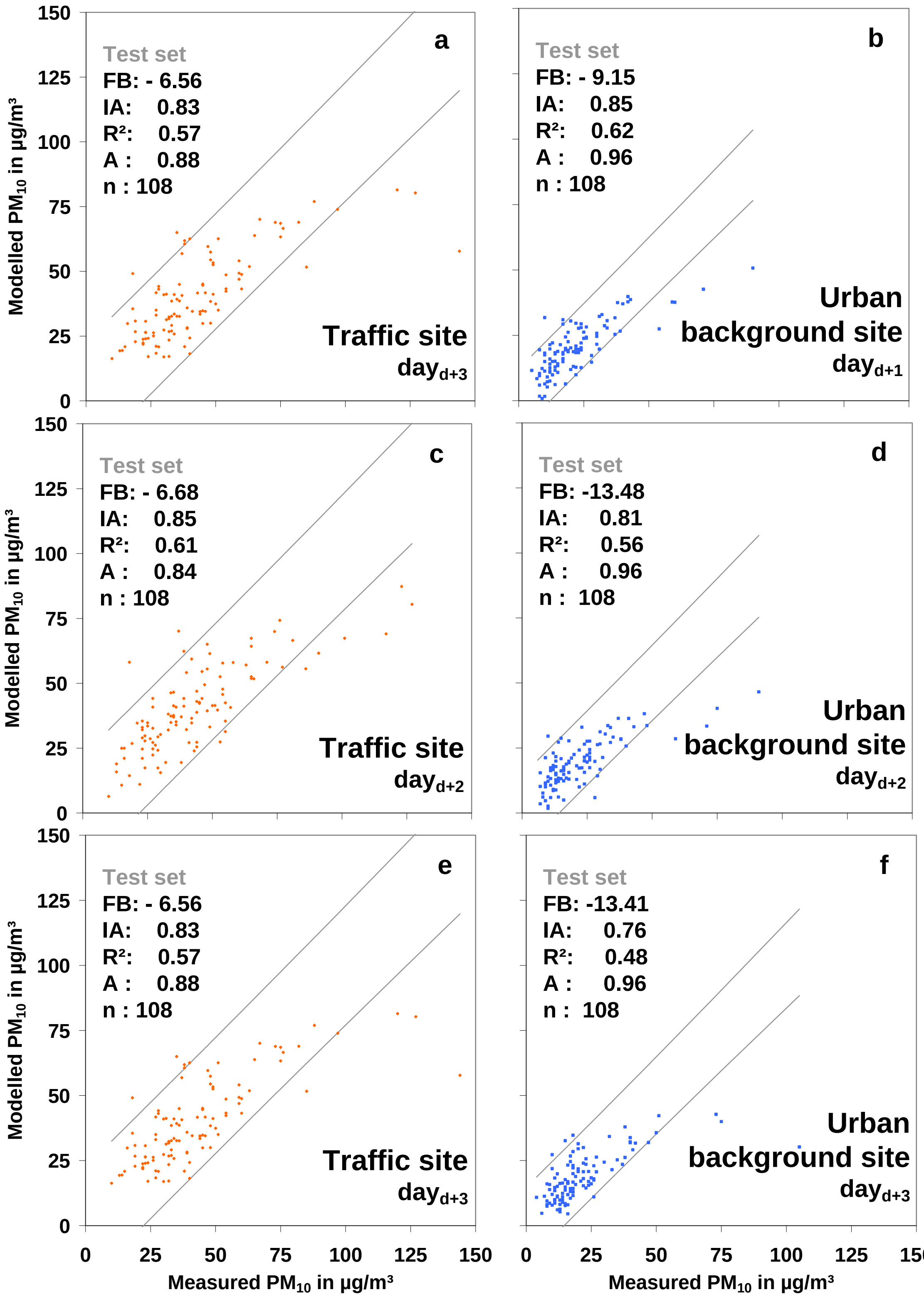

Fig. 5.20a-f: **Boosting method:**
Scatter plots of modelled and measured 24 h average PM_{10} concentrations at the traffic and urban background sites with 95 % confidence intervals for the period 01.05.2005 to 30.04.2008 (from test set only)

In Fig. 5.21a to 5.21c, and Fig. 5.22a to 5.22c, the error residuals of the test model for the investigated period from 01.05.2007 to 30.04.2008 at the traffic and urban background sites for day_{d+1}, day_{d+2} and day_{d+3}, are presented respectively. Although the trends of the temporal courses for the error residuals were somewhat similar to those depicted in Fig. 5.15a to 5.15c, and Fig. 5.16a to 5.16c, the computation of the average PM_{10} values revealed the differences.

In Table 5.16, the average PM_{10} overprediction and underprediction values over the entire investigation period are listed. These averages were calculated based on results from the Forecasting model trained with the boosting method, and as well as from the test model. The overprediction of average PM_{10} concentrations with both models were of the same magnitude for all three days of forecasts; the differences ranged from 0.19 µg/m³ to 0.52 µg/m³ at the traffic site, and 0.07 µg/m³ to 0.18 µg/m³ at the urban background site. The effect of the boosting training method became evident when comparing the average underprediction values; the magnitudes of underprediction with the test model were clearly greater compared to the model trained with the boosting method. This discrepancy can be explained by the training process of the former model, during which more weights are assigned to the rare observations containing high PM_{10} concentrations that are more difficult to simulate. In the

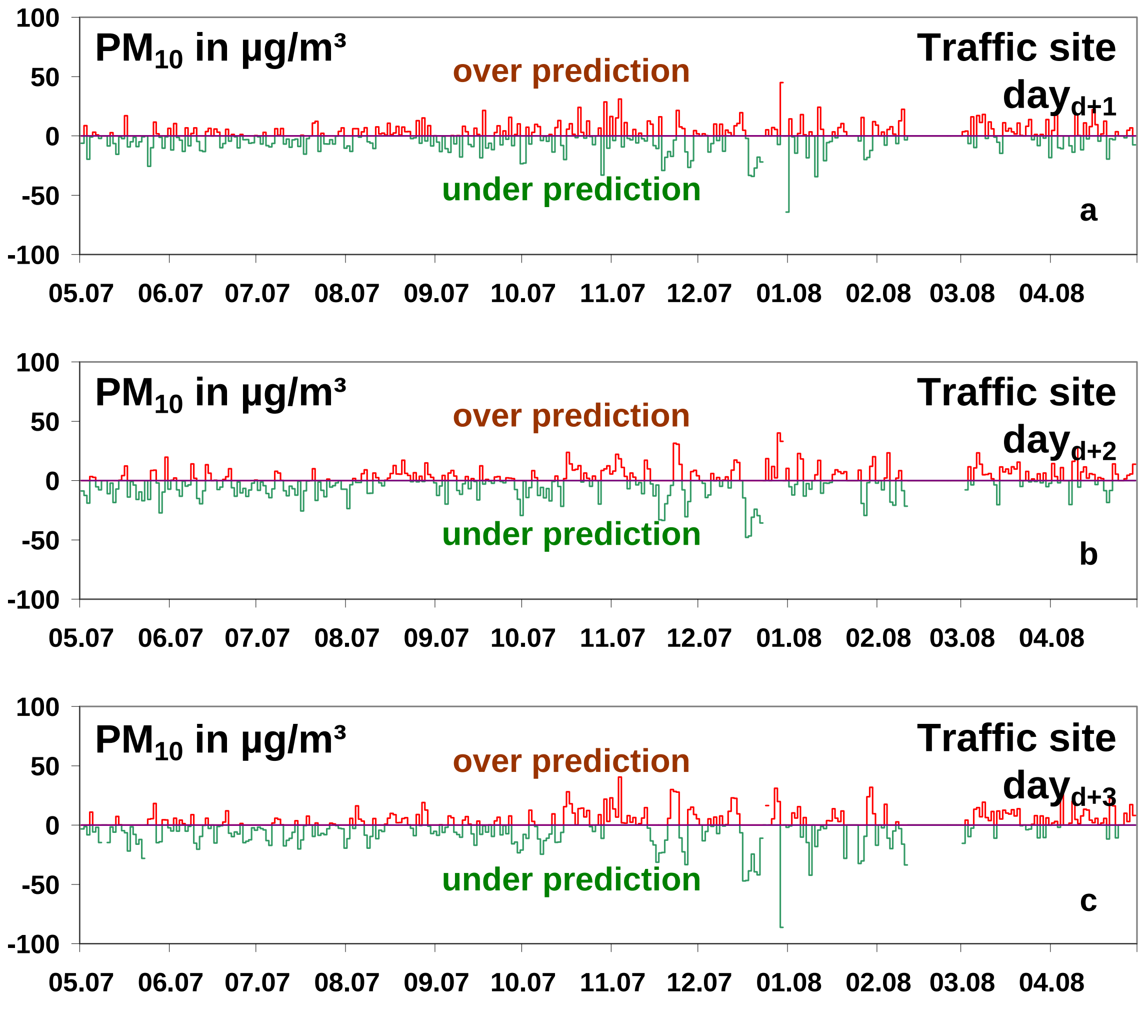

Fig. 5.21a-c: Error residuals of modelled 24 h average PM_{10} concentrations at the traffic site for day_{d+1}, day_{d+2} and day_{d+3} for the period 01.05.2007 to 30.04.2008

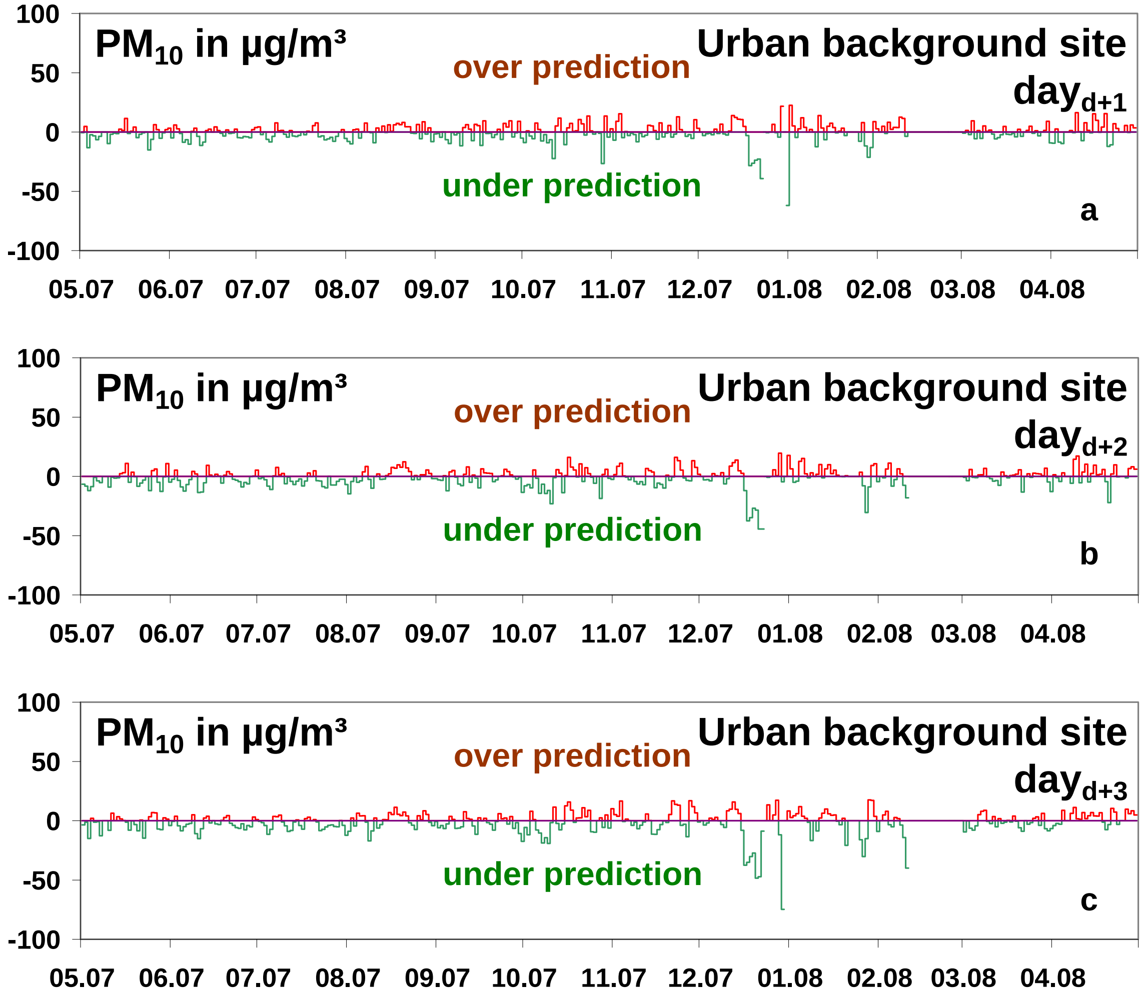

Fig. 5.22a-c: Error residuals of modelled 24 h average PM_{10} concentrations at the urban background site for day_{d+1}, day_{d+2} and day_{d+3} for the period 01.05.2007 to 30.04.2008

Table 5.16: Average PM_{10} overprediction and underprediction values for the period 01.05.2007 to 30.04.2008

Site	**Average PM_{10} concentrations in µg/m³**			
	PM_{10} Forecasting model *trained with boosting method*		**PM_{10} Forecasting model** *with similar data distribution in training, validation and test sets*	
	Overprediction	**Underprediction**	**Overprediction**	**Underprediction**
day_{d+1}				
Traffic	7.85	-9.35	7.61	-11.26
Urban background	5.29	-5.63	5.22	-7.26
day_{d+2}				
Traffic	8.43	-9.83	8.62	-11.47
Urban background	5.10	-6.48	5.28	-7.05
day_{d+3}				
Traffic	9.06	-10.38	9.58	-11.55
Urban background	5.42	-6.87	6.54	-7.79

case of the test model, the model was unable to respond to these observations as effectively as the former as only a third of the highest PM_{10} values were allocated to the training data set. As a result, although both models were unable to simulate high PM_{10} concentrations accurately during inversion periods, the boosting method improved the overall predictions slightly, as shown by lower average PM_{10} underprediction values. Nevertheless, good agreements between the lower modelled and measured PM_{10} concentrations were observed with both models.

5.3.7.2 Results from bagging method

To investigate on the effect of bagging on the quality of PM_{10} predictions, a second test PM_{10} Forecasting model was developed, and double inclusion of nine exemplary episodic cases (without influence from fireworks) on 10.10.2007, 18.11.2007, 21.11.2007, 22.11.2007, 27.11.2007, 18.12.2007, 27.01.2008, 13.01.2008 and 10.02.2008 in the training data set was performed. On these nine days, the 24 h average PM_{10} concentrations on day_{d+1} exceeded 73 µg/m³ at the traffic site, and 30 µg/m³ at the urban background site. For the validation and test sets, the data distributions were rearranged; each consisting of six data sets with 24 h average PM_{10} concentrations on day_{d+1} exceeding 83 µg/m³ at the traffic site, and 37 µg/m³ at the urban background site. The number of hidden nodes for this test model was varied from one to fifteen, and the best performing test model was eventually derived with a network topology of thirteen hidden nodes.

In Fig. 5.23a to 5.23f, the modelled PM_{10} concentrations from the test set for day_{d+1}, day_{d+2} and day_{d+3} at the traffic and urban background sites were regressed over the corresponding measured data. The results of the analyses with the combined training and validation sets are included in Annex C4. With the bagging method, the test model exhibited a similar tendency to underpredict, as indicated by the negative *FB* values. The overall *IA* values improved slightly, and the model was also able to capture a little more variability in the PM_{10} measured concentrations based on the improved R^2 value. For the test model, it is also worth mentioning that the number of correct predictions of 24 h average PM_{10} exceedances improved at the urban background site.

In Fig. 5.24a to 5.24c, and Fig. 5.25a to 5.25c, the error residuals of the test model for the investigated period from 01.05.2007 to 30.04.2008 at the traffic and urban background sites for day_{d+1}, day_{d+2} and day_{d+3}, are presented respectively. Based on the results, the occurrences of PM_{10} underprediction were still distinguishable during continuous temperature inversion periods at both studied sites, even when using the bagging training method.

In Table 5.17, the average PM_{10} overprediction and underprediction values over the entire investigation period are listed. Results from the first test model (with similar data distribution for the training, validation and test sets) were used as reference. The evaluations showed that the model which was trained with the bagging method overpredicted the PM_{10} concentrations by 8.04 µg/m³ to 9.79 µg/m³ at the traffic site, and 5.23 µg/m to 6.85 µg/m³ at the urban background site. In comparison to the reference model, the difference in overprediction for all three days of forecast ranged from 0.21 µg/m³ to 0.43 µg/m³ at the traffic site, and 0.01 µg/m³ to 0.39 µg/m³ at the urban background site. When considering the underprediction values, the average concentrations ranged from -8.94 µg/m³ to -10.13 µg/m³ at the traffic site, and -5.44 µg/m³ to -7.29 µg/m³ at the urban background site. This implied that the double inclusion of data with high PM_{10} concentrations in the training set did improve the overall prediction accuracy of PM_{10} concentrations during episodic events to a small extent. However, it should be emphasised that the data which were doubled for the model training set were only limited

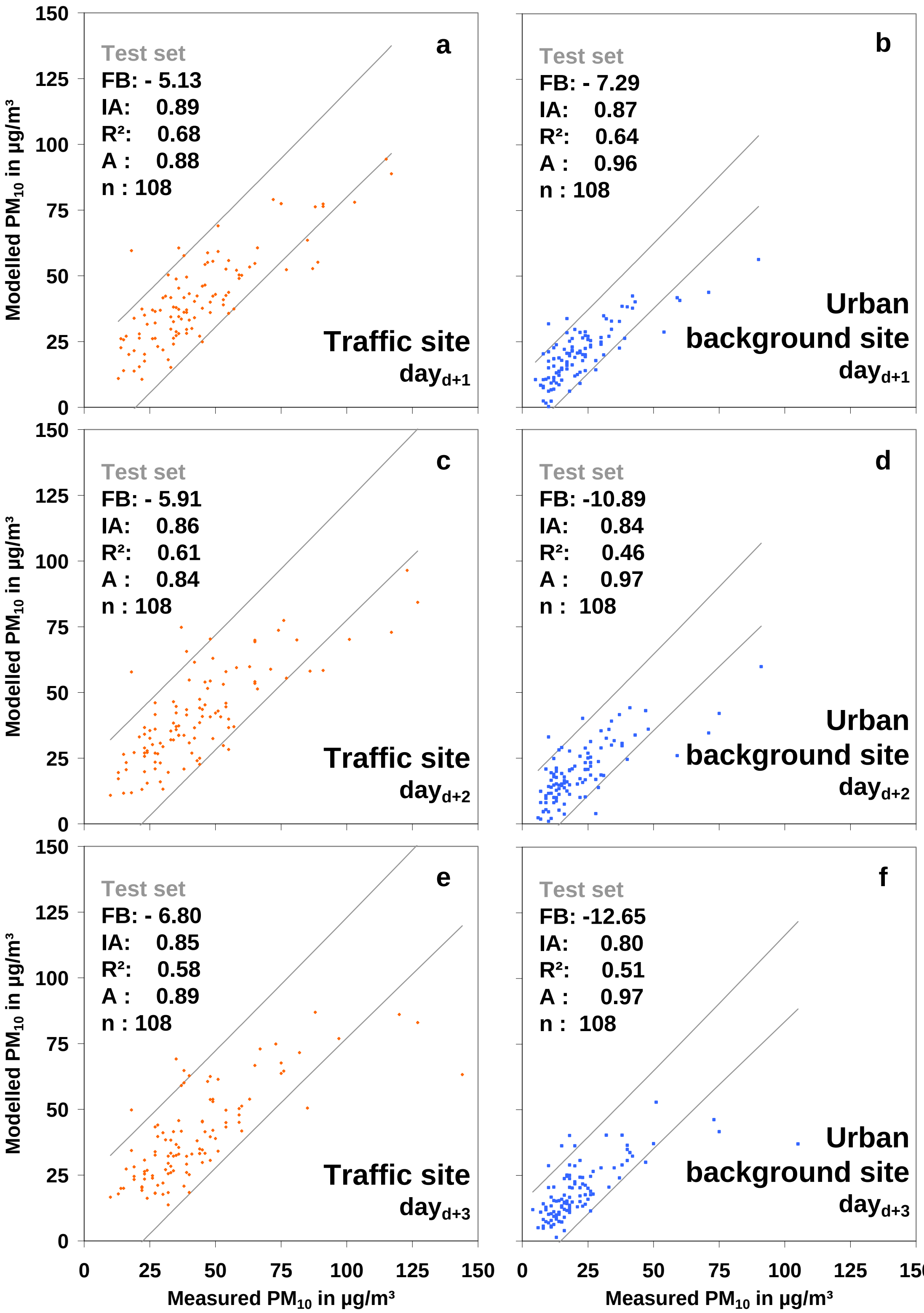

Fig. 5.23a-f: **Bagging method:**
Scatter plots of modelled and measured 24 h average PM_{10} concentrations at the traffic and urban background sites with 95 % confidence intervals for the period 01.05.2005 to 30.04.2008 (from test set only)

to nine. Although more data could be included, caution has to be made for the application of the bagging method. The biggest influence on the model's prediction accuracy strongly depends on the quality of the limited but yet important data with high PM_{10} concentrations during inversions. In a situation whereby the build-up of high PM_{10} concentrations (due to additional local loads or single events) cannot be adequately described by the model input parameters, the weight assigned during the training process with this type of occasions can be expected to low. However, doubling or tripling of such events in the training set implies that larger erroneous weight will now be assigned with the increase in frequency of days with high PM_{10} concentrations. As a result, overprediction of the lower PM_{10} concentrations could eventually be resulted.

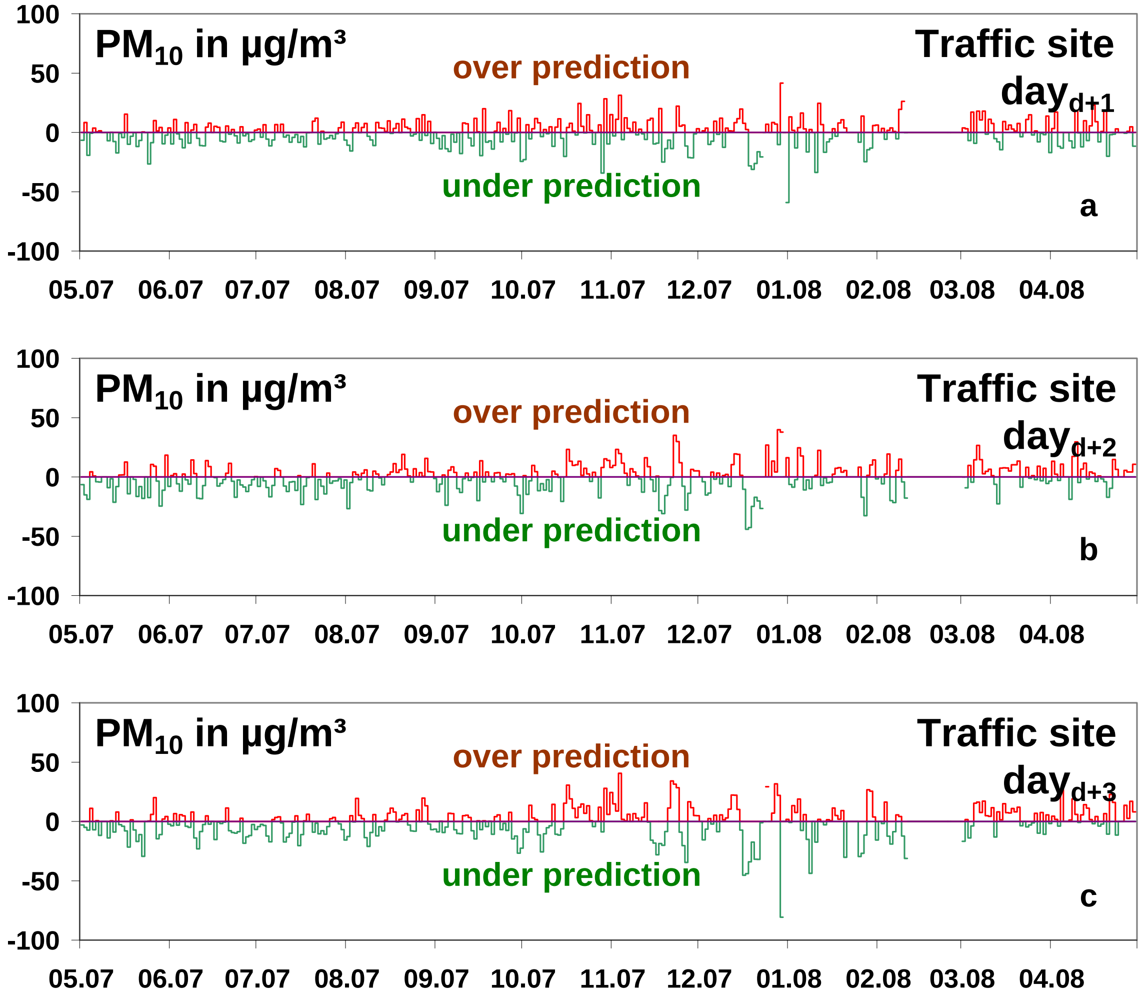

Fig. 5.24a-c: Error residuals of modelled 24 h average PM_{10} concentrations at the traffic site for day_{d+1}, day_{d+2} and day_{d+3} for the period 01.05.2007 to 30.04.2008

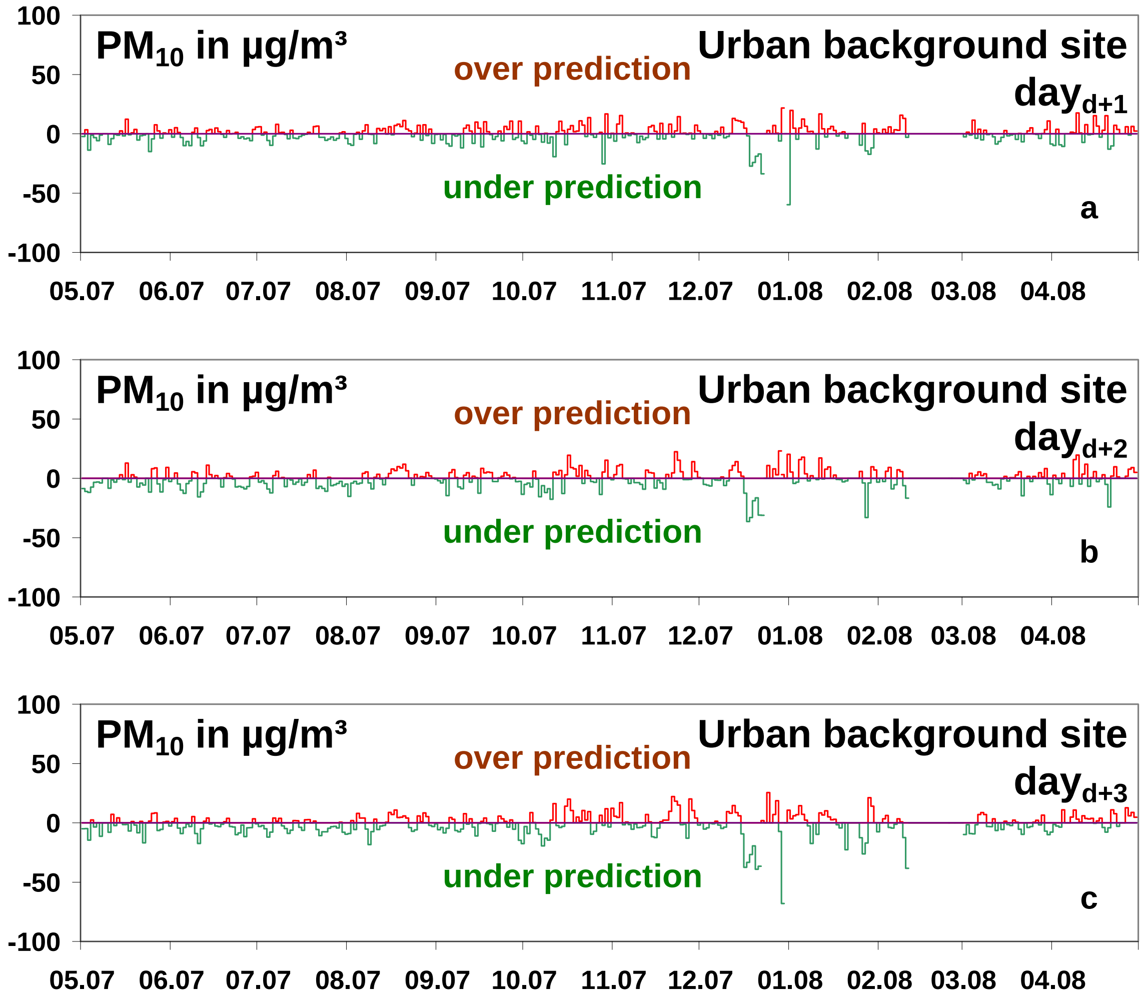

Fig. 5.25a-c: Error residuals of modelled 24 h average PM_{10} concentrations at the urban background site for day_{d+1}, day_{d+2} and day_{d+3} for the period 01.05.2007 to 30.04.2008

Table 5.17: Average PM_{10} overprediction and underprediction values for the period 01.05.2007 to 30.04.2008

Site	Average PM_{10} concentrations in µg/m³			
	PM_{10} Forecasting model *trained with bagging method*		**PM_{10} Forecasting model** *with similar data distribution in training, validation and test sets*	
	Overprediction	**Underprediction**	**Overprediction**	**Underprediction**
day_{d+1}				
Traffic	8.04	-8.94	7.61	-11.26
Urban background	5.23	-5.44	5.22	-7.26
day_{d+2}				
Traffic	8.89	-9.65	8.62	-11.47
Urban background	5.67	-6.27	5.28	-7.05
day_{d+3}				
Traffic	9.79	-10.13	9.58	-11.55
Urban background	6.86	-7.29	6.54	-7.79

5.3.8 Conclusions

An objective of this dissertation was to utilise readily available meteorological forecasts such as wind characteristics, amount of precipitation and radiation as input parameters for a PM_{10} neural network Forecasting model. The benefits of developing such a model are two-folds. Firstly, the modelled results could act as both an alarm for bad weather (from the weather forecaster) and the quality of ambient air (from the PM_{10} Forecasting model). Secondly, the information derived from the model could also aid in public education. The overall PM_{10} Forecasting's results illustrated a possibility of effective use on the operational level for performing future PM_{10} forecasts up to three days at both the traffic and urban background sites. However, the accuracy in simulating high PM_{10} concentrations during continuous temperature inversions was not as satisfactory.

Two neural network training methods could be adopted to improve the overall accuracy in PM_{10} predictions. The first method is a simplified boosting method, which involves the reservation of data containing days with the highest PM_{10} concentrations as the training set for the model. This method has its drawback, as days with high PM_{10} concentrations during inversions will not be reflected at all in the test set. Nevertheless, the reason for the application of the boosting training method is not unfounded. By reserving data with high PM_{10} concentrations in the training set, the developed model will be adequately trained to respond to a larger number of input data variations, in the expectation that the model can cover all the possible behaviours of the input parameters under study. Based on this type of model training method, the overall prediction accuracy of PM_{10} concentrations was found to be slightly better compared to a reference model, which was not trained with the boosting method.

The second method is a simplified bagging method, which involves the doubling of limited events with high PM_{10} concentrations in the training set. It was found that the double inclusion of these data in the training set did improve the overall prediction accuracy of PM_{10} concentrations during inversions to a small extent. However, the accuracy in PM_{10} predictions depends largely on the quality of the few but yet important data which are multiplied in the training set. On one hand, it is necessary that the PM_{10} Forecasting model is able to predict high PM_{10} concentrations accurately during inversions. On the other hand, it is also important that the low PM_{10} concentrations are correctly simulated. Therefore, caution has to be made when selecting the data to be multiplied in the training set, as the accuracy in predicting lower PM_{10} concentrations could be compromised when the data quality in describing high PM_{10} concentrations during temperature inversions is dubious. A possible outcome is the overprediction of lower PM_{10} concentrations due to the erroneous assignment of weights to the higher values.

To conclude, although both training methods could be used in improving the overall prediction accuracy of high PM_{10} concentrations during inversions, the bagging training method was, to some extent, superior to the boosting training method. For the first training method (boosting), the main limitation lies with the few data with high PM_{10} concentrations measured during temperature inversions. Although all these data were reserved for the training set, it was still not possible to accurately simulate the high values for all three days of forecast on both study sites. For the second training method (bagging), the constraint with the limited sets can be easily overcome by multiplying the inclusion of such data. Therefore, there is a possibility that the prediction accuracy could be further improved by repeating more data of high PM_{10} concentrations in the training set. In another words the training data set of the model could be modified to achieve different results.

6 Summary and conclusions

The problem of air pollution is a frequently recurring situation and its management has considerable social and economic effects. On one hand, air pollution control is necessary to prevent the situation from worsening in the long run. On the other hand, forecasting of air quality in days in advance is also necessary in order to adopt preventive and evasive actions during episodes of airborne pollutions.

Dedicated research, technological developments and concerted action have brought air quality modelling in the mainstream of air quality assessment and management. For instance, neural network models can be used as a useful and effective tool for the modelling of complex and poorly understood processes that occur in nature, as they are able to self-extract functional relationships between model inputs and outputs from the data set, without requiring explicit consideration on the actual data generation process. Neural network models are capable of learning to model a relationship during a supervised training procedure, when they are repeatedly presented with series of input and associated output data. In the case of modelling ambient air pollutant concentrations, the input data could consist of measurements of meteorological or air quality data from measurements, and the outputs would be the air pollutant concentration.

In this dissertation, the objectives were to simulate present and future PM_{10} concentrations at urban sites by means of using neural network modelling. For that, two models were developed for PM_{10} Nowcasting and PM_{10} Forecasting.

The two neural network models developed in this dissertation were trained using the backpropagation algorithm. Training involves finding the set of network weights which enable the models to best represent the underlying patterns in the training data set. This is achieved by minimising the overall networks' errors, for all input patterns, with respect to the associated networks' output patterns. In the scope of this dissertation, the resilient backpropagation method was used for the development of the neural networks.

To conduct a thorough and insightful evaluation on the modelled PM_{10} concentrations, a range of performance indices is necessary. The common indices which were used for both the PM_{10} Nowcasting and PM_{10} Forecasting models included the fractional bias (*FB*), the index of agreement (*IA*), the squared correlation coefficient (R^2), the mean absolute error (*MAE*), the mean bias error (*MBE*) and the root mean square error (*RMSE*). For the PM_{10} Forecaster model, additional performance indices to evaluate the correct number of PM_{10} exceedances, false alarms and PM_{10} missed exceedances were considered: the index of success (*IS*), the false alarm value (*FAR*) and the overall accuracy (*A*).

For both models, thorough analyses of the error residuals and quantile-quantile plots were performed for the identification of possible outliers, and for the better understanding in the patterns across the two sets of univariate modelled and measured data.

PM_{10} Nowcasting: From 15.11.2006 to 18.03.2007, a modified mechanical broom and water wash street sweeper was operated along the paved roadway at the Stuttgart Neckartor site. Based on results from single particle analyses and measurements of PM and NO_X concentrations, reductions in ambient PM_{10} concentrations could be suggested. However, an exact quantitative evaluation on the effectiveness of street sweeping was complicated by the possible influence of different meteorological conditions and other unknown effects during sweeping and non-sweeping days. With the neural network approach, these influencing meteorological conditions can be parameterised as functions to PM_{10} concentrations. The PM_{10} Nowcasting model (Multiple-Input Single-Output model) was therefore developed as a tool to simulate the past measurements of PM_{10} concentrations during the street sweeping periods, assuming that no street sweeping would take place.

The parameterised input variables included daily measurement data of air pollutants (excluding PM_{10}) and meteorological parameters from three LUBW ambient air monitoring stations and one meteorological station in Stuttgart. The aim of the developed model is to Nowcast the corresponding 24 h average PM_{10} concentrations at Neckartor during street sweeping days. Based on the modelling results, any positive effects of street sweeping as an ambient PM_{10} abatement strategy at Neckartor would be suggested by higher modelled PM_{10} concentrations in comparison to the corresponding measured PM_{10} values during street sweeping days. Conversely, no influence on the ambient PM_{10} concentrations after street sweeping would be implied by similar or lower modelled PM_{10} concentrations than the measured values.

Through extensive statistical evaluation on the performance of the developed PM_{10} Nowcasting model, it was shown that the model was capable of accurately simulating the daily PM_{10} concentrations from 03.01.2004 to 14.11.2006 at Neckartor. The PM_{10} Nowcasting was subsequently applied for the modelling of PM_{10} concentrations on all the 52 street sweeping days. Although results from linear regression analysis between the modelled PM_{10} concentrations against the measured values showed that the measured PM_{10} values were approximately 4 % lower than the modelled values, trends of lower PM_{10} concentrations were not observable during all sweeping periods. Interesting, this reduction trend from the modelling results was in accordance to the measurement results.

PM_{10} Forecasting: The PM_{10} Forecasting model (Multiple-Input Multiple-Output model) was developed to forecast the 24 h average PM_{10} concentrations in one, two and three days in advance for two urban sites of different characteristics in Stuttgart. The first site represented a heavily trafficked site (Stuttgart Neckartor), and the second site represented an urban background site (Stuttgart Bad Cannstatt). Measured PM_{10} concentrations from two LUBW ambient air monitoring stations and past meteorological forecasts from a Numerical Mesoscale Model (NMM) were considered as the model input parameters. The modelled PM_{10} concentrations obtained from the PM_{10} Forecasting were then compared with the actual measured PM_{10} values.

Relatively good results were obtained for the forecasts of traffic and urban background PM_{10} concentrations. Similar to the PM_{10} Nowcasting, difficulties were encountered in the simulation of very high PM_{10} concentrations. In general, the day-to-day variations in daily PM_{10} concentrations were correctly reproduced, while some underpredictions were detected during colder months. By comparing the error residuals between results for the two sites, the magnitude of errors at the traffic site was significantly larger than at the urban background site. A possible explanation to this discrepancy could be the exposure of the traffic site to varying daily traffic loads, which was clearly absent at the urban background site.

For both sites, the errors for PM_{10} forecasts were observed to increase with the forecasted days. These observations were anticipated due to the inherent characteristics of forecasted meteorological parameters with days; the longer the forecast periods, the larger the errors.

The overall PM_{10} Forecasting's results illustrate a possibility of effective use on the operational level for performing future PM_{10} forecasts up to three days at both the traffic and urban background sites. However, in real-time forecasting conditions, some compromise in performance should be expected, due to the possibility of less accurate meteorological forecasts. Therefore, a prerequisite for the successful implementation for real-time PM_{10} forecasting is the availability of quality meteorological forecasts, as the developed model performs according to the accuracy of these parameters.

Both the PM_{10} Nowcasting and PM_{10} Forecasting models failed to accurately simulate PM_{10} concentrations during several distinct PM_{10} episodes. There are two aspects in explaining the common underpredicting behaviours of both models:

From the mathematical aspect, the underpredicting behaviours of both models during episodic events verifies the general assumption that neural network models will fail to extrapolate on data which have not been presented during the training procedure. There are two approaches to address this issue, aiming to increase the frequency of extreme values in the training process either by reserving most of the available episodes for the training set, or by including each episode case more times.

From the scientific aspect, the underpredicting behaviours of the models could be attributed to the additional loads of PM from episodic events, whose presence could not be accurately modelled by the input parameters. The three most probable types of PM_{10} episodes are the wintertime inversion-induced PM_{10} episodes, recreational PM_{10} episodes and regional and long-range PM_{10} transport.

1. During wintertime inversion-induced PM_{10} episodes, atmospheric inversions can result in the accumulation of PM_{10} components emitted at ground-level, not only the traffic-related species. In addition, the atmospheric stability may also enhance the formation of secondary PM components. As a result, both models encountered the possible difficulties in simulating the PM_{10} formation or the PM accumulation phenomena during such stagnation conditions. As wintertime inversion-induced PM_{10} episodes can last for several days especially during the colder months in winter, it can be expected that this type of PM_{10} episodes will have the greatest influence on the prediction quality of ambient PM_{10} concentrations. Therefore, a typical characteristic of these episodes is the continuous underpredictions of PM_{10} concentrations over several days.

2. Although fireworks events have relatively short duration, the additional anthropogenic loads on the ambient PM_{10} concentrations, which cannot be well accounted for with the meteorological parameters and NO_2 measurement, can be substantial. Hence, it is clear that both models will fail to simulate PM_{10} concentrations on days with fireworks, during which associations between the modelled PM_{10} concentrations and the corresponding input parameters cannot be established. In comparison to the wintertime inversion-induced PM_{10} episodes, underprediction of PM_{10} concentrations on days with fireworks will only be observed on discrete single days.

3. The hypothesis of long-range transport for air masses towards Stuttgart could be suggested by performing back trajectory analysis. However, PM_{10} back trajectories analysis was not performed in the scope of this dissertation, and information on PM_{10} episodes caused by long-range transport for the region of Baden-Württemberg was not documented in literatures during the investigation periods. Although there was

insufficient information to suggest that the underprediction behaviour of PM_{10} concentrations on certain days was due to long-range transport of PM_{10}, the possibility of such occurrence should not be ruled out entirely.

A general conclusion is that neural network models can be useful and fairly accurate tools of assessment in PM_{10} concentrations in urban areas. After such models have been trained using appropriate site- and time-specific data, its utilisation does not require extensive effort. However neural network models have inherent limitations. In this dissertation, the main limitation is that both the PM_{10} Nowcasting and PM_{10} Forecasting models are strictly site-specific. Nevertheless, the general approach can be followed, especially in the case of neural networks, where a number of key decisions on their formulation, topology and operating parameters are necessary for the accurate simulation of PM_{10} concentrations.

For the PM_{10} Forecasting, future model refinements should be compatible with the needs of model users. Correspondingly, a continuous contact and exchange of information between the model implementers and model end-users should be established and maintained. Among the major objectives of such a contact is to identify the needs for specific activities aiming at a further improvement of model documentation and a better assessment of model accuracy.

Annexes A - D

Annex A Resilient backpropagation training algorithm

Multilayer networks typically use sigmoid transfer functions in the hidden layers in order to compress an infinite input range into a finite output range. Sigmoid functions are characterised by the fact that their slope must approach zero as the input gets large. This causes a problem when using the steepest descent method to train a multiplayer network with sigmoid transfer functions. Even though the weights and biases are far from their optimal values, the gradient can have a very small magnitude and therefore result in the small changes in their weights and biases. As a result, the developed network may be too slow for practical problems. In order to shorten the training time via increasing the training rate, the heuristic technique is adopted, whereby the performance of the standard steepest descent algorithm is analysed. One such technique is the resilient backpropagation method [186, 187].

The purpose of the resilient backpropagation training algorithm is to eliminate these “harmful” effects of the magnitudes of the partial derivatives. Only the sign of the derivative is used to determine the direction of the weight update; the magnitude of the derivative has no effect on the update. To achieve this, the individual update value $\Delta_{ij}(t)$ for each respective weight w_{ij} shall be introduced. The estimation on the update value is based on the observed behaviour of the partial derivative during two successive weight-steps from Eq. (A.1) to (A.3):

$$\Delta_{ij}(t) = \eta^{+} \cdot \Delta_{ij}(t-1), \text{ if } \frac{\partial E}{\partial w_{ij}}(t) \cdot \frac{\partial E}{\partial w_{ij}}(t-1) > 0, \tag{A.1}$$

$$\Delta_{ij}(t) = \eta^{-} \cdot \Delta_{ij}(t-1), \text{ if } \frac{\partial E}{\partial w_{ij}}(t) \cdot \frac{\partial E}{\partial w_{ij}}(t-1) < 0, \tag{A.2}$$

$$\Delta_{ij}(t) = \Delta_{ij}(t-1), \qquad \text{else}, \tag{A.3}$$

where η^{-} represents a negative multiplication factor, η^{+} represents a positive multiplication factor, and $0 < \eta^{-} < 1 < \eta^{+}$.

In another words, every time the partial derivative of the corresponding weight w_{ij} changes its sign, which indicates that the last update was too big and the algorithm has jumped over a local minimum, the update-value $\Delta_{ij}(t)$ is decreased by the factor η^{-}. If the derivative retains its sign, the update-value is slightly increased in order to accelerate convergence in the shallow regions. Once the update-value for each weight is adapted, the weight-update itself follows a very simple rule: if the derivative is positive (increasing error), the weight is decreased by its update-value, if the derivative is negative, the update-value is added as shown by Eq. (A.4) to (A.7):

$$\Delta w_{ij}(t) = -\Delta_{ij}(t), \qquad \text{if } \frac{\partial E}{\partial w_{ij}}(t) > 0, \tag{A.4}$$

$$\Delta w_{ij}(t) = \Delta_{ij}(t), \qquad \text{if } \frac{\partial E}{\partial w_{ij}}(t) < 0, \tag{A.5}$$

$$\Delta w_{ij}(t) = 0\,, \qquad \text{else,} \tag{A.6}$$

$$w_{ij}(t+1) = w_{ij}(t) + \Delta w_{ij}(t)\,. \tag{A.7}$$

However, there is one exception. If the partial derivative changes sign, that is the previous step was too large and the minimum was missed, the previous weight-update is reverted as shown by Eq. (A.8)

$$\Delta w_{ij}(t) = -\Delta w_{ij}(t-1)\,, \qquad \text{if } \frac{\partial E}{\partial w_{ij}}(t) \cdot \frac{\partial E}{\partial w_{ij}}(t-1) < 0\,. \tag{A.8}$$

Due to that 'backtracking' weight-step, the derivative is supposed to change its sign once again in the following step. In order to avoid a double computation of the update-value, there should be no adaptation of the update-value in the succeeding step. In practice this can be done by setting Eq. (A.9) in the $\Delta_{ij}(t)$ update-rule as described above.

$$\frac{\partial E}{\partial w_{ij}}(t-1) = 0 \tag{A.9}$$

The partial derivative of the total error is given by Eq. (A.10)

$$\frac{\partial E}{\partial w_{ij}}(t) = \frac{1}{2} \cdot \sum_{i=1}^{R} \frac{\partial E}{\partial w_{ij}}(t)\,. \tag{A.10}$$

Hence, the partial derivatives of the errors must be accumulated for all the input training patterns. This means that the weights are updated only after the presentation of all training patterns. This iteration continues until the connecting weight values allow the network to perform the required mapping of the target values.

Annex B Numerical Mesoscale Models

B1 Forecasted meteorological parameters for day_{d+1} from NMM3 model

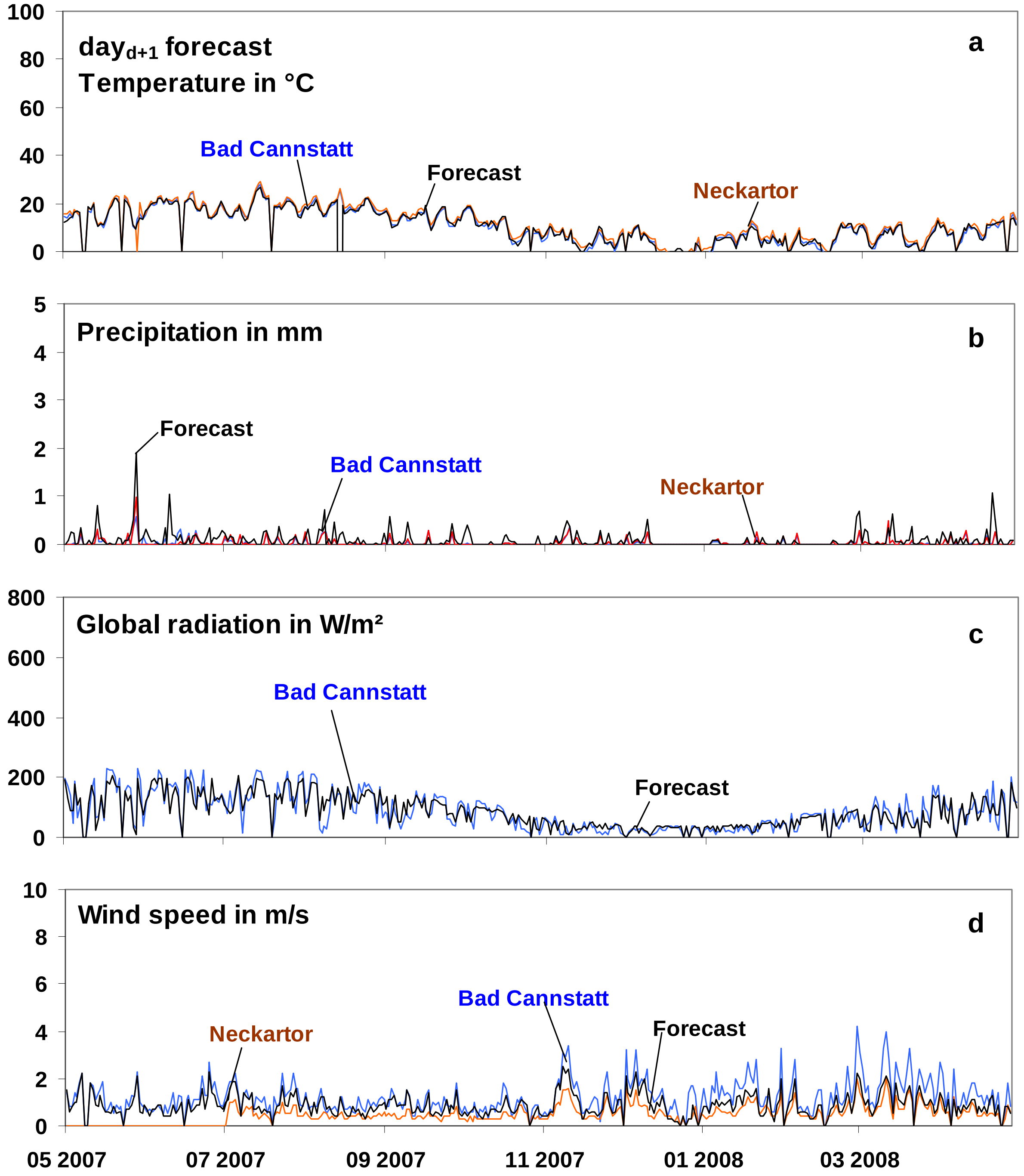

Fig. B.1a-d: Forecasted and measured meteorological parameters at Stuttgart Neckartor and Bad Cannstatt for day_{d+1} for the period 01.05.2007 to 30.04.2008
data source: LUBW and meteoblue AG

B2 Forecasted meteorological parameters for day$_{d+2}$ from NMM3 model

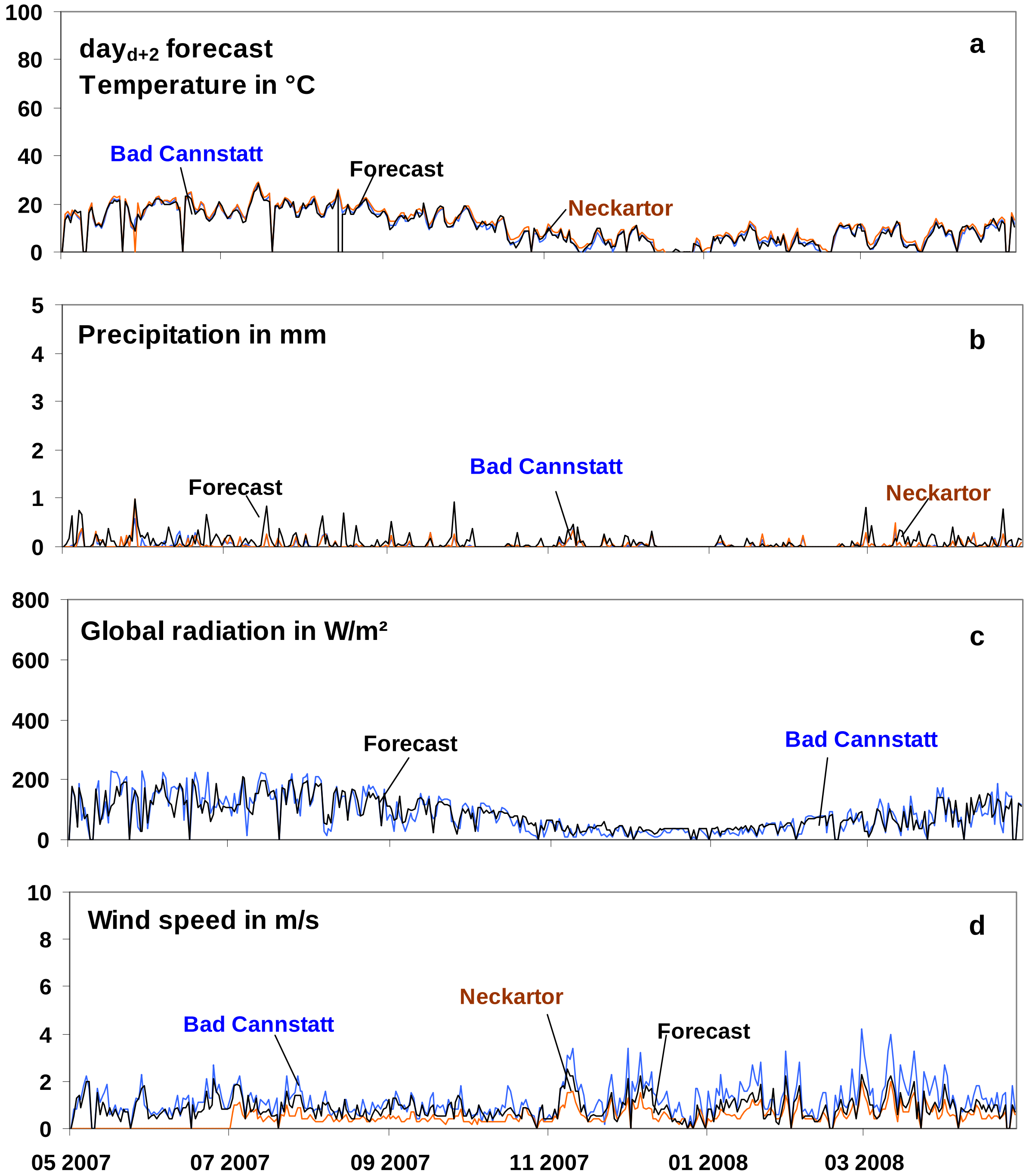

Fig. B.2a-d: Forecasted and measured meteorological parameters at Stuttgart Neckartor and Bad Cannstatt for day$_{d+2}$ for the period 02.05.2007 to 30.04.2008
data source: LUBW and meteoblue AG

B3 Forecasted meteorological parameters for day$_{d+3}$ from NMM12 model

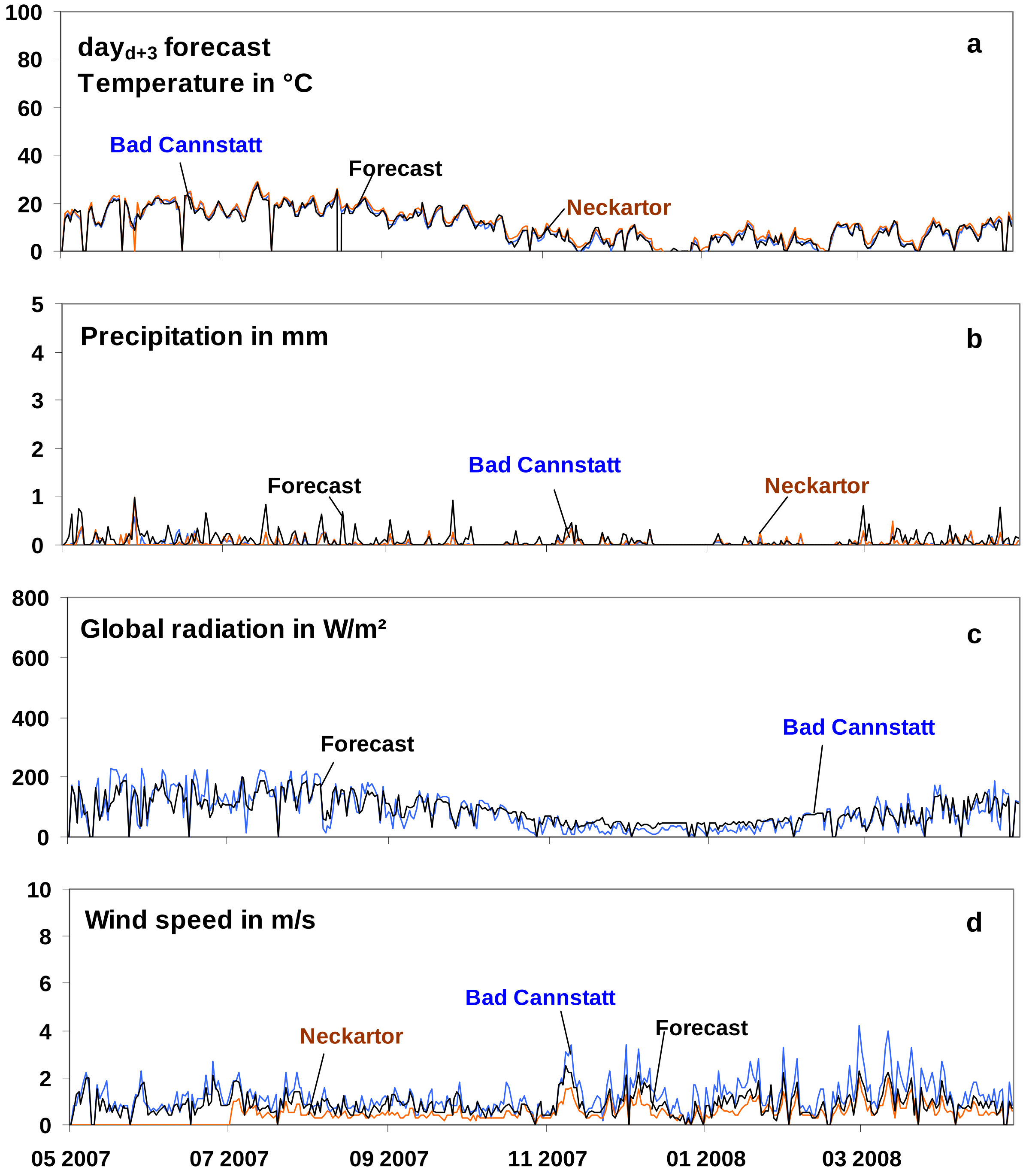

Fig. B.3a-d: Forecasted and measured meteorological parameters at Stuttgart Neckartor and Bad Cannstatt for day$_{d+3}$ for the period 03.05.2007 to 30.04.2008

data source: LUBW and meteoblue AG

Annex C Statistical evaluation of PM_{10} Nowcasting and PM_{10} Forecasting models

C1 PM_{10} Nowcasting models with different network topology

Table C.1: Overall statistical model evaluation parameters of modelled and measured 24 h average PM_{10} concentrations at Stuttgart Neckartor, presented as average values and their standard deviations for the period 03.01.2004 to 14.11.2006

Network topology		**Overall results from training, validation and test sets**					
		FB **in %**	***IA***	***R²***	***MAE*** **in µg/m³**	***MBE*** **in µg/m³**	***RMSE*** **in µg/m³**
20 - 1 - 1		-8.68	0.93	0.81	8.09	-4.40	12.46
	s_D	(2.79)	(0.02)	(0.04)	(2.30)	(1.76)	(3.21)
20 - 2 - 1		-6.55	0.94	0.82	7.70	-3.36	11.90
	s_D	(4.39)	(0.02)	(0.04)	(2.40)	(2.40)	(3.37)
20 - 3 - 1		**-3.35**	**0.97**	**0.89**	**5.86**	**-1.89**	**7.44**
	s_D	**(2.93)**	**(0.03)**	**(0.08)**	**(3.41)**	**(1.73)**	**(4.11)**
20 - 4 - 1		-2.72	0.94	0.83	7.24	-1.42	11.21
	s_D	(1.85)	(0.02)	(0.05)	(2.45)	(1.13)	(3.37)
20 - 5 - 1		-2.57	0.95	0.82	8.14	-1.34	11.80
	s_D	(1.41)	(0.02)	(0.07)	(3.19)	(0.79)	(3.82)
20 - 6 - 1		-5.03	0.95	0.83	7.53	-2.59	11.33
	s_D	(3.45)	(0.02)	(0.06)	(2.71)	(1.89)	(3.53)
20 - 7 - 1		-6.13	0.95	0.82	7.68	-3.15	11.60
	s_D	(4.39)	(0.02)	(0.05)	(2.67)	(2.33)	(3.37)
20 - 8 - 1		-5.07	0.95	0.82	7.85	-2.61	11.61
	s_D	(3.33)	(0.02)	(0.07)	(2.74)	(1.79)	(3.39)
20 - 9 - 1		-7.07	0.94	0.81	8.15	-3.61	11.98
	s_D	(5.04)	(0.02)	(0.05)	(2.95)	(2.62)	(3.58)
20 -10 - 1		-6.67	0.94	0.81	8.07	-3.41	11.96
	s_D	(4.85)	(0.02)	(0.06)	(3.07)	(2.49)	(3.86)
20 -11 - 1		-5.06	0.94	0.81	7.78	-2.61	11.68
	s_D	(3.52)	(0.02)	(0.06)	(2.50)	(1.89)	(3.23)
20 -12 - 1		-3.12	0.94	0.82	7.48	-1.62	11.55
	s_D	(2.07)	(0.02)	(0.05)	(2.35)	(1.19)	(3.28)
20 -13 - 1		-0.55	0.94	0.81	7.75	-0.29	11.48
	s_D	(1.38)	(0.02)	(0.05)	(2.33)	(0.75)	(3.09)
20 -14 - 1		-3.35	0.94	0.81	7.61	-1.75	11.63
	s_D	(2.08)	(0.02)	(0.05)	(2.32)	(1.21)	(3.13)
20 -15 - 1		-4.26	0.94	0.81	7.61	-2.21	11.64
	s_D	(2.72)	(0.02)	(0.04)	(2.36)	(1.54)	(3.24)

FB: fractional bias, IA: index of agreement, R^2: correlation coefficient, MAE: mean absolute error, MBE: mean bias error, RMSE: root mean square error, s_D: standard deviation

C1.1 PM_{10} Nowcasting with three hidden nodes

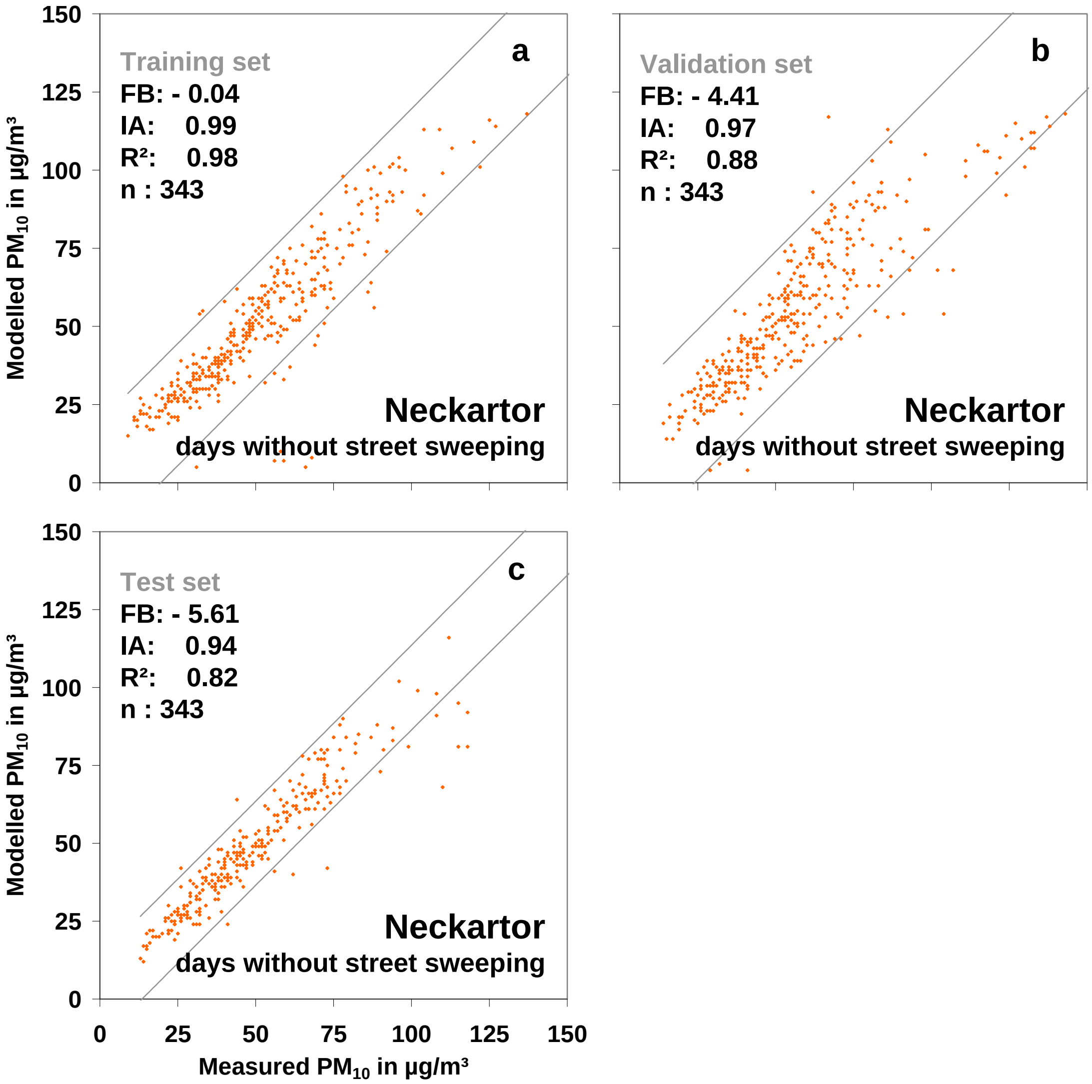

Fig. C.1a-c: Scatter plots of modelled and measured PM_{10} concentrations at Stuttgart Neckartor with 95 % confidence intervals for the period 03.01.2004 to 14.11.2006 (from training, validation and test sets)

C2 PM_{10} Forecasting models with different network topology

Table C.2: Overall statistical model evaluation parameters of modelled and measured 24 h average PM_{10} concentrations at the traffic site on day_{d+1}, presented as average values and their standard deviations for the period 01.05.2007 to 30.04.2008

Network topology		**Overall results from training, validation and test sets**					
		FB **in %**	***IA***	***R²***	***MAE*** **in µg/m³**	***MBE*** **in µg/m³**	***RMSE*** **in µg/m³**
Traffic site, day$_{d+1}$							
18 – 1 – 6		-0.78	0.84	0.58	10.18	-0.33	13.68
	s_D	(5.75)	(0.09)	(0.19)	(2.72)	(2.25)	(4.01)
18 – 2 – 6		0.16	0.79	0.64	10.06	0.07	14.19
	s_D	(10.13)	(0.06)	(0.11)	(3.73)	(4.49)	(6.20)
18 – 3 – 6		-0.04	0.80	0.61	9.80	-0.02	14.03
	s_D	(6.68)	(0.05)	(0.10)	(3.62)	(2.99)	(6.03)
18 – 4 – 6		1.36	0.86	0.64	9.38	0.58	12.87
	s_D	(4.56)	(0.04)	(0.16)	(3.13)	(1.97)	(5.11)
18 – 5 – 6		-3.44	0.82	0.63	9.39	-1.43	13.67
	s_D	(4.94)	(0.06)	(0.09)	(3.71)	(2.32)	(6.22)
18 – 6 – 6		-2.02	0.84	0.61	9.35	-0.85	13.32
	s_D	(4.55)	(0.04)	(0.08)	(3.21)	(2.13)	(5.52)
18 – 7 – 6		-2.83	0.80	0.60	9.80	-1.18	14.10
	s_D	(12.81)	(0.06)	(0.10)	(3.93)	(5.67)	(6.42)
18 – 8 – 6		**-5.84**	**0.86**	**0.63**	**9.10**	**-2.40**	**13.01**
	s_D	**(2.89)**	**(0.04)**	**(0.08)**	**(2.79)**	**(1.48)**	**(4.93)**
18 – 9 – 6		1.08	0.83	0.61	9.63	0.46	13.44
	s_D	(7.94)	(0.04)	(0.09)	(3.09)	(3.51)	(5.36)
18 – 10 – 6		-3.18	0.87	0.64	9.20	-1.33	12.69
	s_D	(2.83)	(0.04)	(0.10)	(2.60)	(1.24)	(4.55)
18 – 11 – 6		-4.91	0.86	0.63	9.31	-2.03	13.08
	s_D	(3.73)	(0.05)	(0.10)	(2.91)	(1.42)	(4.99)
18 – 12 – 6		-3.97	0.87	0.65	9.03	-1.65	12.67
	s_D	(3.19)	(0.04)	(0.10)	(2.52)	(1.51)	(4.62)
18 – 13 – 6		-10.28	0.87	0.63	9.82	-4.14	13.49
	s_D	(2.85)	(0.04)	(0.09)	(2.66)	(1.78)	(4.62)
18 – 14 – 6		-4.00	0.83	0.62	9.44	-1.66	13.50
	s_D	(8.32)	(0.05)	(0.09)	(3.55)	(3.81)	(5.92)
18 – 15 – 6		-8.37	0.88	0.66	9.31	-3.40	12.75
	s_D	(2.27)	(0.05)	(0.11)	(2.26)	(0.94)	(4.05)

FB: fractional bias, IA: index of agreement, R^2: correlation coefficient, MAE: mean absolute error, MBE: mean bias error, RMSE: root mean square error, s_D: standard deviation

Table C.3: Overall statistical model evaluation parameters of modelled and measured 24 h average PM_{10} concentrations at the urban background site on day_{d+1}, presented as average values and their standard deviations for the period 01.05.2007 to 30.04.2008

Network topology		**Overall results from training, validation and test sets**					
		FB **in %**	***IA***	***R²***	***MAE*** **in µg/m³**	***MBE*** **in µg/m³**	***RMSE*** **in µg/m³**
Urban background site, day_{d+1}							
18 – 1 – 6		-4.16	0.81	0.53	5.79	-0.84	9.00
	s_D	(9.71)	(0.09)	(0.17)	(1.31)	(1.75)	(3.21)
18 – 2 – 6		0.62	0.72	0.52	5.98	0.13	9.56
	s_D	(10.53)	(0.08)	(0.06)	(1.87)	(2.28)	(4.51)
18 – 3 – 6		-7.88	0.67	0.46	5.98	-1.57	10.14
	s_D	(7.20)	(0.10)	(0.09)	(2.19)	(1.65)	(4.78)
18 – 4 – 6		-0.49	0.75	0.51	5.79	-0.10	9.36
	s_D	(6.59)	(0.09)	(0.08)	(2.13)	(1.36)	(4.51)
18 – 5 – 6		-6.95	0.72	0.49	5.82	-1.39	9.73
	s_D	(6.86)	(0.09)	(0.07)	(2.05)	(1.37)	(4.53)
18 – 6 – 6		0.93	0.77	0.50	5.83	0.19	9.28
	s_D	(7.37)	(0.07)	(0.07)	(1.78)	(1.58)	(4.14)
18 – 7 – 6		-6.31	0.76	0.55	5.52	-1.26	9.28
	s_D	(11.68)	(0.08)	(0.05)	(2.06)	(2.58)	(4.64)
18 – 8 – 6		**-4.58**	**0.79**	**0.50**	**5.68**	**-0.93**	**9.24**
	s_D	**(5.90)**	**(0.07)**	**(0.07)**	**(1.89)**	**(1.35)**	**(4.15)**
18 – 9 – 6		-1.09	0.76	0.50	5.73	-0.22	9.36
	s_D	(8.91)	(0.08)	(0.06)	(1.91)	(1.95)	(4.41)
18 – 10 – 6		-4.90	0.80	0.52	5.60	-0.99	9.08
	s_D	(5.72)	(0.07)	(0.07)	(1.80)	(1.09)	(4.04)
18 – 11 – 6		-7.67	0.78	0.50	5.86	-1.53	9.40
	s_D	(7.98)	(0.08)	(0.08)	(1.74)	(1.40)	(4.06)
18 – 12 – 6		-3.95	0.78	0.52	5.53	-0.80	9.22
	s_D	(7.35)	(0.08)	(0.06)	(1.81)	(1.64)	(4.33)
18 – 13 – 6		-13.17	0.79	0.52	5.89	-2.55	9.36
	s_D	(4.47)	(0.07)	(0.10)	(1.80)	(1.05)	(4.09)
18 – 14 – 6		-9.43	0.79	0.53	5.70	-1.86	9.22
	s_D	(5.41)	(0.06)	(0.06)	(1.81)	(1.31)	(4.06)
18 – 15 – 6		-11.78	0.81	0.55	5.68	-2.30	9.05
	s_D	(5.69)	(0.06)	(0.07)	(1.48)	(1.00)	(3.70)

FB: fractional bias, IA: index of agreement, R²: correlation coefficient, MAE: mean absolute error, MBE: mean bias error, RMSE: root mean square error, s_D: standard deviation

Table C.4: Overall statistical model evaluation parameters of modelled and measured 24 h average PM_{10} concentrations at the traffic site on day_{d+2}, presented as average values and their standard deviations for the period 02.05.2007 to 30.04.2008

Network topology		Overall results from training, validation and test sets					
		FB **in %**	***IA***	***R^2***	***MAE*** **in µg/m³**	***MBE*** **in µg/m³**	***RMSE*** **in µg/m³**
Traffic site, day_{d+2}							
18 – 1 – 6		-2.21	0.85	0.56	10.25	-0.91	13.74
	s_D	(5.45)	(0.12)	(0.23)	(2.50)	(2.13)	(3.21)
18 – 2 – 6		-3.50	0.75	0.54	10.36	-1.44	14.90
	s_D	(11.83)	(0.07)	(0.13)	(3.88)	(5.28)	(6.28)
18 – 3 – 6		-8.90	0.78	0.56	10.12	-3.56	14.61
	s_D	(8.12)	(0.06)	(0.14)	(3.91)	(3.92)	(6.09)
18 – 4 – 6		4.34	0.81	0.53	10.69	1.86	14.31
	s_D	(8.35)	(0.05)	(0.13)	(2.87)	(3.56)	(4.44)
18 – 5 – 6		3.52	0.80	0.58	10.31	1.50	13.96
	s_D	(9.75)	(0.06)	(0.16)	(2.91)	(4.21)	(4.66)
18 – 6 – 6		2.77	0.80	0.58	10.21	1.18	13.99
	s_D	(7.71)	(0.05)	(0.12)	(3.41)	(3.32)	(5.24)
18 – 7 – 6		-10.01	0.74	0.43	11.38	-3.99	16.08
	s_D	(16.69)	(0.07)	(0.12)	(5.27)	(7.26)	(7.18)
18 – 8 – 6		**-3.28**	**0.86**	**0.61**	**9.73**	**-1.35**	**13.01**
	s_D	**(4.31)**	**(0.05)**	**(0.16)**	**(2.28)**	**(2.07)**	**(3.55)**
18 – 9 – 6		-0.66	0.82	0.58	9.94	-0.28	13.64
	s_D	(5.26)	(0.05)	(0.14)	(3.38)	(2.34)	(4.98)
18 – 10 – 6		-0.30	0.86	0.61	9.69	-0.13	12.96
	s_D	(5.35)	(0.05)	(0.15)	(2.35)	(2.40)	(3.67)
18 – 11 – 6		-1.88	0.85	0.59	9.97	-0.78	13.31
	s_D	(4.17)	(0.06)	(0.15)	(2.61)	(1.63)	(3.88)
18 – 12 – 6		-1.36	0.84	0.58	9.81	-0.56	13.41
	s_D	(7.13)	(0.05)	(0.15)	(2.65)	(3.23)	(4.32)
18 – 13 – 6		-5.09	0.83	0.56	10.08	-2.08	13.84
	s_D	(8.48)	(0.05)	(0.14)	(3.06)	(3.92)	(4.83)
18 – 14 – 6		-2.17	0.79	0.55	10.15	-0.90	14.28
	s_D	(11.58)	(0.05)	(0.15)	(3.55)	(5.14)	(5.42)
18 – 15 – 6		-5.89	0.80	0.58	9.86	-2.39	14.07
	s_D	(7.31)	(0.06)	(0.15)	(3.44)	(3.48)	(5.68)

FB: fractional bias, IA: index of agreement, R^2: correlation coefficient, MAE: mean absolute error, MBE: mean bias error, RMSE: root mean square error, s_D: standard deviation

Table C.5: Overall statistical model evaluation parameters of modelled and measured 24 h average PM_{10} concentrations at the urban background site on day_{d+2}, presented as average values and their standard deviations for the period 02.05.2007 to 30.04.2008

Network topology		**Overall results from training, validation and test sets**					
		FB **in %**	***IA***	***R²***	***MAE*** **in µg/m³**	***MBE*** **in µg/m³**	***RMSE*** **in µg/m³**
Urban background site, day$_{d+2}$							
18 – 1 – 6		-7.54	0.83	0.52	6.20	-1.49	8.95
	s_D	(8.13)	(0.12)	(0.24)	(1.16)	(1.31)	(2.03)
18 – 2 – 6		-7.97	0.69	0.46	6.13	-1.57	9.93
	s_D	(11.44)	(0.08)	(0.10)	(2.18)	(2.57)	(4.50)
18 – 3 – 6		-15.05	0.69	0.48	6.22	-2.87	10.05
	s_D	(7.32)	(0.07)	(0.10)	(2.26)	(1.89)	(4.40)
18 – 4 – 6		6.92	0.75	0.45	6.57	1.47	9.64
	s_D	(8.14)	(0.05)	(0.08)	(1.88)	(1.65)	(3.64)
18 – 5 – 6		-3.64	0.77	0.47	6.14	-0.73	9.33
	s_D	(5.23)	(0.05)	(0.12)	(1.71)	(1.17)	(3.41)
18 – 6 – 6		-4.89	0.77	0.48	6.24	-0.98	9.35
	s_D	(4.36)	(0.05)	(0.10)	(1.81)	(1.04)	(3.63)
18 – 7 – 6		-9.77	0.74	0.47	6.36	-1.91	9.67
	s_D	(16.42)	(0.05)	(0.13)	(2.34)	(3.52)	(4.08)
18 – 8 – 6		**-3.59**	**0.82**	**0.51**	**6.18**	**-0.72**	**8.96**
	s_D	**(5.08)**	**(0.04)**	**(0.13)**	**(1.08)**	**(1.20)**	**(2.73)**
18 – 9 – 6		-1.51	0.77	0.48	6.17	-0.31	9.26
	s_D	(7.21)	(0.05)	(0.09)	(2.00)	(1.61)	(3.63)
18 – 10 – 6		-3.73	0.78	0.48	6.14	-0.75	9.26
	s_D	(5.04)	(0.05)	(0.09)	(1.64)	(1.16)	(3.49)
18 – 11 – 6		-4.20	0.80	0.48	6.47	-0.84	9.30
	s_D	(6.34)	(0.04)	(0.10)	(1.58)	(1.08)	(3.07)
18 – 12 – 6		-1.24	0.78	0.47	6.31	-0.25	9.35
	s_D	(10.03)	(0.04)	(0.12)	(1.47)	(2.20)	(3.21)
18 – 13 – 6		-6.70	0.75	0.49	6.17	-1.33	9.47
	s_D	(7.18)	(0.06)	(0.10)	(2.09)	(1.70)	(3.97)
18 – 14 – 6		-2.72	0.78	0.48	6.29	-0.55	9.24
	s_D	(9.76)	(0.03)	(0.12)	(1.68)	(2.16)	(3.17)
18 – 15 – 6		-8.18	0.71	0.49	6.22	-1.61	9.73
	s_D	(8.33)	(0.07)	(0.12)	(2.25)	(1.96)	(4.32)

FB: fractional bias, IA: index of agreement, R^2: correlation coefficient, MAE: mean absolute error, MBE: mean bias error, RMSE: root mean square error, s_D: standard deviation

Table C.6: Overall statistical model evaluation parameters of modelled and measured 24 h average PM_{10} concentrations at the traffic site on day_{d+3}, presented as average values and their standard deviations for the period 03.05.2007 to 30.04.2008

Network topology		Overall results from training, validation and test sets					
		FB **in %**	***IA***	***R²***	***MAE*** **in µg/m³**	***MBE*** **in µg/m³**	***RMSE*** **in µg/m³**
Traffic site, day$_{d+3}$							
18 – 1 – 6		1.05	0.76	0.38	12.88	0.45	17.34
	s_D	(6.69)	(0.12)	(0.17)	(3.83)	(2.98)	(5.42)
18 – 2 – 6		0.88	0.66	0.37	12.89	0.38	17.60
	s_D	(15.43)	(0.05)	(0.12)	(4.31)	(6.89)	(6.75)
18 – 3 – 6		-8.89	0.73	0.47	11.57	-3.62	16.64
	s_D	(13.40)	(0.06)	(0.09)	(4.97)	(6.27)	(7.84)
18 – 4 – 6		7.90	0.76	0.44	13.63	3.49	16.73
	s_D	(13.75)	(0.03)	(0.10)	(2.87)	(5.98)	(4.34)
18 – 5 – 6		-5.59	0.81	0.50	11.70	-2.31	15.58
	s_D	(6.97)	(0.02)	(0.16)	(2.56)	(2.75)	(4.46)
18 – 6 – 6		1.41	0.77	0.48	11.63	0.60	15.90
	s_D	(8.45)	(0.02)	(0.11)	(3.99)	(3.79)	(6.04)
18 – 7 – 6		-10.08	0.75	0.42	12.46	-4.08	17.03
	s_D	(13.23)	(0.02)	(0.12)	(4.28)	(6.22)	(6.46)
18 – 8 – 6		**1.20**	**0.84**	**0.54**	**10.96**	**0.51**	**14.78**
	s_D	**(7.52)**	**(0.03)**	**(0.15)**	**(2.26)**	**(3.38)**	**(3.82)**
18 – 9 – 6		0.58	0.81	0.51	11.34	0.25	15.29
	s_D	(7.07)	(0.01)	(0.12)	(3.24)	(3.14)	(5.11)
18 – 10 – 6		0.79	0.74	0.47	11.86	0.34	16.18
	s_D	(10.48)	(0.03)	(0.12)	(3.89)	(4.74)	(6.25)
18 – 11 – 6		-0.78	0.83	0.52	11.73	-0.33	15.33
	s_D	(6.26)	(0.03)	(0.14)	(2.18)	(2.43)	(3.74)
18 – 12 – 6		3.73	0.77	0.49	11.67	1.61	15.86
	s_D	(13.50)	(0.01)	(0.12)	(3.28)	(5.99)	(5.03)
18 – 13 – 6		-4.35	0.73	0.48	11.66	-1.81	16.35
	s_D	(11.51)	(0.04)	(0.17)	(4.51)	(5.37)	(6.89)
18 – 14 – 6		-5.29	0.79	0.51	11.23	-2.19	15.54
	s_D	(11.24)	(0.01)	(0.14)	(3.46)	(5.29)	(5.65)
18 – 15 – 6		-7.31	0.66	0.48	11.83	-3.00	17.11
	s_D	(12.47)	(0.07)	(0.13)	(5.32)	(5.87)	(8.20)

FB: fractional bias, IA: index of agreement, R^2: correlation coefficient, MAE: mean absolute error, MBE: mean bias error, RMSE: root mean square error, s_D: standard deviation

Table C.7: Overall statistical model evaluation parameters of modelled and measured 24 h average PM_{10} concentrations at the urban background site on day_{d+3}, presented as average values and their standard deviations for the period 03.05.2007 to 30.04.2008

Network topology		**Overall results from training, validation and test sets**					
		***FB* in %**	***IA***	***R^2***	***MAE* in µg/m³**	***MBE* in µg/m³**	***RMSE* in µg/m³**
Urban background site, day_{d+3}							
18 – 1 – 6		-4.76	0.76	0.39	7.46	-0.98	10.98
	s_D	(4.77)	(0.13)	(0.19)	(2.35)	(0.98)	(4.09)
18 – 2 – 6		-3.97	0.64	0.36	7.16	-0.82	11.36
	s_D	(15.61)	(0.10)	(0.08)	(2.64)	(3.50)	(5.64)
18 – 3 – 6		-7.94	0.68	0.42	6.62	-1.61	10.96
	s_D	(14.65)	(0.09)	(0.06)	(2.62)	(3.36)	(5.65)
18 – 4 – 6		7.45	0.73	0.40	7.36	1.63	10.93
	s_D	(13.38)	(0.05)	(0.06)	(1.99)	(2.85)	(4.26)
18 – 5 – 6		-6.32	0.78	0.45	7.06	-1.29	10.41
	s_D	(5.97)	(0.03)	(0.13)	(1.38)	(1.14)	(3.67)
18 – 6 – 6		-4.46	0.73	0.41	6.68	-0.92	10.73
	s_D	(6.25)	(0.06)	(0.07)	(2.30)	(1.51)	(4.84)
18 – 7 – 6		-5.16	0.75	0.41	7.10	-1.06	10.70
	s_D	(13.03)	(0.03)	(0.11)	(1.66)	(2.98)	(4.23)
18 – 8 – 6		**-5.07**	**0.80**	**0.48**	**6.87**	**-1.04**	**10.12**
	s_D	**(4.67)**	**(0.03)**	**(0.13)**	**(1.40)**	**(1.17)**	**(3.65)**
18 – 9 – 6		-0.85	0.77	0.44	6.93	-0.18	10.43
	s_D	(7.42)	(0.03)	(0.10)	(1.80)	(1.71)	(4.14)
18 – 10 – 6		-1.65	0.69	0.41	6.85	-0.34	10.86
	s_D	(10.10)	(0.08)	(0.09)	(2.49)	(2.32)	(5.27)
18 – 11 – 6		-4.29	0.80	0.46	7.36	-0.88	10.39
	s_D	(6.15)	(0.03)	(0.10)	(1.37)	(1.05)	(3.41)
18 – 12 – 6		2.71	0.73	0.41	6.84	0.58	10.76
	s_D	(16.45)	(0.04)	(0.11)	(1.57)	(3.61)	(4.12)
18 – 13 – 6		-7.40	0.69	0.43	6.59	-1.50	10.89
	s_D	(10.08)	(0.07)	(0.11)	(2.42)	(2.65)	(5.35)
18 – 14 – 6		-7.20	0.78	0.46	6.91	-1.46	10.37
	s_D	(10.71)	(0.02)	(0.12)	(1.34)	(2.55)	(3.89)
18 – 15 – 6		-11.36	0.62	0.43	6.78	-2.26	11.37
	s_D	(12.90)	(0.08)	(0.13)	(2.89)	(3.08)	(5.89)

FB: fractional bias, IA: index of agreement, R^2: correlation coefficient, MAE: mean absolute error, MBE: mean bias error, RMSE: root mean square error, s_D: standard deviation

C2.1 PM_{10} Forecasting with eight hidden nodes

Table C.8: Performance indices on the successful predictions of exceedances of 24 h average PM_{10} concentrations at the traffic and urban background sites with the training set

Site	Training set					
	TP	***FP***	***FN***	***IS***	***FAR***	***A***
day$_{d+1}$						
Traffic	42	5	5	0.81	0.11	0.91
Urban background	0	0	8	0.00	N.A.	0.93
day$_{d+2}$						
Traffic	40	7	6	0.75	0.15	0.88
Urban background	0	0	8	0.00	N.A.	0.93
day$_{d+3}$						
Traffic	42	8	6	0.75	0.16	0.87
Urban background	0	0	11	0.00	N.A.	0.90

TP: number of correct predictions of exceedances, FP: number of false alarms, FN: number of missed exceedances, IS: index of success, FAR: false alarms value, A: overall accuracy

Table C.9: Performance indices on the successful predictions of exceedances of 24 h average PM_{10} concentrations at the traffic and urban background sites with the validation set

Site	Validation set					
	TP	***FP***	***FN***	***IS***	***FAR***	***A***
day$_{d+1}$						
Traffic	18	8	1	0.67	0.31	0.92
Urban background	0	0	2	0.00	N.A.	0.98
day$_{d+2}$						
Traffic	18	9	1	0.64	0.33	0.91
Urban background	0	0	2	0.00	N.A.	0.98
day$_{d+3}$						
Traffic	17	14	3	0.50	0.45	0.84
Urban background	0	0	1	0.00	N.A.	0.99

TP: number of correct predictions of exceedances, FP: number of false alarms, FN: number of missed exceedances, IS: index of success, FAR: false alarms value, A: overall accuracy

Table C.10: Performance indices on the successful predictions of exceedances of 24 h average PM_{10} concentrations at the traffic and urban background sites with the test set

Site	**Test set**					
	TP	***FP***	***FN***	***IS***	***FAR***	***A***
day$_{d+1}$						
Traffic	6	3	7	0.38	0.33	0.91
Urban background	0	0	0	0.00	N.A.	1.00
day$_{d+2}$						
Traffic	4	6	8	0.22	0.60	0.87
Urban background	0	0	0	0.00	N.A.	1.00
day$_{d+3}$						
Traffic	5	11	5	0.24	0.69	0.85
Urban background	0	0	0	0.00	N.A.	1.00

TP: number of correct predictions of exceedances, FP: number of false alarms, FN: number of missed exceedances, IS: index of success, FAR: false alarms value, A: overall accuracy

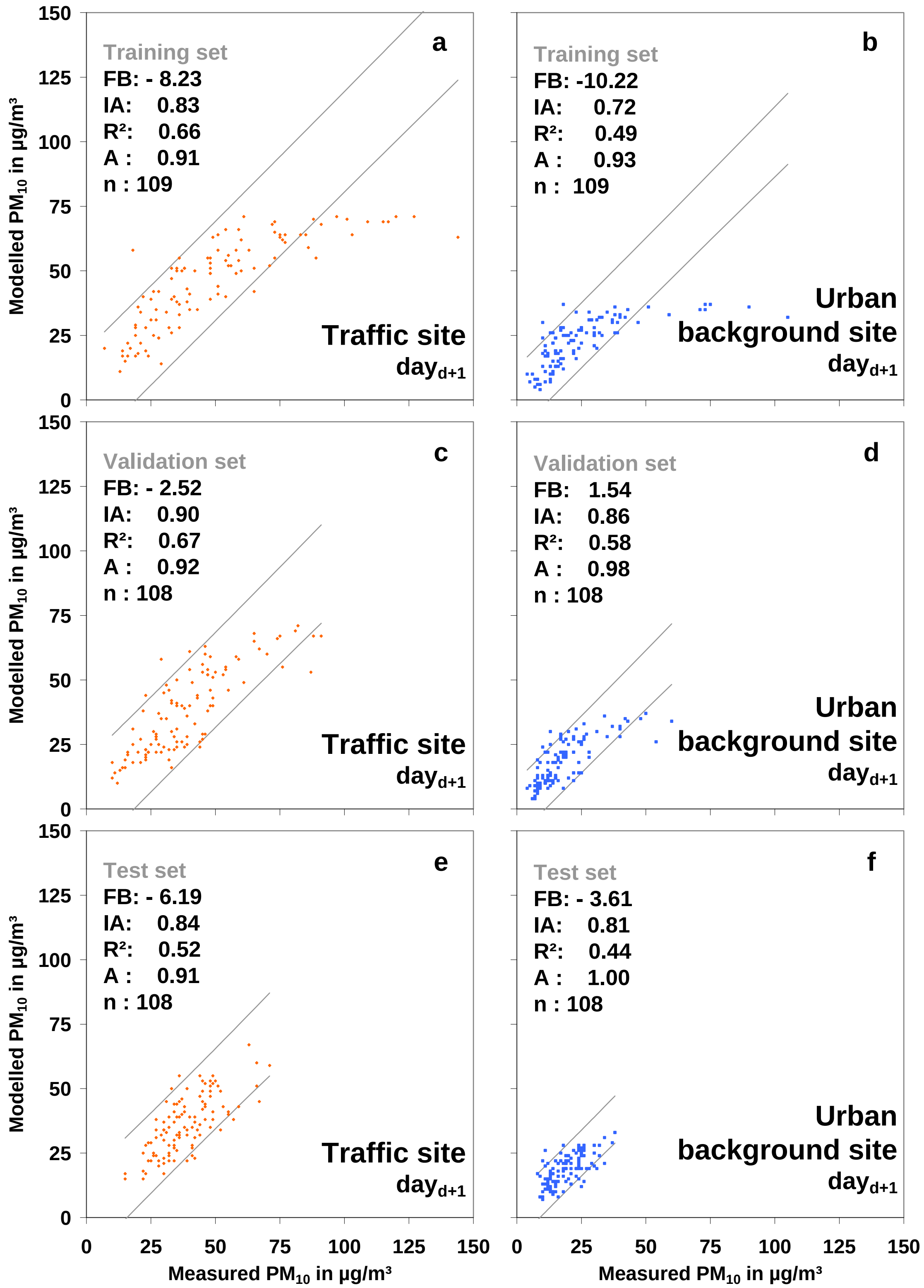

Fig. C.2a-f: Scatter plots of modelled and measured PM_{10} concentrations at the traffic and urban background sites with 95 % confidence intervals for day_{d+1} (from training, validation and test sets)

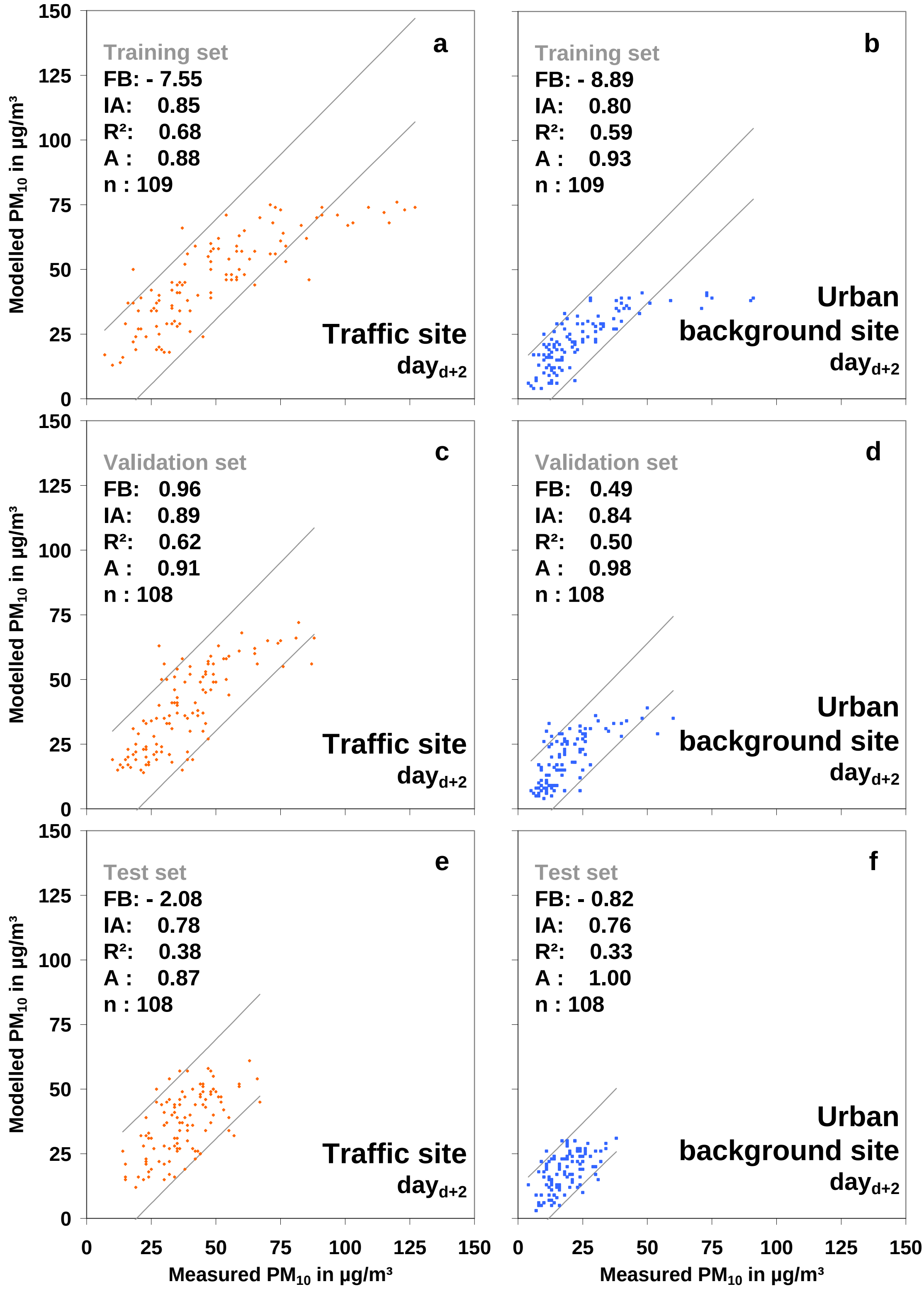

Fig. C.3a-f: Scatter plots of modelled and measured PM_{10} concentrations at the traffic and urban background sites with 95 % confidence intervals for day_{d+2} (from training, validation and test sets)

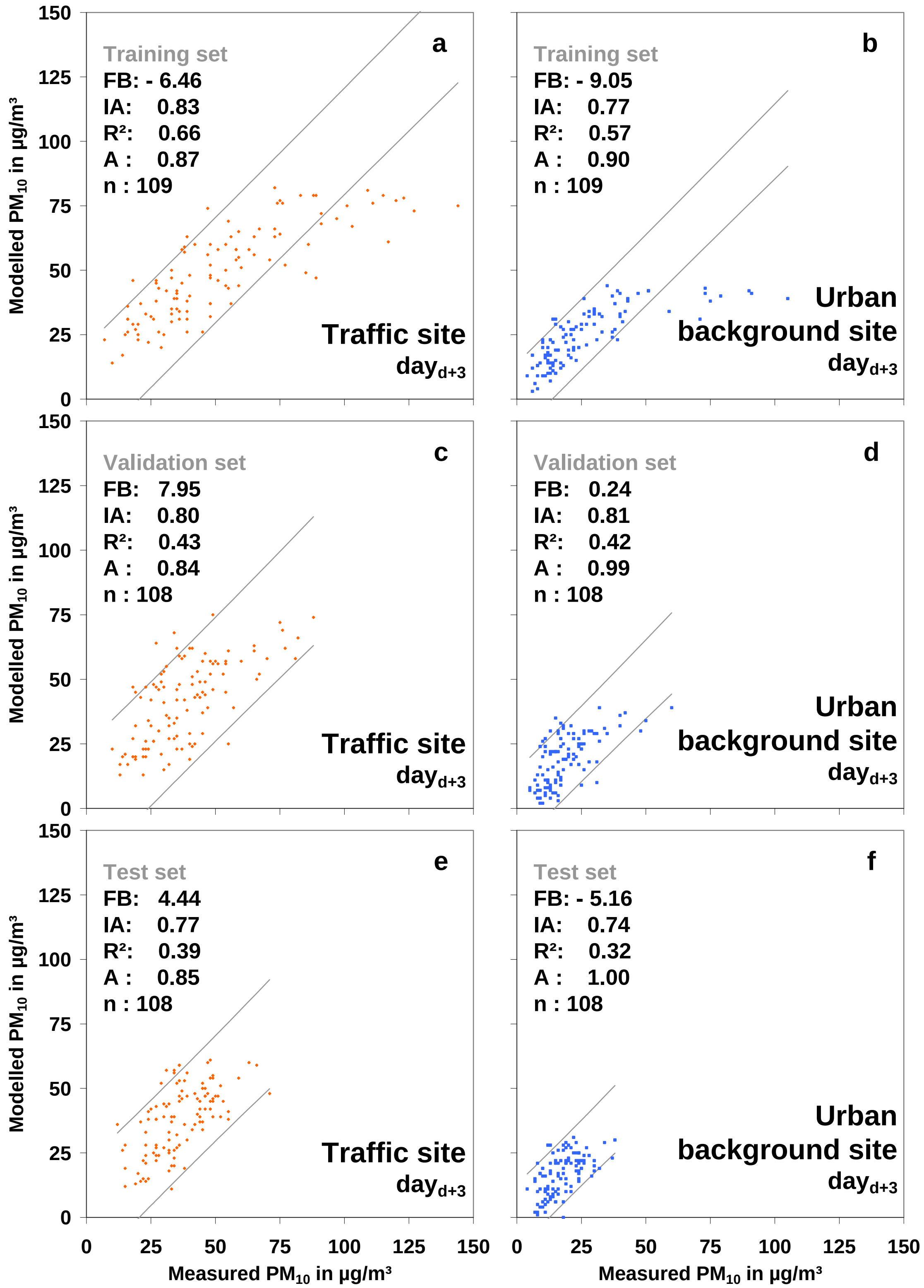

Fig. C.4a-f: Scatter plots of modelled and measured PM_{10} concentrations at the traffic and urban background sites with 95 % confidence intervals for day_{d+3} (from training, validation and test sets)

C3 Test PM_{10} Forecasting model with fourteen hidden nodes

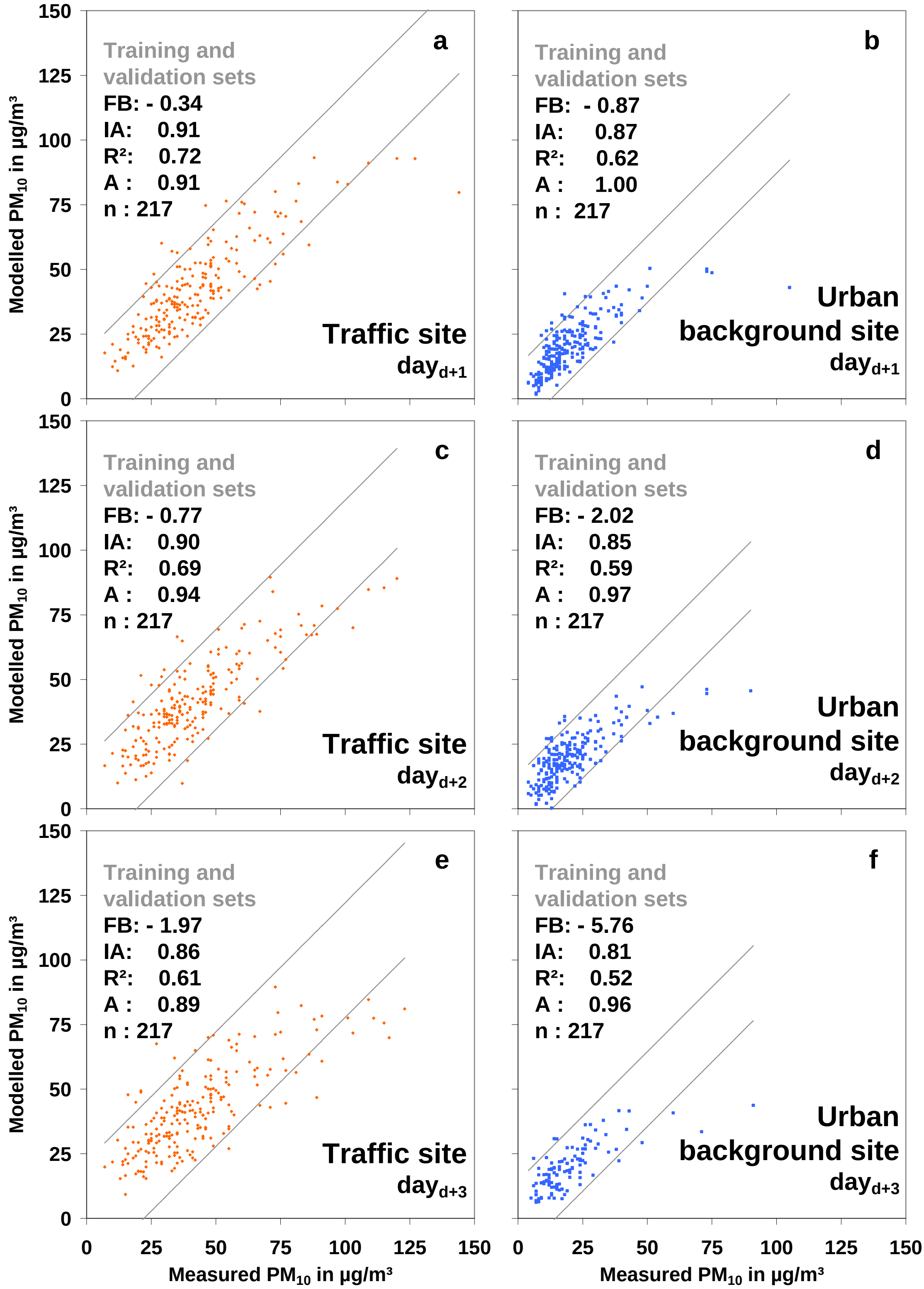

Fig. C.5a-f: Scatter plots of modelled and measured PM_{10} concentrations at the traffic and urban background sites with 95 % confidence intervals for day_{d+1}, day_{d+2} and day_{d+3} (from training and validation sets)

Table C.11: Performance indices on the successful predictions of exceedances of 24 h average PM_{10} concentrations at the traffic and urban background sites with the training set

Site	**Training and validation sets**					
	TP	***FP***	***FN***	***IS***	***FAR***	***A***
day_{d+1}						
Traffic	39	10	10	0.67	0.21	0.91
Urban background	4	0	1	0.75	0.00	1.00
day_{d+2}						
Traffic	41	6	7	0.76	0.13	0.94
Urban background	0	0	6	0.00	N.A.	0.97
day_{d+3}						
Traffic	41	12	13	0.63	0.23	0.89
Urban background	0	0	8	0.00	N.A.	0.96

TP: number of correct predictions of exceedances, FP: number of false alarms, FN: number of missed exceedances, IS: index of success, FAR: false alarms value, A: overall accuracy

Table C.12: Performance indices on the successful predictions of exceedances of 24 h average PM_{10} concentrations at the traffic and urban background sites with the validation set

Site	**Test set**					
	TP	***FP***	***FN***	***IS***	***FAR***	***A***
day_{d+1}						
Traffic	24	7	6	0.65	0.23	0.88
Urban background	1	0	4	0.20	0.00	0.96
day_{d+2}						
Traffic	21	9	8	0.55	0.30	0.84
Urban background	0	0	4	0.00	N.A.	0.96
day_{d+3}						
Traffic	19	8	5	0.59	0.30	0.88
Urban background	0	0	4	0.00	N.A.	0.96

TP: number of correct predictions of exceedances, FP: number of false alarms, FN: number of missed exceedances, IS: index of success, FAR: false alarms value, A: overall accuracy

C4 Test PM_{10} Forecasting model with thirteen hidden nodes

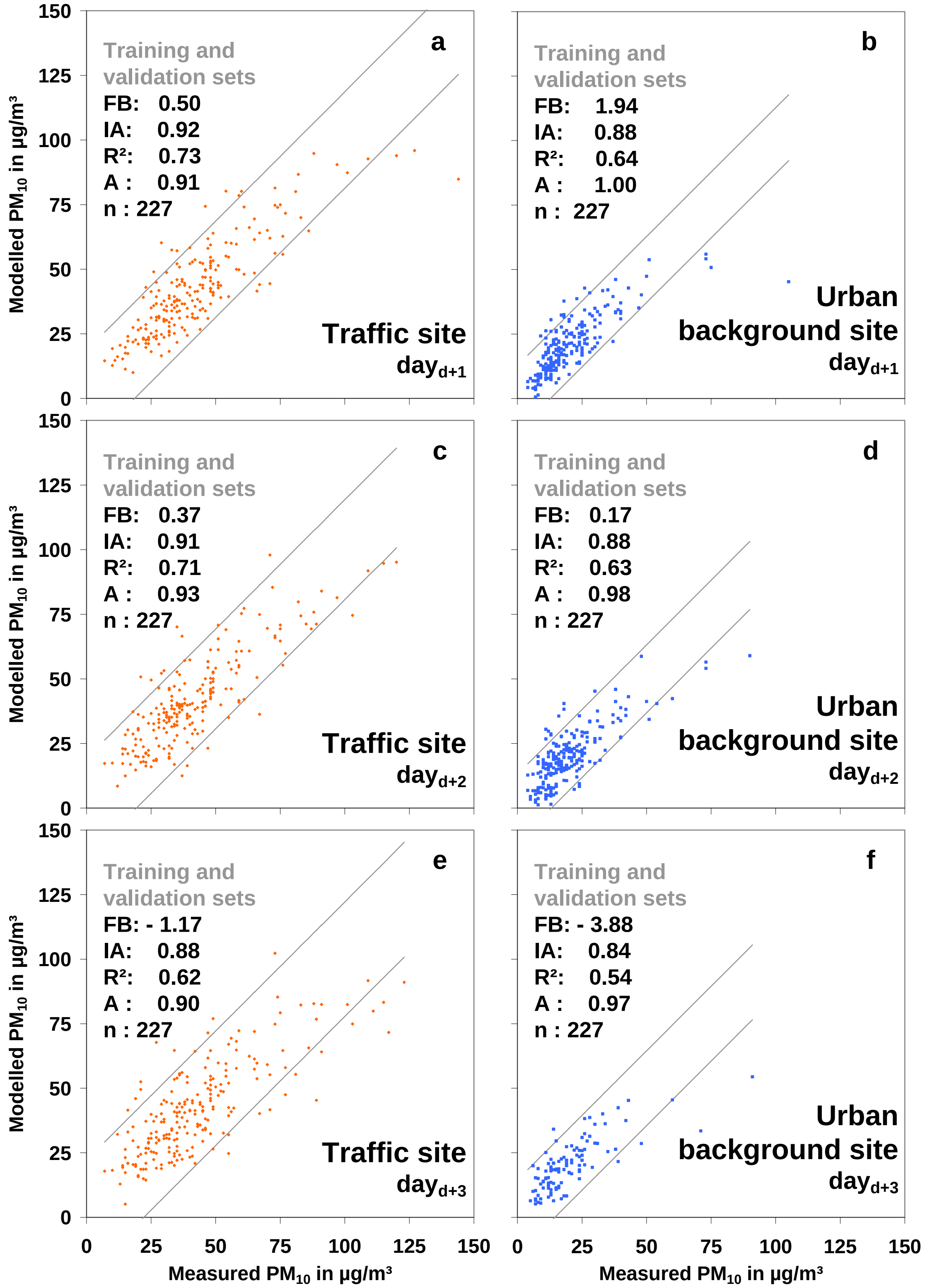

Fig. C.6a-f: Scatter plots of modelled and measured PM_{10} concentrations at the traffic and urban background sites with 95 % confidence intervals for day_{d+1}, day_{d+2} and day_{d+3} (from training and validation sets)

Table C.13: Performance indices on the successful predictions of exceedances of 24 h average PM_{10} concentrations at the traffic and urban background sites with the training set

Site	**Training and validation sets**					
	TP	***FP***	***FN***	***IS***	***FAR***	***A***
day$_{d+1}$						
Traffic	40	10	9	0.68	0.21	0.91
Urban background	4	0	1	0.75	0.00	1.00
day$_{d+2}$						
Traffic	40	8	8	0.71	0.17	0.93
Urban background	3	1	3	0.42	0.17	0.98
day$_{d+3}$						
Traffic	44	13	10	0.66	0.23	0.90
Urban background	3	1	5	0.33	0.17	0.97

TP: number of correct predictions of exceedances, FP: number of false alarms, FN: number of missed exceedances, IS: index of success, FAR: false alarms value, A: overall accuracy

Table C.14: Performance indices on the successful predictions of exceedances of 24 h average PM_{10} concentrations at the traffic and urban background sites with the validation set

Site	**Test set**					
	TP	***FP***	***FN***	***IS***	***FAR***	***A***
day$_{d+1}$						
Traffic	24	7	6	0.65	0.23	0.88
Urban background	1	0	4	0.20	0.00	0.96
day$_{d+2}$						
Traffic	20	8	9	0.54	0.29	0.84
Urban background	1	0	3	0.25	0.00	0.97
day$_{d+3}$						
Traffic	19	7	5	0.61	0.27	0.89
Urban background	1	0	3	0.25	0.00	0.97

TP: number of correct predictions of exceedances, FP: number of false alarms, FN: number of missed exceedances, IS: index of success, FAR: false alarms value, A: overall accuracy

Annex D Nowcast of PM_{10} concentrations at Neckartor on street sweeping days

Table D.1: Modelled and measured PM_{10} concentrations at Stuttgart Neckartor from 15.11.2006 to 18.03.2007

Date	Modelled PM_{10} in µg/m³	Measured PM_{10} in µg/m³	η_1 in %
17.11.2006	87	86	-1.2
18.11.2006	71	68	-4.2
20.11.2006	43	41	-4.7
21.11.2006	35	31	-11.4
24.11.2006	77	69	-10.4
25.11.2006	72	70	-2.8
05.01.2007	26	20	-23.1
06.01.2007	13	12	-7.7
12.01.2007	31	32	3.2
13.01.2007	30	32	6.7
14.01.2007	27	29	7.4
15.01.2007	77	69	-10.4
16.01.2007	88	81	-8.0
18.01.2007	22	16	-27.3
19.01.2007	24	13	-45.8
20.01.2007	19	19	0.0
21.01.2007	14	16	14.3
22.01.2007	61	51	-16.4
23.01.2007	38	36	-5.3
26.01.2007	52	46	-11.5
27.01.2007	29	28	-3.4
28.01.2007	14	21	50.0
29.01.2007	28	25	-10.7
30.01.2007	80	86	7.5
10.02.2007	38	41	7.9
11.02.2007	21	18	-14.3
12.02.2007	40	38	-5.0
13.02.2007	20	18	-10.0
16.02.2007	77	71	-7.8
17.02.2007	55	62	12.7
18.02.2007	67	69	3.0
19.02.2007	90	91	1.1
20.02.2007	113	98	-13.3
23.02.2007	84	93	10.7
24.02.2007	47	53	12.8
25.02.2007	21	19	-9.5
26.02.2007	25	19	-24.0
27.02.2007	30	23	-23.3
02.02.2007	25	27	8.0
03.02.2007	20	15	-25.0

η_1: effect of street sweeping on ambient PM_{10} concentrations

References

[1] Lahl, U., 2005. Feinstaub – eine gesundheitspolitische Herausforderung. 46. Kongress der Deutsche Sesellschaft für Pneumologie. 17 März 2005.

[2] UBA Umweltbundesamt, 2005. Hintergrundpapier zum Thema Staub/Feinstaub (PM).

[3] WHO World Health Organisation, 2003. Health aspects of air pollutants with particulate matter, ozone, and nitrogen dioxide. Report on a WHO working group. Copenhagen, WHO Regional Office for Europe, Denmark.

[4] WHO, World Health Organisation, 2004. Health aspects of air pollution. Results from the WHO project "Systematic review of health aspects of air pollution in Europe". Copenhagen, WHO Regional Office for Europe, Denmark.

[5] Harrison R.M., Yin, J., 2000. Particulate matter in the atmosphere: which particle properties are important for its effects on health? The Science of the Total Environment 249, 85-101.

[6] European Community 2008. Council Directive 2008/50/EC of 21 May 2008 on ambient air quality and cleaner air for Europe. Official Journal of the European Union, L152/1.

[7] European Community 1999. Council Directive 1999/30/EC of 22 April 1999 relating to the limit values for sulphur dioxide, nitrogen dioxide and oxides of nitrogen, particulate matter and lead in ambient air. Official Journal of the European Union, L163/41.

[8] 22. Verordnung zur Durchführung des Bundes-Immissionsschutzgesetzes (Verordnung über Immissionswerte für Schadstoffe in der Luft – 22. BImSchV), 11 September 2002, BGBI I, 3626.

[9] Lahl, U., Steven, W., 2004. Reduzierung von Partikelimmissionen – eine gesunheitspolitische Schwerpunktaufgabe. Teil 1: Luftbelastung durch Partikeln und gesundheitliche Auswirkungen. Gefahrstoffe Reinhaltung der Luft 64(7/8), 325-331.

[10] Lahl, U., Steven, W., 2004. Reduzierung von Partikelimmissionen – eine gesunheitspolitische Schwerpunktaufgabe. Teil 2: Maßnahmenprogramm zur Reduzierung der Emission von Partikeln. Gefahrstoffe Reinhaltung der Luft 64(9), 381-385.

[11] Kukkonen, J., Pohjola, M., Sokhi, R.S., Luhana, L., Kitwiroon, N., Fragkou, L., Rantamaki, M., Berge, E., Odegaard, V., Havard Slordal, L., Denby, B., Finardi, S., 2005. Analysis and evaluation of selected local-scale PM_{10} air pollution episodes in four European cities: Helsinki, London, Milan and Oslo. Atmospheric Environment 39, 2759-2773.

[12] Bruckmann P., Niemenn, K., Wurzler, S., Engel, I., Hoogerbrugge, R, Garus, G., Olschewski, A., 2008. High PM_{10} levels covering large parts of Europe caused by

long range transport. Gefahrstoffe Reinhaltung der Luft 5, 189-195.

[13] Bruckmann P., Birmili W., Straub, W., Pitz, M., Gladtke, D., Pfeffer, U., Hebbinghaus, H., Wurzler, S., Olschewski, A., 2008. An outbreak of Saharan dust causing high PM_{10} levels north of the Alps. Gefahrstoffe Reinhaltung der Luft 11/12, 490-498.

[14] Kocak, M., Mihalopoulos, N., Kubilay, N., 2009. Origin and source regions of PM_{10} in the Eastern Mediterranean atmosphere. Atmospheric Research 92, 464-474.

[15] The World Bank Group, 1999. Urban air quality management. Pollution prevention and abatement handbook 1998. Toward cleaner production, 96-100. Washington, D.C.

[16] Regierungsprasidium Stuttgart Baden-Württemberg, 2005. Luftreinhalte-/Aktionsplan für den Regierungsbezirk Stuttgart Teilplan Landeshauptstadt Stuttgart.

[17] Umweltministerium Baden-Württemberg, 2008. Umweltzonen in Baden-Württemberg.

[18] Düring, I., Jacob, J., Lohmeyer, A., Lutz, M., Reichenbacher, W., 2002. Estimation of the “non-exhaust pipe” PM_{10} emissions of roads for practical traffic air pollution modelling. Proceedings of the 11^{th} International Symposium Transport and Air Pollution. June 2002, Graz, Austria. Vol. I, 309-316.

[19] Chang, Y.M., Chou, C.M., Su, K.T., Tseng, C.H., 2005. Effectiveness of street sweeping and washing for controlling ambient TSP. Atmospheric Environment 39, 1897-1902.

[20] Chow, J.C., Watson, J.G., Egami, R.T., Frazier, C.A., Lu, Z., Goodrich, A., Bird, A., 1990. Evaluation of regenerative-air vacuum street sweeping on geological contributions to PM_{10}. Journal of the Air & Waste Management Association 40, 1134-1142.

[21] Gertler, A., Kuhns, H., Abu-Allaban, M., Damm, C., Gillies, J., Etyemezian, V., Clayton, R., Proffitt, D., 2006. A case study of the impact of Winter road sand/salt and street sweeping on road dust re-entrainment. Atmospheric Environment 40, 5976-5985.

[22] Kuhns, H., Etyemezian, V., Green, M., Henrickson, K., McGown, M., Barton, K., Pitchford, M., 2003. Vehicle-based road dust emission measurement Part II: Effect of precipitation, wintertime road sanding, and street sweepers on inferred PM_{10} emission potentials from paved and unpaved roads. Atmospheric Environment 37, 4573-4582.

[23] Norman, M., Johansson, C., 2006. Studies of some measures to reduce road dust emissions from paved roads in Scandinavia. Atmospheric Environment 40, 6154-6164.

[24] Tandon, A., Yadav, S., Attri, A.K., 2008. City-wide sweeping a source for respirable particulate matter in the atmosphere. Atmospheric Environment 42, 1064-1069.

[25] Baumbach, G., Ang, K.B., Staub, D., Vogt, U., Kapp, R., Reiser, M., Dreher, W., Pesch, P., Brumbach, M., 2009. Measurement strategy to determine the effects of street cleaning as PM abatement measure. Proceedings of the 7th International Conference on Air Quality. March 2009. Istanbul, Turkey.

[26] Kobe, A., 2007. The European ambient air policy – Developments and the role of modelling. 11th International Conference on Harmonisation within Atmospheric Dispersion Modelling for Regulatory Purposes. Cambridge, UK, July 2-5.

[27] Pfeiffer, H., Baumbach G., Sarachaga-Ruiz, L., Kleanthous, S., Poulida, O., Beyaz, E., 2009. Neural modelling of the spatial distribution of air pollutants. Atmospheric Environment 43, 3289-3297.

[28] Monteiro, A, Lopes, M., Miranda, A.I., Borrego, C., Vautard, R., 2005. Air pollution forecast in Portugal: a demand from the new air quality framework directive. International Journal of Environment and Pollution 5, 1-9.

[29] CENR Committee on Environment and Natural Resources, 2001. Air quality forecasting. A review of federal programs and research needs. NOAA Aeronomy Laboratory. Boulder Colorado.

[30] Sharma, P., Khare, M., 2001. Modelling of vehicular exhausts – a review. Transportation Research-D6, 179-198.

[31] Vardoulakis, S., Fischer, B.E.A., Pericleous, K., Gonzalez-Flesca, N., 2003. Modelling air quality in street canyons: a review. Atmospheric Environment 37, 155-182.

[32] VDI 3782 Part 1, 2001. Environmental meteorology. Atmospheric dispersion models. Gaussian plume model for air quality management. Berlin, Beuth.

[33] VDI 3782 Part 3, 1985. Dispersion of air pollutants in the atmosphere. Berlin, Beuth.

[34] Heymann, M., 2006. Modeling reality. Practice, knowledge, and uncertainty in atmospheric transport simulation. Historical Studies in the Physical and Biological Sciences 37(1), 49-85.

[35] Morris, R.E., Meyers, T.C., 1990. User's guide for the urban airshed model Volume I: User's Manual for UAM (CB-IV). EPA-450/4-90-007A. U.S. Environmental Protection Agency, Research Triangle Park, NC.

[36] Lamb, R.G., 1983. A regional scale (1000 km) Model of Photochemical Air Pollution, Part I: Theoretical Formulation. EPA 600/3-83-035. U.S. Environmental Protection Agency, Research Triangle, NC.

[37] Lamb, R.G., 1983. A regional scale (1000 km) Model of Photochemical Air Pollution, Part II: Input Process Network Design. EPA 600/3-84-085, U.S. Environmental Protection Agency, Research Triangle Park, NC.

[38] Carmichael G.R., Peters, L.K., 1984. An Eulerian/transport/transformation/removal for SO_2 and sulphate-I. Model development. Atmospheric Environment 18, 937-952.

[39] Carmichael G.R., Peters, L.K., 1984. An Eulerian/transport/transformation/removal for SO_2 and sulphate-II. Model calculation of SO_X transport in the Eastern in the United States. Atmospheric Environment 20, 173-188.

[40] Carmichael G.R., Peters, L.K., Saylor, R.D., 1991. The STEM-II regional scale acid deposition and photochemical oxidant model-I. An overview of model development and application, Atmospheric Environment, 25A, 2077-2090.

[41] Byun, D.J., Young, J., Gipson, J., Godowitch, J., Binkowski, F., Roselle, S., Benjey, B., Pleim, J., Ching, J., Novak, J., Coats, C., Odman, T., Hanna, A., Alapaty, K., Mathur, R., Mchenry, J., Sankar, U., Fine, S., Xiu, A., Jang, C., 1998. Description of the Models-3 Community Multiscale Air Quality (CMAQ) model. Proceedings of the American Meteorological Society 78th Annual Meeting, January 11-16, Phoenix, AZ.

[42] Jose, R.S., Baklanov, A., Sokhi, R.S., Karatzas, K., Perez, J.L., 2006. Air quality modelling: State-of-the-art. In: Voinv, A., Jake, A.J., Rizzoli, A.E. (eds). Proceedings of the iEMSs Third Biennial Meeting: “Summit on Environmental Modelling and Software”. International Environmental Modelling and Software Society, Burlington, USA, July 2006.

[43] Carslaw, D., Beevers, S., 2002. The efficacy of low emission zones in central London as a means of reducing nitrogen dioxide concentrations. Atmospheric Environment 7(1), 46-64.

[44] Carslaw, D., Beevers, S.D., Fuller, G., 2001. An empirical approach for the prediction of annual mean nitrogen dioxide concentration in London. Atmospheric Environment 35(8), 1505-1515.

[45] Düring, I., Lohmeyer, A., 2003. Machbarkeitstudie zu kombinierten Lärmminderungs-/Luftreinhaltungplänen in BBG. – Teil Vergleichende Bewertung von Maßnahmen zur Reduzierung der PM_{10}-Belastung-Wirkungsuntersuchungen zur OU Nauen. Projekt 2464.

[46] Duc, H., Shannon, I., Azzi, M., 2000. Spatial distribution characteristics of some air pollutants in Sydney. Mathematics and Computers in Simulation 54, 1-21.

[47] Britter, R.E., Hanna, S.R., 2003. Flow and dispersion in urban areas. Annual Review of Fluid Mechanics 35(1), 469-496.

[48] Milliez, M., Carissimo, B., 2007. Numerical simulations of pollutant dispersion in an idealized urban area, for different meteorological conditions. Boundary-Layer Meteorology 122, 321-342.

[49] Lohmeyer, A., Eichorn, J., Flassak, T., Kunz, W., 2002. WinMISKAM 4.2, microscale flow and dispersion model for built up areas, recent developments. Proceedings of the 11th International Symposium Transport and Air Pollution. June 2002, Graz, Austria.

[50] Louka, P., Ketzel, M., Sahm, P., Guilloteau, E., Moussiopoulos, N., Sini, J.-F., 2001. CFD inter-comparison on a full-scale street-canyon. 7th International Conference on Harmonisation within Atmospheric Dispersion Modelling for Regulatory Purposes in

Belgirate, Italy, 28-31 May 2001. European Commission, Joint Research Centre, Environment Institute, Ispra, Italy. Proceedings, pp. 299-303.

[51] Kukkonen, J., Partanen, L., Karppinen, A., Ruuskanen, J., Junninen, H., Kolehmainen, M., Niska, H., Dorling, S., Chatterton, T., Cawley, G., 2003. Extensive evaluation of neural network models for the prediction of NO_2 and PM_{10} concentrations, compared with a deterministic modelling system and measurements in central Helsinki. Atmospheric Environment 37, 4539-4550.

[52] Schlink, U., Dorling, S., Pelikan, E., Nunnari, G., Cawley, G., Junninen, H., Greig, A., Foxall, R., Eben, K., Chatterton, T., Vonfracek, J., Richter, M., Dostal, M., Bertucco, L., Kolehmainen, M., Doyle, M., 2003. A rigorous inter-comparison of ground-level ozone predictions. Atmospheric Environment 37, 3237-3253.

[53] Dutot, A-L., Rynkiewicz, J., Steiner, F.E., Rude, J., 2007. A 24-h forecast of ozone peaks and exceedances levels using neural classifiers and weather predictions. Environmental Modelling & Software 22(9), 1261-1269.

[54] Agirre-Basurko, E., Ibarra-Berasteigi, G., Madariaga, I., 2006. Regression and multilayer perceptron-based models to forecast hourly O_3 and NO_2 levels in the Bilbao area. Environmental Modelling & Software 21, 430-446.

[55] Slini, T., Kaprara, A., Moussiopoulos, N., 2006. PM_{10} forecasting for Thessaloniki, Greece. Environmental Modelling & Software 21, 559-565.

[56] Zolghadri, A., Cazaurang, F., 2006. Adaptive nonlinear state-space modelling for the prediction of daily mean PM_{10} concentrations. Environmental Modelling & Software 21, 885-894.

[57] Brandt, J., Christensen, J.H., Frohn, L.M., Palmgren, F., Berkowicz, R., Zlatev, Z., 2001. Operational air pollution forecasts from Europe to local scale. Atmospheric Environment 35(1), 91-98.

[58] Vanghan, J., Lamb, B., 2003. AIRPACT: A numerical air-quality forecasting system for the Seattle area, presented at U.S. EPA & A&WMA National Air Quality Conference San Antonio, February 4th.

[59] AIRNow
http://www.airnow.gov/

[60] Air Quality – Forecast
http://www.eurad.uni-koeln.de/index_e.html

[61] Baklanov, A., Hänninen, O., Slordal, L.H., Kukkonen, J., Bjergene, N., Fay, B., Finardi., S., Hoe, S.C., Jantunen, M., Karppinen, A., Rasmussen, A., Skouloudis, A., Sokhi, R.S., Sorensen, J.H., 2007. Integrated systems for forecasting urban meteorology, air pollution and population exposure. Atmospheric Chemistry and Physics 7, 855-874.

[62] Finardi, S., De Maria, R., D’Allura, A., Cascone, C., Calori, G., Lollobrigida, F., 2008. A deterministic air quality forecasting system for Torino urban area, Italy.

Environmental modelling & Software 23, 344-355.

[63] Slodal, L.H., Laupsa, H., Wind, P., Tarrason, L., 2004. Local and regional description of particulate matter in the Oslo. The Norwegian Meteorological Institute. Joint MSC-W & NILU Technical Report 5/04.

[64] Carpenter, W.A., 1975. The theory and mathematical development of AIRPOL-4, Report, VHTRC-75-R49. Virginia Highway and Transportation Research Council, Clemena, G.G., Charlottesvilla, V.A.

[65] U.S. Environmental Protection Agency, 1995. User's guide for the Industrial Source Complex (ISC3) Dispersion Models (revised) Volume I – User Instructions. EPA-454/b-95-003a. Research Triangle Park, NC.

[66] Peterson, W.B., 1980. User's guide for highway air pollution model. EPA-60018-80-018.

[67] Zimmerman, J.P., Thompson, R.S., 1975. User's guide for HIWAY. A Highway Air Pollutant Model, EPA – 650/4-74-008.

[68] Benson, P.E., 1979. CALINE 3: A versatile dispersion model for predicting air pollutant levels near highway and arterial roads. Final Report, FHWA/CA/TL. -79/23. California Department of Transportation, Sacramento, CA.

[69] Benson, P.E., 1989. CALINE 4: A dispersion model for predicting air pollutant concentrations near roadway. Final Report, FHWA/CA/TL. – 84/15. California Department of Transportation, Sacramento, CA.

[70] Ward, C.E., Rangier, A.J., Shirley, E.C., 1977. CALINE 2 – An improved microscale-model for the dispersion of air pollutants from a line source. Federal Highway Administration Report, FHQA-RD-77-74, Washington, DC.

[71] VDI 3945 Part 3, 2000. Atmospheric dispersion models; Particle model. Berlin, Beuth.

[72] Joseph, S.S., Strimaitis, D.G., Yamartino, R.J., 1990. Model formulation and user's guide for the CALPUFF dispersion model. Report no. A025-2. California Air Resources Board, Sacramento, California, USA.

[73] Villasenor, R., Lopez-Villegas, M.T., Eidels-Dubovio, S., Quintanar, A., Gallardo, J.C., 2003. A mesoscale modeling study of wind blown dust on the Mexico City Basin. Atmospheric Environment 37, 2451-2462.

[74] Nester, K., Panitz, H.J., Fiedler, F., 1995. Comparison of the DRAIS and EURAD model simulations od air pollution in a mesoscale area. Meteorology and Atmospheric Physics 57, 135-158.

[75] Nester, K., Panitz, H.J., 2005. Sensitivity analysis by the adjoint chemistry transport model DRAIS for an episode in the Berlin ozone (BERLIOZ) experiment. Atmoshperic Chemistry and Physics Discussions 5., 8715-8754.

[76] Stern, R., Yamartino, R.J., 2001. Development and first evaluation of micro-calgrid: a 3-D, urban-canopy-scale photochemical model. Atmospheric Environment 35, S149-165.

[77] Eichhorn, J., Schrodin, R., Zdunkowski, W., 1988. Three-dimensional numerical simulation of the urban climate. Beiträge zur Physik der Atmosphäre 61(3), 187-203.

[78] Eichhorn, J., 1989. Entwicklung und Anwendung eines dreidimensionalen mikroskaligen Staftklima-Modells. Dissertation, Johannes-Gutenberg-Universität Mainz.

[79] Diaz-Robles, L.A., Ortega, J.C., Fu, J.S., Reed, G.D., Chow, J.C., Watson, J.G., Moncada-Herrera, J.A., 2008. A hybrid ARIMA and artificial neural networks model to forecast particulate matter in urban areas: The case of Temuco, Chile. Atmospheric Environment 42, 8331-8340.

[80] Liu, P.-W.G., 2009. Simulation of the daily average PM_{10} concentrations at Ta-Liao with Box-Jenkins time series models and multivariate analysis. Atmospheric Environment 43, 2104-2113.

[81] McKendry, I.G., 2002. Evaluation of artificial neural networks for fine particulate pollution (PM_{10} and $PM_{2.5}$) forecasting. Journal of the Air & Waste Management Association 52, 1096-1101.

[82] Perez, P., Trier, A., Reyes, J., 2000. Prediction of $PM_{2.5}$ concentrations several hours in advance using neural networks in Santiago, Chile. Atmospheric Environment 34, 1189-1196.

[83] Perez, P., Reyes, J., 2002. Prediction of maximum of 24-h average of PM_{10} concentrations 30-h in advance in Santiago, Chile. Atmospheric Environment 36, 4555-4561.

[84] Perez, P., Salini, G., 2008. $PM_{2.5}$ forecasting in a large city: Comparison of three methods. Atmospheric Environment 42, 8219-8224.

[85] Chaloulakou, A., Grivas, G., Spyrellis, N., 2003. Neural network and multiple regression models for PM_{10} prediction in Athens: A comparative assessment. Journal of the Air & Waste Management Association 53, 1183-1190.

[86] Stadlober, E., Hörmann, S., Pfeiler, B., 2007. Quality and performance of a PM_{10} daily forecasting model. Atmospheric Environment 42, 1098-1109.

[87] Hoi, K.I., Yuen, K.V., Mok, K.M., 2009. Prediction of daily averaged PM_{10} concentrations by statistical time-varying model. Atmospheric Environment 43, 2579-2581.

[88] Assael, M.J., Delaki, M., Kakosimos, K.E., 2008. Applying the OSPM model to the calculation of PM_{10} concentration levels in the historical centre of the city of Thessaloniki. Atmospheric Environment 42, 65-77.

[89] Grivas, G., Chaloulakou, A., 2006. Artificial neural network models for prediction of

PM_{10} hourly concentrations, in Greater Area of Athens, Greece. Atmospheric Environment 40, 1216-1229.

[90] Hooyberghs, J., Mensink, C., Dumont, G., Fierens, F., Brasseur, O., 2005. A neural network forecast for daily average PM_{10} concentrations in Belgium. Atmospheric Environment 39, 3279-3289.

[91] Kurt, A., Gulbagci, B., Karaca, F., Alagha, O., 2008. An online air pollution forecasting system using neural networks. Environment International 34, 592-598.

[92] Perez, P., Reyes, J., 2006. An integrated neural network model for PM_{10} forecasting. Atmospheric Environment 40, 2845-2851.

[93] Zickus, E., Greig, A.J., Niranjan, M. 2002. Comparison of four machine learning methods for predicting PM_{10} concentrations in Helsinki, Finland. Water, Air, and Soil Pollution: Focus 2, 717-729.

[94] European Environment Agency, 1997. Ambient air quality, pollutants dispersion and transport models. Topic report no. 19/1996. Copenhagen, Denmark.

[95] Gardner, M.W., Dorling, S.R., 1998. Artificial neural networks: the multilayer perceptron – a review of applications in atmospheric science, Atmospheric Environment 32(14/15), 2627-2636.

[96] Kao, J.J., Huang, S.S., 2000. Forecast using neural network versus Box-Jenkins methodology for ambient air quality monitoring data. Journal of Air & Waste Management Association 50, 219-226.

[97] Jackman, A.J., Simpson, R.W., Taylor, J.A., 1988. Modelling distributions of air pollutant concentrations-III. The hybrid deterministic statistical distribution approach. Atmospheric Environment 22(1), 163-174.

[98] Chelani, A.B., Gajghate, D.G., Hasan, M.Z., 2002. Prediction of ambient PM_{10} and toxic metals using artificial neural networks. Journal of the Air & Waste Management Association 52, 805-810.

[99] Oussar, Y., Dreyfus, G., 2001. How to be a gray box: Dynamic semi-physical modelling. Neural Networks 14, 1161-1172.

[100] Gardner, M.W., Dorling, S.R., 1999. Neural network modelling and prediction of hourly NO_X and NO_2 concentrations in urban air in London. Atmospheric Environment 33, 709-719.

[101] Elminir, H,K., Abdel-Galil, H., 2006. Estimation of air pollutant concentrations from meteorological parameters using artificial neural network. Journal of Electrical Engineering 57(2), 105-110.

[102] Leonard, J.A., Leonard, M.A., Ungar, L.H., 1992. A neural network architecture that computes its own reliability. Computers & Chemical Engineering 16, 819-835.

[103] Wolfram Mathematica Neural Networks

http://www.wolfram.com/products/applications/neuralnetworks/

[104] A MORE flexible neural network package
http://cran.r-project.org/web/packages/AMORE/index.html

[105] MathWorks Neural Network Toolbox
http://www.mathworks.com/products/neuralnet/

[106] GBLearn2 library in Lisp Universal Shell
http://lush.sourceforge.net/index.html

[107] Colvile, R.N., Hutchinson, E.J., Mindell, J.S., Warren, R.F., 2001. The transport sector as a source of air pollution. Atmospheric Environment 35, 1537-1565.

[108] Diegmann, V., Pfäfflin, F., Wiegand, G., Wursthorn, H., Dünnebeil, F., Helms, H., Lambrecht, U., 2006. Verkehrliche Massnahmen zur Reduzierung von Feinstaub – Möglichkeiten und Minderungspotenziale. Studie im Auftrag des Umweltbundesamt, Juli 2006. Dessau-Rosslau.

[109] LUBW Landesanstalt für Umwelt, Messungen und Naturschutz Baden-Württemberg, 2006. Besondere Immissionssituationen während der Inversionswetterlagen Januar/Februar 2006. Karlsruhe.

[110] LUBW Landesanstalt für Umwelt, Messungen und Naturschutz Baden-Württemberg, 2002. Besondere Immissionsverhältnisse waehrend der Inversionswetterlagen im Januar 2002. Karlsruhe.

[111] Baumbach, G., Ang, K.B., Bari, A., Vogt, U., Zeng, Y., 2006. Untersuchung der Ursachen hoher Feinstaubbelastung an verkehrsreichen Straßen und der Eigenschaften und Herkunft der gesammelten PM_{10}-Stäube des Messortes Stuttgart-Neckartor. Bericht-Nr.:52-2006, Sprint-Druck, Stuttgart, Bundesrepublik Deutschland.

[112] Görgen, R., Lambrecht, U., 2007. Particulate matter in ambient air. The debate on the PM_{10} daily limit value. Journal for European Environmental & Planning Law 4, 278-288.

[113] Lenschow, P., Abraham, H.-J., Kutzner, K., Lutz, M., Press, J.-D., Reichenbaecher, W., 2001. Some ideas about the sources of PM_{10}. Atmospheric Environment 35(1), S23-S33.

[114] Zeng, Y., 2005. Investigation of correlation between PM_{10} concentrations and meteorological parameters in urban areas. Master Thesis no. 2807. Universität Stuttgart, Institute of Process Engineering and Powerplant Technology.

[115] Janhäll, S., Olofson, K.F.G., Andersson, P.U., Pettersson, J.B.C., Hallquist, M., 2006. Evolution of the urban aerosol during winter temperature inversion episodes. Atmospheric Environment 40, 5355-5366.

[116] Pernigotti, D., Rossa, A.M., Ferrario, M.E., Sansone, M., Benassi, A., 2007. Influence of ABL stability on the diurnal cycle of PM_{10} concentration: illustration of the

potential of the new Veneto network of MW-radiometers and SODAR. Meteorologische Zeitschrift, doi: 10.1127/0941-2948/2007/0204.

[117] Ahrens, D., Anke, K., Drechsler, S., Gromes, B., Holst, J., Lumpp, R., Sähn, E., Scheu-Hactel, H., Scholz, W., 2007. Einflussgrößen auf die zeitliche und räumliche Struktur der Feinstaubkonzentrationen. LUBW Landesanstalt für Umwelt, Messungen und Naturschutz Baden-Württemberg, Karlsruhe.

[118] Putaud, J.P., Raes, F., van Dingenen, R., Brüggemann, E., Facchini, M.C., Decesari, S., Fuzzi, S., Gehrig, R., Hüclin, C., Laj, P., Lorbeer, G., Maenhout, W., Mihalopoulos, N., Müller, K., Querol, X., Rodriguez, S., Chneider, J., Spindler, G., Ten Brink, H., Torseth, K., Wiedensohler, A., 2004. A European aerosol phenomenology-2: chemical characteristics of particulate matter at kerbside, urban, rural and background sites in Europe. Atmospheric Environment 38, 2579-2595.

[119] Madhavi Latha, K., Highwood., E.J., 2006. Studies on particulate matter (PM_{10}) and its precursors over urban environment of Reading, UK. Journal of Quantitative Spectroscopy & Radiation Transfer 101, 367-379.

[120] Parameswaran, K., Rajeev, K., Sen Dupta, K., 1997. An observational study of nighttime concentrations in the lower atmosphere at a tropical coastal station. Journal of Atmospheric and Solar-Terrestrial Physics 59, 1727-1737.

[121] Drechsler, D., Ahrens, D., Lumpp, R., Holst, T.H., Uhrner, U., 2006. Hohe Feinstaubbelastung als Folge der Aerosolbildung. Immissionsschutz 2, 56-62.

[122] Rauterberg-Wulff, A., 2000. Untersuchung über die Bedeutung der Staubaufwirbelung für PM_{10}-Immission an einer Hauptverkehrsstrasse. Im Auftrag der Senatsverwaltung für Stadtenwicklung und Technologie. TU Berlin, Fachgebiet Luftreinhaltung. Berlin.

[123] U.S. Environmental Protection Agency, 1995. Emission factor documentation for AP-42. Research Triangle Park, NC.

[124] DIN 18123, 1996. Baugrund, Untersuchung von Bodenproben – Bestimmung der Korngroessemverteilung, Beuth Verlag GmbH. Berlin.

[125] Ketzel, M., Omstedt, G., Johansson, C., Düring, I., Pohjola, M., Oettl, D., Gidhagen, L., Wahlin, P., Lohmeyer, A., Haakana, M., Berkowicz, R., 2007. Estimation and validation of $PM_{2.5}$/PM_{10} exhaust and non-exhaust emission factors for practical street pollution modelling. Atmospheric Environment 41, 9370-9385.

[126] McColloch, W.S., Pitts, W., 1943. A logical calculus of ideas immanent in nervous activity. Bulletin of Mathematical Biophysics 5, 115-133.

[127] Goodlett, C.R. and Horn, K.H., 2001. Mechanisms of alcohol-induced damage to the developing nervous system. Alcohol Research & Health 25(3), 175-184.

[128] Neal, R., 1996. Lecture notes in statistics. Bayesian learning for neural networks. Springer-Verlag, New York.

[129] Casey, M., 1996. The dynamics of discrete-time computation, with application to recurrent neural networks and finite state machine extraction. Neural Computation 8(6), 1135-1178.

[130] Gardner, M.W., Dorling, S.R., 2000. Statistical surface ozone models: an improved methodology to account for non-linear behaviour. Atmospheric Environment 34, 21-34.

[131] Lu, H.C., Chang, T.S., 2005. Meteorologically adjusted trends of daily maximum ozone concentrations in Taipei, Taiwan. Atmospheric Environment 39, 6491-6501.

[132] Bishop, C., 1995. Neural networks for pattern recognition. University Press, Oxford.

[133] Willmott, C.J., 1981. On the validation of models. Physical Geography 2, 184-194.

[134] Kolehmainen, M., Martikainen, H., Ruuskanen, J., 2001. Neural networks and periodic components used in air quality forecasting. Atmospheric Environment 35, 815-825.

[135] Fang, M., Chan, C.K., Yao, X., 2009. Managing air quality in a rapidly developing nation: China. Atmospheric Environment 43, 79-86.

[136] Weather forecast data, meteoblue AG, Basel, Switzerland
http://www.meteoblue.com/

[137] Ciu, X., Shin, K.G., 1994. Design of a general-purpose MIMO predictor with neural networks. Journal of Intelligent Material Systems and Structures 5, 198-210.

[138] Huang, S.J., Lian, R.J., 2000. A combination of fuzzy logic and neural network controller for multiple-input multiple-output systems. International Journal of System Science 31(3), 343-157.

[139] Holst, J., Mayer, H., Holst, T., 2008. Effect of meteorological exchange conditions on PM_{10} conditions. Meteorologische Zeitschrift 17(3), 273-282.

[140] Junker, C., Wang, J.-L., Lee, C.-T., 2009. Evaluation of the effect of long-range transport of air pollutants on coastal atmospheric monitoring sites in and around Taiwan. Atmospheric Environment 43, 3374-3384.

[141] Niemi, J.V., Saarikoski, S., Aurela, M., Tervahattu, H., Hillamo, R., Westphal, D.L., Aarnio, P., Koskentalo, T., Makkonen, U., Vehkamaeki, H., Kulmale, M., 2009. Long-range transport episodes of fine particles in southern Finland during 1999-2007. Atmospheric Environment 53, 1255-1264.

[142] Vecchi, R., Bernardoni, V., Cricchio, D., D’Alessandro, A., Fermo, P., Lucarelli, F., Nava, S., Piazzalunga, A., Valli, G., 2008. The impact of fireworks on airborne particles. Atmospheric Environment 42, 1121-1132.

[143] Bondietti, E.A., Papastefanou, C., 1993. Estimates of residence time of sulphate aerosols in ambient air. The Science of the Total Environment 136, 25-31.

[144] Wiman, B.L.B., Unsworth, M.H., Linberg, S.E., Bergkvist, B., Jaenicke, R., Hannsson, H.C., 1990. Perspectives on aerosol deposition to natural surfaces: interactions between aerosol residence times, removal processes, the biosphere and global environmental change. Journal of Aerosol Science 21(3), 313-338.

[145] Kumar, P., Fennel, P., Britter, R., 2008. Effect of wind direction and speed on the dispersion of nucleation and accumulation mode particles in an urban street canyon. Science of the Total Environment 402(1), 82-94.

[146] Baumbach, G., Vogt, U., 2003. Influence of inversion layers on the distribution of air pollutants in urban areas. Water, Air, Soil Pollution 3, 65-76.

[147] Stull, R.B., 1988. An introduction to boundary layer meteorology. Kluwer Academic Publishers, Dordrecht.

[148] LUBW Landesanstalt für Umwelt, Messungen und Naturschutz Baden-Württemberg, 2004. Entwicklung der Stickstoffoxid-Immissionen in Baden-Württtemberg zwischen 1995 und 2003. Karlsruhe.

[149] Hatzianastassiou, N., Katsoulis, B.D., Antakis, B., 2007. Extreme nitrogen oxide and ozone concentrations in Athens atmosphere in relation to meteorological conditions. Environmental Monitoring and Assessment 128, 447-464.

[150] Velders, G.J., Matthijsen, J., 2009. Meteorological variability in NO_2 and PM_{10} concentrations in the Netherlands and its relation with EU limit values. Atmospheric Environment, doi:10.1016/j.atmosenv.2009.05.009.

[151] Mysliwiec, M.J., Kleeman M.J., 2001. Source apportionment of secondary airborne particulate matter in a polluted atmosphere. Environmental Science & Technology 36(24), 5376-5384.

[152] Charron, A., Harrison, R.M., 2005. Fine ($PM_{2.5}$) and coarse ($PM_{2.5-10}$) particulate matter on a heavily trafficked London Highway: sources and processes. Environmental Science & Technology 39, 7768-7776.

[153] Harrison, R.M., Deacon, A.R., Jones, M.R., Appleby, R.S., 1997. Sources and processes affecting concentrations of PM_{10} and $PM_{2.5}$ particulate matter in Birmingham (U.K.). Atmospheric Environment 31(24), 4103-4117.

[154] Bouchlaghem, K., Nsom, B., Latrache, N., Kacem, H.H., 2009. Impact of Sahatan dust on PM_{10} concentration in the Mediterranean Tunisian coasts. Atmospheric Research 92, 531-539.

[155] Chang, L.S., Park, S.U., 2004. Direct radioactive forcing due to anthropogenic aerosols in East Asia during April 2001. Atmospheric Environment 38, 4467-4482.

[156] Zhang, K., Wang, Y., Wen, T., Yousef, M., Frank, M., 2007. Properties of nitrate, sulfate and ammonium in typical polluted atmospheric aerosols (PM_{10}) in Beijing. Atmospheric Research 84, 67-77.

[157] Latha, K.M., Badarinath, K., 2005. Shortwave radioactive forcing efficiency of urban

aerosols – a case study using ground based measurements. Chemosphere 57, 217-220.

[158] Lee, Y.L., Sequeira, R., 2002. Water-soluble aerosol and visibility degradation in Hong Kong during autumn and early winter, 1998. Environmental Pollution 116, 225-233.

[159] Ulke, A.G., Mazzeo, N.A., 1998. Climatological aspects of the daytime mixing height in Buenos Aires city, Argentina. Atmospheric Environment 32, 1615-1622.

[160] Seibert, P., Beyrich, F., Gryning, S.E., Joffre, S., Rasmussen, A., Tercier, P., 2000. Review and intercomparison of operational methods for the determination of the mixing height. Review Article, Atmospheric Environment 34, 1001-1027.

[161] Karppinen, A., Joffre, S.M., Kukkonen, J., Bremer, P., 2001. Evaluation of inversion strengths and mixing heights during extremely stable atmospheric stratification. International Journal of Environment and Pollution 16, 603-613.

[162] Sicard, M., Perez, C., Rocadenbosch, F., Baldasano, J.M., Garcia-Vizcaino, D., 2006. Mixed-Layer depth determination in the Barcelona coastal area from regular lidar measurements: methods, results and limitation. Boundary-Layer Meteorology 1999, 135-157.

[163] Khare, M., Nagendra, S., 2007. Artificial neural networks in vehicular pollution modelling. Springer Verlag, Germany.

[164] Swingler, K., 1996. Applying neural networks: a practical guide. Academic Press, London.

[165] Berry, T., Linoff, J., 1997. Data mining techniques. John Wiley and Sons, New York.

[166] Salcedo, D., Onasch, T.B., Dzepina, K., Canagaratna, M.R., Zhang, Q., Huffman, J.A., DeCarlo, P.F., Jayne, J.T., Mortimer, P., Worsnop, D.R., Kolb, C.E., Johnson, K.S., Zuberi, B., Marr, L.C., Volkamer, R., Molina, L.T., Molina, M.J., Cardenas, B., Bernabe, R.M., Marquez, C., Gaffney, J.S., Marley, N.A., Laskin, A., Shutthanandan, V., Xie, Y., Lesher, R., Shirley, T., Jimenez, J.L., 2006. Characterization of ambient aerosols in Mexico city during the MCMA-2003 campaign with Aerosol Mass Spectrometry: results from the CENICA Supersite. Atmospheric Chemistry and Physics 6, 925-946.

[167] Silva, P.J., Vawdrey, E.L., Corbett, M., Erupe, M., 2007. Fine particle concentrations and compositions during wintertime inversions in Logan, Utah, USA. Atmospheric Environment 41, 5410-5422.

[168] Monero, T., Querol, X., Alastuey, A., Minguillon, M.C., Pey, J., Rodriguez, S., Miro, J.V., Felis, C., Gibbons, W., 2007. Recreational atmospheric pollution episodes: Inhalable metalliferous particles from fireworks displays. Atmospheric Environment 41, 913-922.

[169] Ravindra, K., Mor, S., Kaushik, C.P., 2003. Short-term variation in air quality associated with fireworks events: A case study. Journal of Environmental Monitoring 5, 260-264.

[170] Karaca, F., Anil, F., Alagha, O., 2009. Long-range potential source contributions of episodic aerosol events to PM_{10} profile of a megacity. Atmospheric Environment, doi: 10.1016/j.atmosenv.2009.08.005.

[171] Pey, J., Querol, X., de la Rosa, J., Gonzazaez-Castanedo, Y., Alastuey, A., Gangoiti, G., Sanchez de la Campa, A., Alados-Arboledas, L., Sorribas, M., Pio, C., Cachorro, V., Pineiro, M., Lopez-Mahia, P., Garcia-Gacio, D., 2008. Characterization of a long range transport pollution episode affecting PM in SW Spain. Journal of Environmental Monitoring 10, 1158-1171.

[172] Watson, J.G., Chow, J.C., Lurmann, F.W., Musarra, S.P., 1994. Ammonium nitrate, nitric acid, and ammonium equilibrium in wintertime Phoenix, Arizona. Journal of the Air & Waste Management Association 44, 405-412.

[173] Silva, P.J., Vawdrey, E.L., Corbett, M., Erupe, M., 2007. Fine particle concentrations and composition during wintertime inversions in Logan, Utah, USA. Atmospheric Environment 41, 5410-5422.

[174] Karaca, F., Alagha, O., Ertürk, F., Yilmaz, Y.Z., Özkara, T., 2008. Seasonal variation of source contributions to atmospheric fine and coarse particles. Environmental Engineering Science 25(5), 767-781.

[175] Birmili, W., Schepamski, K., Ansmann, A., Spindler, G., Tegen, I., Wehner, B., Nowak, A., Reimer, E., Mattis, I., Müller, K., Brüggemann, E., Gnauk, T., Herrmann, H., Wiedensohler, A., Althausen, D., Schladitz, A., Tuch, T., Löschau, G., 2008. A case of extreme particulate matter concentrations over Central Europe caused by dust emitted over the southern Ukraine. Atmospheric Chemistry and Physics 8, 997-1016.

[176] Salvador, P., Artinano, B., Pio, C.A., Afonso, J., Puxbaum, H., Legrand, M., Hammer, S., Kaiser, A., 2009. Evaluation of aerosol sources at European high altitude background sites with trajectory statistical methods. Geophysical Research Abstracts 11, EGU2009-9728.

[177] Ordieres, J.B., Vergara, E.P., Capuz, R.S., Salazar, R.E., 2005. Neural network prediction model for fine particulate matter ($PM_{2.5}$) on the US-Mexico border in El Paso (Texas) and Ciudad Juarez (Chihuahua). Environmental Modelling & Software 20, 547-559.

[178] Hanna, S.R., Chang, J., Britter, R., Neophytou, M., 2003. Overview of model evaluation history and procedures in the atmospheric air quality area, QNET-CFD Network Newsletter 2(5), 1-4.

[179] Piringer, M., Baumann-Stanzer, K., 2009. Selected results of a model validation exercise. Advances Sciences and Research 3, 13-16.

[180] Chang, J.C., Hanna, S.R., 2004. Air quality model performance evaluation. Meteorology and Atmospheric Physics 87, 1-3.

[181] Kousa, A., Kukkonen, J., Karppinen, A., Aarnio, P., Koskentalo, T., 2001. Statistical and diagnostic evaluation of a new-generation urban dispersion modelling system against an extensive dataset in the Helsinki area. Atmospheric Environment 35, 4617-

4628.

[182] LUWG Landesamt für Umwelt Wasserwirtschaft und Gewerbaufsicht, 2007. Feinstaubbelastungsepisode Ende Dezember 2007 in Rheinland-Pfalz.

[183] Freund, Y., Schapire, R., 1996. Experiments with a new boosting algorithm. Proceedings of the Thirteen International Conference on Machine Learning, 148-156.

[184] Maclin, R., Opitz, D., 1997. An empirical evaluation of bagging and boosting. Proceedings of the Fourteenth National Conference on Artificial Intelligence, 546-551.

[185] Breiman, L., 1996. Bagging predictors. Machine Learning 24(2), 123-140.

[186] Riedmiller, M., Braun, H., 1993. A direct adaptive method for faster backpropagation learning: The RPROP algorithm. Proceedings of the IEEE International Conference on Neural Networks (ICNN), 586-591. San Francisco, USA.

[187] Reidmiller, M., 1994. Advanced supervised learning in multi-layer perceptrons from backpropagation to adaptive learning algorithms. International Journal on Computer Standards and Interfaces 16, 265-278.